United States
Environmental Protection
Agency

Region III
Philadelphia, PA

Final Report
December 5, 2000

EPA

Hydrodynamic and Water Quality Model of Christina River Basin

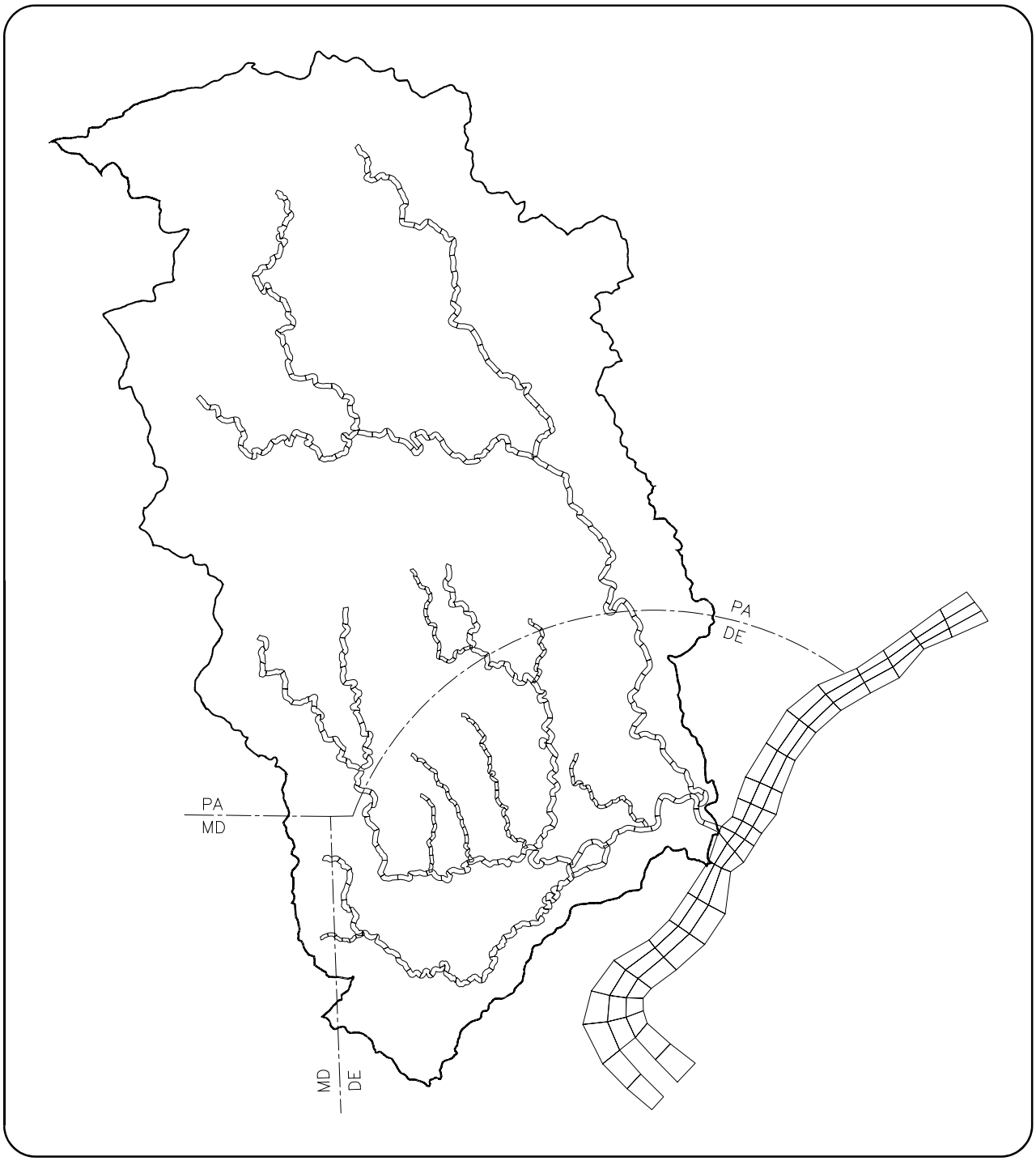

Acknowledgments

Funding for this study was provided through the U.S. Environmental Protection Agency, Region 3, under contracts #68-C7-0018 and #68-C-99-249. The EPA Work Assignment Manager was Mr. Leo Essenthier. The EPA Region 3 TMDL Coordinator was Mr. Tom Henry. Technical direction was provided by Mr. George Golliday and Mr. Larry Merrill, EPA Region 3. Coordination of the various agencies involved in the study was provided by Mr. David Pollison, Mr. Thomas Fikslin, and Mr. Jason Tsai of the Delaware River Basin Commission. Data and technical review were provided by Mr. Richard Greene, Mr. Hassan Mirsajadi, and Ms. Xia Xie of Delaware Department of Natural Resources and Environmental Control and by Mr. William Goman and Ms. Nancy Crickman of Pennsylvania Department of Environmental Protection. Field monitoring data from August 1997 and solar radiation data were provided by Dr. John Davis, Widener University. Discharge monitoring data for some Pennsylvania NPDES discharges were provided by Mr. Bob Struble, Brandywine Valley Association. ArcINFO GIS coverage for the NPDES point sources and HSPF watersheds as well as water withdrawal data were provided by Mr. Jerry Kaufman, New Castle County Water Resources Agency.

This report should be cited as:

USEPA. 2000. *Hydrodynamic and Water Quality Model of Christina River Basin*. Final Report. United States Environmental Protection Agency, Region III, Philadelphia, PA. December 5, 2000. 464 pp.

CONTENTS

FIGURES

TABLES

This page intentionally left blank

1 - INTRODUCTION

Section 303(d) of the Federal Clean Water Act requires the states to identify waterbodies that need Total Maximum Daily Loads (TMDLs) to assure compliance with water quality standards. TMDLs, as defined by U.S. Environmental Protection Agency (EPA), are the sum of individual waste load allocations (WLAs) for point sources and load allocations (LAs) for nonpoint sources of pollution. Not all waterbodies require the development of a TMDL. Both Pennsylvania and Delaware have developed 303(d) lists of impaired waters in the Christina River Basin. This study is concerned only with the 303(d) waters listed for nutrients and low dissolved oxygen.

A hydrodynamic and water quality model of the Christina River Basin (see Figure 1-1) has been developed for use in TMDL calculations. The Environmental Fluid Dynamics Code (EFDC) hydrodynamic and water quality model has been selected for use in this study. The model includes a portion of the tidal Delaware River, and tidal Christina River, as well as other nontidal streams, including the upper Christina River, Brandywine Creek, East Branch Brandywine Creek, West Branch Brandywine Creek, Buck Run, Red Clay Creek, and White Clay Creek. The model consists of 406 depth-averaged, computational grid cells. The grid cells in the nontidal streams have lengths ranging from about 500 to 1,000 meters to provide sufficient longitudinal resolution.

The United States Geological Survey (USGS) is currently developing a watershed runoff model for the Christina River Basin using the Hydrologic Simulation Program-Fortran (HSPF) model. The HSPF model is scheduled to be completed approximately 2 years hence. When it is available, dynamic nonpoint source flows and nutrient loadings computed by the HSPF model will be coupled with the EFDC receiving water model to form a powerful tool for management of both point and nonpoint sources in the basin. This report discusses the first phase of the TMDL for the Christina River Basin, namely, the low-flow analysis for nutrients and dissolved oxygen. Since the HSPF model is not yet available to provide dynamic, time-varying nonpoint source flows and loads, this phase of the TMDL will consider only low-flow summer conditions. The flow rates and nutrient loading rates from the point and nonpoint sources in the EFDC model for this phase were time-varying inputs. The point source loads generally varied on a monthly time step based on discharge monitoring records (DMRs). The nonpoint source loads varied on a daily time step as estimated from daily flow records and constant background concentrations. The tidal boundary conditions were also configured as time-varying concentrations, as were the atmospheric meteorological conditions.

1.1 Purpose of the Study

The purpose of this project is to construct a numerical model of the major features of estuarine and nontidal circulation and eutrophication processes for the Christina River Basin system. This numerical model is a tool for the development of TMDLs for nutrients, dissolved oxygen, and zinc. The objectives of the water quality model are as follows:

- Develop a water quality model that can be used to support development of TMDLs for nutrients and dissolved oxygen for the Brandywine Creek and Christina River basins.
- Configure the EFDC model so that it is consistent with the HSPF watershed runoff loading model being developed concurrently by the USGS.
- Develop and present a one-day workshop to transfer the water quality model technology to the U.S. Environmental Protection Agency (EPA), Delaware Department of Natural Resources and Environmental Control (DNREC), Pennsylvania Department of Environmental Protection (PADEP), Delaware River Basin Commission (DRBC), and other interested parties.
- Document the development and calibration of the water quality model in the form of a summary report
- Deliver the model source and executable code along with a low-flow data set that can be used for TMDL analyses.

1.2 Scope of the Study

The scope of the study has been expanded beyond the scope of work described in the original proposal for this project to include (1) the use of a multidimensional, finite-difference hydrodynamic and water quality model (EFDC) instead of the DYNHYD/WASP framework; (2) the use of a sediment process model to predict the response of benthic sediment nutrient fluxes and sediment oxygen demand due to changes in loading to the system; and (3) the calibration of the model over a dynamic summer period beginning in May and continuing through September 1997. The stream reaches cited for nutrients and low dissolved oxygen on the Pennsylvania 303(d) list are shown in Table 1-1; those cited on the Delaware 303(d) list are given in Table 1-2. The stream reaches listed for nutrients and low dissolved oxygen where the potential causes are point sources, nonpoint sources, or other reasons are shown in Figure 1-2. The stream reaches on the 303(d) lists cited for nutrients and low dissolved oxygen having potential causes related to point sources only are shown in Figure 1-3. The stream segments shown in Figure 1-3 will be the primary focus of this initial phase of the TMDL for low-flow conditions.

Calibration of the model was to be achieved using available data, and no field sampling to support model development was included in the scope of this study. An extensive data monitoring program for the Christina River Basin managed by DNREC and PADEP has been in place since at least 1995. Under this program various stations have been sampled generally on a monthly or bimonthly basis. Data for calibration were obtained from various sources including STORET, USGS, DNREC, PADEP, NOAA, and a special field sampling study conducted by Dr. John Davis in August 1997. The resulting

data set provided reasonably complete coverage for all the stream reaches included in the model during the summer 1997 calibration period.

1.3 The EFDC Model Package

The hydrodynamic and water quality model chosen for the study is EFDC, the Environmental Fluid Dynamics Code (Hamrick 1992a; Park et al. 1995) because it contained features not available in DYNHYD/WASP that were necessary for simulating the flow and eutrophication processes in the Christina River Basin. A number of low-head dams and submerged weirs have been built in the streams in the study area. DYNHYD does not have any means of handling flow through a hydraulic structure whereas EFDC has that capability. The EFDC water quality module also contains a sediment process submodel that is useful for determining the changes in sediment oxygen and nutrient flux rates due to changes in external loadings to the system. The WASP model does not have this advanced capability. The EFDC model was developed to comply with the requirements for the eutrophication model study of the Christina River Basin. The EFDC hydrodynamic model produces three-dimensional (3-D) predictions of velocity, diffusion, surface elevation, salinity, suspended sediment, and temperature on an intratidal time scale (60-second time step). The water quality module, an adaptation of the Corps of Engineers CE-QUAL-ICM (Cerco and Cole 1993), was integrated directly into EFDC and operates on a time step which is double that of the hydrodynamic model. In addition, the water quality model optionally interacts directly with a predictive sediment diagenesis model based on DiToro and Fitzpatrick (1993). Point source and tributary (nonpoint source) loads were developed using water quality and flow monitoring data.

Figure 1-1. Christina River Basin study area.

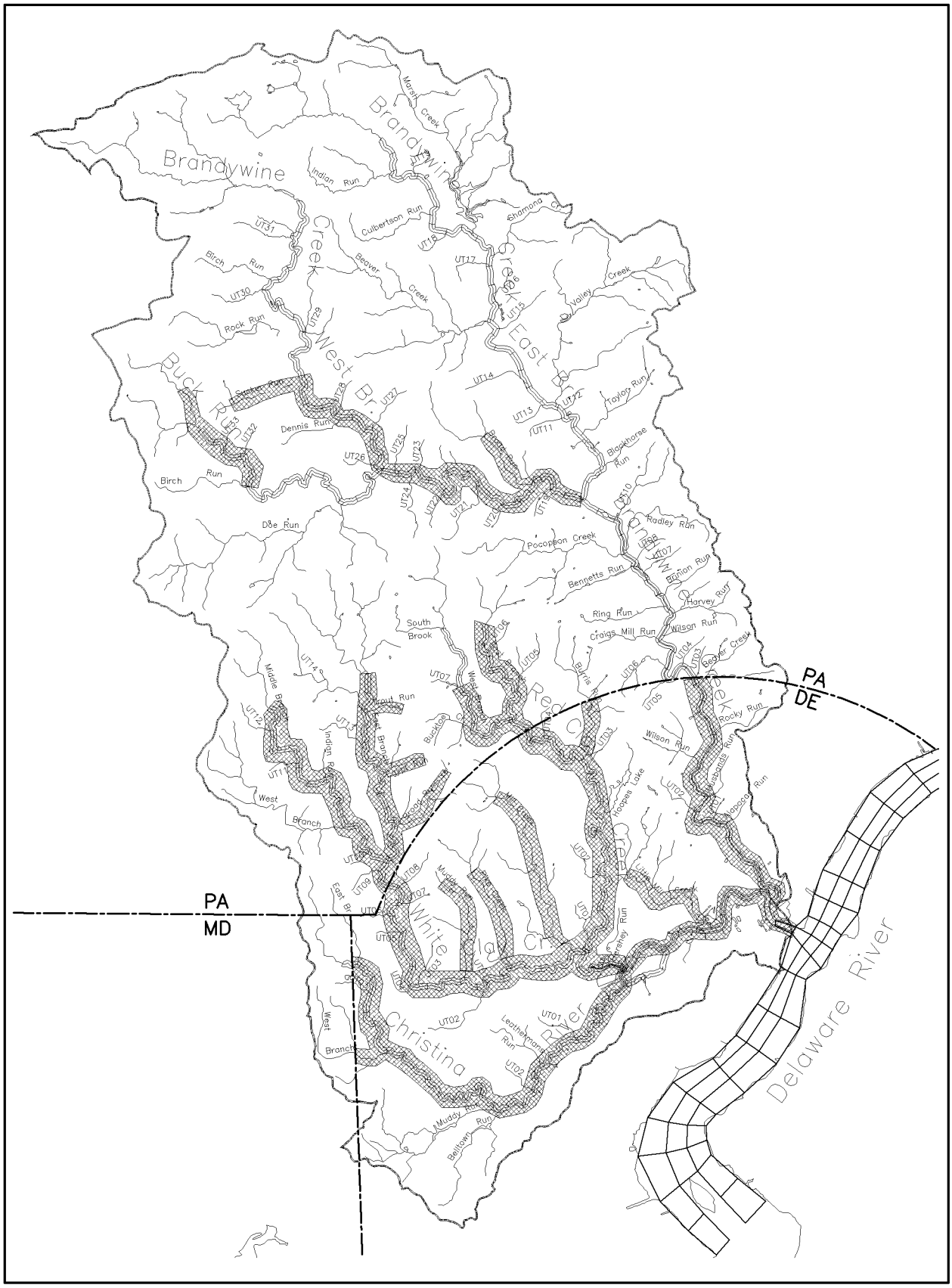

Figure 1-2. 303(d) waters listed for nutrients, low DO (NPS and PS as cause)

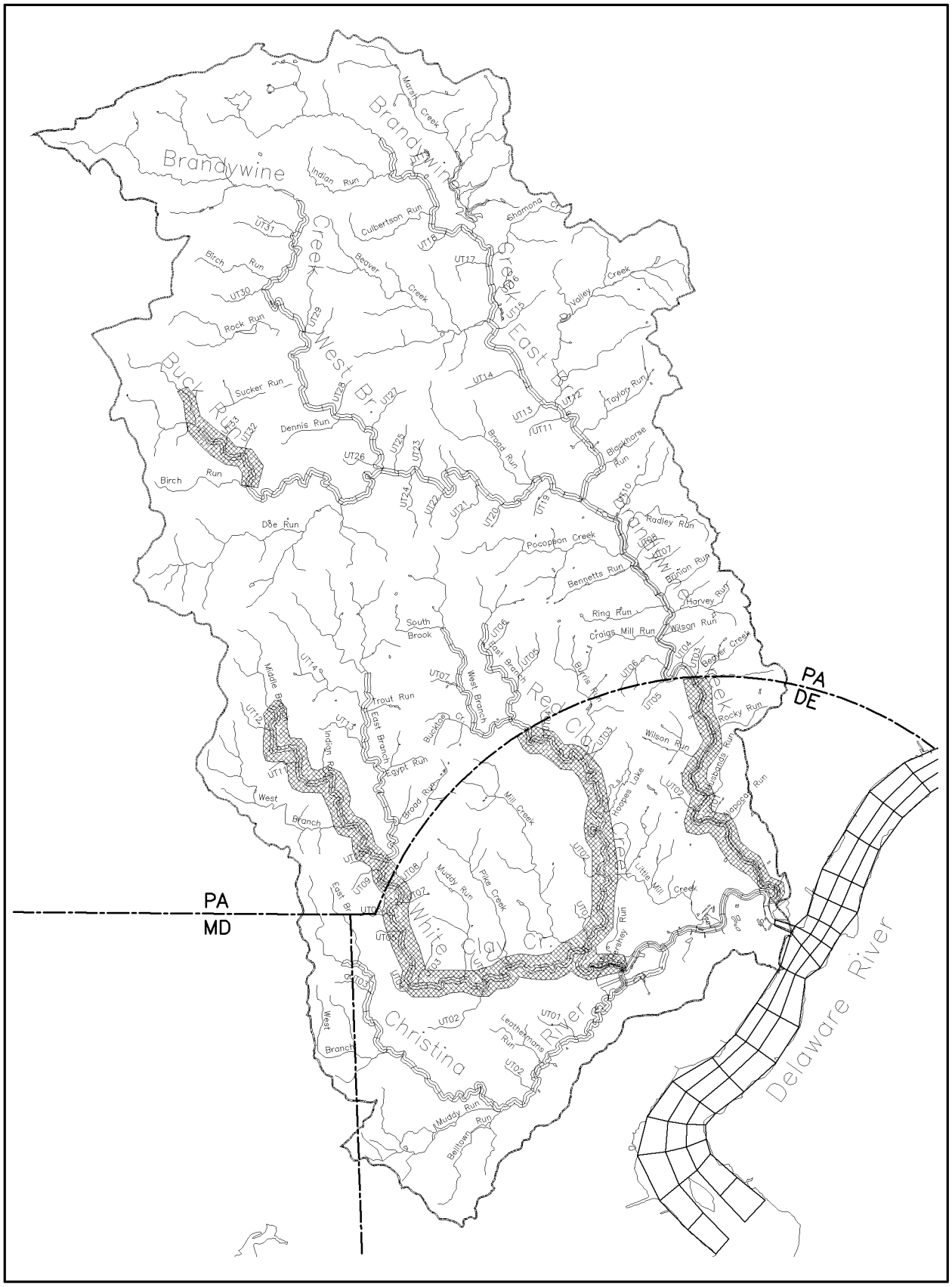

Figure 1-3. 303(d) waters listed for nutrients, low DO (PS as possible cause)

Table 1-1. Stream reaches on the Pennsylvania 303(d) list cited for nutrients and low DO.

Watershed	Stream ID	Segment ID	Miles	Source of Impairment	Cause of Impairment
Brandywine Creek	00004	27	1.28	other	nutrients
Buck Run	00131	50	1.77	municipal point source	nutrients, low DO
Sucker Run	00202	970930-1437-GLW	6.78	agriculture	nutrients
W.Br. Brandywine Cr.	00085	various	16.05	agriculture	nutrients
Broad Run	00434	971209-1445-ACW	4.10	hydromodification, agriculture	low DO, nutrients
E.Br. Red Clay Creek	00413	various	11.62	agriculture	low DO
E.Br. White Clay Creek	00432	various	29.55	agriculture	nutrients, low DO
Egypt Run	00440	970508-1245-ACE	3.66	agriculture	low DO
Indian Run	00475	115	1.09	agriculture, municipal point source	nutrients
Middle Br. White Clay	00462	115	17.33	agriculture, municipal point source	nutrients
Red Clay Creek	00374	971203-1400-ACW	0.76	agriculture	low DO
Trout Run	00402	970506-1425-MRB	2.74	agriculture	nutrients
Walnut Run	00435	971209-1445-ACW	1.39	agriculture, hydromodification	nutrients, low DO
W.Br. Red Clay Creek	00391	971023-1145-MRB	4.58	agriculture	low DO
White Clay Creek	00373	971216-1230-GLW	1.13	agriculture	nutrients

Table 1-2. Stream reaches on the Delaware 303(d) list cited for nutrients and low DO.

Waterbody ID	Watershed Name	Segment	Miles	Pollutants/Stressors	Probable Sources
DE040-001	Brandywine Creek	Lower Brandywine	3.8	nutrients	PS, NPS, SF
DE040-002	Brandywine Creek	Upper Brandywine	9.3	nutrients	PS, NPS, SF
DE260-001	Red Clay Creek	Main stem	12.8	nutrients	PS, NPS, SF
DE260-002	Red Clay Creek	Burroughs Run	4.5	nutrients	NPS
DE320-001	White Clay Creek	Main stem	18.2	nutrients	PS, NPS
DE320-002	White Clay Creek	Mill Creek	16.6	nutrients	NPS
DE320-003	White Clay Creek	Pike Creek	9.4	nutrients	NPS
DE320-004	White Clay Creek	Muddy Run	5.8	nutrients	NPS
DE120-001	Christina River	Lower Christina River	1.5	nutrients, DO	NPS, SF
DE120-002	Christina River	Middle Christina River	7.5	nutrients	NPS, SF
DE120-003	Christina River	Upper Christina River	6.3	nutrients	NPS, SF
DE120-003-02	Christina River	Lower Christina Creek	8.4	nutrients	NPS
DE120-005-01	Christina River	West Branch	5.3	nutrients	NPS
DE120-006	Christina River	Upper Christina Creek	8.3	nutrients	NPS
DE120-007-01	Christina River	Little Mill Creek	12.8	nutrients, DO	NPS, SF

PS = point source; NPS = nonpoint source; SF = Superfund site

This page intentionally left blank

2 - THE CHRISTINA RIVER BASIN SYSTEM

2.1 Physical Description

The Christina River Basin covers an area of about 565 square miles in Chester County, Pennsylvania; New Castle County, Delaware; and a small portion of Cecil County, Maryland (Figure 1-1). The basin drains to the tidal Delaware River at Wilmington, Delaware. The major streams in the watershed include the upper Christina River, Brandywine Creek, Red Clay Creek, and White Clay Creek. The watershed is composed of diverse land uses and includes urban, rural, and agricultural areas. The streams in the basin are used as municipal and industrial water supplies as well as for recreational purposes.

2.2 Hydrology

The Christina River basin was delineated into 39 subwatersheds for the HSPF model. There are a number of long-term stream gages in the basin maintained by the USGS. Data from these gaging stations were used to determine the 7-day, 10-year (7Q10) low-flow discharge rates (see Section 6.5). These same subwatersheds were used to determine daily nonpoint source inflows and loads to the EFDC model. For model calibration, a daily-average flow rate per unit area (cfs/mi^2) was estimated for each of the 39 basins and was then distributed to the appropriate EFDC model grid cell. The flow balance was checked by comparing model results to the daily flow rates at selected USGS stream gage stations for the period May 1 to September 21, 1997 (see Section 9.4 for details).

2.3 Eutrophication Processes

Algae in the water column eventually become deposited as organic matter and decay in the bottom sediments, which contributes to oxygen demand. Nutrients in the estuary are taken up by algae and predation as well as algal mortality which results in the transfer of nutrients to the benthic sediments. In the summer, with increased temperature, the nutrients are mineralized in the sediments and released back into the water column. Nutrients released from the sediments support the summer algal bloom. Carbon produced by algae settles to bottom waters, decays, and consumes oxygen. Diminished oxygen in bottom water enhances the release of sediment nutrients, especially ammonia. The nutrient release continues the cycle of benthic release, algal production, and oxygen consumption. It is this cycle that is simulated by the EFDC predictive sediment processes submodel.

The three major nutrients required by algae for growth are carbon, nitrogen, and phosphorus. Diatoms also require silica from which they synthesize their distinctive skeletons. Algal production is diminished or eliminated by the prolonged absence of one or more of the required nutrients. Nutrients are supplied in various ratios from natural and anthropogenic sources. The ratio of nutrient utilization by

algae is within a limited range, however, largely determined by algal composition. The classic Redfield ratios (Redfield et al. 1963) indicate that the ratio of carbon to nitrogen required by algae is 6 to 1 by mass. The required ratio of carbon to phosphorus is 42 to 1, and the carbon to silica requirement is about 1.25 to 1 (Strickland 1960). The disparity in the ratio of nutrients supplied and nutrients required often leads to depletion of one nutrient, due to algal uptake, while the others remain available. The depleted nutrient is referred to as "limiting", since algal production is limited by the supply of this nutrient.

Inorganic carbon is seldom in short supply and is usually not considered in analyses of nutrient limitations. Silica receives little emphasis in management studies since the supply from natural sources is beyond control and usually abundant. The primary emphasis is placed on limitations by nitrogen and phosphorus since the supply of these nutrients can be altered through the management of releases from municipalities, industry, agriculture, and other sources.

A "rule of thumb" is that phosphorus is the limiting nutrient in freshwater systems (Hecky and Kilham 1988) whereas nitrogen is limiting in estuarine and marine waters (Boynton et al. 1982). The phosphorus limit in freshwater is influenced by the relative natural abundance of the two nutrients.

In downstream portions of estuaries and in coastal waters, the ratio of nitrogen to phosphorus is altered from the ratio in runoff by internal recycling processes. Sediment-water interactions greatly diminish the availability of nitrogen relative to phosphorus (Nixon 1981). Particulate organic nitrogen and phosphorus enter the sediments roughly in Redfield proportions as organic matter. Within the sediments, total phosphorus is conservative. The only pathways for removal are recycling of inorganic phosphorus back to the water column or burial to deep, isolated sediments. On the other hand, total nitrogen is a nonconservative parameter. A significant fraction may be lost through denitrification to nitrogen gas. The nitrogen loss is such that the nitrogen returned to the water column is roughly half the amount expected based on the nitrogen to phosphorus ratio of the incoming material. The reduced nitrogen to phosphorus ratio of dissolved fluxes leaving the sediments, compared to particle fluxes entering the sediments, acting over lengthy time scales, pushes the water column toward nitrogen rather than phosphorus limitation.

2.4 Sediment-Water Interactions

Over time scales of years, benthic sediments act as sinks for oxygen, nitrogen, phosphorus, and silica removed from the water column. Oxygen is consumed by the oxygenation of organic carbon and by the nitrification of ammonia. Certain fractions of particulate nitrogen, phosphorus, and silica that settle into bottom sediments are buried to deeper sediment layers from which recycling to the water column is not possible.

Over seasonal time scales, sediments can be significant sources of dissolved nutrients to the overlying water. The role of sediments in the systemwide nutrient budget is especially important during the summer when seasonal low flows diminish tributary nutrient loads. During the summer, warm temperature enhances biological processes in the sediments. The decay (i.e., diagenesis) of organic matter produces phosphate, ammonia, and silica that are released into the overlying water.

A sediment process of potential importance to the management of eutrophication issues is the coupled nitrification/denitrification sequence that occurs in bottom sediments. The nitrification reaction, in which ammonia is oxidized to nitrate, requires oxygen. The denitrification reaction, in which nitrate is reduced to nitrogen gas, normally takes place under anoxic conditions. Denitrification is therefore a potential pathway for removal of nitrogen from the system. The primary source of nitrate for denitrification is previously nitrified ammonia. The maximum denitrification occurs when oxygen is available for nitrification. When oxygen is absent in the sediments, denitrification is diminished and limited to the rate at which nitrate is supplied by diffusion from the water column.

When oxygen is freely available, a large fraction of ammonia produced in the sediments is nitrified/denitrified to nitrogen gas, which is unavailable to algae. When oxygen is absent, virtually all the ammonia produced is released to the overlying water and is available for algal consumption. The coupling of nitrification and denitrification suggests the existence of an antagonistic cycle in the eutrophication process. Conditions that lead to hypoxia diminish denitrification leading to increased ammonia released to the water column that feeds algal production. Algal carbon settles to the bottom, consumes oxygen, and further diminishes denitrification. This same mechanism suggests that a slight improvement in bottom dissolved oxygen can start a positive feedback reaction which would promote denitrification at the expense of ammonia release. The diminished ammonia release would limit algal production and reduce the supply of carbon to the bottom sediments. The diminished carbonaceous oxygen demand leads to increased dissolved oxygen, which leads to still more denitrification.

This page intentionally left blank

3 - EFDC HYDRODYNAMIC MODEL

Modeling the physics, chemistry, and biology of the receiving waters of streams, lakes, estuaries, or coastal regions requires a model that incorporates all the major processes. Transport processes for this study were simulated using the three-dimensional EFDC hydrodynamic model that includes temperature transport. The EFDC hydrodynamic model was developed by Hamrick (1992a). The model formulation was based on the principles expressed by the equations of motion, conservation of volume, and conservation of mass. Quantities computed by the model included three-dimensional velocities, surface elevation, vertical viscosity and diffusivity, temperature, salinity, and density.

3.1 General

The Environmental Fluid Dynamics Code is a general purpose modeling package for simulating three-dimensional flow, transport, and biogeochemical processes in surface water systems including rivers, lakes, estuaries, reservoirs, wetlands, and coastal regions. The EFDC model was originally developed at the Virginia Institute of Marine Science for estuarine and coastal applications and is considered public domain software. In addition to hydrodynamic and salinity and temperature transport simulation capabilities, EFDC is capable of simulating cohesive and noncohesive sediment transport, near field and far field discharge dilution from multiple sources, eutrophication processes, the transport and fate of toxic contaminants in the water and sediment phases, and the transport and fate of various life stages of finfish and shellfish. Special enhancements to the hydrodynamic portion of the code, including vegetation resistance, drying and wetting, hydraulic structure representation, wave-current boundary layer interaction, and wave-induced currents, allow refined modeling of wetland marsh systems, controlled flow systems, and nearshore wave induced currents and sediment transport. The EFDC model has been extensively tested and documented for more than 20 modeling studies. The model is presently being used by a number of organizations including universities, governmental agencies, and environmental consulting firms.

The structure of the EFDC model includes four major modules: (1) a hydrodynamic model, (2) a water quality model, (3) a sediment transport model, and (4) a toxics model (see Figure 3-1). The EFDC hydrodynamic model itself, which was used for this study, is composed of six transport modules including dynamics, dye, temperature, salinity, near field plume, and drifter (see Figure 3-2). Various products of the dynamics module (i.e., water depth, velocity, and mixing) are directly coupled to the water quality, sediment transport, and toxics models as shown in the following figures. Schematic diagrams for the water quality model, the sediment transport model, and the toxics model are shown in Figures 3-3, 3-4, and 3-5, respectively.

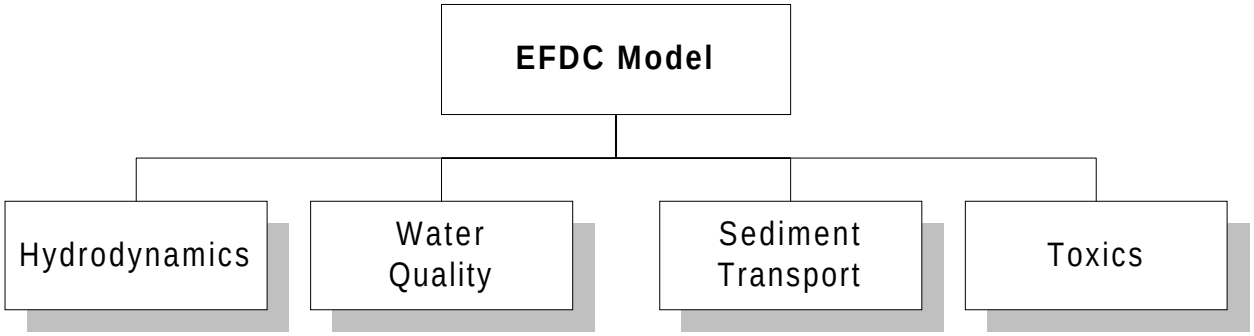

Figure 3-1. Primary modules of the EFDC model.

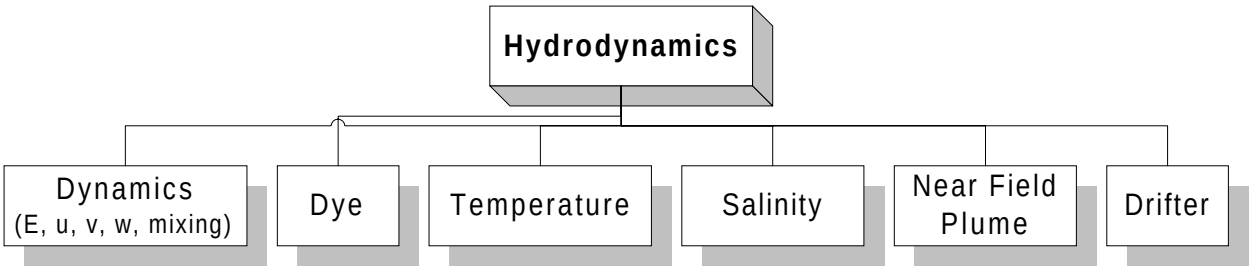

Figure 3-2. Structure of the EFDC hydrodynamic model.

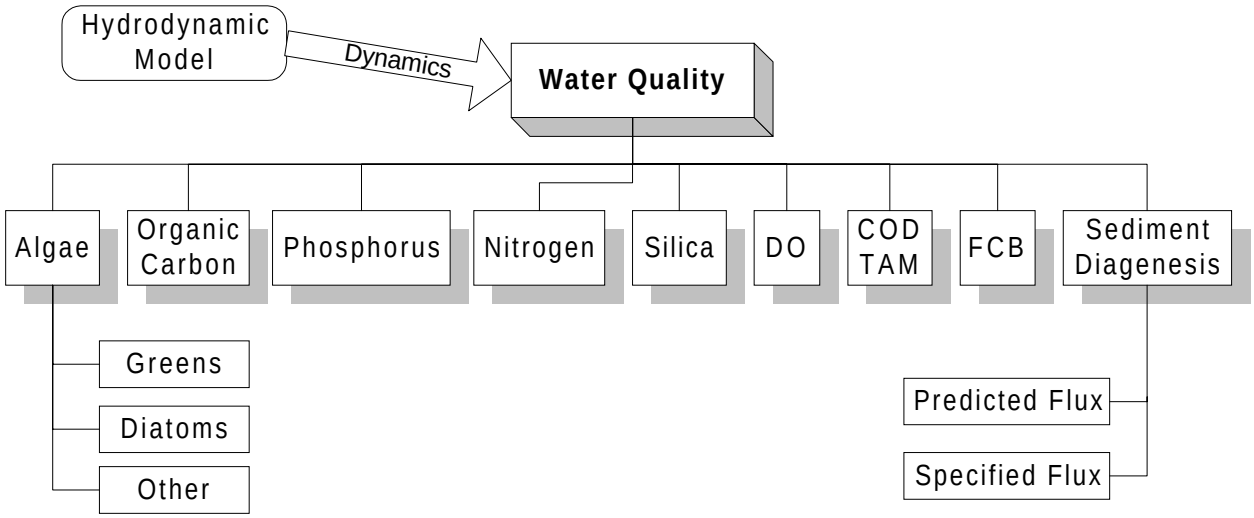

Figure 3-3. Structure of the EFDC water quality model.

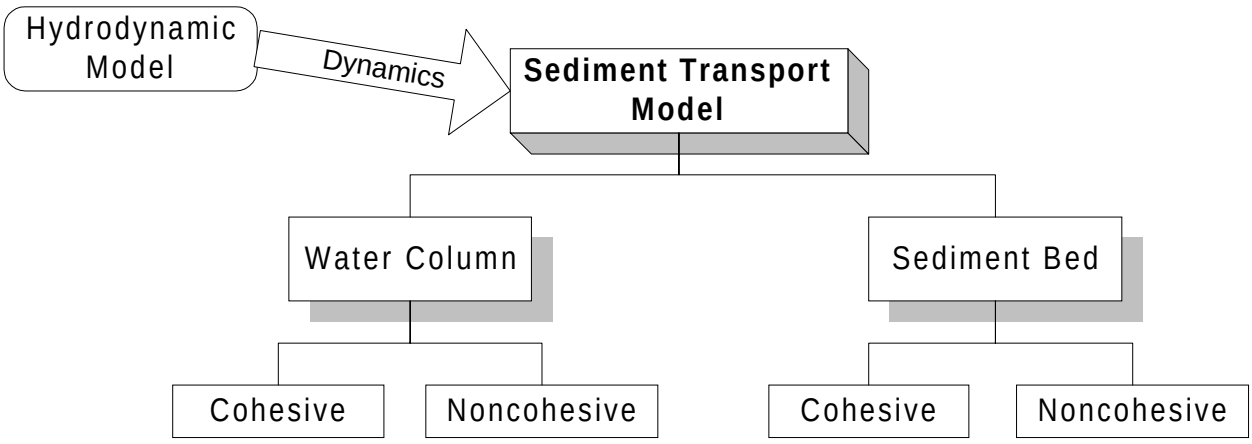

Figure 3-4. Structure of the EFDC sediment transport model.

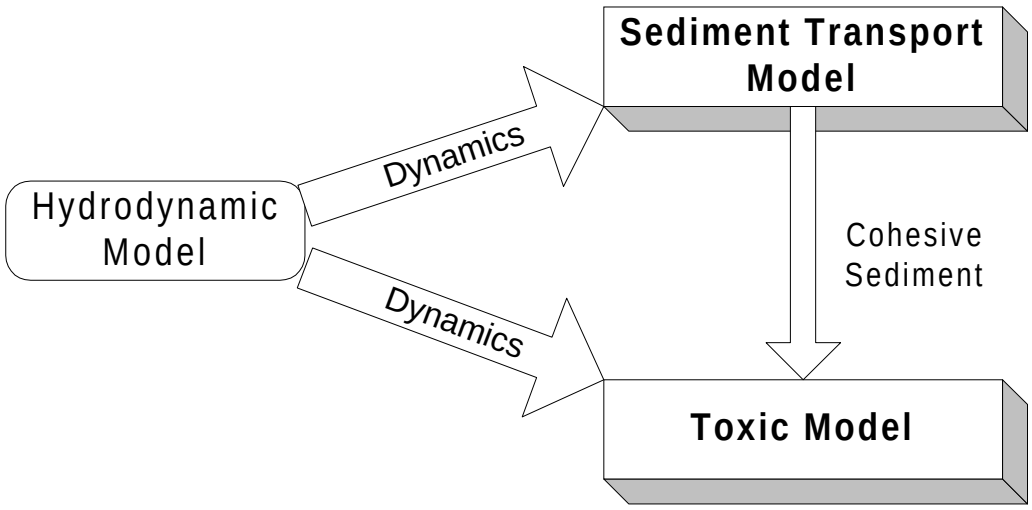

Figure 3-5. Structure of the EFDC toxics model.

3.2 Hydrodynamics and Salinity and Temperature Transport

The physics of the EFDC model and many aspects of the computational scheme are equivalent to the widely used Blumberg-Mellor model (Blumberg and Mellor 1987). The EFDC model solves the three-dimensional, vertically hydrostatic, free surface, turbulent averaged equations of motions for a variable density fluid. Dynamically coupled transport equations for turbulent kinetic energy, turbulent length scale, salinity, and temperature are also solved. The two turbulence parameter transport equations implement the Mellor-Yamada level 2.5 turbulence closure scheme (Mellor and Yamada 1982; Galperin et al. 1988). The EFDC model uses a stretched or sigma vertical coordinate and Cartesian, or curvilinear, orthogonal horizontal coordinates.

The numerical scheme employed in EFDC to solve the equations of motion uses second order accurate spatial finite differencing on a staggered or C grid. The model's time integration employs a second order accurate three-time level, finite difference scheme with an internal-external mode splitting procedure to separate the internal shear or baroclinic mode from the external free surface gravity wave or barotropic mode. The external mode solution is semi-implicit and simultaneously computes the two-dimensional (2-D) surface elevation field by a preconditioned conjugate gradient procedure. The external solution is completed by the calculation of the depth average barotropic velocities using the new surface elevation field. The model's semi-implicit external solution allows large time steps that are constrained only by the stability criteria of the explicit central difference or high order upwind advection scheme (Smolarkiewicz and Margolin 1993) used for the nonlinear accelerations. Horizontal boundary conditions for the external mode solution include options for simultaneously specifying the surface elevation only, the characteristic of an incoming wave (Bennett and McIntosh 1982), free radiation of an outgoing wave (Bennett 1976; Blumberg and Kantha 1985), or the normal volumetric flux on arbitrary portions of the boundary. The EFDC model's internal momentum equation solution, at the same time step as the external solution, is implicit with respect to vertical diffusion. The internal solution of the momentum equations is in terms of the vertical profile of shear stress and velocity shear, which results in the simplest and most accurate form of the baroclinic pressure gradients and eliminates the over determined character of alternate internal mode formulations. Time splitting inherent in the three-time-level scheme is controlled by periodic insertion of a second order accurate two-time-level trapezoidal step. EFDC is also readily configured as a 2-D model in either the horizontal or vertical planes.

The EFDC model implements a second order accurate in space and time, mass conservation fractional step solution scheme for the Eulerian transport equations for salinity, temperature, suspended sediment, water quality constituents, and toxic contaminants. The transport equations are temporally integrated at the same time step or twice the time step of the momentum equation solution (Smolarkiewicz and Margolin 1993). The advective step of the transport solution uses either the central

difference scheme used in the Blumberg-Mellor model or a hierarchy of positive definite upwind difference schemes. The highest accuracy upwind scheme, second order accurate in space and time, is based on a flux-corrected transport version Smolarkiewicz's multidimensional positive-definite advection transport algorithm (Smolarkiewicz and Clark, 1986; Smolarkiewicz and Grabowski 1990), which is monotonic and minimizes numerical diffusion. The horizontal diffusion step, if required, is explicit in time, whereas the vertical diffusion step is implicit. Horizontal boundary conditions include time variable material inflow concentrations, upwind outflow, and a damping relaxation specification of climatological boundary concentration. The NOAA Geophysical Fluid Dynamics Laboratory's atmospheric heat exchange model (Rosati and Miyakoda 1988) is implemented for the temperature transport equation.

3.3 Sediment Transport

The EFDC code is capable of simulating the transport and fate of multiple size classes of cohesive and noncohesive suspended sediment including bed deposition and resuspension. Water column transport is based on the same high order advection-diffusion scheme used for salinity and temperature. A number of options are included for the specification of settling velocities. For the transport of multiple size classes of cohesive sediment, an optional flocculation model (Burban et al. 1989, 1990) can be activated. Sediment mass conservative deposited bed formulations are included for both cohesive and noncohesive sediment. The deposited bed may be represented by a single layer or multiple layers. The multiple bed layer option provides a time since deposition versus vertical position in the bed relationship to be established. Water column/sediment bed interface elevation changes can be optionally incorporated into the hydrodynamic continuity equation. An optional one-dimensional (1-D) in the vertical, bed consolidation calculation can be performed for cohesive beds.

3.4 Water Quality and Eutrophication Simulation

The EFDC code includes two internal eutrophication submodels for water quality simulation (Park et al. 1995). The simple or reduced eutrophication model is functionally equivalent to the WASP5 EUTRO model (Ambrose et al. 1993). The complex or full eutrophication model is functionally equivalent to the CE-QUAL-ICM or Chesapeake Bay Water Quality model (Cerco and Cole 1993). Both water column eutrophication models are coupled to a functionally equivalent implementation of the CE-QUAL-ICM sediment diagenesis or biogeochemical processes model (DiToro and Fitzpatrick 1993). The eutrophication models can be executed simultaneously with the hydrodynamic component of EFDC, or EFDC simulated hydrodynamic transport fields can be saved, allowing the EFDC code to be executed in a water quality only simulation mode.

The computational scheme used in the internal eutrophication models employs a fractional step extension of the same advective and diffusive algorithms used for salinity and temperature, which

guarantee positive constituent concentrations. A novel ordering of the reaction sequence in the reactive source and sink fractional step allows the linearized reactions to be solved implicitly, further guaranteeing positive concentrations. The eutrophication models accept an arbitrary number of point and nonpoint source loadings as well as atmospheric and ground water loadings.

In addition to the internal eutrophication models, the EFDC model can be externally linked to the WASP5 model. In the external linking mode, the EFDC model generates WASP5 input files describing cell geometry and connectivity as well as advective and diffusive transport fields. For estuary simulation, the transport fields may be intratidally time averaged or intertidally time averaged using the averaging procedure described by Hamrick (1994).

3.5 Toxic Contaminant Transport and Fate

The EFDC code includes two internal submodels for simulating the transport and fate of toxic contaminants. A simple, single contaminant submodel can be activated from the master input file. The simple model accounts for water and suspended sediment phase transport with equilibrium partitioning and a lumped first order reaction. Contaminant mass per unit area in the sediment bed is also simulated. The second, more complex, submodel simulates the transport and fate of an arbitrary number of reacting contaminants in the water and sediment phases of both the water column and sediment bed. In this mode, the contaminant transport and fate simulation is functionally similar to the WASP5 TOXIC model (Ambrose et al. 1993), with the added flexibility of simulating an arbitrary number of contaminants, and the improved accuracy of utilizing more complex three-dimensional physical transport fields in a highly accurate numerical transport scheme. Water-sediment phases interaction may be represented by equilibrium or nonlinear sorption processes. In this mode, the multilayer sediment bed formulation is active, with sediment bed water volume and dissolved contaminant mass balances activated to allow contaminants to reenter the water column by sediment resuspension, pore water expulsion due to consolidation, and diffusion from the pore water into the water column. The complex contaminant model activates a subroutine describing reaction processes with appropriate reaction parameters provided by the toxic reaction processes input file.

3.6 Finfish and Shellfish Transport

The EFDC code includes the capability of simulating the transport and fate of various life stages of finfish and shellfish. In addition to advection and diffusion by the ambient flow, mortality, predation, toxicity, and swimming behavior are simulated. Organism age and ambient environment queued vertical and horizontal swimming and settling is simulated. Environmental queues include light intensity, temperature, salinity, and tidal phases.

3.7 Near-Field Discharge Dilution and Mixing Zone Analysis

In addition to the far-field transport and fate simulation capability incorporated into the EFDC code's water quality and toxic contaminant modules, the code includes a near-field discharge dilution and mixing zone module. The near field model is based on a Lagrangian buoyant jet and plume model (Frick 1984; Lee and Cheung 1990) and allows representation of submerged single and multiple port diffusers and buoyant surface jets. The near field model provides analysis capabilities similar to CORMIX (Jirka and Doneker 1991; Jirka and Akar 1991) while offering two distinct advantages. The first advantage is that a more realistic representation of ambient current and stratification conditions, provided directly by the EFDC hydrodynamic module, is incorporated into the analysis. The second advantage is that multiple discharges and multiple near field analysis times may be specified to account for varying ambient current and stratification conditions. For example, the analysis of 10 discharges under six ambient conditions each would require 60 executions of CORMIX, while the entire analysis of the 60 situations would be produced in a single EFDC simulation. The near-field simulation may be executed in two modes. The first provides virtual source information for representing the discharges in a standard EFDC far field transport and fate simulation. In the second mode the near-field and far-field transport are directly coupled, using a virtual source formulation, to provide simultaneous near and far field transport and fate simulation.

3.8 Spill Trajectory and Search and Rescue Simulation

In addition to the Eulerian transport equation formulation used for far field analysis and the Lagrangian jet and plume module used for near field analysis, the EFDC code incorporates a number of Lagrangian particle transport formulations based on an implicit trilinear interpolation scheme (Bennett and Clites 1987). The first formulation allows release of neutrally buoyant or buoyant drifters at user specified locations and times. This formulation is useful in simulating spill trajectories, search and rescue operations, and oceanographic instrument drifters. The second formulation releases drifters in each three-dimensional model cell at a specified sequence of times and calculates the generalized Lagrangian mean velocity field (Andrews and McIntyre 1978) relative to a user-specified averaging interval.

3.9 Wetland, Marsh, and Tidal Flat Simulation Extension

The EFDC model provides a number of enhancements for the simulation of flow and transport in wetlands, marshes, and tidal flats. The code allows for drying and wetting in shallow areas by a mass conservative scheme. The drying and wetting formulation is coupled to the mass transport equations in a manner that prevents negative concentrations of dissolved and suspended materials. A number of alternatives are in place in the model to simulate general discharge control structures such as weirs, spillways, culverts, and water surface elevation activated pumps. The effect of submerged and emergent plants is incorporated into the turbulence closure model and flow resistance formulation. Plant density

and geometric characteristics of individual and composite plants are required as input for the vegetation resistance formulation. A simple soil moisture model, allowing rainfall infiltration and soil water loss due to evapotranspiration under dry conditions, is implemented. To represent narrow channels and canals in wetland, marsh and tidal flat systems, a subgrid scale channel model is implemented. The subgrid channel model allows a 1-D network in the horizontal channels to be dynamically coupled to the two-dimensional horizontal grid representing the wetland, marsh, or tidal flat system. Volume and mass exchanges between 2-D wetland cells and the 1-D channels are accounted for. The channels may continue to flow when the 2-D wetland cells become dry.

3.10 Nearshore Wave-Induced Currents and Sediment Transport Extensions

The EFDC code includes a number of extensions for simulation of nearshore wave-induced currents and noncohesive sediment transport. The extensions include a wave-current boundary layer formulation similar to that of Grant and Madsen (1986); modifications of the hydrodynamic model's momentum equations to represent wave period averaged Eulerian mean quantities; the inclusion of the three-dimensional wave-induced radiation or Reynold's stresses in the momentum equations; and modifications of the velocity fields in the transport equations to include advective transport by the wave-induced Stoke's drift. High frequency surface wave fields are provide by an external wave refraction-diffraction model or by an internal mild slope equation submodel similar to that of Madsen and Larsen (1987). The internal refraction-diffraction computation is executed on a refined horizontal grid coincident with the main model's horizontal grid.

3.11 User Interface

The EFDC modeling package's user interface is based on text input file templates. This choice was selected in the interest of maintaining model portability across a range of computing platforms and readily allows the model user to modify input files using most text editing software. The text interface also allows modification of model files on remote computing systems and in hetrogeneous network environments. All input files have standard templates available with the EFDC code and in the digital version of the user's manual. The file templates include extensive built-in documentation and an explanation of numerical input data quantities. Actual numerical input data are inserted into the text template in a flexible free format as internally specified in the file templates. Extensive checking of input files is implemented in the code and diagnostic on screen messages indicate the location and nature of input file errors. All input files involving dimensional data have unit conversion specifications for the Meters-Kilograms-Seconds (MKS) international system of units used internally in the model.

3.12 Preprocessing Software

The EFDC modeling package includes a grid generating preprocessor code, GEFDC, which is used to construct the horizontal model grid, and interpolate bathymetry and initial fields such as water surface elevation, salinity, to the grid cells. EFDC inputs files specifying the grid geometry and initial fields are generated by the preprocessor. The preprocessor is capable of generating Cartesian and curvilinear-orthogonal grids using a number of grid generation schemes (Mobley and Stewart 1980; Ryskin and Leal 1983; Kang and Leal 1992).

3.13 Program Configuration

The EFDC code exists in only one generic version. A model application is specified entirely by information in the input files. To minimize memory requirements for specific applications, an executable file is created by adjusting the appropriate variable array size in the model's parameter file and compiling the source code. The EFDC model can be configured to execute all or a portion of a model application in reduced spatial dimension mode including 2-D depth or width averaged and 1-D cross section averaged. The number of layers used in the 3-D mode or 2-D width averaged mode is readily changed by one line of model input. Model grid sections specified as 2-D width averaged are allowed to have depth varying widths to provide representations equivalent to those of 2-D width averaged estuarine and reservoir models such as CE-QUAL-W2 (Cole and Buchak 1994).

3.14 Run-Time Diagnostics

The EFDC modeling package includes extensive built-in run-time diagnostics that may be activated in the master input file by the model user. Representative diagnostics include records of maximum CFL numbers, times and locations of negative depths, a variety of volume and mass balance checks, and global mass and energy balances. An on screen print of model variables in a specified cell can be activated during modeling execution. The model generates a number of log files that allow additional diagnostics of any run-time problems encountered during the set-up of a new application.

3.15 Model Output Options

A wide variety of output options are available for the EFDC model, including (1) specification of output files for horizontal plane and vertical plane transect plotting of vector and scalar field at a specified time; (2) the generation of time series of model variables at selected locations and time intervals; (3) grab sample simulation at specified times and locations; and (4) the specification of least squares analysis of selected model variables at a defined location over a specified interval. A general three-dimensional output option allows saving of all major model variables in a compressed-file format at specified times. A restart file is generated at user-specified intervals during model execution.

3.16 Postprocessing, Graphics, and Visualization

The generic model output files can be readily processed by a number of third party graphics and visualization software packages, often without the need for intermediate processing (Rennie and Hamrick 1992). The availability of the source code to the user allows the code to be modified for specific output options. Graphics and visualization software successfully used with EFDC output include: APE, AVS, IDL, Mathematica, MatLab, NCAR Graphics, PV-Wave, Techplot, SiteView, Spyglass Transform and Slicer, Voxelview, and GrADS. The model developer currently uses Spyglass and Voxelview and a number of postprocessor applications are available for special image enhancement for these products.

3.17 Documentation

Extensive documentation of the EFDC model is available. Theoretical and computational aspects of the model are described by Hamrick (1992a). The model user's manual (Hamrick 1996) provides details on use of the GEFDC preprocessor and set-up of the EFDC input files. Input file templates are also included. A number of papers describe model applications and capabilities (Hamrick 1992b; Hamrick 1994; Moustafa and Hamrick 1994; Hamrick and Wu 1996; and Wu et al. 1996).

3.18 Computer Requirements

The EFDC modeling system is written in FORTRAN 77. The few nonstandard VAX FORTRAN language extensions in the code are supported by a wide variety of ANSI standard FORTRAN 77 compilers. The generic or universal source code has been compiled and executed on most UNIX workstations (DEC Alpha, Hewlett-Packard, IBM RISC6000, Silicon Graphics, Sun and Sparc compatibles) Cray and Convex supercomputers, and PC compatible and Macintosh personal computers. Absoft, Lahey, and Microsoft compilers are supported on PC compatibles, while Absoft, Language Systems, and Motorola compilers are supported on Macintosh and compatible systems.

4 - EFDC WATER QUALITY MODEL

4.1 Introduction

The central issues in the water quality model are primary production of carbon by algae and concentration of dissolved oxygen. Primary production provides the energy required by the ecosystem to function. However, excessive primary production is detrimental since its decomposition in the water and sediments consumes oxygen. Dissolved oxygen is necessary to support the life functions of higher organisms and is considered an indicator of the health of estuarine systems. To predict primary production and dissolved oxygen, a large suite of model state variables is necessary (Table 4-1). The nitrate state variable in the model represents the sum of nitrate and nitrite nitrogen. The three variables (salinity, water temperature, and total suspended solids) needed for computation of the above 21 state variables are provided by the EFDC hydrodynamic model. The interactions among the state variables is illustrated in Figure 4-1. The kinetic processes included in the EFDC water quality model are mostly from the Chesapeake Bay three-dimensional water quality model, CE-QUAL-ICM (Cerco and Cole 1994). The kinetic sources and sinks, as well as the external loads for each state variable, are described in Sections 4.3 to 4.11. The kinetic processes include the exchange of fluxes at the sediment-water interface, including sediment oxygen demand, which are explained in Section 5 (EFDC Sediment Process Model) of this report. The description of the EFDC water column water quality model in this section is from Park et al. (1995).

Table 4-1. EFDC model water quality state variables.

(1) cyanobacteria	(12) labile particulate organic nitrogen
(2) diatom algae	(13) dissolved organic nitrogen
(3) green algae	(14) ammonia nitrogen
(4) refractory particulate organic carbon	(15) nitrate nitrogen
(5) labile particulate organic carbon	(16) particulate biogenic silica
(6) dissolved organic carbon	(17) dissolved available silica
(7) refractory particulate organic phosphorus	(18) chemical oxygen demand
(8) labile particulate organic phosphorus	(19) dissolved oxygen
(9) dissolved organic phosphorus	(20) total active metal
(10) total phosphate	(21) fecal coliform bacteria
(11) refractory particulate organic nitrogen	(22) macroalgae

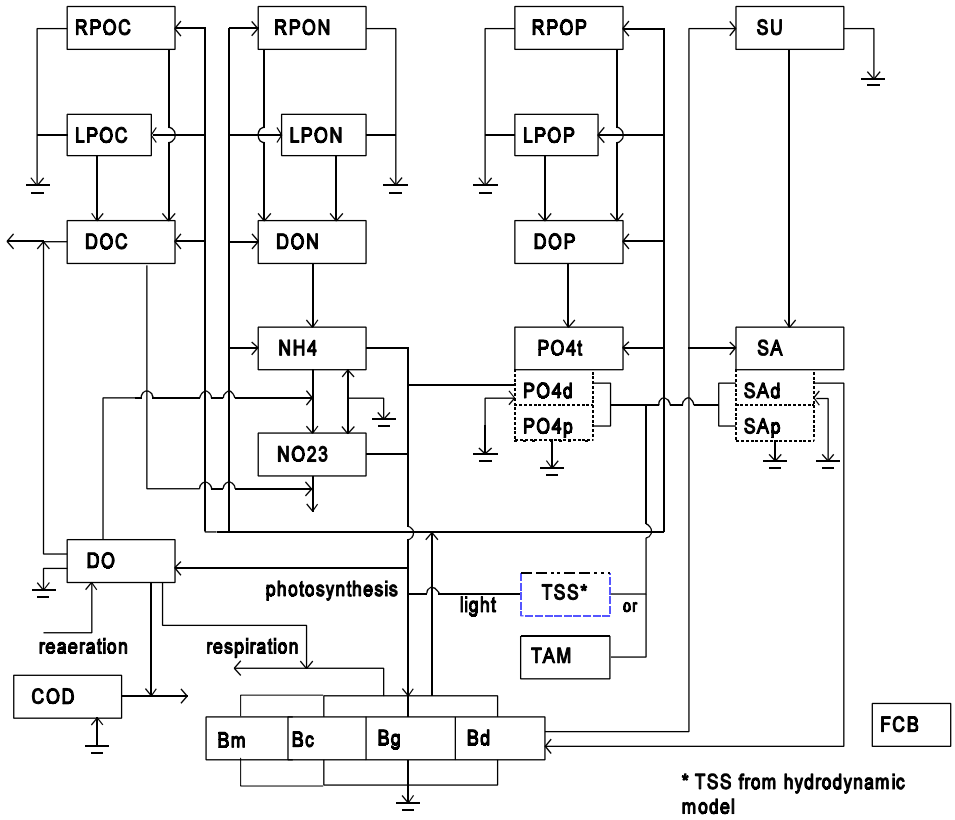

Figure 4-1. Schematic diagram for the EFDC water column water quality model.

4.1.1 Algae

Algae are grouped into four model classes: cyanobacteria, diatoms, greens, and macroalgae. The grouping is based upon the distinctive characteristics of each class and upon the significant role the characteristics play in the ecosystem. Cyanobacteria, commonly called blue-green algae, are characterized by their abundance (as picoplankton) in saline water and by their bloom-forming characteristics in fresh water. Cyanobacteria are unique in that some species fix atmospheric nitrogen, although nitrogen fixers are not believed to be predominant in many river systems. Diatoms are distinguished by their requirement of silica as a nutrient to form cell walls. Diatoms are large algae characterized by high settling velocities. Settling of spring diatom blooms to the sediments may be a significant source of carbon for sediment oxygen demand. Algae that do not fall into the preceding two groups are lumped into the heading of green algae. Green algae settle at a rate intermediate between

cyanobacteria and diatoms and are subject to greater grazing pressure than cyanobacteria. Macroalgae are almost always attached to a stable substrate and are therefore most abundant in the areas of harbors and near shore. The waters in many stream systems are characterized by various rooted macrophytes and periphyton. All species of macroalgae in this study have been lumped into a single class of macroalgae. Because of their attachment to the substrate, they are limited to growing in the bottom water-column layer and are not subject to physical transport.

4.1.2 Organic Carbon

Three organic carbon state variables are considered: dissolved, labile particulate, and refractory particulate. Labile and refractory distinctions are based upon the time scale of decomposition. Labile organic carbon decomposes on a time scale of days to weeks whereas refractory organic carbon requires more time. Labile organic carbon decomposes rapidly in the water column or the sediments. Refractory organic carbon decomposes slowly, primarily in the sediments, and may contribute to sediment oxygen demand years after deposition.

4.1.3 Nitrogen

Nitrogen is first divided into organic and mineral fractions. Organic nitrogen state variables are dissolved organic nitrogen, labile particulate organic nitrogen, and refractory particulate organic nitrogen. Two mineral nitrogen forms are considered: ammonium and nitrate. Both are utilized to satisfy algal nutrient requirements, although ammonium is preferred from thermodynamic considerations. The primary reason for distinguishing the two is that ammonium is oxidized by nitrifying bacteria into nitrate. This oxidation can be a significant sink of oxygen in the water column and sediments. An intermediate in the complete oxidation of ammonium, nitrite, also exists. Nitrite concentrations are usually much less than nitrate, and for modeling purposes, nitrite is combined with nitrate. Hence the nitrate state variable actually represents the sum of nitrate plus nitrite.

4.1.4 Phosphorus

As with carbon and nitrogen, organic phosphorus is considered in three states: dissolved, labile particulate, and refractory particulate. Only a single mineral form, total phosphate, is considered. Total phosphate exists as several states within the model ecosystem: dissolved phosphate, phosphate sorbed to inorganic solids, and phosphate incorporated in algal cells. Equilibrium partition coefficients are used to distribute the total among the three states.

4.1.5 Silica

Silica is divided into two state variables: available silica and particulate biogenic silica. Available silica is primarily dissolved and can be utilized by diatoms. Particulate biogenic silica cannot

be utilized. In the model, particulate biogenic silica is produced through diatom mortality. Particulate biogenic silica undergoes dissolution to available silica or else settles to the bottom sediments.

4.1.6 Chemical Oxygen Demand

In the context of this study, chemical oxygen demand is the concentration of reduced substances that are oxidizable by inorganic means. The primary component of chemical oxygen demand is sulfide released from sediments. Oxidation of sulfide to sulfate may remove substantial quantities of dissolved oxygen from the water column.

4.1.7 Dissolved Oxygen

Dissolved oxygen is required for the existence of higher life forms. Oxygen availability determines the distribution of organisms and the flows of energy and nutrients in an ecosystem. Dissolved oxygen is a central component of the water quality model.

4.1.8 Total Active Metal

Both phosphate and dissolved silica sorb to inorganic solids, primarily iron and manganese. Sorption and subsequent settling is one pathway for removal of phosphate and silica from the water column. Consequently, the concentration and transport of iron and manganese are represented in the model. Limited data do not allow a complete treatment of iron and manganese chemistry, however. Rather, a single-state variable, total active metal, is defined as the total concentration of metals that are active in phosphate and silica transport. Total active metal is partitioned between particulate and dissolved phases by an oxygen-dependent partition coefficient.

4.1.9 Salinity

Salinity is a conservative tracer that provides verification of the transport component of the model and facilitates examination of conservation of mass. Salinity also influences the dissolved oxygen saturation concentration and is used in the determination of kinetics constants that differ in saline and fresh water.

4.1.10 Temperature

Temperature is a primary determinant of the rate of biochemical reactions. Reaction rates increase as a function of temperature, although extreme temperatures result in the mortality of organisms.

4.2 Conservation of Mass Equation

The governing mass-balance equation for each of the water quality state variables may be expressed as:

$$\frac{\partial C}{\partial t} + \frac{\partial (uC)}{\partial x} + \frac{\partial (vC)}{\partial y} + \frac{\partial (wC)}{\partial z} =$$

$$\frac{\partial}{\partial x}\left(K_x \frac{\partial C}{\partial x} \right) + \frac{\partial}{\partial y}\left(K_y \frac{\partial C}{\partial y} \right) + \frac{\partial}{\partial z}\left(K_z \frac{\partial C}{\partial z} \right) + S_C \qquad (4\text{-}1)$$

C = concentration of a water quality state variable

u, v, w = velocity components in the x-, y-, and z-directions, respectively

K_x, K_y, K_z = turbulent diffusivities in the x-, y-, and z-directions, respectively

S_C = internal and external sources and sinks per unit volume.

The last three terms on the left-hand side (LHS) of Eq. 4-1 account for the advective transport, and the first three terms on the right-hand side (RHS) of Eq. 4-1 account for the diffusive transport. These six terms for physical transport are analogous to, and thus the numerical method of solution is the same as, those in the mass-balance equation for salinity in the hydrodynamic model (Hamrick 1992a). The last term in Eq. 4-1 represents the kinetic processes and external loads for each of the state variables. The present model solves Eq. 4-1 after decoupling the kinetic terms from the physical transport terms. The solution scheme for both the physical transport (Hamrick 1992a) and the kinetic equations is second-order accurate.

The governing mass-balance equation for water quality state variables (Eq. 4-1) consists of physical transport, advective and diffusive, and kinetic processes. When solving Eq. 4-1, the kinetic terms are decoupled from the physical transport terms. The mass-balance equation for physical transport only, which takes the same form as the salt-balance equation, is:

$$\frac{\partial C}{\partial t} + \frac{\partial (uC)}{\partial x} + \frac{\partial (vC)}{\partial y} + \frac{\partial (wC)}{\partial z} = \frac{\partial}{\partial x}\left(K_x \frac{\partial C}{\partial x} \right) + \frac{\partial}{\partial y}\left(K_y \frac{\partial C}{\partial y} \right) + \frac{\partial}{\partial z}\left(K_z \frac{\partial C}{\partial z} \right) \qquad (4\text{-}2)$$

The equation for kinetic processes only, which will be referred to as the kinetic equation, is:

$$\frac{\partial C}{\partial t} = S_C \qquad (4\text{-}3)$$

which may be expressed as:

$$\frac{\partial C}{\partial t} = K \cdot C + R \qquad (4\text{-}4)$$

where K is kinetic rate (time^{-1}) and R is source/sink term (mass volume^{-1} time^{-1}). Equation 4-4 is obtained by linearizing some terms in the kinetic equations, mostly Monod type expressions. Hence, K

and R are known values in Eq. 4-4. Equation 4-2 is identical to, and thus its numerical method of solution is the same as, the mass-balance equation for salinity (Hamrick 1992a).

The remainder of this chapter details the kinetics portion of the mass-conservation equation for each state variable. Parameters are defined where they first appear. All parameters are listed, in alphabetical order, in an appendix. For consistency with reported rate coefficients, kinetics are detailed using a temporal dimension of days. Within the CE-QUAL-ICM computer code, kinetics sources and sinks are converted to a dimension of seconds before employment in the mass-conservation equation.

4.3 Algae

Algae, which occupies a central role in the model (Figure 4-1), are grouped into three model state variables: cyanobacteria (blue-green algae), diatoms, and green algae. The subscript, **x**, is used to denote four algal groups: **c** for cyanobacteria, **d** for diatoms, **g** for green algae, and **m** for macroalgae. Sources and sinks included in the model are

- growth (production)
- basal metabolism
- predation
- settling
- external loads

Equations describing these processes are largely the same for the four algal groups with differences in the values of parameters in the equations. The kinetic equation describing these processes is:

$$\frac{\partial B_x}{\partial t} = (P_x - BM_x - PR_x)B_x + \frac{\partial}{\partial z}(WS_x \cdot B_x) + \frac{WB_x}{V} \quad (4\text{-}5)$$

B_x = algal biomass of algal group x (g C m^{-3})
t = time (day)
P_x = production rate of algal group x (day^{-1})
BM_x = basal metabolism rate of algal group x (day^{-1})
PR_x = predation rate of algal group x (day^{-1})
WS_x = settling velocity of algal group x (m day^{-1})
WB_x = external loads of algal group x (g C day^{-1})
V = cell volume (m^3).

The model simulates the total biomass of the macroalgae rather than the size of the macroalgae; therefore, they can be treated as other groups of algae. Since macroalgae attach to the bottom, they are limited to growing in the bottom layer only and are not be transported through water movement.

4.3.1 Production (Algal Growth)

Algal growth depends on nutrient availability, ambient light, and temperature. The effects of these processes are considered to be multiplicative:

$$P_x = PM_x \cdot f_1(N) \cdot f_2(I) \cdot f_3(T) \quad (4\text{-}6)$$

PM_x = maximum growth rate under optimal conditions for algal group x (day^{-1})
$f_1(N)$ = effect of suboptimal nutrient concentration ($0 \le f_1 \le 1$)
$f_2(I)$ = effect of suboptimal light intensity ($0 \le f_2 \le 1$)
$f_3(T)$ = effect of suboptimal temperature ($0 \le f_3 \le 1$).

The freshwater cyanobacteria may undergo rapid mortality in salt water, e.g., freshwater organisms in the Potomac River (Thomann et al. 1985). For the freshwater organisms, the increased mortality may be included in the model by retaining the salinity toxicity term in the growth equation for cyanobacteria:

$$P_c = PM_c \cdot f_1(N) \cdot f_2(I) \cdot f_3(T) \cdot f_4(S) \quad (4\text{-}7)$$

$f_4(S)$ = effect of salinity on cyanobacteria growth ($0 \le f_4 \le 1$).

Activation of the salinity toxicity term, $f_4(S)$, is an option in the source code.

4.3.2 Effect of Nutrients on Algal Growth

Using Liebig's "law of the minimum" (Odum 1971) that growth is determined by the nutrient in least supply, the nutrient limitation for growth of cyanobacteria and green algae is expressed as:

$$f_1(N) = minimum\left(\frac{NH4 + NO3}{KHN_x + NH4 + NO3}, \frac{PO4d}{KHP_x + PO4d}\right) \quad (4\text{-}8)$$

NH4 = ammonium nitrogen concentration (g N m^{-3})
NO3 = nitrate nitrogen concentration (g N m^{-3})
KHN_x = half-saturation constant for nitrogen uptake for algal group x (g N m^{-3})
PO4d = dissolved phosphate phosphorus concentration (g P m^{-3})
KHP_x = half-saturation constant for phosphorus uptake for algal group x (g P m^{-3}).

Some cyanobacteria, e.g., *Anabaena*, can fix nitrogen from atmosphere and thus are not limited by nitrogen. Hence, Eq. 4-8 is not applicable to the growth of nitrogen fixers.

Since diatoms require silica as well as nitrogen and phosphorus for growth, the nutrient limitation for diatoms is expressed as:

$$f_1(N) = minimum\left(\frac{NH4 + NO3}{KHN_d + NH4 + NO3}, \frac{PO4d}{KHP_d + PO4d}, \frac{SAd}{KHS + SAd}\right) \quad (4\text{-}9)$$

SAd = concentration of dissolved available silica (g Si m^{-3})

KHS = half-saturation constant for silica uptake for diatoms (g Si m^{-3}).

4.3.3 Effect of Light on Algal Growth

The daily and vertically integrated form of Steele's equation is:

$$f_2(I) = \frac{2.718 \cdot FD}{Kess \cdot \Delta z}\left(e^{-\alpha_B} - e^{-\alpha_T}\right) \quad (4\text{-}10)$$

$$\alpha_B = \frac{I_o}{FD \cdot (I_s)_x} \cdot \exp\left(-Kess[H_T + \Delta z]\right) \quad (4\text{-}11)$$

$$\alpha_T = \frac{I_o}{FD \cdot (I_s)_x} \cdot \exp\left(-Kess \cdot H_T\right) \quad (4\text{-}12)$$

FD = fractional daylength ($0 \le FD \le 1$)

Kess = total light extinction coefficient (m^{-1})

Δz = layer thickness (m)

I_o = daily total light intensity at water surface (langleys day^{-1})

$(I_s)_x$ = optimal light intensity for algal group x (langleys day^{-1})

H_T = depth from the free surface to the top of the layer (m).

Light extinction in the water column consists of three fractions in the model: a background value dependent on water color, extinction due to suspended particles, and extinction due to light absorption by ambient chlorophyll:

$$Kess = Ke_b + Ke_{TSS} \cdot TSS + Ke_{Chl} \cdot \sum_{x=c,d,g} \left(\frac{B_x}{CChl_x}\right) \quad (4\text{-}13)$$

Ke_b = background light extinction (m^{-1})

Ke_{TSS} = light extinction coefficient for total suspended solid (m^{-1} per g m^{-3})

TSS = total suspended solid concentration (g m^{-3}) provided from the hydrodynamic model

Ke_{Chl} = light extinction coefficient for chlorophyll 'a' (m^{-1} per mg Chl m^{-3})

$CChl_x$ = carbon-to-chlorophyll ratio in algal group x (g C per mg Chl).

Since macroalgae only attach to the bottom, they are not included in computation of the light extinction Self shading is not considered for macroalgae for the present model. For a model application

that does not simulate TSS, the Ke_{TSS} term may be set to zero and Ke_b may be estimated to include light extinction due to suspended solid.

Optimal light intensity (I_s) for photosynthesis depends on algal taxonomy, duration of exposure, temperature, nutritional status, and previous acclimation. Variations in I_s are largely due to adaptations by algae intended to maximize production in a variable environment. Steel (1962) noted the result of adaptations is that optimal intensity is a consistent fraction (approximately 50%) of daily intensity. Kremer and Nixon (1978) reported an analogous finding that maximum algal growth occurs at a constant depth (approximately 1 m) in the water column. Their approach is adopted so that optimal intensity is expressed as:

$$(I_s)_x = maximum \left\{(I_o)_{avg} \cdot e^{-Kess\cdot(D_{opt})_x}, (I_s)_{\min}\right\} \quad (4\text{-}14)$$

$(D_{opt})_x$ = depth of maximum algal growth for algal group x (m)
$(I_o)_{avg}$ = adjusted surface light intensity (langleys day^{-1}).

A minimum, $(I_s)_{min}$, in Eq. 4-14 is specified so that algae do not thrive at extremely low light levels. The time required for algae to adapt to changes in light intensity is recognized by estimating $(I_s)_x$ based on a time-weighted average of daily light intensity:

$$(I_o)_{avg} = CI_a \cdot I_o + CI_b \cdot I_1 + CI_c \cdot I_2 \quad (4\text{-}15)$$

I_1 = daily light intensity 1 day preceding model day (langleys day^{-1})
I_2 = daily light intensity 2 days preceding model day (langleys day^{-1})
CI_a, CI_b, CI_c = weighting factors for I_0, I_1 and I_2, respectively: $CI_a + CI_b + CI_c = 1$.

4.3.4 Effect of Temperature on Algal Growth

A Gaussian probability curve is used to represent temperature dependency of algal growth:

$$\begin{aligned} f_3(T) &= \exp(-KTG1_x[T - TM_x]^2) && if \quad T \le TM_x \\ &= \exp(-KTG2_x[TM_x - T]^2) && if \quad T > TM_x \end{aligned} \quad (4\text{-}16)$$

T = temperature (°C) provided from the hydrodynamic model
TM_x = optimal temperature for algal growth for algal group x (°C)
$KTG1_x$ = effect of temperature below TM_x on growth for algal group x ($°C^{-2}$)
$KTG2_x$ = effect of temperature above TM_x on growth for algal group x ($°C^{-2}$).

4.3.5 Effect of Salinity on Growth of Freshwater Cyanobacteria

The growth of freshwater cyanobacteria in salt water is limited by:

$$f_4(S) = \frac{STOX^2}{STOX^2 + S^2} \quad (4\text{-}17)$$

STOX = salinity at which Microcystis growth is halved (ppt)
S = salinity in water column (ppt) provided from the hydrodynamic model.

4.3.6 Algal Basal Metabolism

Algal biomass in the present model decreases through basal metabolism (respiration and excretion) and predation. Basal metabolism in the present model is the sum of all internal processes that decrease algal biomass and consists of two parts; respiration and excretion. In basal metabolism, algal matter (carbon, nitrogen, phosphorus, and silica) is returned to organic and inorganic pools in the environment, mainly to dissolved organic and inorganic matter. Respiration, which may be viewed as a reversal of production, consumes dissolved oxygen. Basal metabolism is considered to be an exponentially increasing function of temperature:

$$BM_x = BMR_x \cdot \exp(KTB_x[T - TR_x]) \quad (4\text{-}18)$$

BMR_x = basal metabolism rate at TR_x for algal group x (day^{-1})
KTB_x = effect of temperature on metabolism for algal group x ($^\circ C^{-1}$)
TR_x = reference temperature for basal metabolism for algal group x ($^\circ C$).

4.3.7 Algal Predation

The present model does not include zooplankton. Instead, a constant rate is specified for algal predation, which implicitly assumes zooplankton biomass is a constant fraction of algal biomass. An equation similar to that for basal metabolism (Eq. 4-18) is used for predation:

$$PR_x = PRR_x \cdot \exp(KTB_x[T - TR_x]) \quad (4\text{-}19)$$

PRR_x = predation rate at TR_x for algal group x (day^{-1}).

The difference between predation and basal metabolism lies in the distribution of the end products of the two processes. In predation, algal matter (carbon, nitrogen, phosphorus, and silica) is returned to organic and inorganic pools in the environment, mainly to particulate organic matter. The predation for macroalgae is a lumped parameter that includes losses due to grazing, frond breakage, and other losses. This implicitly assumes that the losses are a fraction of the biomass.

4.3.8 Algal Settling

Settling velocities for four algal groups, WS_c, WS_d , WS_g, and WS_m, are specified as an input. Seasonal variations in settling velocity of diatoms can be accounted for by specifying time-varying WS_d.

4.4 Organic Carbon

The present model has three state variables for organic carbon: refractory particulate, labile particulate, and dissolved.

4.4.1 Particulate Organic Carbon

Labile and refractory distinctions are based on the time scale of decomposition. Labile particulate organic carbon with a decomposition time scale of days to weeks decomposes rapidly in the water column or in the sediments. Refractory particulate organic carbon with a longer-than-weeks decomposition time scale decomposes slowly, primarily in the sediments, and may contribute to sediment oxygen demand years after decomposition. For labile and refractory particulate organic carbon, sources and sinks included in the model are (Fig. 4-1):

- algal predation
- dissolution to dissolved organic carbon
- settling
- external loads.

The governing equations for refractory and labile particulate organic carbons are:

$$\frac{\partial RPOC}{\partial t} = \sum_{x=c,d,g,m} FCRP \cdot PR_x \cdot B_x - K_{RPOC} \cdot RPOC + \frac{\partial}{\partial z}(WS_{RP} \cdot RPOC) + \frac{WRPOC}{V} \qquad (4\text{-}20)$$

$$\frac{\partial LPOC}{\partial t} = \sum_{x=c,d,g,m} FCLP \cdot PR_x \cdot B_x - K_{LPOC} \cdot LPOC + \frac{\partial}{\partial z}(WS_{LP} \cdot LPOC) + \frac{WLPOC}{V} \qquad (4\text{-}21)$$

RPOC = concentration of refractory particulate organic carbon (g C m^{-3})

LPOC = concentration of labile particulate organic carbon (g C m^{-3})

FCRP = fraction of predated carbon produced as refractory particulate organic carbon

FCLP = fraction of predated carbon produced as labile particulate organic carbon

K_{RPOC} = dissolution rate of refractory particulate organic carbon (day^{-1})

K_{LPOC} = dissolution rate of labile particulate organic carbon (day^{-1})

WS_{RP} = settling velocity of refractory particulate organic matter (m day^{-1})

WS_{LP} = settling velocity of labile particulate organic matter (m day^{-1})

WRPOC = external loads of refractory particulate organic carbon (g C day^{-1})

WLPOC = external loads of labile particulate organic carbon (g C day^{-1}).

4.4.2 Dissolved Organic Carbon

Sources and sinks for dissolved organic carbon included in the model are (Fig. 4-1):

- algal excretion (exudation) and predation
- dissolution from refractory and labile particulate organic carbon

- heterotrophic respiration of dissolved organic carbon (decomposition)
- denitrification
- external loads

The kinetic equation describing these processes is:

$$\frac{\partial DOC}{\partial t} = \sum_{x=c,d,g,m} \left(\left[FCD_x + (1 - FCD_x) \frac{KHR_x}{KHR_x + DO} \right] BM_x + FCDP \cdot PR_x \right) \cdot B_x$$

$$+ K_{RPOC} \cdot RPOC + K_{LPOC} \cdot LPOC - K_{HR} \cdot DOC - Denit \cdot DOC + \frac{WDOC}{V} \qquad (4\text{-}22)$$

DOC = concentration of dissolved organic carbon (g C m^{-3})

FCD_x = fraction of basal metabolism exuded as dissolved organic carbon at infinite dissolved oxygen concentration for algal group x

KHR_x = half-saturation constant of dissolved oxygen for algal dissolved organic carbon excretion for group x (g O_2 m^{-3})

DO = dissolved oxygen concentration (g O_2 m^{-3})

FCDP = fraction of predated carbon produced as dissolved organic carbon

K_{HR} = heterotrophic respiration rate of dissolved organic carbon (day^{-1})

Denit = denitrification rate (day^{-1}) given in Eq. 4-34

WDOC = external loads of dissolved organic carbon (g C day^{-1}).

The remainder of this section explains each term in Equations 4-20 to 4-22.

4.4.3 Effect of Algae on Organic Carbon

The terms within summation ($\sum$) in Equations 4-20 to 4-22 account for the effects of algae on organic carbon through basal metabolism and predation.

4.4.3.1 Basal metabolism. Basal metabolism, consisting of respiration and excretion, returns algal matter (carbon, nitrogen, phosphorus, and silica) back to the environment. Loss of algal biomass through basal metabolism is (Eq. 4-18):

$$\frac{\partial B_x}{\partial t} = -BM_x \cdot B_x \qquad (4\text{-}23)$$

which indicates that the total loss of algal biomass due to basal metabolism is independent of ambient dissolved oxygen concentration. In this model, it is assumed that the distribution of total loss between respiration and excretion is constant as long as there is sufficient dissolved oxygen for algae to respire. Under that condition, the losses by respiration and excretion may be written as:

$(1 - FCD_x) \cdot BM_x \cdot B_x$ due to respiration (4-24)

$$FCD_x \cdot BM_x \cdot B_x \qquad \text{due to excretion} \qquad (4\text{-}25)$$

where FCD_x is a constant of value between 0 and 1. Algae cannot respire in the absence of oxygen, however. Although the total loss of algal biomass due to basal metabolism is oxygen-independent (Eq. 4-23), the distribution of total loss between respiration and excretion is oxygen-dependent. When oxygen level is high, respiration is a large fraction of the total. As dissolved oxygen becomes scarce, excretion becomes dominant. Thus, Eq. 4-24 represents the loss by respiration only at high oxygen levels. In general, Eq. 4-24 can be decomposed into two fractions as a function of dissolved oxygen availability:

$$(1 - FCD_x)\frac{DO}{KHR_x + DO} BM_x \cdot B_x \qquad \text{due to respiration} \qquad (4\text{-}26)$$

$$(1 - FCD_x)\frac{KHR_x}{KHR_x + DO} BM_x \cdot B_x \qquad \text{due to excretion} \qquad (4\text{-}27)$$

Equation 4-26 represents the loss of algal biomass by respiration, and Eq. 4-27 represents additional excretion due to insufficient dissolved oxygen concentration. The parameter KHR_x, which is defined as the half-saturation constant of dissolved oxygen for algal dissolved organic carbon excretion in Eq. 4-22, can also be defined as the half-saturation constant of dissolved oxygen for algal respiration in Eq. 4-26.

Combining Equations 4-25 and 4-27, the total loss due to excretion is:

$$\left(FCD_x + (1 - FCD_x)\frac{KHR_x}{KHR_x + DO} \right) BM_x \cdot B_x \qquad (4\text{-}28)$$

Equations 4-26 and 4-28 combine to give the total loss of algal biomass due to basal metabolism, $BM_x \cdot B_x$ (Eq. 4-23). The definition of FCD_x in Eq. 4-22 becomes apparent in Eq. 4-28; i.e., fraction of basal metabolism exuded as dissolved organic carbon at infinite dissolved oxygen concentration. At zero oxygen level, 100% of total loss due to basal metabolism is by excretion regardless of FCD_x. The end carbon product of respiration is primarily carbon dioxide, an inorganic form not considered in the present model, while the end carbon product of excretion is primarily dissolved organic carbon. Therefore, Eq. 4-28, that appears in Eq. 4-22, represents the contribution of excretion to dissolved organic carbon, and there is no source term for particulate organic carbon from algal basal metabolism in Equations 4-20 and 4-21.

4.4.3.2 Predation. Algae produce organic carbon through the effects of predation. Zooplankton take up and redistribute algal carbon through grazing, assimilation, respiration, and excretion. Since

zooplankton are not included in the model, routing of algal carbon through zooplankton predation is simulated by empirical distribution coefficients in Equations 4-20 to 4-22; FCRP, FCLP, and FCDP. The sum of these three predation fractions should be unity.

4.4.4 Heterotrophic Respiration and Dissolution

The second term on the RHS of Equations 4-20 and 4-21 represents dissolution of particulate to dissolved organic carbon and the third term in the second line of Eq. 4-22 represents heterotrophic respiration of dissolved organic carbon. The oxic heterotrophic respiration is a function of dissolved oxygen: the lower the dissolved oxygen, the smaller the respiration term becomes. Heterotrophic respiration rate, therefore, is expressed using a Monod function of dissolved oxygen:

$$K_{HR} = \frac{DO}{KHOR_{DO} + DO} K_{DOC} \tag{4-29}$$

$KHOR_{DO}$ = oxic respiration half-saturation constant for dissolved oxygen (g O_2 m^{-3})

K_{DOC} = heterotrophic respiration rate of dissolved organic carbon at infinite dissolved oxygen concentration (day^{-1}).

Dissolution and heterotrophic respiration rates depend on the availability of carbonaceous substrate and on heterotrophic activity. Algae produce labile carbon that fuels heterotrophic activity: dissolution and heterotrophic respiration do not require the presence of algae though, and may be fueled entirely by external carbon inputs. In the model, algal biomass, as a surrogate for heterotrophic activity, is incorporated into formulations of dissolution and heterotrophic respiration rates. Formulations of these rates require specification of algal-dependent and algal-independent rates:

$$K_{RPOC} = (K_{RC} + K_{RCalg} \sum_{x=c,d,g} B_x) \cdot \exp(KT_{HDR}[T - TR_{HDR}]) \tag{4-30}$$

$$K_{LPOC} = (K_{LC} + K_{LCalg} \sum_{x=c,d,g} B_x) \cdot \exp(KT_{HDR}[T - TR_{HDR}]) \tag{4-31}$$

$$K_{DOC} = (K_{DC} + K_{DCalg} \sum_{x=c,d,g} B_x) \cdot \exp(KT_{MNL}[T - TR_{MNL}]) \tag{4-32}$$

K_{RC} = minimum dissolution rate of refractory particulate organic carbon (day^{-1})

K_{LC} = minimum dissolution rate of labile particulate organic carbon (day^{-1})

K_{DC} = minimum respiration rate of dissolved organic carbon (day^{-1})

K_{RCalg}, K_{LCalg} = constants that relate dissolution of refractory and labile particulate organic carbon, respectively, to algal biomass (day^{-1} per g C m^{-3})

K_{DCalg} = constant that relates respiration to algal biomass (day^{-1} per g C m^{-3})

KT_{HDR} = effect of temperature on hydrolysis of particulate organic matter ($^{\circ}C^{-1}$)

TR_{HDR} = reference temperature for hydrolysis of particulate organic matter (°C)
KT_{MNL} = effect of temperature on mineralization of dissolved organic matter ($°C^{-1}$)
TR_{MNL} = reference temperature for mineralization of dissolved organic matter (°C).
Equations 4-30 to 4-32 have exponential functions that relate rates to temperature.

In the present model, the term "hydrolysis" is defined as the process by which particulate organic matter is converted to dissolved organic form, and thus includes both dissolution of particulate carbon and hydrolysis of particulate phosphorus and nitrogen. Therefore, the parameters, KT_{HDR} and TR_{HDR}, are also used for the temperature effects on hydrolysis of particulate phosphorus (Equations 4-28 and 4-29) and nitrogen (Equations 4-54 and 4-55). The term "mineralization" is defined as the process by which dissolved organic matter is converted to dissolved inorganic form, and thus includes both heterotrophic respiration of dissolved organic carbon and mineralization of dissolved organic phosphorus and nitrogen. Therefore, the parameters, KT_{MNL} and TR_{MNL}, are also used for the temperature effects on mineralization of dissolved phosphorus (Eq. 4-46) and nitrogen (Eq. 4-56).

4.4.5 Effect of Denitrification on Dissolved Organic Carbon

As oxygen is depleted from natural systems, organic matter is oxidized by the reduction of alternate electron acceptors. Thermodynamically, the first alternate acceptor reduced in the absence of oxygen is nitrate. The reduction of nitrate by a large number of heterotrophic anaerobes is referred to as denitrification, and the stoichiometry of this reaction is (Stumm and Morgan 1981):

$$4NO_3^- + 4H^+ + 5CH_2O \rightarrow 2N_2 + 7H_2O + 5CO_2 \quad (4\text{-}33)$$

The last term in Eq. 4-22 accounts for the effect of denitrification on dissolved organic carbon. The kinetics of denitrification in the model are first-order:

$$Denit = \frac{KHOR_{DO}}{KHOR_{DO} + DO} \frac{NO3}{KHDN_N + NO3} AANOX \cdot K_{DOC} \quad (4\text{-}34)$$

$KHDN_N$ = denitrification half-saturation constant for nitrate (g N m^{-3})
AANOX = ratio of denitrification rate to oxic dissolved organic carbon respiration rate.

In Eq. 4-34, the dissolved organic carbon respiration rate, K_{DOC}, is modified so that significant decomposition via denitrification occurs only when nitrate is freely available and dissolved oxygen is depleted. The ratio, AANOX, makes the anoxic respiration slower than oxic respiration. Note that K_{DOC}, defined in Eq. 4-32, includes the temperature effect on denitrification.

4.5 Phosphorus

The present model has four state variables for phosphorus: three organic forms (refractory particulate, labile particulate, and dissolved) and one inorganic form (total phosphate).

4.5.1 Particulate Organic Phosphorus

For refractory and labile particulate organic phosphorus, sources and sinks included in the model are (Fig. 4-1):

- algal basal metabolism and predation
- dissolution to dissolved organic phosphorus
- settling
- external loads.

The kinetic equations for refractory and labile particulate organic phosphorus are:

$$\frac{\partial RPOP}{\partial t} = \sum_{x=c,d,g,m} (FPR_x \cdot BM_x + FPRP \cdot PR_x) APC \cdot B_x - K_{RPOP} \cdot RPOP + \frac{\partial}{\partial z}(WS_{RP} \cdot RPOP) + \frac{WRPOP}{V} \quad (4\text{-}35)$$

$$\frac{\partial LPOP}{\partial t} = \sum_{x=c,d,g,m} (FPL_x \cdot BM_x + FPLP \cdot PR_x) APC \cdot B_x - K_{LPOP} \cdot LPOP + \frac{\partial}{\partial z}(WS_{LP} \cdot LPOP) + \frac{WLPOP}{V} \quad (4\text{-}36)$$

RPOP = concentration of refractory particulate organic phosphorus (g P m^{-3})

LPOP = concentration of labile particulate organic phosphorus (g P m^{-3})

FPR_x = fraction of metabolized phosphorus by algal group x produced as refractory particulate organic phosphorus

FPL_x = fraction of metabolized phosphorus by algal group x produced as labile particulate organic phosphorus

FPRP = fraction of predated phosphorus produced as refractory particulate organic phosphorus

FPLP = fraction of predated phosphorus produced as labile particulate organic phosphorus

APC = mean algal phosphorus-to-carbon ratio for all algal groups (g P per g C)

K_{RPOP} = hydrolysis rate of refractory particulate organic phosphorus (day^{-1})

K_{LPOP} = hydrolysis rate of labile particulate organic phosphorus (day^{-1})

WRPOP = external loads of refractory particulate organic phosphorus (g P day^{-1})

WLPOP = external loads of labile particulate organic phosphorus (g P day^{-1}).

4.5.2 Dissolved Organic Phosphorus

Sources and sinks for dissolved organic phosphorus included in the model are (Fig. 4-1):

- algal basal metabolism and predation
- dissolution from refractory and labile particulate organic phosphorus
- mineralization to phosphate phosphorus
- external loads.

The kinetic equation describing these processes is:

$$\frac{\partial DOP}{\partial t} = \sum_{x=c,d,g,m} (FPD_x \cdot BM_x + FPDP \cdot PR_x) APC \cdot B_x$$

$$+ K_{RPOP} \cdot RPOP + K_{LPOP} \cdot LPOP - K_{DOP} \cdot DOP + \frac{WDOP}{V} \quad (4\text{-}37)$$

DOP = concentration of dissolved organic phosphorus (g P m^{-3})

FPD_x = fraction of metabolized phosphorus by algal group x produced as dissolved organic phosphorus

FPDP = fraction of predated phosphorus produced as dissolved organic phosphorus

K_{DOP} = mineralization rate of dissolved organic phosphorus (day^{-1})

WDOP = external loads of dissolved organic phosphorus (g P day^{-1}).

4.5.3 Total Phosphate

For total phosphate that includes both dissolved and sorbed phosphate (Section 4.5.4), sources and sinks included in the model are (Fig. 4-1):

- algal basal metabolism, predation, and uptake
- mineralization from dissolved organic phosphorus
- settling of sorbed phosphate
- sediment-water exchange of dissolved phosphate for the bottom layer only
- external loads.

The kinetic equation describing these processes is:

$$\frac{\partial PO4t}{\partial t} = \sum_{x=c,d,g,m} (FPI_x \cdot BM_x + FPIP \cdot PR_x - P_x) APC \cdot B_x + K_{DOP} \cdot DOP$$

$$+ \frac{\partial}{\partial z}(WS_{TSS} \cdot PO4p) + \frac{BFPO4d}{\Delta z} + \frac{WPO4t}{V} \quad (4\text{-}38)$$

PO4t = total phosphate (g P m^{-3}) = PO4d + PO4p (4-39)

PO4d = dissolved phosphate (g P m^{-3})

PO4p = particulate (sorbed) phosphate (g P m^{-3})

FPI_x = fraction of metabolized phosphorus by algal group x produced as inorganic phosphorus

FPIP = fraction of predated phosphorus produced as inorganic phosphorus
WS_{TSS} = settling velocity of suspended solid (m day^{-1}), provided by the hydrodynamic model
BFPO4d = sediment-water exchange flux of phosphate (g P m^{-2} day^{-1}), applied to the bottom layer only
WPO4t = external loads of total phosphate (g P day^{-1}).

In Eq. 4-38, if total active metal is chosen as a measure of sorption site, the settling velocity of total suspended solid, WS_{TSS}, is replaced by that of particulate metal, WS_s (Sections 4.5.4 and 4.10). The remainder of this section explains each term in Equations 4-35 to 4-38, except BFPO4d (benthic flux of dissolved orthophosphate), which is described in Chapter 5.

4.5.4 Total Phosphate System

Suspended and bottom sediment particles (clay, silt, and metal hydroxides) adsorb and desorb phosphate in river and estuarine waters. This adsorption-desorption process has been suggested to buffer phosphate concentration in water column and to enhance the transport of phosphate away from its external sources (Carritt and Goodgal 1954; Froelich 1988; Lebo 1991). To ease the computational complication due to the adsorption-desorption of phosphate, dissolved and sorbed phosphate are treated and transported as a single state variable. Therefore, the model phosphate state variable, total phosphate, is defined as the sum of dissolved and sorbed phosphate (Eq. 4-39), and the concentrations for each fraction are determined by equilibrium partitioning of their sum.

In CE-QUAL-ICM, sorption of phosphate to particulate species of metals including iron and manganese was considered based on a phenomenon observed in the monitoring data from the mainstem of the Chesapeake Bay: phosphate was rapidly depleted from anoxic bottom waters during the autumn reaeration event (Cerco and Cole 1993). Their hypothesis was that reaeration of bottom waters caused dissolved iron and manganese to precipitate, and phosphate sorbed to newly formed metal particles and rapidly settled to the bottom. One state variable, total active metal, in CE-QUAL-ICM was defined as the sum of all metals that act as sorption sites, and the total active metal was partitioned into particulate and dissolved fractions via an equilibrium partitioning coefficient (Section 4.10). Then phosphate was assumed to sorb to only the particulate fraction of the total active metal.

In the treatment of phosphate sorption in CE-QUAL-ICM, the particulate fraction of metal hydroxides was emphasized as a sorption site in bottom waters under anoxic conditions. Phosphorus is a highly particle-reactive element, and phosphate in solution reacts quickly with a wide variety of surfaces, being taken up by and released from particles (Froelich 1988). The present model has two options, total suspended solid and total active metal, as a measure of a sorption site for phosphate, and dissolved and

sorbed fractions are determined by equilibrium partitioning of their sum as a function of total suspended solid or total active metal concentration:

$$PO4p = \frac{K_{PO4p} \cdot TSS}{1 + K_{PO4p} \cdot TSS} PO4t \quad \text{or} \quad PO4p = \frac{K_{PO4p} \cdot TAMp}{1 + K_{PO4p} \cdot TAMp} PO4t \tag{4-40}$$

$$PO4d = \frac{1}{1 + K_{PO4p} \cdot TSS} PO4t \quad \text{or} \quad PO4d = \frac{1}{1 + K_{PO4p} \cdot TAMp} PO4t$$

$$= PO4t - PO4p \tag{4-41}$$

K_{PO4p} = empirical coefficient relating phosphate sorption to total suspended solid (per g m^{-3}) or particulate total active metal (per mol m^{-3}) concentration

TAMp = particulate total active metal (mol m^{-3}).

Dividing Eq. 4-40 by Eq. 4-41 gives:

$$K_{PO4p} = \frac{PO4p}{PO4d} \frac{1}{TSS} \quad \text{or} \quad K_{PO4p} = \frac{PO4p}{PO4d} \frac{1}{TAMp} \tag{4-42}$$

where the meaning of K_{PO4p} becomes apparent, i.e., the ratio of sorbed to dissolved phosphate per unit concentration of total suspended solid or particulate total active metal (i.e., per unit sorption site available).

4.5.5 Algal Phosphorus-to-Carbon Ratio (APC)

Algal biomass is quantified in units of carbon per volume of water. In order to express the effects of algal biomass on phosphorus and nitrogen, the ratios of phosphorus-to-carbon and nitrogen-to-carbon in algal biomass must be specified. Although global mean values of these ratios are well known (Redfield et al. 1963), algal composition varies especially as a function of nutrient availability. As phosphorus and nitrogen become scarce, algae adjust their composition so that smaller quantities of these vital nutrients are required to produce carbonaceous biomass (DiToro 1980; Parsons et al. 1984). Examining the field data from the surface of upper Chesapeake Bay, Cerco and Cole (1993) showed that the variation of nitrogen-to-carbon stoichiometry was small and thus used a constant algal nitrogen-to-carbon ratio, ANC_x. Large variations, however, were observed for algal phosphorus-to-carbon ratio indicating the adaptation of algae to ambient phosphorus concentration (Cerco and Cole 1993): algal phosphorus content is high when ambient phosphorus is abundant and is low when ambient phosphorus is scarce. Thus, a variable algal phosphorus-to-carbon ratio, APC, is used in model formulation. A mean

ratio for all algal groups, APC, is described by an empirical approximation to the trend observed in field data (Cerco & Cole 1994):

$$APC = \left(CP_{prm1} + CP_{prm2} \cdot \exp[-CP_{prm3} \cdot PO4d]\right)^{-1} \quad (4\text{-}43)$$

CP_{prm1} = minimum carbon-to-phosphorus ratio (g C per g P)

CP_{prm2} = difference between minimum and maximum carbon-to-phosphorus ratio (g C per g P)

CP_{prm3} = effect of dissolved phosphate concentration on carbon-to-phosphorus ratio (per g P m^{-3}).

4.5.6 Effect of Algae on Phosphorus

The terms within summation ($\sum$) in Equations 4-35 to 4-38 account for the effects of algae on phosphorus. Both basal metabolism (respiration and excretion) and predation are considered, and thus formulated, to contribute to organic and phosphate phosphorus. That is, the total loss by basal metabolism ($BM_x \cdot B_x$ in Eq. 4-5) is distributed using distribution coefficients; FPR_x, FPL_x, FPD_x, and FPI_x. The total loss by predation ($PR_x \cdot B_x$ in Eq. 4-5), is also distributed using distribution coefficients; FPRP, FPLP, FPDP, and FPIP. The sum of four distribution coefficients for basal metabolism should be unity, and so is that for predation. Algae take up dissolved phosphate for growth, and algae uptake of phosphate is represented by ($-\sum P_x \cdot APC \cdot B_x$) in Eq. 4-38.

4.5.7 Mineralization and Hydrolysis

The third term on the RHS of Equations 4-35 and 4-36 represents hydrolysis of particulate organic phosphorus, and the last term in Eq. 3-7 represents mineralization of dissolved organic phosphorus. Mineralization of organic phosphorus is mediated by the release of nucleotidase and phosphatase enzymes by bacteria (Chróst and Overbek 1987) and algae (Boni et al. 1989). Since the algae themselves release the enzymes and bacterial abundance is related to algal biomass, the rate of organic phosphorus mineralization is related to algal biomass in model formulation. Another mechanism included in model formulation is that algae stimulate production of an enzyme that mineralizes organic phosphorus to phosphate when phosphate is scarce (Chróst and Overbek 1987; Boni et al. 1989). The formulations for hydrolysis and mineralization rates including these processes are:

$$K_{RPOP} = \left(K_{RP} + \frac{KHP}{KHP + PO4d} K_{RPalg} \sum_{x=c,d,g} B_x\right) \cdot \exp\left(KT_{HDR}[T - TR_{HDR}]\right) \quad (4\text{-}44)$$

$$K_{LPOP} = \left(K_{LP} + \frac{KHP}{KHP + PO4d} K_{LPalg} \sum_{x=c,d,g} B_x\right) \cdot \exp\left(KT_{HDR}[T - TR_{HDR}]\right) \quad (4\text{-}45)$$

$$K_{DOP} = \left(K_{DP} + \frac{KHP}{KHP + PO4d} K_{DPalg} \sum_{x=c,d,g} B_x\right) \cdot \exp\left(KT_{MNL}[T - TR_{MNL}]\right) \quad (4\text{-}46)$$

K_{RP} = minimum hydrolysis rate of refractory particulate organic phosphorus (day^{-1})

K_{LP} = minimum hydrolysis rate of labile particulate organic phosphorus (day^{-1})

K_{DP} = minimum mineralization rate of dissolved organic phosphorus (day^{-1})

K_{RPalg}, K_{LPalg} = constants that relate hydrolysis of refractory and labile particulate organic phosphorus, respectively, to algal biomass (day^{-1} per g C m^{-3})

K_{DPalg} = constant that relates mineralization to algal biomass (day^{-1} per g C m^{-3})

KHP = mean half-saturation constant for algal phosphorus uptake (g P m^{-3}).

$$= \frac{1}{3}\sum_{x=c,d,g} KHP_x \tag{4-47}$$

When phosphate is abundant relative to KHP, the rates become close to the minimum values with little influence from algal biomass. When phosphate becomes scarce relative to KHP, the rates increase with the magnitude of increase depending on algal biomass. Equations 4-44 to 4-46 have exponential functions that relate rates to temperature.

4.6 Nitrogen

The present model has five state variables for nitrogen: three organic forms (refractory particulate, labile particulate, and dissolved) and two inorganic forms (ammonium and nitrate). The nitrate state variable in the model represents the sum of nitrate and nitrite.

4.6.1 Particulate Organic Nitrogen

For refractory and labile particulate organic nitrogen, sources and sinks included in the model are (Figure 4-1):

- algal basal metabolism and predation
- dissolution to dissolved organic nitrogen
- settling
- external loads.

The kinetic equations for refractory and labile particulate organic nitrogen are:

$$\frac{\partial RPON}{\partial t} = \sum_{x=c,d,g,m} (FNR_x \cdot BM_x + FNRP \cdot PR_x) ANC_x \cdot B_x - K_{RPON} \cdot RPON$$

$$+ \frac{\partial}{\partial z}(WS_{RP} \cdot RPON) + \frac{WRPON}{V} \tag{4-48}$$

$$\frac{\partial LPON}{\partial t} = \sum_{x=c,d,g,m} (FNL_x \cdot BM_x + FNLP \cdot PR_x) ANC_x \cdot B_x - K_{LPON} \cdot LPON$$

$$+ \frac{\partial}{\partial z}(WS_{LP} \cdot LPON) + \frac{WLPON}{V} \quad (4\text{-}49)$$

RPON = concentration of refractory particulate organic nitrogen (g N m^{-3})

LPON = concentration of labile particulate organic nitrogen (g N m^{-3})

FNR_x = fraction metabolized nitrogen by algal group x as refractory particulate organic nitrogen

FNL_x = fraction of metabolized nitrogen by algal group x produced as labile particulate organic nitrogen

FNRP = fraction of predated nitrogen produced as refractory particulate organic nitrogen

FNLP = fraction of predated nitrogen produced as labile particulate organic nitrogen

ANC_x = nitrogen-to-carbon ratio in algal group x (g N per g C)

K_{RPON} = hydrolysis rate of refractory particulate organic nitrogen (day^{-1})

K_{LPON} = hydrolysis rate of labile particulate organic nitrogen (day^{-1})

WRPON = external loads of refractory particulate organic nitrogen (g N day^{-1})

WLPON = external loads of labile particulate organic nitrogen (g N day^{-1}).

4.6.2 Dissolved Organic Nitrogen

Sources and sinks for dissolved organic nitrogen included in the model are (Fig. 4-1):

- algal basal metabolism and predation
- dissolution from refractory and labile particulate organic nitrogen
- mineralization to ammonium
- external loads.

The kinetic equation describing these processes is:

$$\frac{\partial DON}{\partial t} = \sum_{x=c,d,g,m} (FND_x \cdot BM_x + FNDP \cdot PR_x) ANC_x \cdot B_x$$

$$+ K_{RPON} \cdot RPON + K_{LPON} \cdot LPON - K_{DON} \cdot DON + \frac{WDON}{V} \quad (4\text{-}50)$$

DON = concentration of dissolved organic nitrogen (g N m^{-3})

FND_x = fraction of metabolized nitrogen by algal group x produced as dissolved organic nitrogen

FNDP = fraction of predated nitrogen produced as dissolved organic nitrogen

K_{DON} = mineralization rate of dissolved organic nitrogen (day^{-1})

WDON = external loads of dissolved organic nitrogen (g N day^{-1}).

4.6.3 Ammonium Nitrogen

Sources and sinks for ammonia nitrogen included in the model are (Fig. 4-1):

- algal basal metabolism, predation, and uptake
- mineralization from dissolved organic nitrogen

- nitrification to nitrate
- sediment-water exchange for the bottom layer only
- external loads.

The kinetic equation describing these processes is:

$$\frac{\partial NH4}{\partial t} = \sum_{x=c,d,g,m} (FNI_x \cdot BM_x + FNIP \cdot PR_x - PN_x \cdot P_x) ANC_x \cdot B_x + K_{DON} \cdot DON$$

$$- Nit \cdot NH4 + \frac{BFNH4}{\Delta z} + \frac{WNH4}{V} \qquad (4\text{-}51)$$

FNI_x = fraction of metabolized nitrogen by algal group x produced as inorganic nitrogen

FNIP = fraction of predated nitrogen produced as inorganic nitrogen

PN_x = preference for ammonium uptake by algal group x ($0 \le PN_x \le 1$)

Nit = nitrification rate (day^{-1}) given in Eq. 4-59

BFNH4 = sediment-water exchange flux of ammonium (g N m^{-2} day^{-1}), applied to the bottom layer only

WNH4 = external loads of ammonium (g N day^{-1}).

4.6.4 Nitrate Nitrogen

Sources and sinks for nitrate nitrogen included in the model are (Fig. 4-1):

- algal uptake
- nitrification from ammonium
- denitrification to nitrogen gas
- sediment-water exchange for the bottom layer only
- external loads.

The kinetic equation describing these processes is:

$$\frac{\partial NO3}{\partial t} = - \sum_{x=c,d,g,m} (1 - PN_x) P_x \cdot ANC_x \cdot B_x + Nit \cdot NH4 - ANDC \cdot Denit \cdot DOC$$

$$+ \frac{BFNO3}{\Delta z} + \frac{WNO3}{V} \qquad (4\text{-}52)$$

ANDC = mass of nitrate nitrogen reduced per mass of dissolved organic carbon oxidized (0.933 g N per g C from Eq. 4-33)

BFNO3 = sediment-water exchange flux of nitrate (g N m^{-2} day^{-1}), applied to the bottom layer only

WNO3 = external loads of nitrate (g N day^{-1}).

The remainder of this section explains each term in Equations 4-48 to 4-52, except BFNH4 and BFNO3 which are described in Chapter 5.

4.6.5 Effect of Algae on Nitrogen

The terms within summation ($\sum$) in Equations 4-48 to 4-52 account for the effects of algae on nitrogen. As in phosphorus, both basal metabolism (respiration and excretion) and predation are considered, and thus formulated, to contribute to organic and ammonium nitrogen. That is, algal nitrogen released by both basal metabolism and predation are represented by distribution coefficients; FNR_x, FNL_x, FND_x, FNI_x, FNRP, FNLP, FNDP, and FNIP. The sum of four distribution coefficients for basal metabolism should be unity; the sum of the predation distribution coefficients should also be unity.

Algae take up ammonium and nitrate for growth, and ammonium is preferred from thermodynamic considerations. The preference of algae for ammonium is expressed as:

$$PN_x = NH4\frac{NO3}{(KHN_x + NH4)(KHN_x + NO3)} + NH4\frac{KHN_x}{(NH4 + NO3)(KHN_x + NO3)} \quad (4\text{-}53)$$

This equation forces the preference for ammonium to be unity when nitrate is absent, and to be zero when ammonium is absent.

4.6.6 Mineralization and Hydrolysis

The third term on the RHS of Equations 4-48 and 4-49 represents hydrolysis of particulate organic nitrogen and the last term in Eq. 4-50 represents mineralization of dissolved organic nitrogen. Including a mechanism for accelerated hydrolysis and mineralization during nutrient-limited conditions (Section 4.5.7), the formulations for these processes are:

$$K_{RPON} = (K_{RN} + \frac{KHN}{KHN + NH4 + NO3}K_{RNalg}\sum_{x=c,d,g} B_x)\cdot\exp(KT_{HDR}[T - TR_{HDR}]) \quad (4\text{-}54)$$

$$K_{LPON} = (K_{LN} + \frac{KHN}{KHN + NH4 + NO3}K_{LNalg}\sum_{x=c,d,g} B_x)\cdot\exp(KT_{HDR}[T - TR_{HDR}]) \quad (4\text{-}55)$$

$$K_{DON} = (K_{DN} + \frac{KHN}{KHN + NH4 + NO3}K_{DNalg}\sum_{x=c,d,g} B_x)\cdot\exp(KT_{MNL}[T - TR_{MNL}]) \quad (4\text{-}56)$$

K_{RN} = minimum hydrolysis rate of refractory particulate organic nitrogen (day^{-1})

K_{LN} = minimum hydrolysis rate of labile particulate organic nitrogen (day^{-1})

K_{DN} = minimum mineralization rate of dissolved organic nitrogen (day^{-1})

K_{RNalg}, K_{LNalg} = constants that relate hydrolysis of refractory and labile particulate organic nitrogen, respectively, to algal biomass (day^{-1} per g C m^{-3})

K_{DNalg} = constant that relates mineralization to algal biomass (day^{-1} per g C m^{-3})

KHN = mean half-saturation constant for algal nitrogen uptake (g N m^{-3}).

$$= \frac{1}{3}\sum_{x=c,d,g} KHN_x \tag{4-57}$$

Equations 4-54 to 4-56 have exponential functions that relate rates to temperature.

4.6.7 Nitrification

Nitrification is a process mediated by autotrophic nitrifying bacteria that obtain energy through the oxidation of ammonium to nitrite and of nitrite to nitrate. The stoichiometry of complete reaction is (Bowie et al. 1985):

$$NH_4^+ + 2O_2 \rightarrow NO_3^- + H_2O + 2H^+ \tag{4-58}$$

The first term in the second line of Eq. 4-51 and its corresponding term in Eq. 4-52 represent the effect of nitrification on ammonium and nitrate, respectively. The kinetics of complete nitrification process are formulated as a function of available ammonium, dissolved oxygen and temperature:

$$Nit = \frac{DO}{KHNit_{DO} + DO}\frac{NH4}{KHNit_N + NH4} Nit_m \cdot f_{Nit}(T) \tag{4-59}$$

$$\begin{aligned} f_{Nit}(T) &= \exp(-KNit1[T - TNit]^2) \qquad if \quad T \le TNit \\ &= \exp(-KNit2[TNit - T]^2) \qquad if \quad T > TNit \end{aligned} \tag{4-60}$$

$KHNit_{DO}$ = nitrification half-saturation constant for dissolved oxygen (g O_2 m^{-3})
$KHNit_N$ = nitrification half-saturation constant for ammonium (g N m^{-3})
Nit_m = maximum nitrification rate at TNit (g N m^{-3} day^{-1})
TNit = optimum temperature for nitrification (°C)
KNit1 = effect of temperature below TNit on nitrification rate ($°C^{-2}$)
KNit2 = effect of temperature above TNit on nitrification rate ($°C^{-2}$).

The Monod function of dissolved oxygen in Eq. 4-59 indicates the inhibition of nitrification at low oxygen level. The Monod function of ammonium indicates that when ammonium is abundant, the nitrification rate is limited by the availability of nitrifying bacteria. The effect of suboptimal temperature is represented using Gaussian form.

4.6.8 Denitrification

The effect of denitrification on dissolved organic carbon was described in Section 4.4.5. Denitrification removes nitrate from the system in stoichiometric proportion to carbon removal as determined by Eq. 4-33. The last term in the first line of Eq. 4-52 represents this removal of nitrate.

4.7 Silica

The present model has two state variables for silica: particulate biogenic silica and available silica.

4.7.1 Particulate Biogenic Silica

Sources and sinks for particulate biogenic silica included in the model are (Fig. 4-1):

- diatom basal metabolism and predation
- dissolution to available silica
- settling
- external loads

The kinetic equation describing these processes is:

$$\frac{\partial SU}{\partial t} = (FSP_d \cdot BM_d + FSPP \cdot PR_d) ASC_d \cdot B_d - K_{SUA} \cdot SU + \frac{\partial}{\partial z}(WS_d \cdot SU) + \frac{WSU}{V} \qquad (4\text{-}61)$$

SU = concentration of particulate biogenic silica (g Si m^{-3})

FSP_d = fraction of metabolized silica by diatoms produced as particulate biogenic silica

FSPP = fraction of predated diatom silica produced as particulate biogenic silica

ASC_d = silica-to-carbon ratio of diatoms (g Si per g C)

K_{SUA} = dissolution rate of particulate biogenic silica (day^{-1})

WSU = external loads of particulate biogenic silica (g Si day^{-1}).

4.7.2 Available Silica

Sources and sinks for available silica included in the model are (Fig. 4-1):

- diatom basal metabolism, predation, and uptake
- settling of sorbed (particulate) available silica
- dissolution from particulate biogenic silica
- sediment-water exchange of dissolved silica for the bottom layer only
- external loads.

The kinetic equation describing these processes is:

$$\frac{\partial SA}{\partial t} = (FSI_d \cdot BM_d + FSIP \cdot PR_d - P_d) ASC_d \cdot B_d + K_{SUA} \cdot SU + \frac{\partial}{\partial z}(WS_{TSS} \cdot SAp) + \frac{BFSAd}{\Delta z} + \frac{WSA}{V} \qquad (4\text{-}62)$$

SA = concentration of available silica (g Si m^{-3}) = SAd + SAp (4-63)

SAd = dissolved available silica (g Si m^{-3})

SAp = particulate (sorbed) available silica (g Si m^{-3})

FSI_d = fraction of metabolized silica by diatoms produced as available silica

FSIP = fraction of predated diatom silica produced as available silica

BFSAd = sediment-water exchange flux of available silica (g Si m^{-2} day^{-1}), applied to bottom layer only

WSA = external loads of available silica (g Si day^{-1}).

In Eq. 4-62, if total active metal is chosen as a measure of sorption site, the settling velocity of total suspended solid, WS_{TSS}, is replaced by that of particulate metal, WS_s (Sections 4.7.3 and 4.10).

4.7.3 Available Silica System

Analysis of Chesapeake Bay monitoring data indicates that silica shows similar behavior as phosphate in the adsorption-desorption process (Cerco and Cole 1993). As in phosphate, therefore, available silica is defined to include both dissolved and sorbed fractions (Eq. 4-63). Treatment of available silica is the same as total phosphate, and the same method to partition dissolved and sorbed phosphate is used to partition dissolved and sorbed available silica:

$$SAp = \frac{K_{SAp} \cdot TSS}{1 + K_{SAp} \cdot TSS} SA \quad \text{or} \qquad SAp = \frac{K_{SAp} \cdot TAMp}{1 + K_{SAp} \cdot TAMp} SA \tag{4-64}$$

$$SAd = \frac{1}{1 + K_{SAp} \cdot TSS} SA \quad \text{or} \qquad SAd = \frac{1}{1 + K_{SAp} \cdot TAMp} SA$$

$$= SA - SAp \tag{4-65}$$

K_{SAp} = empirical coefficient relating available silica sorption to total suspended solid (per g m^{-3}) or particulate total active metal (per mol m^{-3}) concentration.

As in K_{PO4p} in Section 4.5.4, K_{SAp} is the ratio of sorbed to dissolved available silica per unit sorption site available.

4.7.4 Effect of Diatoms on Silica

In Equations 4-62 and 4-63, those terms expressed as a function of diatom biomass (B_d) account for the effects of diatoms on silica. As in phosphorus and nitrogen, both basal metabolism (respiration and excretion) and predation are considered, and thus formulated, to contribute to particulate biogenic and available silica. That is, diatom silica released by both basal metabolism and predation are represented by distribution coefficients; FSP_d, FSI_d, FSPP, and FSIP. The sum of two distribution coefficients for basal metabolism should be unity and so is that for predation. Diatoms require silica as well as phosphorus and nitrogen, and diatom uptake of available silica is represented by $(- P_d \cdot ASC_d \cdot B_d)$ in Eq. 4-63.

4.7.5 Dissolution

The term (- K_{SUA}·SU) in Eq. 4-62 and its corresponding term in Eq. 4-63 represent dissolution of particulate biogenic silica to available silica. The dissolution rate is expressed as an exponential function of temperature:

$$K_{SUA} = K_{SU} \cdot \exp(KT_{SUA}[T - TR_{SUA}]) \quad (4\text{-}66)$$

K_{SU} = dissolution rate of particulate biogenic silica at TR_{SUA} (day^{-1})
KT_{SUA} = effect of temperature on dissolution of particulate biogenic silica ($^{\circ}C^{-1}$)
TR_{SUA} = reference temperature for dissolution of particulate biogenic silica ($^{\circ}C$).

4.8 Chemical Oxygen Demand

In the present model, chemical oxygen demand is the concentration of reduced substances that are oxidizable through inorganic means. The source of chemical oxygen demand in saline water is sulfide released from sediments. A cycle occurs in which sulfate is reduced to sulfide in the sediments and reoxidized to sulfate in the water column. In fresh water, methane is released to the water column by the sediment process model. Both sulfide and methane are quantified in units of oxygen demand and are treated with the same kinetic formulation. The kinetic equation, including external loads, if any, is:

$$\frac{\partial COD}{\partial t} = -\frac{DO}{KH_{COD} + DO} KCOD \cdot COD + \frac{BFCOD}{\Delta z} + \frac{WCOD}{V} \quad (4\text{-}67)$$

COD = concentration of chemical oxygen demand (g O_2-equivalents m^{-3})
KH_{COD} = half-saturation constant of dissolved oxygen required for oxidation of chemical oxygen demand (g O_2 m^{-3})
KCOD = oxidation rate of chemical oxygen demand (day^{-1})
BFCOD = sediment flux of chemical oxygen demand (g O_2-equivalents m^{-2} day^{-1}), applied to bottom layer only
WCOD = external loads of chemical oxygen demand (g O_2-equivalents day^{-1}).

An exponential function is used to describe the temperature effect on the oxidation rate of chemical oxygen demand:

$$KCOD = K_{CD} \cdot \exp(KT_{COD}[T - TR_{COD}]) \quad (4\text{-}68)$$

K_{CD} = oxidation rate of chemical oxygen demand at TR_{COD} (day^{-1})
KT_{COD} = effect of temperature on oxidation of chemical oxygen demand ($^{\circ}C^{-1}$)
TR_{COD} = reference temperature for oxidation of chemical oxygen demand ($^{\circ}C$).

4.9 Dissolved Oxygen

Sources and sinks of dissolved oxygen in the water column included in the model are (Fig. 4-1):

- algal photosynthesis and respiration
- nitrification
- heterotrophic respiration of dissolved organic carbon
- oxidation of chemical oxygen demand
- surface reaeration for the surface layer only
- sediment oxygen demand for the bottom layer only
- external loads.

The kinetic equation describing these processes is:

$$\frac{\partial DO}{\partial t} = \sum_{x=c,d,g,m} \left((1.3 - 0.3 \cdot PN_x) P_x - (1 - FCD_x) \frac{DO}{KHR_x + DO} BM_x \right) AOCR \cdot B_x$$

$$- AONT \cdot Nit \cdot NH4 - AOCR \cdot K_{HR} \cdot DOC - \frac{DO}{KH_{COD} + DO} KCOD \cdot COD$$

$$+ K_r (DO_s - DO) + \frac{SOD}{\Delta z} + \frac{WDO}{V} \qquad (4\text{-}69)$$

AONT = mass of dissolved oxygen consumed per unit mass of ammonium nitrogen nitrified (4.33 g O_2 per g N; see Section 4.9.2)

AOCR = dissolved oxygen-to-carbon ratio in respiration (2.67 g O_2 per g C; see Section 4.9.1)

K_r = reaeration coefficient (day^{-1}): the reaeration term is applied to the surface layer only

DO_s = saturated concentration of dissolved oxygen (g O_2 m^{-3})

SOD = sediment oxygen demand (g O_2 m^{-2} day^{-1}), applied to the bottom layer only; positive is to the water column

WDO = external loads of dissolved oxygen (g O_2 day^{-1}).

The two sink terms in Eq. 4-69, heterotrophic respiration and chemical oxygen demand, are explained in Section 4.4.4 (Eq. 4-29) and Section 4.8 (Eq. 4-67), respectively. The remainder of this section explains the effects of algae, nitrification, and surface reaeration.

4.9.1 Effect of Algae on Dissolved Oxygen

The first line on the RHS of Eq. 4-69 accounts for the effects of algae on dissolved oxygen. Algae produce oxygen through photosynthesis and consume oxygen through respiration. The quantity produced depends on the form of nitrogen utilized for growth. Equations describing production of dissolved oxygen are (Morel 1983):

$$106\,CO_2 + 16\,NH_4^+ + H_2PO_4^- + 106\,H_2O \rightarrow protoplasm + 106\,O_2 + 15\,H^+ \quad (4\text{-}70)$$

$$106\,CO_2 + 16\,NO_3^- + H_2PO_4^- + 122\,H_2O + 17\,H^+ \rightarrow protoplasm + 138\,O_2 \quad (4\text{-}71)$$

When ammonium is the nitrogen source, one mole of oxygen is produced per mole of carbon dioxide fixed. When nitrate is the nitrogen source, 1.3 moles of oxygen are produced per mole of carbon dioxide fixed. The quantity, $(1.3 - 0.3 \cdot PN_x)$, in the first term of Eq. 4-69 is the photosynthesis ratio and represents the molar quantity of oxygen produced per mole of carbon dioxide fixed. It approaches unity as the algal preference for ammonium approaches unity.

The last term in the first line of Eq. 4-69 accounts for the oxygen consumption due to algal respiration (Eq. 4-26). A simple representation of respiration process is:

$$CH_2O + O_2 = CO_2 + H_2O \quad (4\text{-}72)$$

from which, AOCR = 2.67 g O_2 per g C.

4.9.2 Effect of Nitrification on Dissolved Oxygen

The stoichiometry of nitrification reaction (Eq. 4-58) indicates that two moles of oxygen are required to nitrify one mole of ammonium into nitrate. However, cell synthesis by nitrifying bacteria is accomplished by the fixation of carbon dioxide so that less than two moles of oxygen are consumed per mole ammonium utilized (Wezernak and Gannon 1968), i.e., AONT = 4.33 g O_2 per g N.

4.9.3 Effect of Surface Reaeration on Dissolved Oxygen

The reaeration rate of dissolved oxygen at the air-water interface is proportional to the oxygen gradient across the interface, $(DO_s - DO)$, when assuming the air is saturated with oxygen. The saturated concentration of dissolved oxygen, which decreases as temperature and salinity increase, is specified using an empirical formula (Genet et al. 1974):

$$DO_s = 14.5532 - 0.38217 \cdot T + 5.4258 \times 10^{-3} \cdot T^2 - CL \cdot (1.665 \times 10^{-4} - 5.866 \times 10^{-6} \cdot T + 9.796 \times 10^{-8} \cdot T^2) \quad (4\text{-}73)$$

CL = chloride concentration (mg/L) = S/1.80655.

The reaeration coefficient includes the effect of turbulence generated by bottom friction (O'Connor and Dobbins 1958) and that by surface wind stress (Banks and Herrera 1977):

$$K_r = \left(K_{ro} \sqrt{\frac{u_{eq}}{h_{eq}}} + W_{rea} \right) \frac{1}{\Delta z} \cdot KT_r^{T-20} \quad (4\text{-}74)$$

K_{ro} = proportionality constant = 3.933 in MKS unit

u_{eq} = weighted velocity over cross-section (m sec^{-1}) = $\sum(u_k V_k)/\sum(V_k)$

h_{eq} = weighted depth over cross-section (m) = $\sum(V_k)/B_\eta$

B_η = width at the free surface (m)

W_{rea} = wind-induced reaeration (m day^{-1})

$$= 0.728 U_w^{½} - 0.317 U_w + 0.0372 U_w^2 \quad (4\text{-}75)$$

U_w = wind speed (m sec^{-1}) at the height of 10 m above surface

KT_r = constant for temperature adjustment of DO reaeration rate.

4.10 Total Active Metal

The present model requires simulation of total active metal for adsorption of phosphate and silica if that option is chosen (Fig. 4-1). The total active metal state variable is the sum of iron and manganese concentrations, both particulate and dissolved. In the model, the origin of total active metal is benthic sediments. Since sediment release of metal is not explicit in the sediment model (see Chapter 5), release is specified in the kinetic portion of the water column model. The only other term included is settling of the particulate fraction. Then the kinetic equation for total active metal, including external loads, if any, may be written as:

$$\frac{\partial TAM}{\partial t} = \frac{KHbmf}{KHbmf + DO} \frac{BFTAM}{\Delta z} e^{Ktam(T - Ttam)} + \frac{\partial}{\partial z}(WS_s \cdot TAMp) + \frac{WTAM}{V} \quad (4\text{-}76)$$

TAM = total active metal concentration (mol m^{-3}) = TAMd + TAMp (4-77)

TAMd = dissolved total active metal (mol m^{-3})

TAMp= particulate total active metal (mol m^{-3})

KHbmf = dissolved oxygen concentration at which total active metal release is half the anoxic release rate (g O_2 m^{-3})

BFTAM = anoxic release rate of total active metal (mol m^{-2} day^{-1}), applied to the bottom layer only

Ktam = effect of temperature on sediment release of total active metal ($^\circ C^{-1}$)

Ttam = reference temperature for sediment release of total active metal ($^\circ C$)

WS_s = settling velocity of particulate metal (m day^{-1})

WTAM = external loads of total active metal (mol day^{-1}).

In estuaries, iron and manganese exist in particular and dissolved forms depending on dissolved oxygen concentration. In the oxygenated water, most of the iron and manganese exist as particulate while under anoxic conditions, large fractions are dissolved, although solid-phase sulfides and carbonates exist and may predominate. The partitioning between particulate and dissolved phases is expressed using

a concept that total active metal concentration must achieve a minimum level, which is a function of dissolved oxygen, before precipitation occurs:

$$TAMd = minimum\{TAMdmx \cdot \exp(-Kdotam \cdot DO) \ , \ TAM\} \tag{4-78}$$

$$TAMp = TAM - TAMd \tag{4-79}$$

TAMdmx = solubility of total active metal under anoxic conditions (mol m^{-3})

Kdotam = constant that relates total active metal solubility to dissolved oxygen (per g O_2 m^{-3}).

4.11 Fecal Coliform Bacteria

Fecal coliform bacteria are indicative of organisms from the intestinal tract of humans and other animals and can be used as an indicator bacteria as a measure of public health (Thomann and Mueller 1987). In the present model, fecal coliform bacteria have no interaction with other state variables, and have only one sink term, die-off. The kinetic equation, including external loads, may be written as:

$$\frac{\partial FCB}{\partial t} = - KFCB \cdot TFCB^{T-20} \cdot FCB + \frac{WFCB}{V} \tag{4-80}$$

FCB = bacteria concentration (MPN per 100 ml)

KFCB = first order die-off rate at 20°C (day^{-1})

TFCB = effect of temperature on decay of bacteria ($°C^{-1}$)

WFCB = external loads of fecal coliform bacteria (MPN per 100 ml m^3 day^{-1}).

4.12 Method of Solution

The kinetic equations for the 21 state variables in the EFDC water column water quality model can be expressed in a 21 × 21 matrix after linearizing some terms, mostly Monod type expressions:

$$\frac{\partial}{\partial t}[C] = [K] \cdot [C] + [R] \tag{4-81}$$

where [C] is in mass $volume^{-1}$, [K] is in $time^{-1}$, and [R] is in mass $volume^{-1}$ $time^{-1}$. Since the settling of particulate matter from the overlying cell acts as an input for a given cell, when Eq. 4-81 is applied to a cell of finite volume, it may be expressed as:

$$\frac{\partial}{\partial t}[C]_k = [K1]_k \cdot [C]_k + \lambda \cdot [K2]_k \cdot [C]_{k+1} + [R]_k \tag{4-82}$$

where the four matrices [C], [K1], [K2], and [R] are defined in Appendix A of Park et al. (1995). The subscript k designates a cell at the k^{th} vertical layer. The layer index k increases upward with KC vertical layers; k = 1 is the bottom layer and k = KC is the surface layer. Then $\lambda = 0$ for k = KC; otherwise,

$\lambda = 1$. The matrix [K2] is a diagonal matrix, and the non-zero elements account for the settling of particulate matter from the overlying cell.

Equation 4-82 is solved using a second-order accurate trapezoidal scheme over a time step of θ, which may be expressed as:

$$[C]_k^N = \left([I] - \frac{\theta}{2}[K1]_k^O \right)^{-1} \cdot \left([C]_k^O + \frac{\theta}{2}\left\{ [K1]_k^O \cdot [C]_k^O + \lambda [K2]_k^O \cdot [C]_{k+1}^A \right\} + \theta [R]_k^O \right) \quad (4\text{-}83)$$

where $\theta = 2 \cdot m \cdot \Delta t$ is the time step for the kinetic equations; [I] is a unit matrix; $[C]^A = [C]^N + [C]^O$; the superscripts O and N designate the variables before and after being adjusted for the relevant kinetic processes. Since Eq. 4-83 is solved from the surface layer downward, the term with $[C]_{k+1}{}^A$ is known for the k^{th} layer and thus placed on the RHS. In Eq. 4-83, inversion of a matrix can be avoided if the 21 state variables are solved in a proper order. The kinetic equations are solved in the order of the variables in the matrix [C] defined in Appendix A of Park et al. (1995).

4.13 Macroalgae (Periphyton) State Variable

The EFDC water quality model was augmented to represent benthic attached algae (often referred to as macroalgae in estuarine waters and periphyton in fresh waters) using the existing framework for phytoplankton growth kinetics. Mathematical relationships based on the impacts of temperature, available light, available nutrients, stream velocity, and density-dependent interactions were incorporated into the algae growth kinetics framework within EFDC. The major differences between modeling techniques for attached and free-floating algae are: (1) attached algae are expressed in terms of areal densities rather than volumetric concentrations; (2) attached algae growth can be limited by the availability of bottom substrate; (3) the availability of nutrients to the macroalgae matrix can be influenced by stream velocity; and (4) macroalgae are not subject to hydrodynamic transport. A good description of periphyton kinetics as it relates to water quality modeling can be found in Warwick et al. (1997) and has been used to develop this section of the report.

A mass-balance approach was used to model macroalgae growth, with carbon serving as the measure of standing crop size or biomass. For each model grid cell the equation for macroalgae growth is slightly different than the one for free-floating algae (Eq. 4-6):

$$P_m = PM_m \cdot f_1(N) \cdot f_2(I) \cdot f_3(T) \cdot f_4(V) \cdot f_5(D) \quad (4\text{-}84)$$

where

Pm_m = maximum growth rate under optimal conditions for macroalgae

$f_1(N)$ = effect of suboptimal nutrient concentration ($0 \le f_1 \le 1$)

$f_2(I)$ = effect of suboptimal light intensity ($0 \le f_2 \le 1$)

$f_3(T)$ = effect of suboptimal temperature ($0 \le f_3 \le 1$)

$f_4(V)$ = velocity limitation factor ($0 \le f_4 \le 1$)

$f_5(D)$ = density-dependent growth rate reduction factor ($0 \le f_5 \le 1$).

The basic growth kinetics for macroalgae were developed from those supplied by EFDC and others developed by Runke (1985). The macroalgae population as a whole is characterized by the total biomass present without considering the different species and their associated environmental processes. The optimum growth for the given temperature is adjusted for light, nutrients, velocity, and density-dependent limitations. Each growth limitation factor can vary from 0 to 1. A value of 1 indicates the factor does not limit growth, and a value of 0 means the factor is so severely limiting that growth is stopped entirely (Bowie et al. 1985).

Stream velocity has a twofold effect on periphyton productivity in freshwater streams: velocity increases to a certain level to enhance biomass accrual, but further increases result in substantial scouring (Horner et al. 1990). A benthic algal population is typified as a plant community with an understory and an overstory. The entire community is called a matrix. As the matrix develops, the periphyton community is composed of an outer layer of photosynthetically active cells and inner layers of senescent and decomposing cells. Layering can also develop among different species of periphyton. Environmental conditions within the matrix are altered by the physical structure of the periphyton. This influences nutrient uptake and primary production rates of the algae (Sand-Jensen 1983). Above a certain level, current has a simulating effect on periphyton metabolism by mixing the overlying waters with nutrient-poor waters that develop around cells (Whitford and Schumacher 1964). The physical structure of the periphyton community and nutrient uptake by periphyton interfere with nutrient flux through the microbial matrix (Stevenson and Glover 1993).

Current is constantly scouring periphyton from its substrate. At high enough velocities, shear stress can result in substantial biomass reduction. Even at low velocities, sudden increases in velocity raise instantaneous loss rates substantially, but these high rates persist only briefly (Horner et al. 1990). An increase in velocity above that to which benthic algae are accustomed leads to increased loss rates and temporarily reduced biomass. However, recolonization and growth after biomass reduction are usually rapid. The effects of suboptimal velocity upon growth rate are represented in the model by a velocity limitation function. Two options are available in the model for specifying the velocity limitation: (1) a Michaelis-Menton (or Monod) equation (4-85) and (2) a five-parameter logistic function (4-86). The Monod equation limits macroalgae growth due to low velocities, whereas the five-parameter logistic function can be configured to limit growth due to either low or high velocities (Figure 4-2).

Velocity limitation option 1, the Michaelis-Menton equation, is written as follows:

$$f_4(V) = \frac{U}{KMV + U} \tag{4-85}$$

where

U = stream velocity (m/sec)
KMV = half-saturation velocity (m/sec)

Velocity limitation option 2, the five-parameter logistic function is as follows:

$$f_4(V) = d + \frac{a - d}{[\ 1 + (\frac{U}{c})^b\ ]^e} \tag{4-86}$$

where

U = stream velocity (m/sec)
a = asymptote at minimum x
b = slope after asymptote a
c = x-translation
d = asymptote at maximum x
e = slope before asymptote d

The half-saturation velocity in Eq. 4-85 is the velocity at which half the maximum growth rate occurs. This effect is analogous to the nutrient limitation because the effect of velocity at suboptimal levels on periphyton growth is due to increasing the exchange of nutrients between the algal matrix and the overlying water (Runke 1985). However, this formula can be too limiting at low velocities. This function does not allow periphyton growth in still waters, but periphyton does grow in still waters such as lakes. Therefore, the function is applied only at velocities above a minimum threshold level (KMVmin). When velocities are at or below this lower level, the limitation function is applied at the minimum level. Above this velocity, the current produces a steeper diffusion gradient around the periphyton (Whitford and Schumacher 1964). A minimum formulation is used to combine the limiting factors for nitrogen, phosphorus, and velocity. The most severely limiting factor alone limits periphyton growth. Note that Eq. 4-86 can be configured so that low velocities are limiting by setting parameter *d* greater than parameter *a*, and viceversa to limit growth due to high velocities. In waters that are rich in nutrients, low velocities will not limit growth. However, high velocities may cause scouring and detachment of the macroalgae, resulting in a reduction in biomass. The five-parameter logistic function can be configured to approximate this reduction by limiting growth at high velocities.

Macroalgae (periphyton) growth can also be limited by the availability of suitable substrate (Ross 1983). Macroalgae communities reach maximum rates of primary productivity at low levels of

biomass (McIntire 1973; Pfeifer and McDiffett 1975). The relationship between standing crop and production employs the Michaelis-Menton kinetic equation:

$$f_5(D) = \frac{KBP}{KBP + P_m} \tag{4-87}$$

where

KBP = half-saturation biomass level (g C/m^2)
P_m = macroalgae biomass level (g C/m^2).

The half-saturation biomass level (KBP) is the biomass at which half the maximum growth rate occurs. Caupp et al. (1991) used a KBP value of 5.0 g C/m^2 (assuming 50% of ash free dry mass is carbon) for a region of the Truckee River system in California. The function in Eq. 4-87 allows maximum rates of primary productivity at low levels of biomass with decreasing rates of primary productivity as the community matrix expands.

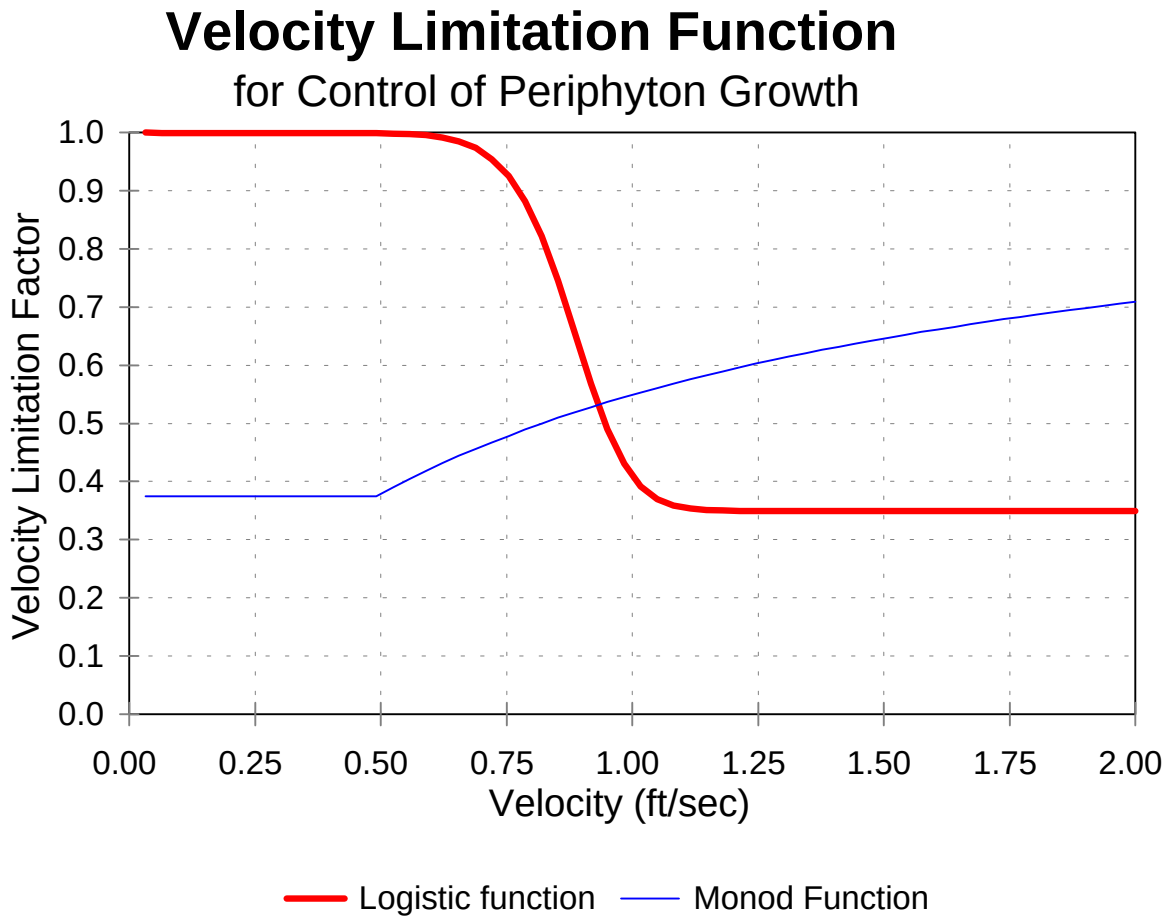

Figure 4-2. Velocity limitation function for (Option 1) the Monod equation where KMV = 0.25 m/sec and KMVmin=0.15 m/sec, and (Option 2) the five-parameter logistic function where *a*=1.0, **b**=12.0, *c*=0.3, *d*=0.35, and e=*3*.0 (high velocities are limiting).

5 - EFDC SEDIMENT PROCESS MODEL

A sediment process model developed by DiToro and Fitzpatrick (1993; hereinafter referred to as D&F) and was coupled with CE-QUAL-ICM for Chesapeake Bay water quality modeling (Cerco and Cole 1993). The sediment process model was slightly modified and incorporated into the EFDC water quality model to simulate the processes in the sediment and at the sediment-water interface. The description of the EFDC sediment process model in this section is from Park et al. (1995). The sediment process model has 27 water-quality related state variables and fluxes (Table 5-1).

Table 5-1. EFDC sediment process model state variables and flux terms

(1) particulate organic carbon G1 class in layer 2	(15) nitrate nitrogen in layer 1
(2) particulate organic carbon G2 class in layer 2	(16) nitrate nitrogen in layer 2
(3) particulate organic carbon G3 class in layer 2	(17) phosphate phosphorus in layer 1
(4) particulate organic nitrogen G1 class in layer 2	(18) phosphate phosphorus in layer 2
(5) particulate organic nitrogen G2 class in layer 2	(19) available silica in layer 1
(6) particulate organic nitrogen G3 class in layer 2	(20) available silica in layer 2
(7) particulate organic phosphorus G1 class in layer 2	(21) ammonia nitrogen flux
(8) particulate organic phosphorus G2 class in layer 2	(22) nitrate nitrogen flux
(9) particulate organic phosphorus G3 class in layer 2	(23) phosphate phosphorus flux
(10) particulate biogenic silica in layer 2	(24) silica flux
(11) sulfide/methane in layer 1	(25) sediment oxygen demand
(12) sulfide/methane in layer 2	(26) release of chemical oxygen demand
(13) ammonia nitrogen in layer 1	(27) sediment temperature
(14) ammonia nitrogen in layer 2	

The nitrate state variables, (15), (16), and (22), in the model represent the sum of nitrate and nitrite nitrogen. The three G classes for particulate organic matter (POM) in Layer 2 and the two layers for inorganic substances are described below.

In the sediment model, benthic sediments are represented as two layers (Fig. 5-1). The upper layer (Layer 1) is in contact with the water column and may be oxic or anoxic depending on dissolved oxygen concentration in the overlying water. The lower layer (Layer 2) is permanently anoxic. The upper layer depth, which is determined by the penetration of oxygen into the sediments, is at its maximum only a small fraction of the total depth. Because H_1 (~ 0.1 cm) « H_2,

$$H = H_1 + H_2 \approx H_2 \tag{5-1}$$

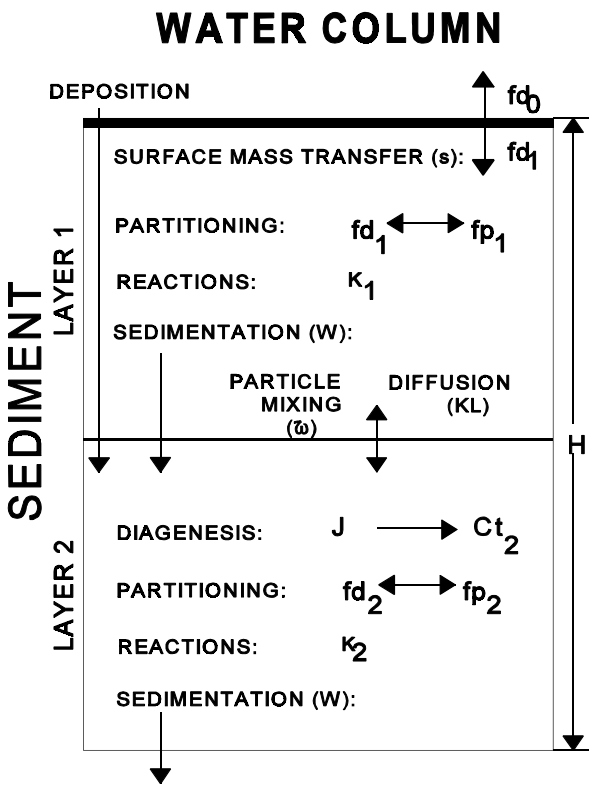

Figure 5-1. Sediment layers and processes included in sediment process model.

where H is the total depth (approximately 10 cm), H_1 is the upper layer depth and H_2 is the lower layer depth.

The model incorporates three basic processes (Fig. 5-2): (1) depositional flux of POM, (2) the diagenesis of POM, and (3) the resulting sediment flux. The sediment model is driven by net settling of particulate organic carbon, nitrogen, phosphorus, and silica from the overlying water to the sediments (**depositional flux**). Because of the negligible thickness of the upper layer (Eq. 5-1), deposition is considered to proceed from the water column directly to the lower layer. Within the lower layer, the model simulates the diagenesis (mineralization or decay) of deposited POM, which produces oxygen demand and inorganic nutrients (**diagenesis flux**). The third basic process is the flux of substances produced by diagenesis (**sediment flux**). Oxygen demand, as sulfide (in salt water) or methane (in fresh water), takes three paths out of the sediments: (1) oxidation at the sediment-water interface as sediment oxygen demand, (2) export to the water column as chemical oxygen demand, or (3) burial to deep,

inactive sediments. Inorganic nutrients produced by diagenesis take two paths out of the sediments: (1) release to the water column or (2) burial to deep, inactive sediments (Fig. 5-2).

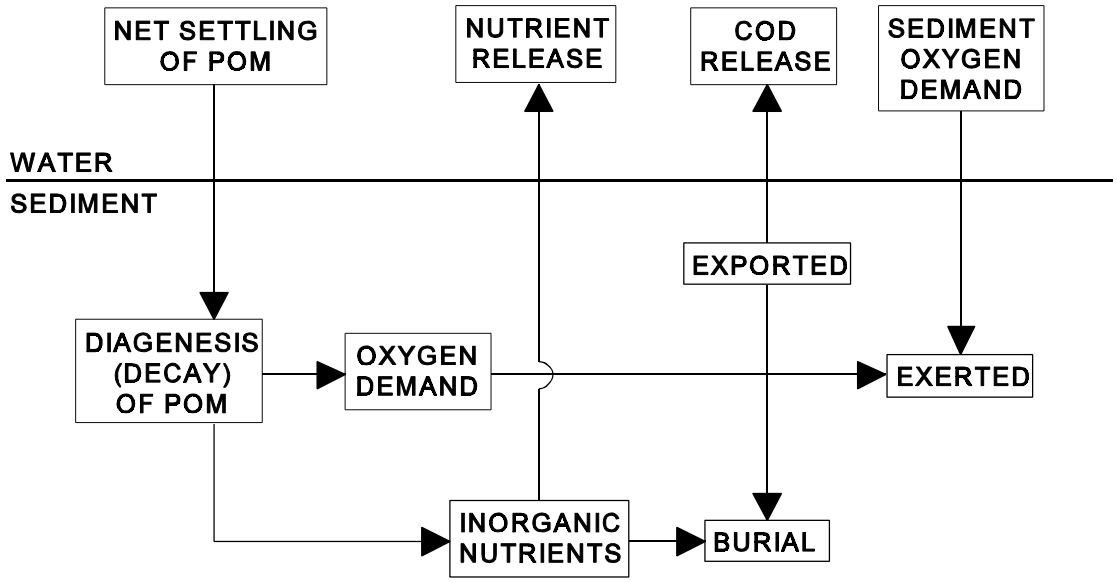

Figure 5-2. Schematic diagram for sediment process model.

This section describes the three basic processes with reactions and sources/sinks for each state variable. The method of solution includes finite difference equations, solution scheme, boundary, and initial conditions. Complete model documentation can be found in D&F (1993).

5.1 Depositional Flux

Deposition is one process that couples the water column model with the sediment model. Consequently, deposition is represented in both the water column and sediment models. In the water column model, the governing mass-balance equations for the following state variables contain settling terms, which represent the depositional fluxes:

- three algal groups, cyanobacteria, diatoms and green algae (Eq. 4-5)
- refractory and labile particulate organic carbon (Equations 4-20 and 4-21)
- refractory and labile particulate organic phosphorus (Equations 4-35 and 4-36) and total phosphate (Eq. 4-38)
- refractory and labile particulate organic nitrogen (Equations 4-48 and 4-49)
- particulate biogenic silica (Eq. 4-61) and available silica (Eq. 4-62).

The sediment model receives these depositional fluxes of particulate organic carbon (POC), particulate organic nitrogen (PON), particulate organic phosphorus (POP), and particulate biogenic silica (PSi). Because of the negligible thickness of the upper layer (Eq. 5-1), deposition is considered to proceed from the water column directly to the lower layer. Since the sediment model has three G classes of POM, G_i (i = 1, 2, or 3), depending on the time scales of reactivity (Section 5.2), the POM fluxes from the water column should be mapped into three G classes based on their reactivity. Then the depositional fluxes for the i^{th} G class (i = 1, 2, or 3) may be expressed as:

$$J_{POC,i} = FCLP_i \cdot WS_{LP} \cdot LPOC^N + FCRP_i \cdot WS_{RP} \cdot RPOC^N + \sum_{x=c,d,g} FCB_{x,i} \cdot WS_x \cdot B_x^N \quad (5\text{-}2)$$

$$J_{PON,i} = FNLP_i \cdot WS_{LP} \cdot LPON^N + FNRP_i \cdot WS_{RP} \cdot RPON^N + \sum_{x=c,d,g} FNB_{x,i} \cdot ANC_x \cdot WS_x \cdot B_x^N \quad (5\text{-}3)$$

$$J_{POP,i} = FPLP_i \cdot WS_{LP} \cdot LPOP^N + FPRP_i \cdot WS_{RP} \cdot RPOP^N + \sum_{x=c,d,g} FPB_{x,i} \cdot APC \cdot WS_x \cdot B_x^N + \gamma_i \cdot WS_{TSS} \cdot PO4p^N \quad (5\text{-}4)$$

$$J_{PSi} = WS_d \cdot SU^N + ASC_d \cdot WS_d \cdot B_d^N + WS_{TSS} \cdot SAp^N \quad (5\text{-}5)$$

$J_{POM,i}$ = depositional flux of POM (M = C, N or P) routed into the i^{th} G class (g m^{-2} day^{-1})

J_{PSi} = depositional flux of PSi (g Si m^{-2} day^{-1})

$FCLP_i$, $FNLP_i$, $FPLP_i$ = fraction of water column labile POC, PON, and POP, respectively, routed into the i^{th} G class in sediment

$FCRP_i$, $FNRP_i$, $FPRP_i$ = fraction of water column refractory POC, PON, and POP, respectively, routed into the i^{th} G class in sediment

$FCB_{x,i}$, $FNB_{x,i}$, $FPB_{x,i}$ = fraction of POC, PON, and POP, respectively, in the algal group x routed into the i^{th} G class in sediment

γ_i = 1 for i = 1

0 for i = 2 or 3.

In the source code, the sediment process model is solved after the water column water quality model, and the calculated fluxes using the water column conditions at $t = t_n$ are used for the computation of the water quality variables at $t = t_n + \theta$. The superscript N indicates the variables after being updated for the kinetic processes, as defined in Eq. 4-82.

The settling of sorbed phosphate is considered to contribute to the labile G_1 pool in Eq. 5-4, and settling of sorbed silica contributes to J_{PSi} in Eq. 5-5 to avoid creation of additional depositional fluxes

for inorganic particulates. The sum of distribution coefficients should be unity: $\sum_i FCLP_i = \sum_i FNLP_i = \sum_i FPLP_i = \sum_i FCRP_i = \sum_i FNRP_i = \sum_i FPRP_i = \sum_i FCB_{x,i} = \sum_i FNB_{x,i} = \sum_i FPB_{x,i} = 1$. The settling velocities, WS_{LP}, WS_{RP}, WS_x, and WS_{TSS}, as defined in the EFDC water column model (Section 4), are net settling velocities. If total active metal is selected as a measure of sorption site, WS_{TSS} is replaced by WS_s in Equations 5-4 and 5-5 (see Sections 4.5 and 4.7).

5.2 Diagenesis Flux

Another coupling point of the sediment model to the water column model is the sediment flux, which is described in Section 5.3. The computation of sediment flux requires that the magnitude of the diagenesis flux be known. The diagenesis flux is explicitly computed using mass-balance equations for deposited POC, PON, and POP. (Dissolved silica is produced in the sediments as the result of the dissolution of PSi. Since the dissolution process is different from the bacterial-mediated diagenesis process, it is presented separately in Section 5.4.) In the mass-balance equations, the depositional fluxes of POM are the source terms and the decay of POM in the sediments produces the diagenesis fluxes. The integration of the mass-balance equations for POM provides the diagenesis fluxes that are the inputs for the mass-balance equations for ammonium, nitrate, phosphate, and sulfide/methane in the sediments (Section 5.3).

The difference in decay rates of POM is accounted for by assigning a fraction of POM to various decay classes (Westrisch and Berner 1984). POM in the sediments is divided into three G classes, or fractions, representing three scales of reactivity. The G_1 (labile) fraction has a half life of 20 days, and the G_2 (refractory) fraction has a half life of one year. The G_3 (inert) fraction is nonreactive, i.e., it undergoes no significant decay before burial into deep, inactive sediments. The varying reactivity of the G classes controls the time scale over which changes in depositional flux will be reflected in changes in diagenesis flux. If the G_1 class would dominate the POM input into the sediments, then there would be no significant time lag introduced by POM diagenesis and any changes in depositional flux would be readily reflected in diagenesis flux.

Because the upper layer thickness is negligible (Eq. 5-1) and thus depositional flux is considered to proceed directly to the lower layer (Equations 5-2 to 5-5), diagenesis is considered to occur in the lower layer only. The mass-balance equations are similar for POC, PON, and POP, and for different G classes. The mass-balance equation in the anoxic lower layer for the i^{th} G class (i = 1, 2, or 3) may be expressed as:

$$H_2 \frac{\partial G_{POM,i}}{\partial t} = - K_{POM,i} \cdot \theta_{POM,i}^{T-20} \cdot G_{POM,i} \cdot H_2 - W \cdot G_{POM,i} + J_{POM,i} \quad (5\text{-}6)$$

$G_{POM,i}$ = concentration of POM (M = C, N, or P) in the i^{th} G class in Layer 2 (g m^{-3})

$K_{POM,i}$ = decay rate of the i^{th} G class POM at 20 °C in Layer 2 (day^{-1})

$\theta_{POM,i}$ = constant for temperature adjustment for $K_{POM,i}$

T = sediment temperature (°C)

W = burial rate (m day^{-1}).

Since the G_3 class is inert, $K_{POM,3} = 0$.

Once the mass-balance equations for $G_{POM,1}$ and $G_{POM,2}$ are solved, the diagenesis fluxes are computed from the rate of mineralization of the two reactive G classes:

$$J_M = \sum_{i=1}^{2} K_{POM,i} \cdot \theta_{POM,i}^{T-20} \cdot G_{POM,i} \cdot H_2 \quad (5\text{-}7)$$

J_M = diagenesis flux (g m^{-2} day^{-1}) of carbon (M = C), nitrogen (M = N), or phosphorus (M = P).

5.3 Sediment Flux

The mineralization of POM produces soluble intermediates, which are quantified as diagenesis fluxes in the previous section. The intermediates react in the oxic and anoxic layers, and portions are returned to the overlying water as sediment fluxes. Computation of sediment fluxes requires mass-balance equations for ammonium, nitrate, phosphate, sulfide/methane, and available silica. This section describes the flux portion for ammonium, nitrate, phosphate, and sulfide/methane of the model. Available silica is described in Section 5.4.

In the upper layer, the processes included in the flux portion are (Fig. 5-1)

- exchange of dissolved fraction between Layer 1 and the overlying water
- exchange of dissolved fraction between Layer 1 and 2 via diffusive transport
- exchange of particulate fraction between Layer 1 and 2 via particle mixing
- loss by burial to the lower layer (Layer 2)
- removal (sink) by reaction
- internal sources.

Since the upper layer is quite thin, $H_1 \sim 0.1$ cm (Eq. 5-1) and the surface mass transfer coefficient (s) is on the order of 0.1 m day^{-1}, then the residence time in the upper layer is $H_1/s \sim 10^{-2}$ days. Hence, a

steady-state approximation is made in the upper layer. Then the mass-balance equation for ammonium, nitrate, phosphate, or sulfide/methane in the upper layer is:

$$H_1 \frac{\partial Ct_1}{\partial t} = 0 = s(fd_0 \cdot Ct_0 - fd_1 \cdot Ct_1) + KL(fd_2 \cdot Ct_2 - fd_1 \cdot Ct_1) + \omega(fp_2 \cdot Ct_2 - fp_1 \cdot Ct_1) - W \cdot Ct_1 - \frac{\kappa_1^2}{s} Ct_1 + J_1 \quad (5\text{-}8)$$

Ct_1 & Ct_2 = total concentrations in Layer 1 and 2, respectively (g m^{-3})

Ct_o = total concentration in the overlying water (g m^{-3})

s = surface mass transfer coefficient (m day^{-1})

KL = diffusion velocity for dissolved fraction between Layer 1 and 2 (m day^{-1})

ω = particle mixing velocity between Layer 1 and 2 (m day^{-1})

fd_o = dissolved fraction of total substance in the overlying water ($0 \le fd_o \le 1$)

fd_1 = dissolved fraction of total substance in Layer 1 ($0 \le fd_1 \le 1$)

fp_1 = particulate fraction of total substance in Layer 1 (= 1 - fd_1)

fd_2 = dissolved fraction of total substance in Layer 2 ($0 \le fd_2 \le 1$)

fp_2 = particulate fraction of total substance in Layer 2 (= 1 - fd_2)

κ_1 = reaction velocity in Layer 1 (m day^{-1})

J_1 = sum of all internal sources in Layer 1 (g m^{-2} day^{-1}).

The first term on the RHS of Eq. 5-8 represents the exchange across sediment-water interface. Then the sediment flux from Layer 1 to the overlying water, which couples the sediment model to the water column model, may be expressed as:

$$J_{aq} = s(fd_1 \cdot Ct_1 - fd_o \cdot Ct_o) \quad (5\text{-}9)$$

J_{aq} = sediment flux of ammonium, nitrate, phosphate, or sulfide/methane to the overlying water (g m^{-2} day^{-1}).

The convention used in Eq. 5-9 is that positive flux is from the sediment to the overlying water.

In the lower layer, the processes included in the flux portion are (Fig. 5-1)

- exchange of dissolved fraction between Layer 1 and 2 via diffusive transport
- exchange of particulate fraction between Layer 1 and 2 via particle mixing
- deposition from Layer 1 and burial to the deep inactive sediments
- removal (sink) by reaction
- internal sources including diagenetic source.

The mass-balance equation for ammonium, nitrate, phosphate or sulfide/methane in the lower layer is:

$$H_2 \frac{\partial Ct_2}{\partial t} = - KL(fd_2 \cdot Ct_2 - fd_1 \cdot Ct_1) - \omega(fp_2 \cdot Ct_2 - fp_1 \cdot Ct_1)$$

$$+ W(Ct_1 - Ct_2) - \kappa_2 \cdot Ct_2 + J_2 \qquad (5\text{-}10)$$

κ_2 = reaction velocity in Layer 2 (m day^{-1})

J_2 = sum of all internal sources including diagenesis in Layer 2 (g m^{-2} day^{-1}).

The substances produced by mineralization of POM in sediments may be present in both dissolved and particulate phases. This distribution directly affects the magnitude of the substance that is returned to the overlying water. In Equations 5-8 to 5-10, the distribution of a substance between the dissolved and particulate phases in a sediment is parameterized using a linear partitioning coefficient. The dissolved and particulate fractions are computed from the partitioning equations:

$$fd_1 = \frac{1}{1 + m_1 \cdot \pi_1} \qquad fp_1 = 1 - fd_1 \qquad (5\text{-}11)$$

$$fd_2 = \frac{1}{1 + m_2 \cdot \pi_2} \qquad fp_2 = 1 - fd_2 \qquad (5\text{-}12)$$

m_1, m_2 = solid concentrations in Layer 1 and 2, respectively (kg L^{-1})

π_1, π_2 = partition coefficients in Layer 1 and 2, respectively (per kg L^{-1}).

The partition coefficient is the ratio of particulate to dissolved fraction per unit solid concentration (i.e., per unit sorption site available).

All terms, except the last two terms, in Equations 5-8 and 5-10 are common to all state variables and are described in Section 5.3.1. The last two terms represent the reaction and source/sink terms, respectively. These terms, which take different mathematical formulations for different state variables, are described in Sections 5.3.2 to 5.3.5 for ammonium, nitrate, phosphate, and sulfide/methane, respectively.

5.3.1 Common Parameters for Sediment Flux

Parameters that are needed for the sediment fluxes are *s*, ω, KL, W, H_2, m_1, m_2, π_1, π_2, κ_1, κ_2, J_1, and J_2 in Equations 5-8 to 5-12. Of these, κ_1, κ_2, J_1, and J_2 are variable-specific. Among the other common parameters, W, H_2, m_1, and m_2, are specified as input. The modeling of the remaining three parameters, *s*, ω, and KL, is described in this section.

5.3.1.1 Surface mass transfer coefficient. Owing to the observation that the surface mass transfer coefficient, *s*, can be related to the sediment oxygen demand, SOD (DiToro et al. 1990), *s* can be estimated from the ratio of SOD and overlying water oxygen concentration:

$$s = \frac{D_1}{H_1} = \frac{SOD}{DO_0} \tag{5-13}$$

D_1 = diffusion coefficient in Layer 1 (m^2 day^{-1}).

Knowing *s*, it is possible to estimate the other model parameters.

5.3.1.2 Particulate phase mixing coefficient. The particle mixing velocity between Layer 1 and 2 is parameterized as:

$$\omega = \frac{D_p \cdot \theta_{Dp}^{T-20}}{H_2} \frac{G_{POC,1}}{G_{POC,R}} \frac{DO_0}{KM_{Dp} + DO_0} \tag{5-14}$$

D_p = apparent diffusion coefficient for particle mixing (m^2 day^{-1})

θ_{Dp} = constant for temperature adjustment for D_p

$G_{POC,R}$ = reference concentration for $G_{POC,1}$ (g C m^{-3})

KM_{Dp} = particle mixing half-saturation constant for oxygen (g O_2 m^{-3}).

The enhanced mixing of sediment particles by macrobenthos (bioturbation) is quantified by estimating D_p. The particle mixing appears to be proportional to the benthic biomass (Matisoff 1982), which is correlated to the carbon input to the sediment (Robbins et al. 1989). This is parameterized by assuming that benthic biomass is proportional to the available labile carbon, $G_{POC,1}$, and $G_{POC,R}$ is the reference concentration at which the particle mixing velocity is at its nominal value. The Monod-type oxygen dependency accounts for the oxygen dependency of benthic biomass.

It has been observed that a hysteresis exists in the relationship between the bottom water oxygen and benthic biomass. Benthic biomass increases as the summer progresses. However, the occurrence of anoxia/hypoxia reduces the biomass drastically and also imposes stress on benthic activities. After full overturn, the bottom water oxygen increases, but the population does not recover immediately. Hence, the particle mixing velocity, which is proportional to the benthic biomass, does not increase in response to the increased bottom water oxygen. Recovery of benthic biomass following hypoxic events depends on many factors including severity and longevity of hypoxia, constituent species, and salinity (Diaz and Rosenberg 1995).

This phenomenon of reduced benthic activities and hysteresis is parameterized based on the idea of stress that low oxygen imposes on the benthic population. It is analogous to the modeling of the toxic effect of chemicals on organisms (Mancini 1983). A first order differential equation is employed, in which the benthic stress (1) accumulates only when overlying oxygen is below KM_{Dp} and (2) is dissipated at a first order rate (Fig. 5-3a):

$$\frac{\partial ST}{\partial t} = - K_{ST} \cdot ST + \left(1 - \frac{DO_0}{KM_{Dp}} \right) \qquad if \quad DO_0 < KM_{Dp}$$

$$\frac{\partial ST}{\partial t} = - K_{ST} \cdot ST \qquad if \quad DO_0 > KM_{Dp} \tag{5-15}$$

ST = accumulated benthic stress (day)

K_{ST} = first order decay rate for ST (day^{-1}).

The behavior of this formulation can be understood by evaluating the steady-state stresses at two extreme conditions of overlying water oxygen, DO_0:

as $DO_0 = 0$ $\quad K_{ST} \cdot ST = 1$ $\quad f(ST) = (1 - K_{ST} \cdot ST) = 0$

as $DO_0 \geq KM_{Dp}$ $\quad K_{ST} \cdot ST = 0$ $\quad f(ST) = (1 - K_{ST} \cdot ST) = 1$

The dimensionless expression, $f(ST) = 1 - K_{ST} \cdot ST$, appears to be the proper variable to quantify the effect of benthic stress on benthic biomass and thus particle mixing (Fig. 5-3b).

The final formulation for the particle mixing velocity, including the benthic stress, is:

$$\omega = \frac{D_p \cdot \theta_{Dp}^{T-20}}{H_2} \frac{G_{POC,1}}{G_{POC,R}} \frac{DO_0}{KM_{Dp} + DO_0} f(ST) + \frac{Dp_{\min}}{H_2} \tag{5-16}$$

Dp_{min} = minimum diffusion coefficient for particle mixing (m^2 day^{-1}).

The reduction in particle mixing due to the benthic stress, f(ST), is estimated by employing the following procedure. The stress, ST, is normally calculated with Eq. 5-15. Once DO_0 drops below a critical concentration, $DO_{ST,c}$, for $NC_{hypoxia}$ consecutive days or more, the calculated stress is not allowed to decrease until t_{MBS} days of $DO_0 > DO_{ST,c}$. That is, only when hypoxic days are longer than critical hypoxia days ($NC_{hypoxia}$), the maximum stress, or minimum ($1 - K_{ST} \cdot ST$), is retained for a specified period (t_{MBS} days) after DO_0 recovery (Fig. 5-3). No hysteresis occurs if DO_0 does not drop below $DO_{ST,c}$ or if hypoxia lasts less than $NC_{hypoxia}$ days. When applying maximum stress for t_{MBS} days, the subsequent hypoxic days are not included in t_{MBS}. This parameterization of hysteresis essentially assumes seasonal

hypoxia, i.e., one or two major hypoxic events during summer, and might be unsuitable for systems with multiple hypoxic events throughout a year.

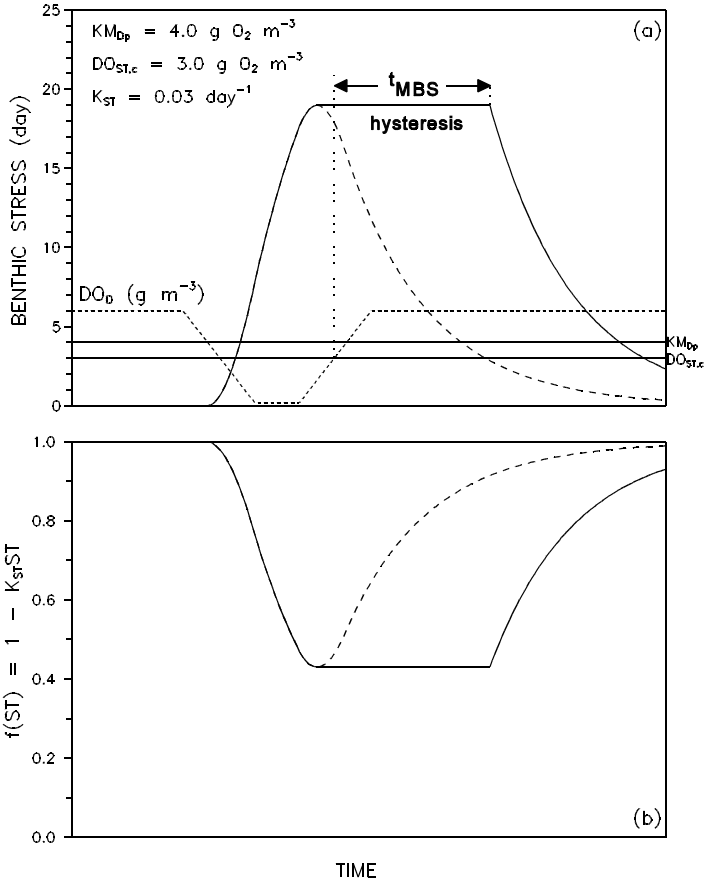

Figure 5-3. Benthic stress (a) and its effect on particle mixing (b) as a function of overlying water column dissolved oxygen concentration.

Three parameters relating to hysteresis, $DO_{ST,c}$, $NC_{hypoxia}$, and t_{MBS}, are functions of many factors including severity and longevity of hypoxia, constituent species, and salinity, and thus have site-specific variabilities (Diaz and Rosenberg 1995). The critical overlying oxygen concentration, $DO_{ST,c}$, also depends on the distance from the bottom of the location of $DO_{0.}$ The critical hypoxia days, $NC_{hypoxia}$, depend on tolerance of benthic organisms to hypoxia and thus on benthic community structure (Diaz and Rosenberg 1995). The time lag for the recovery of benthic biomass following hypoxic events, t_{MBS}, tends to be longer for higher salinity. The above three parameters are considered to be spatially constant input parameters.

5.3.1.3 Dissolved phase mixing coefficient. Dissolved phase mixing between Layer 1 and 2 is via passive molecular diffusion, which is enhanced by the mixing activities of the benthic organisms

(bio-irrigation). This is modeled by increasing the diffusion coefficient relative to the molecular diffusion coefficient:

$$KL = \frac{D_d \cdot \theta_{Dd}^{T-20}}{H_2} + R_{BI,BT} \cdot \omega \tag{5-17}$$

D_d = diffusion coefficient in pore water (m^2 day^{-1})

θ_{Dd} = constant for temperature adjustment for D_d

$R_{BI,BT}$ = ratio of bio-irrigation to bioturbation.

The last term in Eq. 5-17 accounts for the enhanced mixing by organism activities.

5.3.2 Ammonia Nitrogen

Diagenesis is assumed not to occur in the upper layer because of its shallow depth, and ammonium is produced by diagenesis in the lower layer:

$$J_{1,NH4} = 0 \qquad J_{2,NH4} = J_N \quad (from\ Eq.\ 5\text{-}7) \tag{5-18}$$

Ammonium is nitrified to nitrate in the presence of oxygen. A Monod-type expression is used for the ammonium and oxygen dependency of the nitrification rate. Then the oxic layer reaction velocity in Eq. 5-8 for ammonium may be expressed as:

$$\kappa_{1,NH4}^2 = \frac{DO_0}{2 \cdot KM_{NH4,O2} + DO_0} \frac{KM_{NH4}}{KM_{NH4} + NH4_1} \kappa_{NH4}^2 \cdot \theta_{NH4}^{T-20} \tag{5-19}$$

and then the nitrification flux becomes:

$$J_{Nit} = \frac{\kappa_{1,NH4}^2}{s} \cdot NH4_1 \tag{5-20}$$

$KM_{NH4,O2}$ = nitrification half-saturation constant for dissolved oxygen (g O_2 m^{-3})

$NH4_1$ = total ammonium nitrogen concentration in Layer 1 (g N m^{-3})

KM_{NH4} = nitrification half-saturation constant for ammonium (g N m^{-3})

κ_{NH4} = optimal reaction velocity for nitrification at 20°C (m day^{-1})

θ_{NH4} = constant for temperature adjustment for κ_{NH4}

J_{Nit} = nitrification flux (g N m^{-2} day^{-1}).

Nitrification does not occur in the anoxic lower layer:

$$\kappa_{2,NH4} = 0 \tag{5-21}$$

Once Equations 5-8 and 5-10 are solved for $NH4_1$ and $NH4_2$, the sediment flux of ammonium to the overlying water, $J_{aq,NH4}$, can be calculated using Eq. 5-9. Note that it is not $NH4_1$ and $NH4_2$ that determine the magnitude of $J_{aq,NH4}$ (Section X-B-2 in D&F 1993). The magnitude is determined by (1) the diagenesis flux, (2) the fraction that is nitrified, and (3) the surface mass transfer coefficient (*s*) that mixes the remaining portion.

5.3.3 Nitrate Nitrogen

Nitrification flux is the only source of nitrate in the upper layer, and there is no diagenetic source for nitrate in both layers:

$$J_{1,NO3} = J_{Nit} \quad (from\ Eq.\ 5\text{-}19) \qquad J_{2,NO3} = 0 \tag{5-22}$$

Nitrate is present in sediments as dissolved substance, i.e., $\pi_{1,NO3} = \pi_{2,NO3} = 0$, making $fd_{1,NO3} = fd_{2,NO3} = 1$ (Equations 5-11 and 5-12): it also makes $\tilde{\omega}$ meaningless, hence $\tilde{\omega} = 0$. Nitrate is removed by denitrification in both oxic and anoxic layers with the carbon required for denitrification supplied by carbon diagenesis. The reaction velocities in Equations 5-8 and 5-10 for nitrate may be expressed as:

$$\kappa^2_{1,NO3} = \kappa^2_{NO3,1} \cdot \theta^{T-20}_{NO3} \tag{5-23}$$

$$\kappa_{2,NO3} = \kappa_{NO3,2} \cdot \theta^{T-20}_{NO3} \tag{5-24}$$

and the denitrification flux out of sediments as a nitrogen gas becomes:

$$J_{N2(g)} = \frac{\kappa^2_{1,NO3}}{s} NO3_1 + \kappa_{2,NO3} \cdot NO3_2 \tag{5-25}$$

$\kappa_{NO3,1}$ = reaction velocity for denitrification in Layer 1 at 20°C (m day^{-1})
$\kappa_{NO3,2}$ = reaction velocity for denitrification in Layer 2 at 20°C (m day^{-1})
θ_{NO3} = constant for temperature adjustment for $\kappa_{NO3,1}$ and $\kappa_{NO3,2}$
$J_{N2(g)}$ = denitrification flux (g N m^{-2} day^{-1})
$NO3_1$ = total nitrate nitrogen concentration in Layer 1 (g N m^{-3})
$NO3_2$ = total nitrate nitrogen concentration in Layer 2 (g N m^{-3}).

Once Equations 5-8 and 5-10 are solved for $NO3_1$ and $NO3_2$, the sediment flux of nitrate to the overlying water, $J_{aq,NO3}$, can be calculated using Eq. 5-9. The steady-state solution for nitrate showed that the nitrate flux is a linear function of $NO3_0$ (Eq. III-15 in D&F 1993): the intercept quantifies the amount of ammonium in the sediment that is nitrified but not denitrified (thus releases as $J_{aq,NO3}$), and the slope quantifies the extent to which overlying water nitrate is denitrified in the sediment. It also revealed that

if the internal production of nitrate is small relative to the flux of nitrate from the overlying water, the normalized nitrate flux to the sediment, - $J_{aq,NO3}/NO3_0$, is linear in *s* for small *s* and constant for large *s* (Section III-C in D&F 1993). For small *s* (~ 0.01 m day^{-1}), H_1 is large (Eq. 5-13) so that oxic layer denitrification predominates and $J_{aq,NO3}$ is essentially zero independent of $NO3_0$ (Fig. III-4 in D&F 1993).

5.3.4 Phosphate Phosphorus

Phosphate is produced by the diagenetic breakdown of POP in the lower layer:

$$J_{1,PO4} = 0 \qquad J_{2,PO4} = J_P \quad (from\ Eq.\ 5\text{-}7) \tag{5-26}$$

A portion of the liberated phosphate remains in the dissolved form and a portion becomes particulate phosphate, either via precipitation of phosphate-containing minerals (Troup 1974), e.g., vivianite, $Fe_3(PO_4)_2(s)$, or by partitioning to phosphate sorption sites (Lijklema 1980; Barrow 1983; Giordani and Astorri 1986). The extent of particulate formation is determined by the magnitude of the partition coefficients, $\pi_{1,PO4}$ and $\pi_{2,PO4}$, in Equations 5-11 and 5-12. Phosphate flux is strongly affected by DO_0, the overlying water oxygen concentration. As DO_0 approaches zero, the phosphate flux from the sediments increases. This mechanism is incorporated by making $\pi_{1,PO4}$ larger, under oxic conditions, than $\pi_{2,PO4}$. In the model, when DO_0 exceeds a critical concentration, $(DO_0)_{crit,PO4}$, sorption in the upper layer is enhanced by an amount $\Delta\pi_{PO4,1}$:

$$\pi_{1,PO4} = \pi_{2,PO4} \cdot (\Delta\pi_{PO4,1}) \qquad DO_0 > (DO_0)_{crit,PO4} \tag{5-27}$$

When oxygen falls below $(DO_0)_{crit,PO4}$, then:

$$\pi_{1,PO4} = \pi_{2,PO4} \cdot (\Delta\pi_{PO4,1})^{DO_0/(DO_0)_{crit,PO4}} \qquad DO_0 \leq (DO_0)_{crit,PO4} \tag{5-28}$$

which smoothly reduces $\pi_{1,PO4}$ to $\pi_{2,PO4}$ as DO_0 goes to zero. There is no removal reaction for phosphate in both layers:

$$\kappa_{1,PO4} = \kappa_{2,PO4} = 0 \tag{5-29}$$

Once Equations 5-8 and 5-10 are solved for $PO4_1$ and $PO4_2$, the sediment flux of phosphate to the overlying water, $J_{aq,PO4}$, can be calculated using Eq. 5-9.

5.3.5 Sulfide/Methane and Oxygen Demand

5.3.5.1 Sulfide. No diagenetic production of sulfide occurs in the upper layer. In the lower layer, sulfide is produced by carbon diagenesis (Eq. 5-7) decremented by the organic carbon consumed by denitrification (Eq. 5-25). Then:

$$J_{1,H2S} = 0 \qquad J_{2,H2S} = a_{O2,C} \cdot J_C - a_{O2,NO3} \cdot J_{N2(g)} \tag{5-30}$$

$a_{O2,C}$ = stoichiometric coefficient for carbon diagenesis consumed by sulfide oxidation (2.6667 g O_2-equivalents per g C)

$a_{O2,NO3}$ = stoichiometric coefficient for carbon diagenesis consumed by denitrification (2.8571 g O_2-equivalents per g N).

A portion of the dissolved sulfide that is produced in the anoxic layer reacts with the iron to form particulate iron monosulfide, FeS(s) (Morse et al. 1987). The particulate fraction is mixed into the oxic layer where it can be oxidized to ferric oxyhydroxide, Fe_2O_3(s). The remaining dissolved fraction also diffuses into the oxic layer where it is oxidized to sulfate. Partitioning between dissolved and particulate sulfide in the model represents the formation of FeS(s), which is parameterized using partition coefficients, $\pi_{1,H2S}$ and $\pi_{2,H2S}$, in Equations 5-11 and 5-12.

The present sediment model has three pathways for sulfide, the reduced end product of carbon diagenesis: (1) sulfide oxidation, (2) aqueous sulfide flux, and (3) burial. The distribution of sulfide among the three pathways is controlled by the partitioning coefficients and the oxidation reaction velocities (Section V-E in D&F 1993). Both dissolved and particulate sulfide are oxidized in the oxic layer, consuming oxygen in the process. In the oxic upper layer, the oxidation rate that is linear in oxygen concentration is used (Cline and Richards 1969; Millero 1986; Boudreau 1991). In the anoxic lower layer, no oxidation can occur. Then the reaction velocities in Equations 5-8 and 5-10 may be expressed as:

$$\kappa^2_{1,H2S} = \left(\kappa^2_{H2S,d1} \cdot fd_{1,H2S} + \kappa^2_{H2S,p1} \cdot fp_{1,H2S}\right)\theta^{T-20}_{H2S} \frac{DO_0}{2 \cdot KM_{H2S,O2}} \tag{5-31}$$

$$\kappa_{2,H2S} = 0 \tag{5-32}$$

$\kappa_{H2S,d1}$ = reaction velocity for dissolved sulfide oxidation in Layer 1 at 20 °C (m day^{-1})

$\kappa_{H2S,p1}$ = reaction velocity for particulate sulfide oxidation in Layer 1 at 20 °C (m day^{-1})

θ_{H2S} = constant for temperature adjustment for $\kappa_{H2S,d1}$ and $\kappa_{H2S,p1}$

$KM_{H2S,O2}$ = constant to normalize the sulfide oxidation rate for oxygen (g O_2 m^{-3}).

The constant, $KM_{H2S,O2}$, which is included for convenience only, is used to scale the oxygen concentration in the overlying water. At $DO_0 = KM_{H2S,O2}$, the reaction velocity for sulfide oxidation rate is at its nominal value.

The oxidation reactions in the oxic upper layer cause oxygen flux to the sediment, which exerts SOD. By convention, SOD is positive: SOD = $-J_{aq,O2}$. The SOD in the model consists of two components, carbonaceous sediment oxygen demand (CSOD) due to sulfide oxidation and nitrogenous sediment oxygen demand (NSOD) due to nitrification:

$$SOD = CSOD + NSOD = \frac{\kappa_{1,H2S}^2}{s} H2S_1 + a_{O2,NH4} \cdot J_{Nit} \tag{5-33}$$

$H2S_1$ = total sulfide concentration in Layer 1 (g O_2-equivalents m^{-3})

$a_{O2,NH4}$ = stoichiometric coefficient for oxygen consumed by nitrification (4.33 g O_2 per g N).

Equation 4-29 is nonlinear for SOD because the RHS contains *s* (= SOD/DO_0) so that SOD appears on both sides of the equation: note that J_{Nit} (Eq. 5-20) is also a function of *s*. A simple back substitution method is used, as explained in Section 5.6.1.

If the overlying water oxygen is low, then the sulfide that is not completely oxidized in the upper layer can diffuse into the overlying water. This aqueous sulfide flux out of the sediments, which contributes to the chemical oxygen demand in the water column model, is modeled using

$$J_{aq,H2S} = s(fd_{1,H2S} \cdot H2S_1 - COD) \tag{5-34}$$

The sulfide released from the sediment reacts very quickly in the water column when oxygen is available, but can accumulate in the water column under anoxic conditions. The COD, quantified as oxygen equivalents, is entirely supplied by benthic release in the water column model (Eq. 3-16). Since sulfide also is quantified as oxygen equivalents, COD is used as a measure of sulfide in the water column in Eq. 5-34.

5.3.5.2 Methane. When sulfate is used up, methane can be produced by carbon diagenesis and methane oxidation consumes oxygen (DiToro et al. 1990). Owing to the abundant sulfate in the saltwater, only the aforementioned sulfide production and oxidation are considered to occur in the saltwater. Since the sulfate concentration in fresh water is generally insignificant, methane production is considered to replace sulfide production in fresh water. In fresh water, methane is produced by carbon diagenesis in the lower layer decremented by the organic carbon consumed by denitrification, and no diagenetic production of methane occurs in the upper layer (Eq. 5-30):

$$J_{1,CH4} = 0 \qquad J_{2,CH4} = a_{O2,C} \cdot J_C - a_{O2,NO3} \cdot J_{N2(g)} \tag{5-35}$$

The dissolved methane produced takes two pathways: (1) oxidation in the oxic upper layer causing CSOD or (2) escape from the sediment as aqueous flux or as gas flux:

$$J_{2,CH4} = CSOD + J_{aq,CH4} + J_{CH4(g)} \quad (5\text{-}36)$$

$J_{aq,CH4}$ = aqueous methane flux (g O_2-equivalents m^{-2} day^{-1})

$J_{CH4(g)}$ = gaseous methane flux (g O_2-equivalents m^{-2} day^{-1}).

A portion of dissolved methane that is produced in the anoxic layer diffuses into the oxic layer where it is oxidized. This methane oxidation causes CSOD in the freshwater sediment (DiToro et al. 1990):

$$CSOD = CSOD_{\max} \cdot \left(1 - sech[\frac{\kappa_{CH4} \cdot \theta_{CH4}^{T-20}}{s}] \right) \quad (5\text{-}37)$$

$$CSOD_{\max} = minimum\left\{ \sqrt{2 \cdot KL \cdot CH4_{sat} \cdot J_{2,CH4}},\ J_{2,CH4} \right\} \quad (5\text{-}38)$$

$$CH4_{sat} = 100\left(1 + \frac{h + H_2}{10} \right) 1.024^{20-T} \quad (5\text{-}39)$$

$CSOD_{max}$ = maximum CSOD occurring when all the dissolved methane transported to the oxic layer is oxidized

κ_{CH4} = reaction velocity for dissolved methane oxidation in Layer 1 at 20°C (m day^{-1})

θ_{CH4} = constant for temperature adjustment for κ_{CH4}

$CH4_{sat}$ = saturation concentration of methane in the pore water (g O_2-equivalents m^{-3}).

The term, $(h + H_2)/10$ where h and H_2 are in meters, in Eq. 5-39 is the depth from the water surface that corrects for the in situ pressure. Equation 5-39 is accurate to within 3% of the reported methane solubility between 5 and 20°C (Yamamoto et al. 1976).

If the overlying water oxygen is low, the methane that is not completely oxidized can escape the sediment into the overlying water either as aqueous flux or as gas flux. The aqueous methane flux, which contributes to the chemical oxygen demand in the water column model, is modeled using (DiToro et al. 1990):

$$J_{aq,CH4} = CSOD_{\max} \cdot sech[\frac{\kappa_{CH4} \cdot \theta_{CH4}^{T-20}}{s}] = CSOD_{\max} - CSOD \quad (5\text{-}40)$$

Methane is only slightly soluble in water. If its solubility, $CH4_{sat}$ given by Eq. 5-39, is exceeded in the pore water, it forms a gas phase that escapes as bubbles. The loss of methane as bubbles, i.e., the gaseous methane flux, is modeled using Eq. 5-36 with $J_{2,CH4}$ from Eq. 5-35, CSOD from Eq. 5-37, and $J_{aq,CH4}$ from Eq. 5-40 (DiToro et al. 1990).

5.4 Silica

The production of ammonium, nitrate, and phosphate in sediments is the result of the mineralization of POM by bacteria. The production of dissolved silica in sediments is the result of the dissolution of particulate biogenic or opaline silica, which is thought to be independent of bacterial processes.

The depositional flux of particulate biogenic silica from the overlying water to the sediments is modeled using Eq. 5-5. With this source, the mass-balance equation for particulate biogenic silica may be written as:

$$H_2 \frac{\partial PSi}{\partial t} = - S_{Si} \cdot H_2 - W \cdot PSi + J_{PSi} + J_{DSi} \quad (5\text{-}41)$$

PSi = concentration of particulate biogenic silica in the sediment (g Si m^{-3})

S_{Si} = dissolution rate of PSi in Layer 2 (g Si m^{-3} day^{-1})

J_{PSi} = depositional flux of PSi (g Si m^{-2} day^{-1}) given by Eq. 5-5

J_{DSi} = detrital flux of PSi (g Si m^{-2} day^{-1}) to account for PSi settling to the sediment that is not associated with the algal flux of biogenic silica.

The processes included in Eq. 5-41 are dissolution (i.e., production of dissolved silica), burial, and depositional and detrital fluxes from the overlying water. Equation 5-41 can be viewed as the analog of the diagenesis equations for POM (Eq. 5-6). The dissolution rate is formulated using a reversible reaction that is first order in silica solubility deficit and follows a Monod-type relationship in particulate silica:

$$S_{Si} = K_{Si} \cdot \theta_{Si}^{T-20} \frac{PSi}{PSi + KM_{PSi}} (Si_{sat} - fd_{2,Si} \cdot Si_2) \quad (5\text{-}42)$$

K_{Si} = first order dissolution rate for PSi at 20°C in Layer 2 (day^{-1})

θ_{Si} = constant for temperature adjustment for K_{Si}

KM_{PSi} = silica dissolution half-saturation constant for PSi (g Si m^{-3})

Si_{sat} = saturation concentration of silica in the pore water (g Si m^{-3}).

The mass-balance equations for mineralized silica can be formulated using the general forms, Equations 5-8 and 5-10. There is no source/sink term and no reaction in the upper layer:

$$J_{1,Si} = \kappa_{1,Si} = 0 \tag{5-43}$$

In the lower layer, silica is produced by the dissolution of particulate biogenic silica, which is modeled using Eq. 5-42. The two terms in Eq. 5-42 correspond to the source term and reaction term in Eq. 5-10:

$$J_{2,Si} = K_{Si} \cdot \theta_{Si}^{T-20} \frac{PSi}{PSi + KM_{PSi}} Si_{sat} \cdot H_2 \tag{5-44}$$

$$\kappa_{2,Si} = K_{Si} \cdot \theta_{Si}^{T-20} \frac{PSi}{PSi + KM_{PSi}} f_{d2,Si} \cdot H_2 \tag{5-45}$$

A portion of silica dissolved from particulate silica sorbs to solids and a portion remains in the dissolved form. Partitioning using the partition coefficients, $\pi_{1,Si}$ and $\pi_{2,Si}$, in Equations 5-11 and 5-12 controls the extent to which dissolved silica sorbs to solids. Since silica shows similar behavior as phosphate in the adsorption-desorption process, the same partitioning method as applied to phosphate (Section 5.3.4) is used for silica. That is, when DO_0 exceeds a critical concentration, $(DO_0)_{crit,Si}$, sorption in the upper layer is enhanced by an amount $\Delta\pi_{Si,1}$:

$$\pi_{1,Si} = \pi_{2,Si} \cdot (\Delta\pi_{Si,1}) \qquad DO_0 > (DO_0)_{crit,Si} \tag{5-46}$$

When oxygen falls below $(DO_0)_{crit,Si}$, then:

$$\pi_{1,Si} = \pi_{2,Si} \cdot (\Delta\pi_{Si,1})^{DO_0/(DO_0)_{crit,Si}} \qquad DO_0 \leq (DO_0)_{crit,Si} \tag{5-47}$$

which smoothly reduces $\pi_{1,Si}$ to $\pi_{2,Si}$ as DO_0 goes to zero.

Once Equations 5-8 and 5-10 are solved for Si_1 and Si_2, the sediment flux of silica to the overlying water, $J_{aq,Si}$, can be calculated using Eq. 5-9.

5.5 Sediment Temperature

All rate coefficients in the aforementioned mass-balance equations are expressed as a function of sediment temperature, T. The sediment temperature is modeled based on the diffusion of heat between the water column and sediment:

$$\frac{\partial T}{\partial t} = \frac{D_T}{H^2}(T_W - T) \tag{5-48}$$

D_T = heat diffusion coefficient between the water column and sediment (m^2 sec^{-1})

T_W = temperature in the overlying water column (°C) calculated by Eq. 4-82.

The model application in D&F and Cerco and Cole (1993) used $D_T = 1.8 \times 10^{-7}$ m^2 sec^{-1}.

5.6 Method of Solution

5.6.1 Finite-Difference Equations and Solution Scheme

An implicit integration scheme is used to solve the governing mass-balance equations. The finite difference form of Eq. 5-8 may be expressed as:

$$0 = s(fd_0 \cdot Ct_0' - fd_1 \cdot Ct_1') + KL(fd_2 \cdot Ct_2' - fd_1 \cdot Ct_1') + \omega(fp_2 \cdot Ct_2' - fp_1 \cdot Ct_1')$$

$$- W \cdot Ct_1' - \frac{\kappa_1^2}{s} Ct_1' + J_1' \tag{5-49}$$

where the primed variables designate the values evaluated at $t+\theta$ and the unprimed variables are those at t, where θ is defined in Eq. 4-82. The finite difference form of Eq. 5-10 may be expressed as:

$$0 = -KL(fd_2 \cdot Ct_2' - fd_1 \cdot Ct_1') - \omega(fp_2 \cdot Ct_2' - fp_1 \cdot Ct_1') + W(Ct_1' - Ct_2')$$

$$- (\kappa_2 + \frac{H_2}{\theta}) Ct_2' + \left(J_2' + \frac{H_2}{\theta} Ct_2 \right) \tag{5-50}$$

The two terms, - $(H_2/\theta)Ct_2'$ and $(H_2/\theta)Ct_2$, are from the derivative term, $H_2(\partial Ct_2/\partial t)$ in Eq. 5-10, each of which simply adds to the Layer 2 removal rate and the forcing function, respectively. Setting these two terms equal to zero results in the steady-state model. The two unknowns, Ct_1' and Ct_2', can be calculated at every time step using:

$$\begin{pmatrix} s \cdot fd_1 + a_1 + \frac{\kappa_1^2}{s} & -a_2 \\ -a_1 & a_2 + W + \kappa_2 + \frac{H_2}{\theta} \end{pmatrix} \begin{pmatrix} Ct_1' \\ Ct_2' \end{pmatrix} = \begin{pmatrix} J_1' + s \cdot fd_0 \cdot Ct_0' \\ J_2' + \frac{H_2}{\theta} Ct_2 \end{pmatrix} \tag{5-51}$$

$$a_1 = KL \cdot fd_1 + \omega \cdot fp_1 + W \qquad a_2 = KL \cdot fd_2 + \omega \cdot fp_2 \tag{5-52}$$

The solution of Eq. 5-51 requires an iterative method since the surface mass transfer coefficient, s, is a function of the SOD (Eq. 5-13), which is also a function of s (Eq. 5-33). A simple back substitution method is used:

(1) Start with an initial estimate of SOD: for example, SOD = $a_{O2,C} \cdot J_C$ or the previous time step SOD.

(2) Solve Eq. 5-51 for ammonium, nitrate, and sulfide/methane.

(3) Compute the SOD using Eq. 5-33.

(4) Refine the estimate of SOD: a root finding method (Brent's method in Press et al. 1986) is used to make the new estimate.

(5) Go to (2) if no convergence.

(6) Solve Eq. 5-51 for phosphate and silica.

For the sake of symmetry, the equations for diagenesis, particulate biogenic silica and sediment temperature are also solved in implicit form. The finite difference form of the diagenesis equation (Eq. 5-6) may be expressed as:

$$G'_{POM,i} = \left(G_{POM,i} + \frac{\theta}{H_2} J_{POM,I} \right) \left(1 + \theta \cdot K_{POM,i} \cdot \theta_{POM,i}^{T-20} + \frac{\theta}{H_2} W \right)^{-1} \tag{5-53}$$

The finite difference form of the PSi equation (Eq. 5-41) may be expressed as:

$$PSi' = \left(PSi + \frac{\theta}{H_2} (J_{PSi} + J_{DSi}) \right) \left(1 + \theta \cdot K_{Si} \cdot \theta_{Si}^{T-20} \frac{Si_{sat} - f_{d2,Si} \cdot Si_2}{PSi + KM_{PSi}} + \frac{\theta}{H_2} W \right)^{-1} \tag{5-54}$$

using Eq. 5-36 for the dissolution term, in which PSi in the Monod-type term has been kept at time level *t* to simplify the solution. The finite difference form of the sediment temperature equation (Eq. 5-48) may be expressed as:

$$T' = \left(T + \frac{\theta}{H^2} D_T \cdot T_W \right) \left(1 + \frac{\theta}{H^2} D_T \right)^{-1} \tag{5-55}$$

5.6.2 Boundary and Initial Conditions

The above finite difference equations constitute an initial boundary-value problem. The boundary conditions are the depositional fluxes ($J_{POM,i}$ and J_{PSi}) and the overlying water conditions (Ct_0 and T_W) as a function of time, which are provided from the water column water quality model. The initial conditions are the concentrations at $t = 0$, $G_{POM,i}(0)$, PSi(0), $Ct_1(0)$, $Ct_2(0)$, and T(0), to start the computations. Strictly speaking, these initial conditions should reflect the past history of the overlying water conditions and depositional fluxes, which is often impractical because of lack of field data for these earlier years.

This page intentionally left blank

6 - DATABASES

6.1 Introduction

In general, historical water quality data sets for specific waterbodies are typically scattered in among numerous federal and state government agencies, universities, and the private sector. Since specific monitoring programs often have differing objectives and sources of funding, coordination of the results of research and monitoring programs into centralized computer databases for on-line retrieval and analysis generally does not exist. If historical data sets are not readily accessible in database management systems, however, comprehensive integrating analyses, hypothesis testing, and model-building efforts using existing data are very costly, if not impossible, tasks. In the absence of environmental evaluations based on such comprehensive data sets, resource and management decisions, with a larger degree of uncertainty, are often made using only a limited portion of the existing available data.

The increasing scientific complexity and public cost implications of aquatic resource management issues related to waste disposal practices in freshwater and estuarine ecosystems thus require the use of large data sets and sophisticated methods, including models, for credible scientific evaluations of public policy options. The technical credibility of a site-specific modeling framework is, in fact, largely determined by the extent of the agreement between model simulation results and observed data sets. Comparison of model results with the observed database provides the only benchmark that is available to test the model under existing loading conditions. Following satisfactory testing of the model against existing hydrologic, hydrographic, and loading conditions, a properly validated model can then be used to evaluate the probable water quality impact based on management controls that alter external loading conditions. This section of the report documents the sources of historical data used in the development of the Christina River Basin hydrodynamic and water quality model.

6.2 Bathymetric and Stream Geometry Data

The Christina River Basin EFDC model incorporates both tidal and nontidal waterbodies into its framework. The tidal portions of the model include the Delaware River from Reedy Point on the south to Marcus Hook on the north, as well as tidal portions of the Christina River, lower Brandywine Creek, and the lower White Clay Creek. Bathymetric data were available for the Delaware River and the mouth of Christina River from the NOAA Geophysical Data System for Hydrographic Survey Data (GEODAS) CD-ROM. GEODAS contains historical hydrographic survey data from 1850 to 1994. Bathymetry data in the tidal Christina River were estimated from depth contours shown on the 7.5-minute USGS quadrangle map for Wilmington South. Shoreline information was obtained from the 1:100,000 Digital Line Graph CD-ROM published by the USGS.

Cross-section and bottom elevation data for the nontidal streams in the EFDC model were obtained from several sources, including the Federal Emergency Management Agency (FEMA), New Castle County Water Resources Agency, and 7.5-minute quadrangle maps of the area. Input data sets for HEC-2 model runs used to develop flood insurance rate maps were obtained from FEMA. Unfortunately, these data were available only in hard copy "print out" format. The bottom elevations and channel widths from the HEC-2 printouts were used to develop channel geometry for certain stream reaches. For other stream reaches lacking HEC-2 information, estimates of channel geometry and bottom elevation were made from the 7.5-minute USGS quadrangle maps.

6.3 Tide Data

Long-term tide measurements at 15-minute intervals were recorded by the USGS at the Port of Wilmington (station 01481602) near the mouth of the Christina River and at Newport (station 01480065) about 11.4 km (7.0 miles) upstream from the mouth of Christina River. Time-series data files including the calibration period May 1997 to September 1997 were provided by DNREC for both tide gage locations. These time-series data were used to assess the hydrodynamic calibration of the tidal estuary portion of the EFDC model.

6.4 Climatology Data

Meteorological data for Wilmington (WBAN station 13781) were obtained from the National Climatic Data Center. These data included both daily and hourly summaries of atmospheric pressure, air temperature, relative humidity, wind speed, wind direction, and precipitation. In addition, daily values of maximum, minimum, and average air temperature, rainfall, and solar radiation measured at the Stroud Water Research Center near Avondale were provided by Dr. John Davis. The daily solar radiation data were used to develop hourly values assuming a sine function distribution from sunrise to sunset. The climatology data were used to develop the meteorological conditions for the study time period (May 1 to September 21, 1997).

6.5 Stream Flow Data

A number of long-term USGS stream gaging stations are found in the Christina River Basin (see Figure 6-1). Statistical analyses were performed on these stations to determine the average flow, harmonic mean flow, and 7Q10 flow rates. The 7Q10 flow rate will be used for the low-flow TMDL analysis. A summary of the flow statistics is provided in Table 6-1. The daily average flow rates from the gages were used to estimate flow contributions from each of the 39 HSPF watersheds in the study area. The daily flows from each watershed were then distributed to the appropriate EFDC model grid cell.

6.6 In-stream Water Quality Monitoring Data

The primary source of water-column water quality data was from EPA's STORET system, which contains data collected and archived by various agencies including the USGS, Delaware DNREC, and Pennsylvania DEP. Water quality monitoring data for the basin were downloaded from STORET for the period 1980 to 1998. Characterization of both the estuary and stream water quality was required for the development of a model that could be used for TMDL analysis. In August 1997, a detailed water quality field survey was undertaken by Dr. John Davis for PADEP and DNREC at four locations: (1) Red Clay Creek near Kennett Square, (2) White Clay Creek near Avondale, (3) East Branch Brandywine Creek near Downingtown, and (4) West Branch Brandywine Creek near Coatesville. A detailed description of the August 1997 field surveys can be found in Davis (1998).

Data from STORET were compiled into a comprehensive and flexible database (dBASE III format) to characterize the spatial and temporal water quality trends of the Christina River Basin study area. The water quality database was used to (1) prepare tributary loads (nonpoint source loads), (2) develop boundary conditions for the ocean boundary of the model, and (3) compile time-series and longitudinal transect data sets for comparison to model results.

The locations of the water quality stations obtained from STORET are shown in Figure 6-2. A computer data management system was developed for analyzing the observed water quality information and for comparison to model results. The approach was based on the use of a common reference to latitude, longitude, time, and depth in both the real-world observations and the model results. The data management system provided a common link between the field monitoring data and the EFDC model output that facilitated the automation of model-data comparisons. A total of 44 parameter fields were included in the Christina River Basin database file (see Table 6-2). The database consisted of more than 40,000 records.

6.7 Discharge Monitoring Data for Point Sources

Discharge Monitoring Records (DMRs) for various point sources in the Brandywine Creek watershed were provided in hard copy form by the Brandywine Valley Association. Other DMRs were provided in electronic format by PADEP and DNREC. The hard-copy data sheets covered the period 1993 to 1997. The hard-copy data were keypunched and the electronic data were reformatted into a database file for use in developing point source loads for the water quality model. The database file (dBASE III format) contained 30 fields as described in Table 6-3. A list of all 120 NPDES discharges included in the model is given in Section 7 (see Table 7-6) and the locations are shown in Figure 6-3. The August 1997 study (Davis 1998) included seven NPDES discharges that were monitored for flow and water quality parameters (see Figure 6-4). Loading values for the various water quality constituents

were computed based on the flow rates and concentrations provided on the DMRs or measured during the August 1997 study.

The NPDES discharges included 19 single residence discharges (SRD) that are not required to submit DMR data. For purposes of model calibration, it was assumed that these SRD discharges operated at their permit discharge limits. Characteristic concentrations for the various water quality parameters were then assigned to the NPDES source based on the type of discharge, and the loading in kg/day for each constituent was computed for input to the EFDC model. The characteristic effluent concentrations used for this study are listed in Table 6-4, and the characteristic effluent parameter ratios are listed in Table 6-5. The characteristic effluent concentrations and parameter ratios were derived from effluent monitoring data collected by Davis (1998) in August 1998 and from literature values reported in the *Technical Guidance Manual for Developing TMDLs* (USEPA 1995).

Table 6-1. Flow statistics for stream gages in Christina River Basin (cfs).

USGS Gage ID	Drainage Area (mi^2)	Years of Record	Average Flow	Harmonic Mean	7Q10 Flow	1Q10 Flow	7Q1 Flow	1Q1 Flow
01478000	20.5	1944-94	28.21	8.31	1.53	0.54	3.79	1.83
01478500	66.7	1952-79	85.91	47.10	11.00	10.15	24.05	22.38
01478650		1994		38.66				
01479000	89.1	1932-94	114.65	62.19	15.60	14.04	31.23	28.45
01479820		1989-96		24.69				
01480000	47.0	1944-94	63.39	36.51	10.25	8.91	18.38	16.37
01480015		1990-94		41.08				
01480300	18.7	1961-96	26.25	12.83	3.40	3.01	6.62	6.19
01480500	45.8	1944-96	66.33	34.64	8.24	7.34	15.41	14.21
01480617	55.0	1970-96	91.31	52.79	19.02	15.54	24.84	21.63
01480650	6.2	1967-68	6.00	3.51				
01480665	33.4	1967-68	36.36	23.45				
01480700	60.6	1966-96	93.46	50.53	13.86	12.17	21.84	19.87
01480800	81.6	1959-68	86.63	44.81	12.56	11.86	20.57	18.81
01480870	89.9	1972-96	153.43	87.17	28.44	23.62	37.66	34.63
01481000	287.0	1912-96	395.13	234.13	70.63	65.04	117.01	107.14
01481500	314.0	1947-94	477.01	266.73	78.13	71.96	123.45	113.32

Table 6-2. File structure of the water quality monitoring database.

Number of data records: 30422

Field	Field Name	Type	Width	Dec	Description
1	SOURCE	Character	10		Agency identifier
2	OTHERID	Character	10		Other identifier
3	STATION	Character	15		Station name
4	DATE	Date	8		calendar date YYYY/MM/DD
5	TIME	Character	4		24-hr clock time (EST) hhmm
6	LAT	Numeric	10	6	latitude (decimal degrees)
7	LON	Numeric	10	6	longitude (decimal degrees)
8	BOTTOM	Numeric	7	2	station bottom depth (ft)
9	DEPTH	Numeric	7	2	station sample depth (ft)
10	TEMP	Numeric	8	2	water temperature (deg C)
11	FLOW	Numeric	8	3	flow rate (cfs)
12	OXY	Numeric	8	2	dissolved oxygen (mg/L)
13	BOD5	Numeric	8	2	BOD 5-day (mg/L)
14	BOD20	Numeric	8	2	BOD 20-day (mg/L)
15	CBOD5	Numeric	8	2	CBOD 5-day (mg/L)
16	CBOD20	Numeric	8	2	CBOD 20-day (mg/L)
17	COD	Numeric	8	2	chemical oxygen demand (mg/L)
18	PH	Numeric	8	2	pH (standard units)
19	ALK	Numeric	8	3	total alkalinity (mg/L as CaCO3)
20	ACID	Numeric	8	3	total acidity (mg/L as CaCO3)
21	TN	Numeric	8	3	total nitrogen (mg/L as N)
22	TON	Numeric	8	3	total organic nitrogen (mg/L as N)
23	NH3	Numeric	8	3	ammonia nitrogen (mg/L as N)
24	NO2	Numeric	8	3	nitrite nitrogen (mg/L as N)
25	NO3	Numeric	8	3	nitrate nitrogen (mg/L as N)
26	NO23	Numeric	8	3	nitrite + nitrate nitrogen (mg/L as N)
27	TKN	Numeric	8	3	total Kjeldahl nitorgen (mg/L as N)
28	TP	Numeric	8	3	total phosphorus (mg/L as P)
29	DISSP	Numeric	8	3	dissolved phosphorus (mg/L as P)
30	OPO4T	Numeric	8	3	total orthophosphate (mg/L as P)
31	OPO4D	Numeric	8	3	dissolved orthophosphate (mg/L as P)
32	TOC	Numeric	8	3	total organic carbon (mg/L as C)
33	DOC	Numeric	8	3	dissolved organic carbon (mg/L as C)
34	DIC	Numeric	8	3	dissolved inorganic carbon (mg/L as C)
35	TC	Numeric	8	3	total carbon (mg/L as C)
36	CHLORIDE	Numeric	8	3	total chloride (mg/L)
37	ZINCDISS	Numeric	8	3	dissolved zinc (ug/L as Zn)
38	ZINCTOT	Numeric	8	3	total zinc (ug/L as Zn)
39	FEC_COLI	Numeric	8	1	fecal coliform bacteria (MPN/100mL)
40	CHLA	Numeric	8	2	chlorophyll-a (ug/L
41	PHEOPHYTN	Numeric	8	2	pheophyton-a (ug/L)
42	TOTRESIDUE	Numeric	8	2	total nonfilterable residue (mg/L)
43	NON	Numeric	8	3	computed: NO2+NO3 nitrogen (mg/L)
44	DOP	Numeric	8	3	computed: dissolved organic phosphorus (mg/L)
** Total **			354		

Table 6-3. File structure of the NPDES point source discharges database.

Number of data records: 348

Field	Field Name	Type	Width	Dec	Description
1	SOURCE	Character	10		Agency identifier
2	OTHERID	Character	10		Other identifier
3	STATION	Character	15		Station name
4	DATE	Date	8		calendar date YYYY/MM/DD
5	TIME	Character	4		24-hr clock time (EST) hhmm
6	LAT	Numeric	10	6	latitude (decimal degrees)
7	LON	Numeric	10	6	longitude (decimal degrees)
8	BOTTOM	Numeric	7	1	(not used)
9	DEPTH	Numeric	7	1	(not used)
10	FLOW	Numeric	10	6	flow rate (MGD)
11	TEMP	Numeric	10	3	temperature (deg C)
12	BOD	Numeric	10	3	BOD (mg/L)
13	SS	Numeric	10	3	total suspended solids (mg/L)
14	NH3	Numeric	10	3	ammonia nitrogen (mg/L as N)
15	P	Numeric	10	3	total phosphorus (mg/L as P)
16	DO	Numeric	10	3	dissolved oxygen (mg/L)
17	FCB	Numeric	10	3	fecal coliform bacteria (MPN/100mL)
18	CL	Numeric	10	3	chloride (mg/L)
19	PHMAX	Numeric	10	3	maximum pH
20	PHMIN	Numeric	10	3	minimum pH
21	ZN	Numeric	10	3	total zinc (ug/L as Zn)
22	CU	Numeric	10	3	total copper (ug/L as Cu)
23	FE	Numeric	10	3	total iron (ug/L as Fe)
24	FEDISS	Numeric	10	3	dissolved iron (ug/L as Fe)
25	AL	Numeric	10	3	total aluminum (ug/L as Al)
26	MN	Numeric	10	3	total manganese (ug/L as Mn)
27	CR	Numeric	10	3	total chromium (ug/L as Cr)
28	NI	Numeric	10	3	total nickel (ug/L as Ni)
29	PB	Numeric	10	3	total lead (ug/L as Pb)
30	OIL_GREASE	Numeric	10	3	oil & grease
** Total **			292		

Table 6-4. Characteristic (default) NPDES effluent concentrations.

Discharge Type	Code	Characteristic Concentration						
		NH3-N (mg/L)	CBOD5 (mg/L)	TP (mg/L)	DO (mg/L)	TSS (mg/L)	CLO (mg/L)	FCB (cfu/100mL)
Municipal WWTP	MUN	1.5	15.0	2.0	5.0	20.0	90	200
Small STP	STP	1.5	15.0	2.0	5.0	20.0	90	200
Advanced Secondary Treatment 1	ATP1	0.1	2.0	1.2	5.0	10.0	70	200
Advanced Secondary Treatment 2	ATP2	0.1	3.0	1.0	5.0	10.0	90	200
Single Residence Discharge	SRD	1.5	10.0	2.0	6.0	20.0	90	200
Water Filtration Plant	WFP	0.1	2.0	0.1	5.0	20.0	90	2
Industrial Treatment Discharge	IND	0.5	30.0	0.3	5.0	30.0	90	200
Noncontact Cooling Water	NCW	0.1	2.0	0.1	5.0	10.0	90	2
Stormwater Runoff	SWR	1.5	15.0	2.0	5.0	100.0	90	200
Groundwater Cleanup discharge	GWC	0.035	2.0	0.11	5.0	10.0	50	2
Exceptions:								
PA0024058	STP		25.0	7.5	3.0			
PA0025488	ATP2			4.0			106	
DE0000451-002	NCW			4.0				

Table 6-5. Characteristic NPDES effluent parameter ratios.

Discharge Type	Code	Characteristic Ratio						
		CBOD5: BOD5	CBODu: COBD5	DOC:TOC	TN:NH3	NO3:NH3	NO2:NH3	OPO4:TP
Municipal WWTP	MUN	1.0	2.84	0.5	2.42	0.84	0.0300	0.92
Small STP	STP	1.0	2.84	0.5	2.42	0.84	0.0300	0.92
Advanced Secondary Treatment 1	ATP1	1.0	2.84	0.5	444.6	314.3	0.3333	0.94
Advanced Secondary Treatment 2	ATP2	1.0	2.84	0.5	222.3	157.2	0.2962	0.92
Single Residence Discharge	SRD	1.0	2.84	0.5	2.42	0.84	0.0300	0.92
Water Filtration Plant	WFP	1.0	2.84	0.5	2.42	0.84	0.0300	0.92
Industrial Treatment Discharge	IND	1.0	2.84	0.5	9.30	0.087	0.0435	0.33
Noncontact Cooling Water	NCW	1.0	2.84	0.5	2.42	0.84	0.0300	0.92
Stormwater Runoff	SWR	1.0	2.84	0.5	2.42	0.84	0.0300	0.92
Groundwater Cleanup discharge	GWC	1.0	2.84	0.5	60.0	40.0	10.000	0.92
Exceptions:								
PA0024058	STP			0.75				
PA0025488	ATP2		3.38	0.75	55.14	30.14	0.1429	

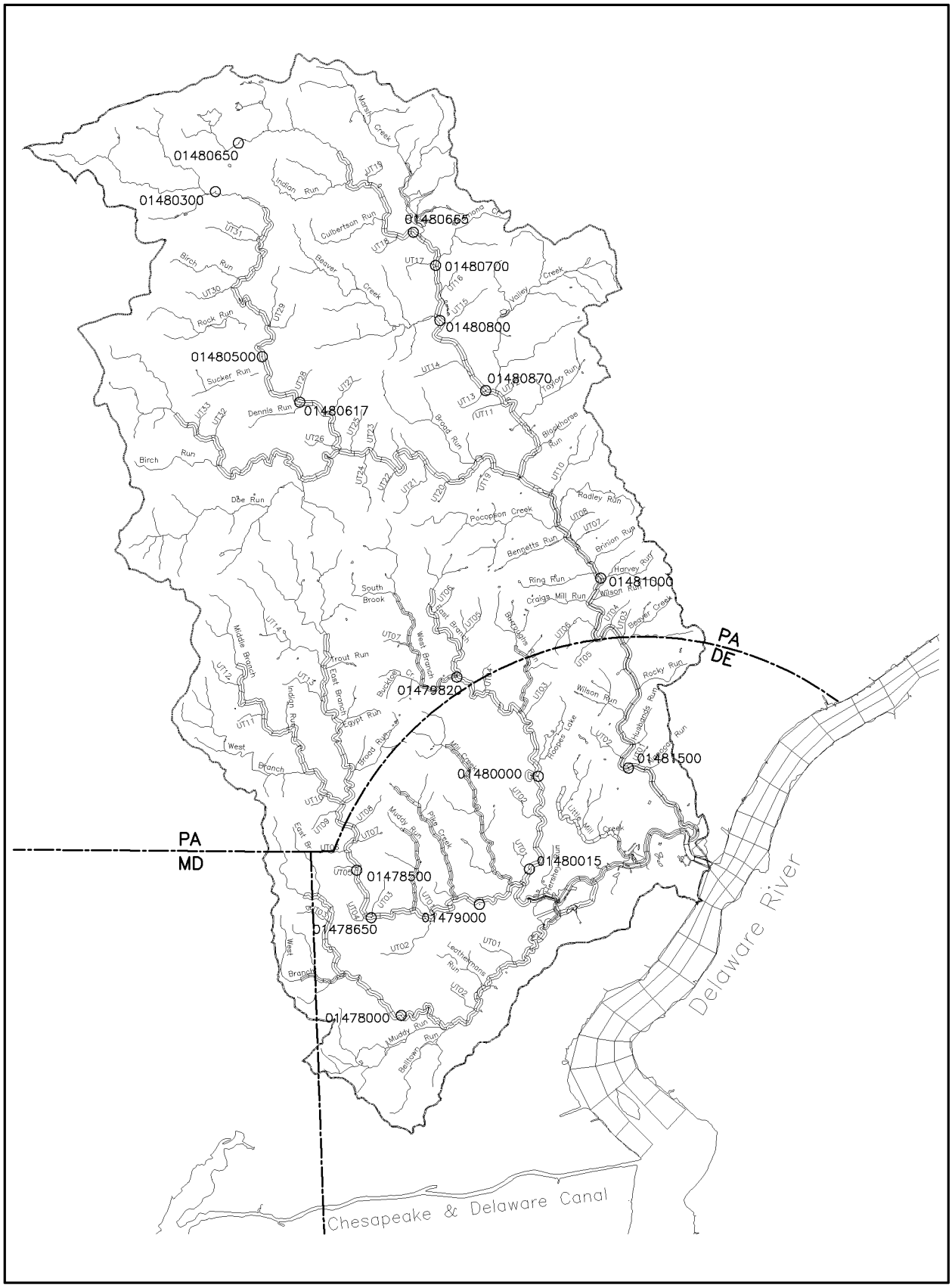

Figure 6-1. Locations of USGS stream gaging stations.

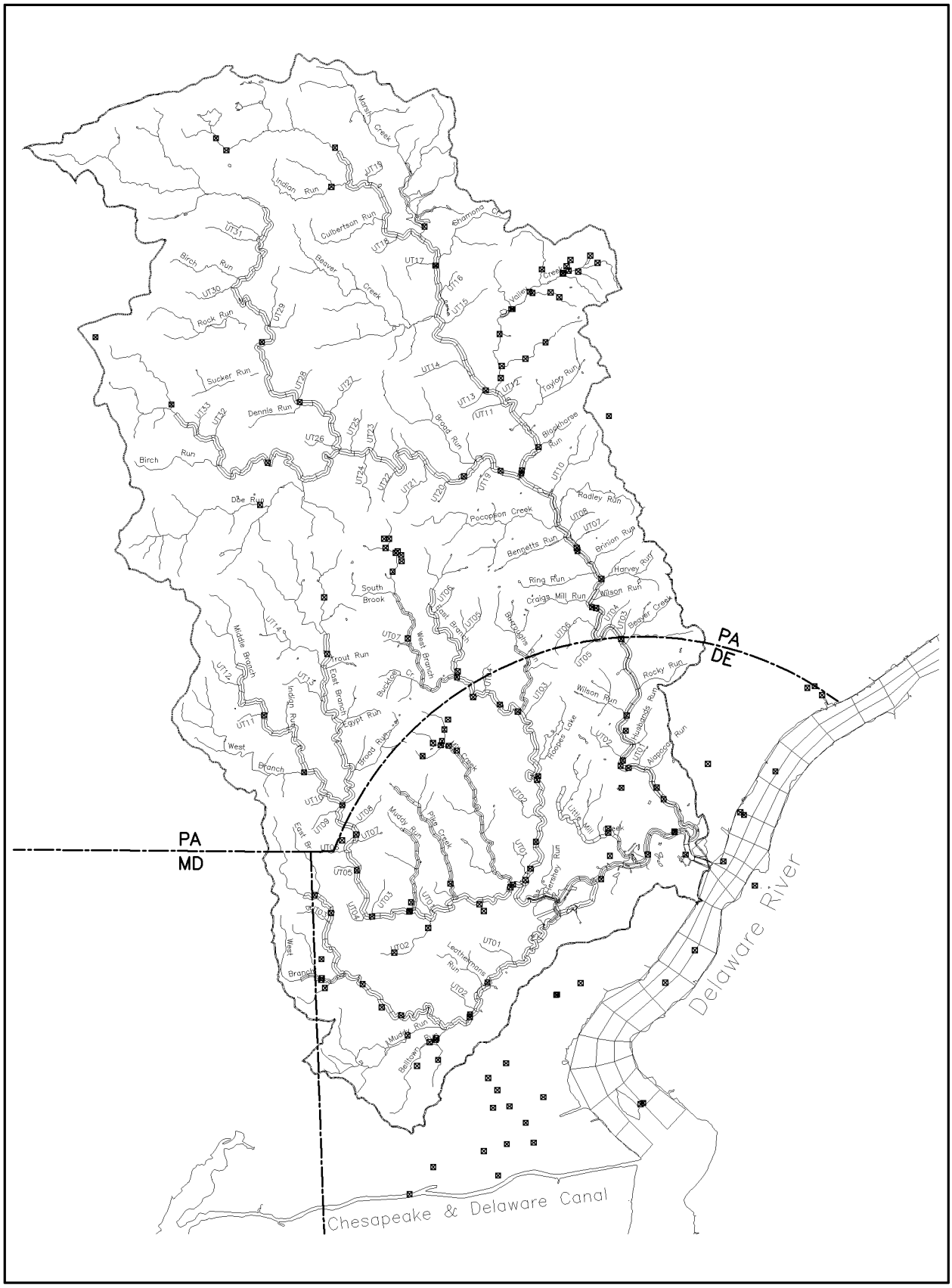

Figure 6-2. Locations of STORET water quality stations.

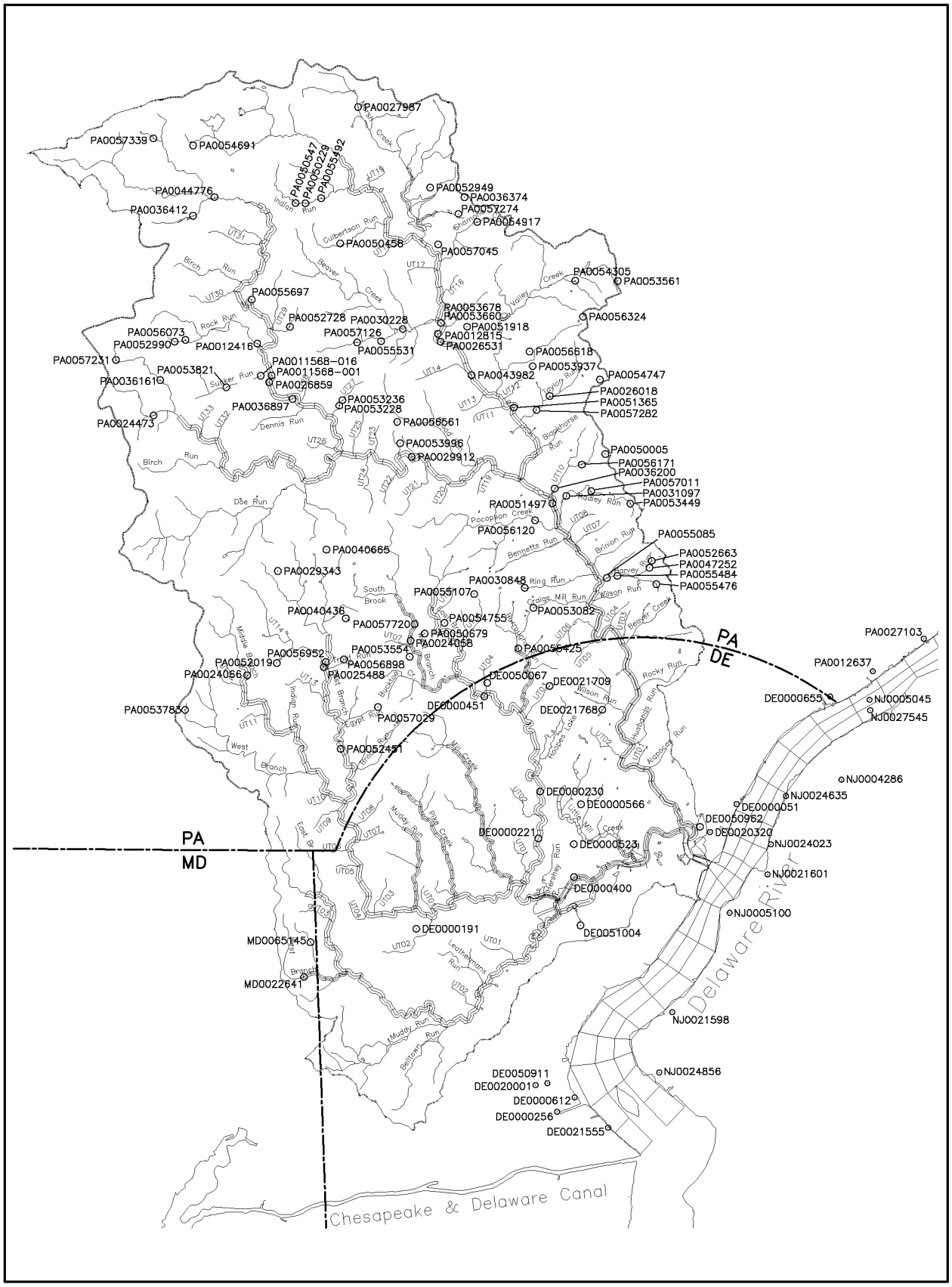

Figure 6-3. Locations of the 120 NPDES point sources included in the model.

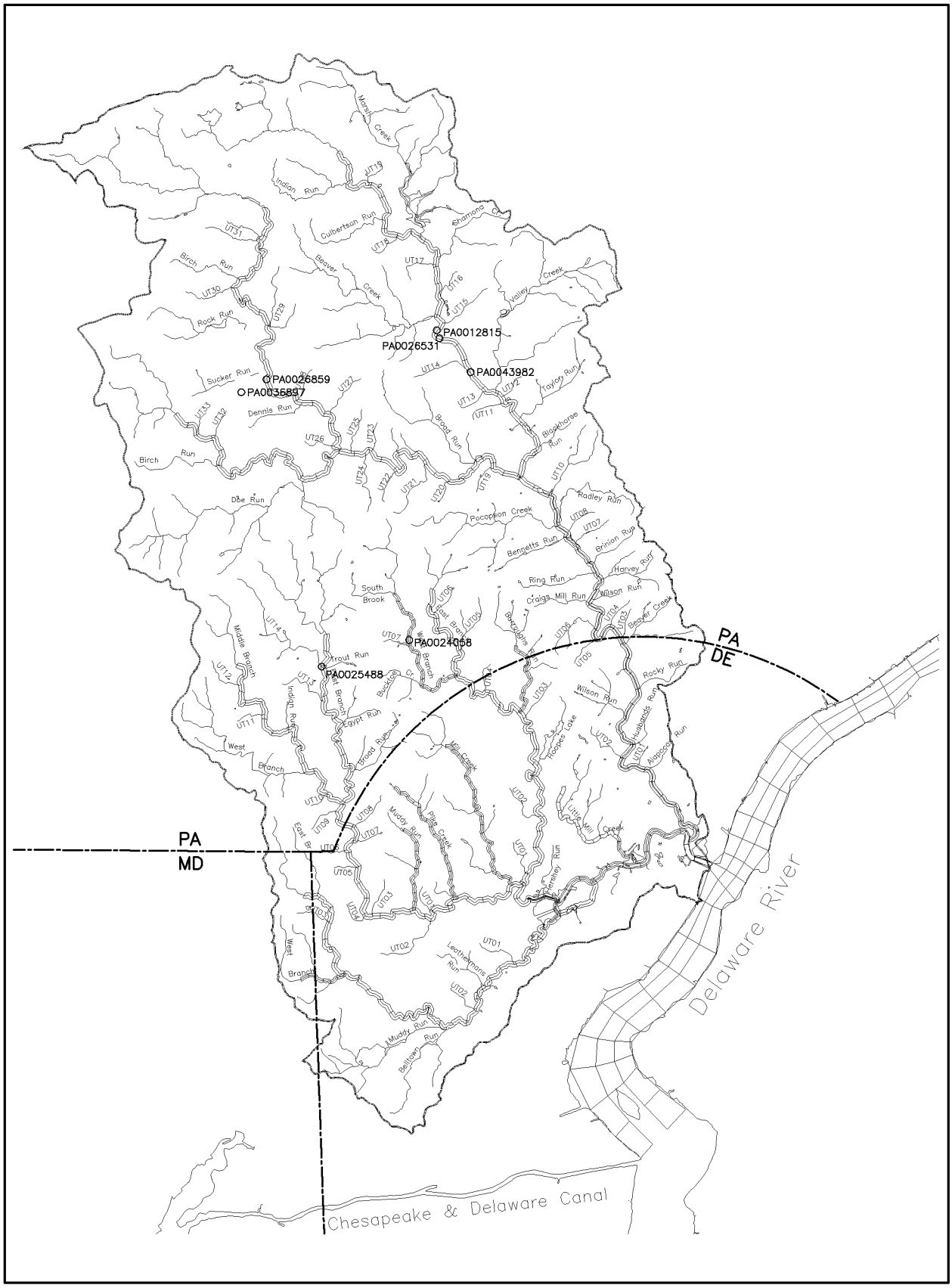

Figure 6-4. Locations of NPDES point sources in August 1997 study (Davis 1998).

7 - LOADS TO THE SYSTEM

External loads of nutrients and oxygen demand were divided into four classes: (1) nonpoint source loads (i.e., diffuse sources) including tributary sources and groundwater sources, (2) point-source loads, (3) water withdrawals, and (4) atmospheric loads. Nonpoint source loads were carried by freshwater flows and groundwater entering the main stream reaches. Point-source loads were discharges from the sewage treatment plants in the study area. Consumptive use water withdrawals were removed from the model system at the appropriate grid cell. Atmospheric loads were transfers from the atmosphere to the water surface via rainfall (wet deposition) and other processes (dry deposition). Atmospheric deposition is not a significant source in the narrow stream channels, but may be more important in the open estuary waterbodies in the lower Christina River and Delaware River because of the larger water surface area in those regions.

7.1 Nonpoint Source Loads

Carbon, nitrogen, phosphorus, dissolved oxygen, and floating algae were treated as mass loads in the model. Nonpoint sources were defined by the delineation of subwatersheds in the HSPF model as shown in Figure 7-1. Ideally, nonpoint source loads are generated by a watershed runoff model to provide predictive nutrient loads to the receiving waters reflective of climatological (rainfall-runoff) characteristics. However, the HSPF watershed loading model for the Christina River Basin is not scheduled to be completed for a few more years. Instead, for this low-flow study, monitoring data in STORET were used to develop tributary loads for the HSPF subwatersheds. Based on water-quality data collected by the USGS (Reif 1999) and baseflow samples collected in 1997 (Senior 1999), estimates of nonpoint source concentrations for sub-basins B1, B5, B6, B8, and B13 were made for nitrite+nitrate nitrogen, ammonia nitrogen, and ortho-phosphate. Estimates of nonpoint source concentrations for other sub-basins were based on instream water quality stations within or downstream of the sub-basin. The lowest flow rates during the calibration period were approximately equal to the 7Q10 flow on certain days in September. The nonpoint source loads (kg/day) for model calibration were computed by multiplying the flow rates for the HSPF subwatersheds by the characteristic concentration for a given water quality constituent. For the low-flow TMDL data set, nonpoint source loads were computed using the daily average flow rates and the characteristic low-flow (or background) concentrations. The estimated 7Q10 flow rates for each subwatershed are listed in Table 7-1. The estimated nonpoint source (background) concentrations for each of the water quality constituents and for each of the 39 subwatersheds are provided in Table 7-2. After the HSPF model is completed, the dynamic nonpoint source loads and flow rates will be computed by HSPF and coupled to the EFDC receiving water model. The HSPF model of the Christina River Basin includes a total of 39 subwatersheds.

7.2 Point Source Loads

For model calibration, a time-series of monthly average loads for the 1997 simulation period was developed for nutrients, dissolved oxygen, chlorides, and total suspended solids at the point sources using the DMR database. The only nutrients reported on the DMR records were ammonia nitrogen and total

phosphorus, if any were reported at all. Thus, a method was developed to estimate the various species of nitrogen, phosphorus, and carbon needed by the EFDC model from the sparse data provided on the DMRs. Fortunately, detailed monitoring of several wastewater treatment plants was conducted in August 1997 by Davis (1998). These plants included Kennett Square, Sunoco, DARA, Broad Run, South Coatesville, and Coatesville (see Table 7-5). The point source monitoring included additional nutrient species for phosphorus and nitrogen not reported on the DMRs. The ratio of each nitrogen species to ammonia nitrogen was computed, as was the ratio of the phosphorus species to total phosphorus (see Table 6-5). These ratios were then used to develop the loadings for each water quality parameter required by the EFDC model according to the rules listed in Table 7-4. The loading rates for the discharges lacking DMR data (mainly the single residence discharges) were estimated using the permit flow limit and the characteristic concentrations shown in Table 6-4 for the associated discharge type. The locations of all 120 NPDES point source discharges included in the model are provided in Table 7-6 arranged according to major stream reach. The river miles are referenced to the mouth of the Christina River (river mile 74.9 according to EPA Reach File 1). The flow limit listed in Table 7-6 is the permit limit for each discharge. The ratios for converting CBOD5 to organic carbon were determined based on data collected during a special study conducted in August-September 1999 from several of the larger WWTPs in the basin. A discussion of the results of the special study is given in Appendix I.

7.3 Water Withdrawals

There are a number of water withdrawals in the Christina River Basin. Only the 28 consumptive use withdrawals were included in the model. For model calibration, the withdrawal rates were held constant for all but four of the locations (DE-02, DE-04, DE-05, and DE-15) where daily withdrawal rates were used in the model. For the other 24 locations, the withdrawal rates were set either to the safe yield rate or to 75% of the pump capacity if the safe yield was not available. The locations of the water withdrawals included in the model are listed in Table 7-7 arranged according to stream reach.

7.4 Atmospheric Loads

Atmospheric loads are typically divided into wet and dry deposition. Wet deposition is associated with dissolved substances in rainfall. The settling of particulate matter during non-rainfall events contributes to dry deposition. Observations of concentrations in rainwater are frequently available, and dry deposition is usually estimated as a fraction of the wet deposition. The atmospheric deposition rates reported in the Long Island Sound Study (Hydro Qual 1991) and the Chesapeake Bay Model Study (Cerco and Cole 1993) as well as information provided by DNREC for Lewes, Delaware, were used to develop both dry and wet deposition loads for the EFDC model of the Christina River Basin. The dry atmospheric deposition rates are presented in Table 7-8, and the wet deposition concentrations are shown in Table 7-9. The loading rate for wet deposition of nutrients was computed internally by the model by multiplying the rainfall rate times the nutrient concentration during each model time step.

Table 7-1. Estimated 7Q10 flow rates for watersheds in Christina River Basin.

WSID	Watershed Description	Area (sq.mi.)	7Q10 unit (cfs/sq.mi.)	7Q10 Flow (cfs)
	Brandywine Creek Watershed:			
B1	Upper West Br. at Honeybrook	18.40	0.3351	6.17
B2	Upper West Br. at Hibernia	27.04	0.3352	9.06
B3	Upper West Br. at Coatesville	17.65	0.2809	4.96
B4	Upper West Br. at Embreeville	17.10	0.1708	2.92
B5	Buck Run	27.51	0.1708	4.70
B6	Doe Run	22.58	0.1708	3.86
B7	Broad Creek	6.44	0.1707	1.10
B8	Upper East Br. at Struble Lake	33.02	0.3765	12.43
B9	Upper East Br. at Shamona Creek	10.02	0.3015	3.02
B10	Lower East Branch	20.93	0.1908	3.99
B11	Marsh Creek	19.98	0.2816	5.62
B12	Beaver Creek	18.09	0.2815	5.09
B13	Valley Creek	20.65	0.1708	3.53
B14	Main Stem above Chadds Ford	24.43	0.1708	4.17
B15	Pocopson Creek	9.20	0.1708	1.57
B16	Main Stem below Chadds Ford	26.55	0.1700	4.51
B17	Main Stem through Wilmington	6.06	0.1801	1.09
	Christina River Watershed:			
C1	Main Stem above Cooches Bridge	14.31	0.0419	0.60
C1wb	West Branch	6.73	0.0223	0.15
C2	Muddy Run	8.67	0.0750	0.65
C3	Belltown Run	6.43	0.0746	0.48
C4	Little Mill Creek	9.23	0.5090	4.70
C5	Main Stem above Smalley's Pond	10.67	0.0749	0.80
C6	Main Stem Lower Tidal	21.20	0.0750	1.59
	White Clay Creek Watershed			
W1	West Branch	10.21	0.2302	2.35
W2	Middle Branch	15.87	0.2306	3.66
W3	East Branch above Avondale	18.74	0.2305	4.32
W4	East Branch below Avondale	14.33	0.1703	2.44
W5	Mill Creek	12.95	0.1698	2.20
W6	Pike Creek	6.65	0.2408	1.60
W7	Middle Run	3.89	0.2389	0.93
W8	Main Stem above Newark	10.13	0.1698	1.72
W9	Main Stem above Delaware Park	9.05	0.2399	2.17
W10	Main Stem at Churchmans Marsh	5.51	0.2196	1.21
	Red Clay Creek Watershed:			
R1	West Branch	17.48	0.2122	3.71
R2	East Branch	9.91	0.1403	1.39
R3	Burroughs Run	7.10	0.1197	0.85
R4	Main Stem above Wooddale	12.46	0.1099	1.37
R5	Main Stem below Wooddale	7.11	0.5092	3.62

Table 7-2. Estimated nonpoint source (background) concentrations for HSPF watersheds in Christina River Basin.

WSID	Watershed Description	CYA (ug/L)	DIA (ug/L)	GRN (ug/L)	RPC (mg/L)	LPC (mg/L)	DOC (mg/L)	RPP (mg/L)	LPP (mg/L)	DOP (mg/L)	P4T (mg/L)	RPN (mg/L)	LPN (mg/L)	DON (mg/L)	NH4 (mg/L)	NO3 (mg/L)	SUU (mg/L)	SAA (mg/L)	COD (mg/L)	DOO (mg/L)	TAM (mg/L)	FCB (#/100mL)	TSS (mg/L)	CLO (mg/L)
	Brandywine Creek Watershed:																							
B1	Upper West Br. at Honeybrook	0.0	0.0	1.0	0.00	0.00	2.10	0.003	0.003	0.004	0.010	0.045	0.045	0.090	0.020	1.80	0.00	0.00	6.00	7.34	0.0	20.0	2.0	11.0
B2	Upper West Br. at Hibernia	0.0	0.0	1.0	0.00	0.00	2.10	0.003	0.003	0.004	0.010	0.045	0.045	0.090	0.020	1.80	0.00	0.00	6.00	7.34	0.0	20.0	2.0	11.0
B3	Upper West Br. at Coatesville	0.0	0.0	1.0	0.00	0.00	2.10	0.003	0.003	0.004	0.010	0.045	0.045	0.090	0.020	1.80	0.00	0.00	6.00	7.34	0.0	20.0	2.0	11.0
B4	Upper West Br. at Embreeville	0.0	0.0	1.0	0.00	0.00	2.10	0.003	0.003	0.004	0.010	0.045	0.045	0.090	0.020	1.80	0.00	0.00	6.00	7.34	0.0	20.0	2.0	11.0
B5	Buck Run	0.0	0.0	1.0	0.00	0.00	2.10	0.003	0.003	0.004	0.010	0.045	0.045	0.090	0.020	1.80	0.00	0.00	6.00	7.34	0.0	20.0	2.0	11.0
B6	Doe Run	0.0	0.0	1.0	0.00	0.00	2.10	0.003	0.003	0.004	0.010	0.045	0.045	0.090	0.020	1.80	0.00	0.00	6.00	7.34	0.0	20.0	2.0	11.0
B7	Broad Creek	0.0	0.0	1.0	0.00	0.00	2.10	0.003	0.003	0.004	0.010	0.045	0.045	0.090	0.020	1.80	0.00	0.00	6.00	7.34	0.0	20.0	2.0	11.0
B8	Upper East Br. at Struble Lake	0.0	0.0	1.0	0.05	0.05	2.40	0.003	0.003	0.005	0.007	0.045	0.045	0.090	0.020	1.16	0.00	0.00	6.00	7.34	0.0	20.0	2.0	11.0
B9	Upper East Br. at Shamona Creek	0.0	0.0	1.0	0.05	0.05	2.40	0.003	0.003	0.005	0.007	0.045	0.045	0.090	0.020	1.16	0.00	0.00	6.00	7.34	0.0	20.0	2.0	11.0
B10	Lower East Branch	0.0	0.0	1.0	0.05	0.05	2.40	0.003	0.003	0.005	0.007	0.045	0.045	0.090	0.020	1.16	0.00	0.00	6.00	7.34	0.0	20.0	2.0	11.0
B11	Marsh Creek	0.0	0.0	1.0	0.05	0.05	2.40	0.003	0.003	0.005	0.007	0.045	0.045	0.090	0.020	1.16	0.00	0.00	6.00	7.34	0.0	20.0	2.0	11.0
B12	Beaver Creek	0.0	0.0	1.0	0.05	0.05	2.40	0.003	0.003	0.005	0.007	0.045	0.045	0.090	0.020	1.16	0.00	0.00	6.00	7.34	0.0	20.0	2.0	11.0
B13	Valley Creek	0.0	0.0	1.0	0.05	0.05	2.40	0.003	0.003	0.005	0.007	0.045	0.045	0.090	0.020	1.16	0.00	0.00	6.00	7.34	0.0	20.0	2.0	11.0
B14	Main Stem above Chadds Ford	0.0	0.0	1.0	0.05	0.05	2.40	0.003	0.003	0.005	0.007	0.045	0.045	0.090	0.020	1.16	0.00	0.00	6.00	7.34	0.0	20.0	2.0	11.0
B15	Pocopson Creek	0.0	0.0	1.0	0.05	0.05	2.40	0.003	0.003	0.005	0.007	0.045	0.045	0.090	0.020	1.16	0.00	0.00	6.00	7.34	0.0	20.0	2.0	11.0
B16	Main Stem below Chadds Ford	0.0	0.0	1.0	0.05	0.05	2.40	0.003	0.003	0.005	0.007	0.045	0.045	0.090	0.020	1.16	0.00	0.00	6.00	7.34	0.0	20.0	2.0	11.0
B17	Main Stem through Wilmington	0.0	0.0	1.0	0.05	0.05	2.40	0.003	0.003	0.005	0.007	0.045	0.045	0.090	0.020	1.16	0.00	0.00	6.00	7.34	0.0	20.0	2.0	11.0
	Christina River Watershed:																							
C1	Christina R. above Cooches Bridge	0.0	0.0	1.0	1.00	1.00	2.00	0.004	0.004	0.002	0.010	0.045	0.045	0.090	0.020	0.80	0.00	0.00	6.00	7.34	0.0	20.0	2.0	11.0
C1wb	Christina R. West Branch	0.0	0.0	1.0	1.00	1.00	2.00	0.004	0.004	0.002	0.010	0.045	0.045	0.090	0.020	0.80	0.00	0.00	6.00	7.34	0.0	20.0	2.0	11.0
C2	Muddy Run	0.0	0.0	1.0	1.00	1.00	2.00	0.004	0.004	0.002	0.010	0.045	0.045	0.090	0.020	0.80	0.00	0.00	6.00	7.34	0.0	20.0	2.0	11.0
C3	Belltown Run	0.0	0.0	1.0	1.00	1.00	2.00	0.004	0.004	0.002	0.010	0.045	0.045	0.090	0.020	0.80	0.00	0.00	6.00	7.34	0.0	20.0	2.0	11.0
C4	Little Mill Creek	0.0	0.0	1.0	1.00	1.00	2.00	0.004	0.004	0.002	0.010	0.045	0.045	0.090	0.020	0.80	0.00	0.00	6.00	7.34	0.0	20.0	2.0	11.0
C5	Main Stem above Smalley's Pond	0.0	0.0	1.0	1.00	1.00	2.00	0.004	0.004	0.002	0.010	0.045	0.045	0.090	0.020	0.80	0.00	0.00	6.00	7.34	0.0	20.0	2.0	11.0
C6	Main Stem Lower Tidal	0.0	0.0	1.0	1.00	1.00	2.00	0.004	0.004	0.002	0.010	0.045	0.045	0.090	0.020	0.80	0.00	0.00	6.00	7.34	0.0	20.0	2.0	11.0
	White Clay Creek Watershed																							
W1	West Branch White Clay Creek	0.0	0.0	1.0	0.15	0.15	1.50	0.007	0.007	0.002	0.004	0.045	0.045	0.090	0.020	1.59	0.00	0.00	6.00	7.34	0.0	20.0	2.0	11.0
W2	Middle Branch White Clay Creek	0.0	0.0	1.0	0.15	0.15	1.50	0.007	0.007	0.002	0.004	0.045	0.045	0.090	0.020	1.59	0.00	0.00	6.00	7.34	0.0	20.0	2.0	11.0
W3	East Branch above Avondale	0.0	0.0	1.0	0.15	0.15	1.50	0.007	0.007	0.002	0.004	0.045	0.045	0.090	0.020	1.59	0.00	0.00	6.00	7.34	0.0	20.0	2.0	11.0
W4	East Branch below Avondale	0.0	0.0	1.0	0.15	0.15	1.50	0.007	0.007	0.002	0.004	0.045	0.045	0.090	0.020	1.59	0.00	0.00	6.00	7.34	0.0	20.0	2.0	11.0
W5	Mill Creek	0.0	0.0	1.0	0.15	0.15	1.50	0.007	0.007	0.002	0.004	0.045	0.045	0.090	0.020	1.59	0.00	0.00	6.00	7.34	0.0	20.0	2.0	11.0
W6	Pike Creek	0.0	0.0	1.0	0.15	0.15	1.50	0.007	0.007	0.002	0.004	0.045	0.045	0.090	0.020	1.59	0.00	0.00	6.00	7.34	0.0	20.0	2.0	11.0
W7	Muddy Run	0.0	0.0	1.0	0.15	0.15	1.50	0.007	0.007	0.002	0.004	0.045	0.045	0.090	0.020	1.59	0.00	0.00	6.00	7.34	0.0	20.0	2.0	11.0
W8	Main Stem above Newark	0.0	0.0	1.0	0.15	0.15	1.50	0.007	0.007	0.002	0.004	0.045	0.045	0.090	0.020	1.59	0.00	0.00	6.00	7.34	0.0	20.0	2.0	11.0
W9	Main Stem above Delaware Park	0.0	0.0	1.0	0.15	0.15	1.50	0.007	0.007	0.002	0.004	0.045	0.045	0.090	0.020	1.59	0.00	0.00	6.00	7.34	0.0	20.0	2.0	11.0
W10	Main Stem at Churchmans Marsh	0.0	0.0	1.0	0.15	0.15	1.50	0.007	0.007	0.002	0.004	0.045	0.045	0.090	0.020	1.59	0.00	0.00	6.00	7.34	0.0	20.0	2.0	11.0
	Red Clay Creek Watershed:																							
R1	West Branch Red Clay Creek	0.0	0.0	1.0	0.00	0.00	2.80	0.014	0.014	0.006	0.011	0.045	0.045	0.090	0.020	1.78	0.00	0.00	6.00	7.34	0.0	20.0	2.0	11.0
R2	East Branch Red Clay Creek	0.0	0.0	1.0	0.00	0.00	2.80	0.014	0.014	0.006	0.011	0.045	0.045	0.090	0.020	1.78	0.00	0.00	6.00	7.34	0.0	20.0	2.0	11.0
R3	Burroughs Run	0.0	0.0	1.0	0.00	0.00	2.80	0.014	0.014	0.006	0.011	0.045	0.045	0.090	0.020	1.78	0.00	0.00	6.00	7.34	0.0	20.0	2.0	11.0
R4	Main Stem above Wooddale	0.0	0.0	1.0	0.00	0.00	2.80	0.014	0.014	0.006	0.011	0.045	0.045	0.090	0.020	1.78	0.00	0.00	6.00	7.34	0.0	20.0	2.0	11.0
R5	Main Stem below Wooddale	0.0	0.0	1.0	0.00	0.00	2.80	0.014	0.014	0.006	0.011	0.045	0.045	0.090	0.020	1.78	0.00	0.00	6.00	7.34	0.0	20.0	2.0	11.0

Key:

CYA = cyanobacteria
DIA = diatom algae
GRN = green algae
RPC = refractory particulate carbon
LPC = labile particulate carbon
DOC = dissolved organic carbon

RPP = refractory particulate phosphorus
LPP = labile particulate phosphorus
DOP = dissolved organic phosphorus
P4T = total orthophosphate

RPN = refractory particulate nitrogen
LPN = labile particulate nitrogen
DON = dissolved organic nitrogen
NH4 = ammonia nitrogen
NO3 = nitrite+nitrate nitrogen

SUU = unavailable silica
SAA = available biogenic silica
COD = chemical oxygen demand
DOO = dissolved oxygen
TAM = total active metal
FCB = fecal coliform bacteria
TSS = total suspended solids
CLO = chlorides

Table 7-3. Wastewater treatment plant monitoring, August 1997.

Parameter	PA0024058 Kennett Sq 08/07/97 (mg/L)	PA0012815 Sunoco 08/13/97 (mg/L)	PA0012815 Sunoco 08/14/97 (mg/L)	PA0026531 DARA 08/13/97 (mg/L)	PA0026531 DARA 08/14/97 (mg/L)	PA0043982 Broad Run 08/13/97 (mg/L)	PA0043982 Broad Run 08/14/97 (mg/L)	PA0036897 S.Coatesville 08/20/97 (mg/L)	PA0026859 Coatesville 08/20/97 (mg/L)	PA0025488 Avondale 08/27/97 (mg/L)
BOD20 inh.	52.000		136.000	5.200	6.900	3.200	2.700	2.400	4.600	6.500
BOD20	121.000		143.000	9.700	16.000	11.200	12.000	8.600	11.000	24.000
BOD5 inh	21.000	29.000	51.000	1.500	2.800	1.500	0.600	0.600	2.500	2.800
BOD5	20.000	30.000	52.000	2.800	4.600	1.700	0.800	0.500	2.700	7.100
Total N	21.800	2.860	4.280	25.200	23.300	36.800	42.100	27.100	20.700	3.860
NH3-N	9.000	0.120	0.460	0.050	0.230	0.050	0.090	0.030	0.060	0.070
NO2-N	0.270	0.010	0.020	0.020	0.030	0.020	0.030	0.010	0.020	0.010
NO3-N	7.580	0.040	0.040	14.800	14.400	27.900	28.070	19.850	16.790	2.110
Total P	5.980	0.060	0.300	0.790	1.460	0.720	0.080	1.200	1.480	8.050
Diss OrthoP	4.850	0.012	0.016	0.770		0.510	0.550	0.870	1.350	6.620
Total OrthoP	5.940	0.020		0.780		0.600			1.390	
TSS (residue total nonvolatile)	62.000	36.000	40.000		10.000	20.000	8.000	10.000	16.000	2.000
Chloride	122.000	44.000	49.000	83.000	79.000	109.000	114.000	55.000	70.000	106.000

Ratios											Secondary Treatment Average	Advanced Treatment Average
BOD20 : BOD5	6.0500		2.7500	3.4643	3.4783	6.5882	15.0000	17.2000	4.0741	3.3803	4.4000	7.5979
(BOD20:BOD5)inh	2.4762		2.6667	3.4667	2.4643	2.1333	4.5000	4.0000	1.8400	2.3200	2.5714	2.9608
TN : NH3	2.4222	23.8333	9.3043	504.0000	101.3043	736.0000	467.7778	903.3333	345.0000	55.1429	11.8533	444.6512
NO2 : NH3	0.0300	0.0833	0.0435	0.4000	0.1304	0.4000	0.3333	0.3333	0.3333	0.1429	0.0523	0.2962
NO3 : NH3	0.8422	0.3333	0.0870	296.0000	62.6087	558.0000	311.8889	661.6667	279.8333	30.1429	0.4208	314.3058
Diss OrthoP : TP	0.8110	0.2000	0.0533	0.9747		0.7083	6.8750	0.7250	0.9122	0.8224	0.3548	1.8363
Total OrthoP : TP	0.9933	0.3333		0.9873		0.8333			0.9392		0.6633	0.9200
TP : NH3	0.6644	0.5000	0.6522	15.8000	6.3478	14.4000	0.8889	40.0000	24.6667	115.0000	0.6055	31.0148

Notes: Secondary treatment: Kennett Square WWTP and Sunoco
Advanced treatment (nitrification): DARA, Broad Run, South Coatesville, and Coatesville

Table 7-4. Methodology for developing EFDC point source loads from DMR data.

Water Quality Parameter	EFDC Code	Calculation
CBOD-5-day		CBOD5 = BOD5 * (CBOD5:BOD5 ratio)
CBOD-ultimate		CBODu = CBOD5 * (CBODu:CBOD5 ratio)
Total organic carbon	TOC	TOC = CBODu * (TOC:CBODu ratio)
Dissolved organic carbon	DOC	DOC = TOC * (DOC:TOC ratio)
Refractory particulate organic carbon	RPOC	0.5 * (TOC - DOC)
Labile particulate organic carbon	LPOC	0.5 * (TOC - DOC)
Total phosphorus Total organic phosphorus		If TP not reported on DMR, use default TP from Table 6-4 TOP = TP - (TP * (OPO4:TP ratio))
Refractory particulate organic phosphorus	RPOP	0.25 TOP
Labile particulate organic phosphorus	LPOP	0.25 TOP
Dissolved organic phosphorus	DOP	0.50 TOP
Total orthophosphate	PO4T	TP * (OPO4:TP ratio)
Total nitrogen Nitrite nitrogen Total organic nitrogen		TN = NH3-N * (TN:NH3 ratio) NO2-N = NH3-n * (NO2:NO3 ratio) TON = TN - NO2-N - NO3-N - NH3-N
Refractory particulate organic nitrogen	RPON	0.25 TON
Labile particulate organic nitrogen	LPON	0.25 TON
Dissolved organic nitrogen	DON	0.50 TON
Ammonia nitrogen	NH3	reported on DMR (or use default NH3-N from Table 6-4)
Nitrate nitrogen	NO3	NO3-N = NH3 * (NO3:NH3 ratio)
Unavailable biogenic silica	SUU	0.10 mg/L (default value)
Dissolved available silica	SAA	1.00 mg/L (default value)
Chemical oxygen demand	COD	9.6 * CBOD5
Dissolved oxygen	DOO	reported on DMR (or use default value from Table 6-4)
Total active metal	TAM	0.0 (not simulated)
Fecal coliform bacteria	FCB	reported on DMR (or use default value from Table 6-4)

Table 7-5. EFDC water quality parameter concentrations for WWTPs monitored in August 1997 study.

Parameter	PA0024058 Kennett Sq 08/07/97 (mg/L)	PA0012815 Sunoco 08/13/97 (mg/L)	PA0012815 Sunoco 08/14/97 (mg/L)	PA0026531 DARA 08/13/97 (mg/L)	PA0026531 DARA 08/14/97 (mg/L)	PA0043982 Broad Run 08/13/97 (mg/L)	PA0043982 Broad Run 08/14/97 (mg/L)	PA0036897 S.Coatesville 08/20/97 (mg/L)	PA0026859 Coatesville 08/20/97 (mg/L)	PA0025488 Avondale 08/27/97 (mg/L)
BOD20 inh.	52.000		136.000	5.200	6.900	3.200	2.700	2.400	4.600	6.500
BOD20	121.000		143.000	9.700	16.000	11.200	12.000	8.600	11.000	24.000
BOD5 inh	21.000	29.000	51.000	1.500	2.800	1.500	0.600	0.600	2.500	2.800
BOD5	20.000	30.000	52.000	2.800	4.600	1.700	0.800	0.500	2.700	7.100
Total N	21.800	2.860	4.280	25.200	23.300	36.800	42.100	27.100	20.700	3.860
NH3-N	9.000	0.120	0.460	0.050	0.230	0.050	0.090	0.030	0.060	0.070
NO2-N	0.270	0.010	0.020	0.020	0.030	0.020	0.030	0.010	0.020	0.010
NO3-N	7.580	0.040	0.040	14.800	14.400	27.900	28.070	19.850	16.790	2.110
Total P	5.980	0.060	0.300	0.790	1.460	0.720	0.800	1.200	1.480	8.050
Diss OrthoP	4.850	0.012	0.016	0.770		0.510	0.550	0.870	1.350	6.620
Total OrthoP	5.940	0.020		0.780		0.600	0.600	0.870	1.390	6.620
TSS (res tot nonvolatile)	62.000	36.000	40.000		10.000	20.000	8.000	10.000	16.000	2.000
Chloride	122.000	44.000	49.000	83.000	79.000	109.000	114.000	55.000	70.000	106.000
EFDC Parameters										
TOC	38.951		97.378	6.605	10.895	7.627	8.172	5.856	7.491	16.343
RPOC	9.738		24.345	1.651	2.724	1.907	2.043	1.464	1.873	4.086
LPOC	9.738		24.345	1.651	2.724	1.907	2.043	1.464	1.873	4.086
DOC	19.476		48.689	3.303	5.448	3.813	4.086	2.928	3.745	8.172
RPOP	0.010	0.010		0.003		0.030	0.050	0.083	0.023	0.358
LPOP	0.010	0.010		0.003		0.030	0.050	0.083	0.023	0.358
DOP	0.020	0.020		0.005		0.060	0.100	0.165	0.045	0.715
P4T	5.940	0.020		0.780		0.600	0.600	0.870	1.390	6.620
RPON	1.238	0.673		2.583		2.208	3.477	1.802	0.958	0.418
LPON	1.238	0.673		2.583		2.208	3.477	1.802	0.958	0.418
DON	2.475	1.345		5.165		4.415	6.955	3.605	1.915	0.835
NH4	9.000	0.120		0.050		0.050	0.090	0.030	0.060	0.070
NO3	7.850	0.050		14.820		27.920	28.100	19.860	16.810	2.120

Table 7-6. Locations of NPDES point source discharges included in the model.

RIVER MILE	CELL I, J	NPDES NUMBER	FLOWLIM MGD	CODE	OWNER	STREAM	TYPE	DESCRIPTION
Brandywine Creek (main stem)								
76.610	54,15	DE0050962	0.0000	SWR	AMTRAK	TB-Brandywine Creek	Industrial	Stormwater
83.554	54,27	DE0021768	0.0250	STP	Winterthur Museum	Clenney Run	Municipal	Small STP
88.644	54,37	PA0053082	0.0206	STP	Mendenhall Inn	TB Brandywine Creek	Commercial	Small STP
89.917	54,38	PA0052663	0.0900	STP	Knight's Bridge Co/Villages at Painters	Harvey Run	Commercial	Small STP
89.917	54,38	PA0055476	0.0400	STP	Birmingham TSA/Ridings at Chadds Ford	TB Harvey Creek	Municipal	Small STP
89.917	54,38	PA0055085	0.0005	SRD	Winslow Nancy Ms.	TB Brandywine Creek	Municipal	Single Residence STP
89.917	54,38	PA0055484	0.0005	SRD	Keating Herbert & Elizabeth	TB Brandywine Creek	Municipal	Single Residence STP
89.917	54,38	PA0047252	0.0700	STP	Pantos Corp/Painters Crossing	Harvey Run		
90.553	54,39	PA0030848	0.0063	STP	Unionville - Chadds Ford Elem. School	Ring Run	Municipal	Small STP
93.098	54,42	PA0056120	0.0005	SRD	Schindler	Pocopson Creek	Municipal	Single Residence STP
92.462	54,43	PA0031097	0.0170	STP	Radley Run C.C.	Radley Run	Municipal	Small STP
92.462	54,43	PA0053449	0.1500	STP	Birmingham Twp. STP	Radley Run	Municipal	Small STP
93.735	54,43	PA0057011	0.0773	STP	Thornbury Twp./Bridlewood Farms STP	Radley Run		
92.462	54,44	PA0036200	0.0320	STP	Radley Run Mews	Plum Run	Municipal	Small STP
94.371	54,44	PA0056171	0.0005	SRD	McGlaughlin Jeffrey	Plum Run	Municipal	Single Residence STP
94.371	54,44	PA0050005	0.1400	GWC	Sun Company	TB Brandywine Creek	GWCleanup	New permit 03/27/98
94.371	54,44	PA0051497	0.0300	NCW	Lenape Forge	Brandywine Creek	Industrial	Cooling Water
Brandywine Creek East Branch								
98.647	54,52	PA0026018	1.8000	MUN	West Chester Borough MUA/Taylor Run	Taylor Run	Municipal	Large STP
98.647	54,52	PA0054747	0.0000	SWR	Trans-Materials, Inc.	Taylor Run	Industrial	Stormwater
98.647	54,52	PA0057282	0.0005	SRD	Jonathan & Susan Pope	TB Valley Creek	Municipal	Single Residence STP
99.276	54,53	PA0051365	0.3690	WFP	West Chester Area Mun. Auth.	EB Brandywine Creek	Municipal	Ingram's Mill-Filter Backwash
100.535	54,55	PA0053937	0.0005	SRD	Johnson Ralph & Gayla	Broad Creek	Municipal	Single Residence STP
100.535	54,55	PA0056324	0.0440	GWC	Mobil SS#16-GPB	TB-WB Valley Run	Commercial	DP
100.535	54,55	PA0056618	0.0005	SRD	O'Cornwell David & Jeanette	Broad Run	Municipal	Single Residence STP
100.535	54,55	PA0054305	0.0000	IND	Sun Co, Inc. (R&M)	TB Valley Creek	Industrial	
100.535	54,55	PA0053561	0.0360	GWC	Johnson Matthey	Valley Creek	GWCleanup	Permitted 03/12/96
101.794	54,57	PA0043982	0.4000	ATP2	Broad Run Sew Co.	EB Brandywine Creek	Municipal	Large STP
103.682	54,61	PA0012815	1.0280	IND	Sunoco Products	EB Brandywine Creek	Industrial	Paper Company - Mill Raceway
103.682	54,60	PA0026531	7.1340	ATP2	Downingtown Area Regional Authority	EB Brandywine Creek	Municipal	Large STP
104.312	54,61	PA0051918	0.1440	NCW	Pepperidge Farms	Parke Run Creek	Industrial	Cooling Water
103.682	54,61	PA0055531	0.0007	STP	Khalife Paul	TB Valley Run	Commercial	Small STP
104.312	54,61	PA0057126	0.0000	IND	Hess Oil - SS #38291	Valley Run	Commercial	DP
104.312	54,61	PA0030228	0.0225	STP	Downingtown I&A School	Beaver Creek	Municipal	No flow since Feb 1994
104.312	54,61	PA0053678	0.0000	IND	Lambert Earl R.	EB Brandywine Creek	Industrial	DP
104.312	54,61	PA0053660	0.0000	IND	Mobil Oil Company #016	EB Brandywine Creek	Commercial	Air stripper at Service Sta
106.830	54,65	PA0054917	0.4750	STP	Uwchlan Twp. Municipal Authority	Shamona Creek	Municipal	Eagleview CC STP
107.459	54,66	PA0057045	0.0000	SWR	Shyrock Brothers, Inc.	EB Brandywine Creek	Commercial	Stormwater
108.088	54,67	PA0027987	0.0500	STP	Pennsylvania Tpk./Caruiel Service Plaza	Marsh Creek	Commercial	Small STP
108.088	54,67	PA0036374	0.0150	STP	Eaglepoint Dev. Assoc.	TB Marsh Creek	Municipal	Small STP
108.088	54,67	PA0052949	0.0000	IND	Phila. Suburban Water Co.	Marsh Creek	Industrial	Uwchlan DP
108.088	54,67	PA0057274	0.0005	SRD	Michael & Antionette Hughes	TB Marsh Creek	Municipal	Single Residence STP
109.977	54,70	PA0050458	0.0531	STP	Little Washington Drainage Co.	Culbertson Run	Municipal	Small STP
112.495	54,74	PA0050229	0.0005	SRD	unknown	Indian Run	Municipal	Single Residence STP
112.495	54,74	PA0050547	0.0375	STP	Indian Run Village MHP	Indian Run	Municipal	Small STP
112.495	54,74	PA0055492	0.0005	SRD	Topp John & Jane	Indian Run	Municipal	Single Residence STP
113.753	54,76	PA0054691	0.0005	SRD	Stoltzfus Ben Z.	TB Brandywine Creek	Municipal	Single Residence STP

Table 7-6. Locations of NPDES point source discharges included in the model (continued).

RIVER MILE	CELL I, J	NPDES NUMBER	FLOWLIM MGD	CODE	OWNER	STREAM	TYPE	DESCRIPTION
Brandywine Creek West Branch								
97.976	46,79	PA0056561	0.0000	SWR	Richard M. Armstrong Co.	Broad Run	Commercial	Stormwater
101.708	40,79	PA0029912	0.1000	STP	Embreeville Hospital	WB Brandywine Creek	Municipal	Large STP
102.330	39,79	PA0053996	0.0005	SRD	Redmond Michael	TB-WB Brandywine Creek	Municipal	Single Residence STP
107.306	29,79	PA0053228	0.0005	SRD	Gramm Jeffery	WB Brandywine Creek	Municipal	Single Residence STP
107.306	29,79	PA0053236	0.0005	SRD	Woodward Raymond Sr. STP	WB Brandywine Creek	Municipal	Single Residence STP
110.416	24,79	PA0036897	0.3900	ATP1	South Coatesville Borough	WB Brandywine Creek	Municipal	Large STP
111.038	23,79	PA0026859	3.8500	ATP1	Coatesville City Authority	WB Brandywine Creek	Municipal	Large STP
111.038	23,79	PA0011568-001	0.5000	IND	Lukens Steel Co.	Sucker Run	Industrial	Large STP
111.038	23,79	PA0011568-016	0.5000	IND	Lukens Steel Co.	Sucker Run	Industrial	Large STP
111.038	23,79	PA0053821	0.0000	SWR	Chester County Aviation Inc.	Sucker Run	Commercial	Stormwater
112.282	20,79	PA0012416	0.1400	WFP	Coatesville Water Plant	Rock Run	Industrial	Water Filtration Plant-Backwash
112.282	20,79	PA0052990	0.0005	SRD	Mitchell Rodney	Rock Run	Municipal	Single Residence STP
112.282	20,79	PA0056073	0.0005	SRD	Vreeland Russell Dr.	TB Rock Run	Municipal	Single Residence STP
113.526	18,79	PA0052728	0.0004	STP	Farmland Industries Inc./Turkey Hill	WB Brandywine Creek	Industrial	Small STP
114.770	16,79	PA0055697	0.0490	STP	Spring Run Estates	WB Brandywine Creek	Commercial	Small STP
120.368	06,79	PA0036412	0.0550	STP	Tel Hai Retirement Community	TB-WB Brandywine Creek	Municipal	Small STP
120.368	06,79	PA0044776	0.6000	STP	NW Chester Co. Municipal Authority	WB Brandywine Creek	Municipal	Large STP
120.368	06,79	PA0057339	0.0005	SRD	Brian & Cheryl Davidson	TB-WB Brandywine Creek	Municipal	Single Residence STP
Buck Run								
117.041	33,61	PA0024473	0.7000	STP	Parkersburg Borough Authority WWTP	TB-Buck Run	Municipal	Small STP-discontinued 06/10/97
117.041	33,61	PA0036161	0.0360	STP	Lincoln Crest MHP STP	Buck Run	Municipal	Small STP
117.041	33,61	PA0057231	0.0005	SRD	Archie & Cloria Shearer	TB-Buck Run	Municipal	Single Residence STP
Christina River (tidal)								
82.274	45,13	DE0000400-001	0.0000	NCW	Ciba-Geigy Corp.	Christina River	Industrial	Cooling Water
83.561	43,09	DE0051004	0.0000	SWR	Boeing	Nonesuch Creek	Industrial	Stormwater
Christina River West Branch								
99.587	16,09	MD0065145	0.0500	STP	Highlands WWTP	WB Christina River	Municipal	Small STP
100.209	14,09	MD0022641	0.4500	STP	Meadowview Utilities, Inc.	WB Christina River	Municipal	Small STP
Red Clay Creek								
89.828	43,26	DE0000221-001	0.0060	NCW	HAVEG/AMTEK (eliminated July 1996)	Red Clay Creek	Industrial	Cooling Water
89.828	43,26	DE0000221-003	0.0040	NCW	HAVEG/AMTEK (eliminated July 1996)	Red Clay Creek	Industrial	Cooling Water
91.746	43,29	DE0000230-001	0.3500	NCW	Hercules Inc.	Red Clay Creek	Industrial	Cooling Water
95.583	43,35	DE0021709-001	0.0150	STP	Greenville Country Club	TB-Red Clay Creek	Municipal	Small STP
96.861	43,37	PA0055425	0.0005	SRD	D'Ambro Anthony Jr.-Lot #22	TB-EB Red Clay Creek	Municipal	Single Residence STP
98.780	43,40	DE0050067	0.0015	STP	Center for Creative Arts	TB-Red Clay Creek	Municipal	Small STP
98.780	43,40	DE0000451-002	2.1700	NCW	NVF Yorklyn	Red Clay Creek	Industrial	Stormwater/Cooling Water
101.337	43,44	PA0055107	0.1500	STP	East Marlborough Township STP	TB-EB Red Clay Creek	Municipal	Large STP
103.255	43,47	PA0054755	0.0000	SWR	Trans-Materials Inc.	EB Red Clay Creek	Industrial	Stormwater
Red Clay Creek West Branch								
103.313	32,43	PA0053554	0.0000	SWR	Earthgro Inc.	WB Red Clay Creek	Industrial	Stormwater
103.950	30,43	PA0024058	1.1000	STP	Kennett Square Boro. WWTP	WB Red Clay Creek	Municipal	Large STP
104.268	29,43	PA0050679	0.2500	NCW	National Vulcanized Fiber (NVF)	TB-WB Red Clay Creek	Industrial	Cooling Water
104.579	28,43	PA0057720-001	0.0500	STP	Sunny Dell Foods, Inc.	WB-Red Clay Creek	Industrial	Mushroom Canning/Process Water
104.579	28,43	PA0057720-003	0.0900	NCW	Sunny Dell Foods, Inc.	WB-Red Clay Creek	Industrial	Mushroom Canning/Cooling Water
White Clay Creek								
93.090	32,18	DE0000191-001	0.0300	NCW	FMC Corp.	Cool Run	Industrial	Stormwater/Cooling Water
102.824	15,18	PA0053783	0.0200	STP	Avon Grove School Dist	TB-WB White Clay Creek	Commercial	Small STP
108.696	06,18	PA0024066	0.2500	STP	West Grove Borough Authority STP	MB White Clay Creek	Municipal	Large STP

Table 7-6. Locations of NPDES point source discharges included in the model (continued).

RIVER MILE	CELL I, J	NPDES NUMBER	FLOWLIM MGD	CODE	OWNER	STREAM	TYPE	DESCRIPTION
White Clay Creek East Branch								
102.750	19,24	PA0052451	0.0012	STP	Frances L. Hamilton Oates STP	EB White Clay Creek	Municipal	Small STP
104.020	19,26	PA0057029	0.1440	GWC	Hewlett Packard Co.	Egypt Run	GWCleanup	Groundwater Cleanup
106.560	19,30	PA0025488	0.3000	ATP2	Avondale Borough Sewer Authority	Indian Run	Municipal	Large STP
106.560	19,30	PA0052019	0.0075	STP	Avon Grove Trailer Court	EB White Clay Creek	Municipal	Small STP
106.560	19,30	PA0056898	0.0650	IND	To-Jo Mushrooms Inc.	Trout Run	Industrial	Small STP-online Jan 98
107.195	19,31	PA0056952	0.0029	IND	Sun Company Inc.	EB White Clay Creek	GWCleanup	Groundwater Cleanup
107.830	19,32	PA0029343	0.0270	STP	Chatham Acres	TB-EB White Clay Creek	Municipal	Small STP
107.830	19,32	PA0040436	0.0090	STP	Chadds Ford Investment Co./Red Fox GC	TB-EB White Clay Creek	Municipal	Small STP
107.830	19,32	PA0040665	0.0100	STP	Stone Barn Restuarantand Apt. Cplx	EB White Clay Creek	Commercial	Small STP
Little Mill Creek								
82.441	41,55	DE0000523-001	0.0000	SWR	General Motors Assembly	Little Mill Creek	Industrial	Stormwater
83.373	38,55	DE0000566	0.0000	SWR	DuPont Chestnut Run	Little Mill Creek	Industrial	Stormwater/Cooling Water
Delaware River								
63.839	57,04	DE0021555-001	0.5500	MUN	Delaware City STP	Delaware River	Municipal	
65.272	57,05	DE0000256-601	13.0000	IND	Star Enterprises	Delaware River	Industrial	
65.272	57,05	DE0000612-001	0.8000	IND	Formosa Plastics Corp.	Delaware River	Industrial	
65.272	57,05	DE0020001-001	0.6800	MUN	Standard Chlorine	Delaware River	Municipal	
65.272	57,05	DE0050911-001	0.3000	MUN	Occidental Chemical Corp.	Delaware River	Municipal	
75.237	57,15	DE0020320-001	90.0000	MUN	City of Wilmington	Delaware River	Municipal	
77.162	57,17	DE0000051-001	5.2000	IND	Dupont-Edgemoor	Delaware River	Industrial	
77.162	57,17	DE0000051-002	3.0000	IND	Dupont-Edgemoor	Delaware River	Industrial	
77.162	57,17	DE0000051-003	6.0000	IND	Dupont-Edgemoor	Delaware River	Industrial	
81.307	57,20	DE0000655-001	33.3000	IND	General Chemical Corporation	Delaware River	Industrial	
83.907	57,22	PA0012637-002	52.3500	IND	Bayway Manufacturing	Delaware River	Industrial	SEE NOTE 1
83.907	57,22	PA0012637-101	69.8000	IND	Bayway Manufacturing	Delaware River	Industrial	SEE NOTE 1
83.907	57,22	PA0012637-201	3.3400	IND	Bayway Manufacturing	Delaware River	Industrial	SEE NOTE 1
85.199	57,23	PA0027103-001	44.0000	MUN	Delcora	Delaware River	Municipal	
82.639	58,21	NJ0005045-001	0.5000	IND	Monsanto	Delaware River	Industrial	SEE NOTE 2
63.839	59,04	NJ0024856-001	1.4450	MUN	City of Salem	Delaware River	Municipal	SEE NOTE 1
69.534	59,09	NJ0021598-001	2.4650	MUN	Pennsville Sewage Authority	Delaware River	Municipal	SEE NOTE 1
73.339	59,12	NJ0005100-661	22.9000	IND	Dupont-Chambers Works	Delaware River	Industrial	SEE NOTE 1
75.237	59,15	NJ0021601-001	1.7290	MUN	Carneys Pt. Sewage Authority	Delaware River	Municipal	SEE NOTE 1
76.045	59,16	NJ0024023-001	0.9500	MUN	Penns Grove Sewage Authority	Delaware River	Municipal	SEE NOTE 1
77.162	59,17	NJ0024635-001	0.0366	MUN	Fort Dix/Pedricktown Facility	Delaware River	Municipal	SEE NOTE 1
79.919	59,19	NJ0004286-001	2.1000	IND	Geon	Delaware River	Industrial	
82.639	59,21	NJ0027545-001	0.9860	MUN	Logan Township MUA	Delaware River	Municipal	SEE NOTE 1

NOTES:
[1] No flow limit available in PCS data base; flow limit shown is maximum reported flow during 01/01/95 to 12/31/98
[2] No flow limit or reported flow available in PCS data base; flow limit shown is an estimate

Table 7-7. Locations of consumptive use water withdrawals included in the model.

RIVER MILE	CELL I, J	WITHDRAWAL NUMBER	FLOWLIM MGD	CODE	OWNER	STREAM	LOCATION
Brandywine Creek							
79.100	54,20	DE-01	16.0000	CUW	City of Wilmington	Brandywine Creek	Brandywine WTP
79.100	54,20	DE-02	20.0000	CUW	City of Wilmington	Brandywine Creek	Porter WTP
79.100	54,20	DE-08	0.7500	CUW	Wilmington Finishing	Brandywine Creek	Wilmington, DE
Brandywine Creek East Branch							
99.906	54,54	PA-4	4.5000	CUW	West Chester MUA	EB Brandywine Creek	West Chester, PA
100.535	54,55	6996-006	0.4650	CUW	General Crushed Stone	Valley Creek	
100.535	54,55	6996-013	0.0030	CUW	General Crushed Stone	Valley Creek	
103.682	54,60	6987-004	0.9900	CUW	Sonoco Products Co.	EB Brandywine Creek	Downingtown, PA
104.312	54,61	250156-022	0.0098	CUW	Ingleside Golf Course	EB Brandywine Creek	
104.312	54,61	6990-004	0.0180	CUW	Brandywine Paperboard	EB Brandywine Creek	Downingtown, PA
104.941	54,62	PA-3	2.5000	CUW	Downingtown MUA	EB Brandywine Creek	Downingtown, PA
106.830	54,65	7266-004	0.0075	CUW	Shyrock Brothers Inc.	EB Brandywine Creek	Uwchlan, PA
Brandywine Creek West Branch							
101.708	40,79	PA-5	0.1500	CUW	Embreeville State Hospital	WB Brandywine Creek	Embreeville, PA
109.172	26,79	7045-004	0.0660	CUW	Sealed Air Corp.	Dennis Run	
111.660	21,79	6971-004	3.4407	CUW	Lukens Steel Co.	WB Brandywine Creek	Coatesville, PA
112.904	19,79	PA-2	2.2500	CUW	City of Coatesville Authority	Rock Run	Rock Run Reservoir
113.526	18,79	450090-002	0.0660	CUW	Byran L. Hawthowne	WB Brandywine Creek	West Brandywine
113.526	18,79	450090-003	0.0113	CUW	Byron L. Hawthorne	WB Brandywine Creek	West Brandywine
116.636	12,79	PA-1	0.7500	CUW	City of Coatesville Authority	Birch Run	Hibernia Reservoir
Christina River (nontidal)							
89.900	32,13	DE-5	0.1500	CUW	Marvin Hershberger	Christina River	Smalley's Pond Headwaters
89.900	32,13	DE-05	4.0000	CUW	United Water Delaware	Christina River	Smalley's Pond WTP
Red Clay Creek							
92.386	43,30	DE-2	0.6750	CUW	Hercules Research Center	Red Clay Creek	Woodale, DE
93.665	43,32	DE-4	0.0225	CUW	Samuel Beard	Red Clay Creek	Wilmington, DE
98.780	43,40	DE-1	2.2500	CUW	National Vulcanized Fiber	Red Clay Creek	Yorklyn, PA
Red Clay Creek West Branch							
103.631	31,43	450088-002	0.0004	CUW	J.H. Thompson, Inc.	WB Red Clay Creek	New Garden, PA
White Clay Creek							
88.557	40,18	DE-04	12.0000	CUW	United Water Delaware	White Clay Creek	Stanton WTP
95.032	28,18	DE-15	1.0000	CUW	Curtis Paper	White Clay Creek	Newark, DE
95.680	27,18	DE-03	0.0001	CUW	City of Newark	White Clay Creek	Papermill WTP
White Clay Creek East Branch							
104.020	19,26	7227-005	0.0239	CUW	Laurel Valley Farms	EB White Clay Creek	New Garden, PA

Table 7-8. Atmospheric dry deposition rates used in Christina River Basin EFDC model.

Parameter	Deposition Rate ($g/m^2/day$)	Parameter	Deposition Rate ($g/m^2/day$)
Refractory Part. Organic Carbon	0.000387	Refractory Part. Organic Nitrogen	0.000530
Labile Part. Organic Carbon	0.000387	Labile Part. Organic Nitrogen	0.000530
Dissolved Organic Carbon	0.000773	Dissolved Organic Nitrogen	0.000771
Dissolved Organic Phosphorus	0.000054	Ammonia Nitrogen	0.000214
Orthophosphate	0.000019	Nitrate+Nitrite Nitrogen	0.000393
Available Silica	0.000247		

Table 7-9. Atmospheric wet deposition concentrations used in Christina River Basin EFDC model.

Parameter	Concentration (mg/L)	Parameter	Concentration (mg/L)
Refractory Part. Organic Carbon	0.325	Refractory Part. Organic Nitrogen	0.0
Labile Part. Organic Carbon	0.325	Labile Part. Organic Nitrogen	0.0
Dissolved Organic Carbon	0.650	Dissolved Organic Nitrogen	0.140
Dissolved Organic Phosphorus	0.045	Ammonia Nitrogen	0.222
Orthophosphate	0.016	Nitrate+Nitrite Nitrogen	0.332
Available Silica	0.0		

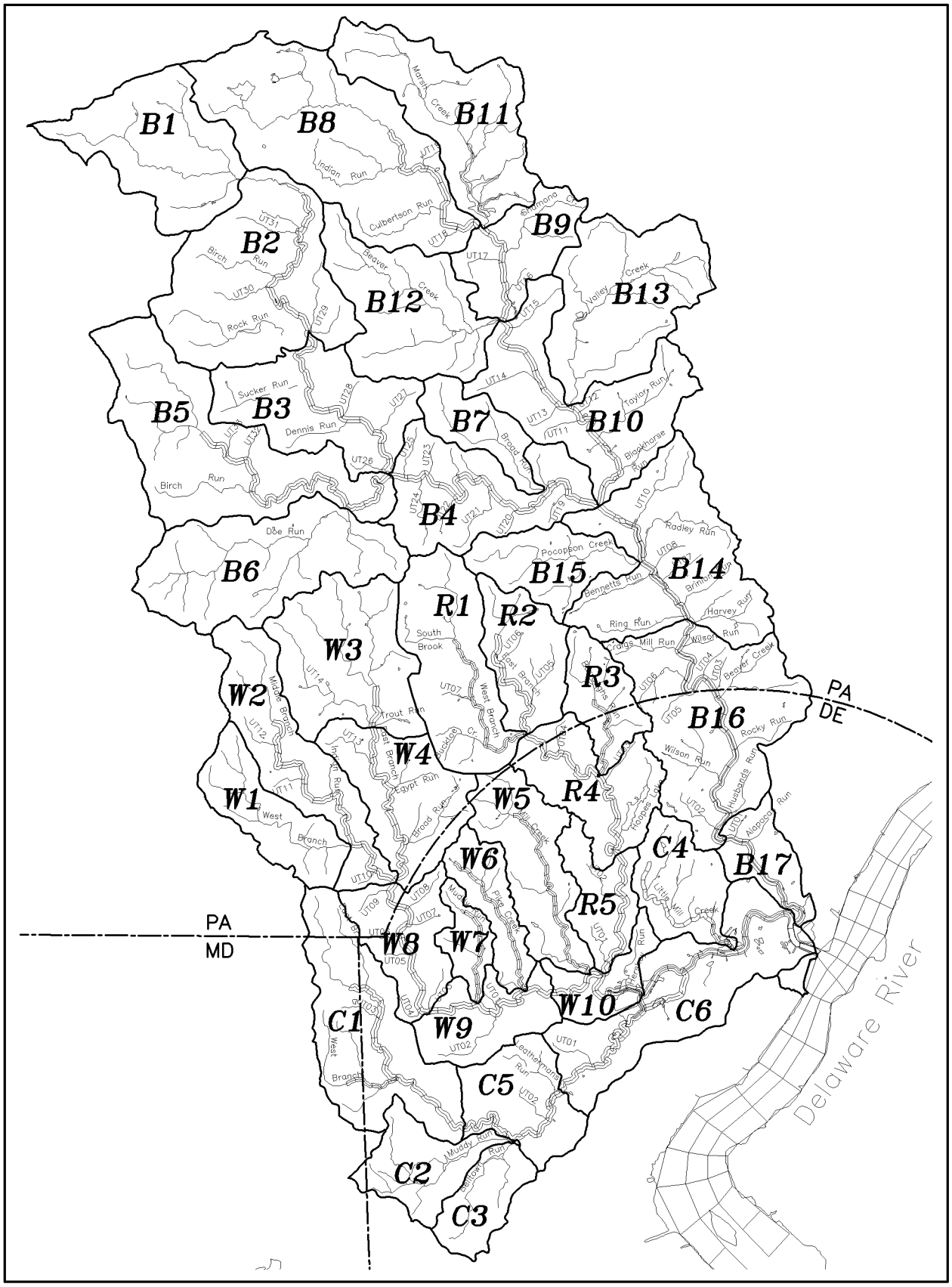

Figure 7-1. Watershed delineation for HSPF model of Christina Basin.

This page intentionally left blank

8 - DELAWARE RIVER BOUNDARY CONDITIONS

Tides were specified at the north and south boundaries in the Delaware River based on the astronomical harmonic constants for the NOAA subordinate tide stations at Reedy Point, Delaware (south boundary) and Chester, Pennsylvania (north boundary). The predicted tides from the harmonic constants will not include any low-frequency influences due to storms or regional low pressure conditions.

The specification of boundary conditions was required at the model north and south interface with the Delaware River. The EFDC water quality model accommodates 21 boundary variables, each specified in an individual time-series data file of concentrations (Table 8-1). Advective boundary conditions in the Peconic Estuary model were of the "upwind" type. Evaluation of the boundary concentration depended on the direction of flow at the boundary. When flow was out of the model, the boundary concentration was assigned the concentration in the model cell immediately upstream of the boundary. When the tidal flow was into the model, the boundary concentration was assigned a specified, time-varying value representative of conditions outside the model domain. To estimate recirculation at the boundary near the time of flow reversal from outgoing to incoming tide, the last outgoing concentration at the boundary is used as the incoming concentration for a certain amount of time specified by the user. This concentration linearly approaches the specified outside boundary concentration over that time period. For the Christina River model, the recirculation time interval was specified as 60 minutes based on experience gained from previous water quality model applications of the EFDC model.

Delaware River boundary conditions for salinity, temperature, total suspended sediment, algae, organic carbon, dissolved oxygen, nitrogen, phosphorus, silica, and fecal coliform bacteria were specified based on available STORET data at stations in the Delaware River. The boundary time-series were created using observations that were averaged by month over the simulation period. If data for a parameter were not available for any given month, then the long-term average (over the period 1988-1998) for that month was used instead. The boundary conditions for two parameters, unavailable silica and COD, were set to constant values because no information was available to produce a time-varying boundary. The boundary condition for unavailable silica was set to 0.10 mg Si/L based on the value used for the Long Island Sound Study model (HydroQual 1991). The boundary condition for COD was set to a nominal value of 1.0 mg/L. Total active metal was not included in the simulation. The time-series boundary conditions for each parameter are shown in Figures 8-1 to 8-7 for the calibration period.

Table 8-1. Specified boundary condition parameters in EFDC water quality model.

(1) cyanobacteria (CYA)	(12) labile particulate organic nitrogen (LPN)
(2) diatom algae (DIA)	(13) dissolved organic nitrogen (DON)
(3) green algae (GRN)	(14) ammonia nitrogen (NH4)
(4) refractory particulate organic carbon (RPC)	(15) nitrate nitrogen (NO3)
(5) labile particulate organic carbon (LPC)	(16) unavailable biogenic silica (SUU)
(6) dissolved organic carbon (DOC)	(17) available dissolved silica (SAA)
(7) refractory particulate organic phosphorus (RPP)	(18) chemical oxygen demand (COD)
(8) labile particulate organic phosphorus (LPP)	(19) dissolved oxygen (DOO)
(9) dissolved organic phosphorus (DOP)	(20) total active metal (not simulated) (TAM)
(10) total orthophosphate (P4T)	(21) fecal coliform bacteria (FCB)
(11) refractory particulate organic nitrogen (RPN)	

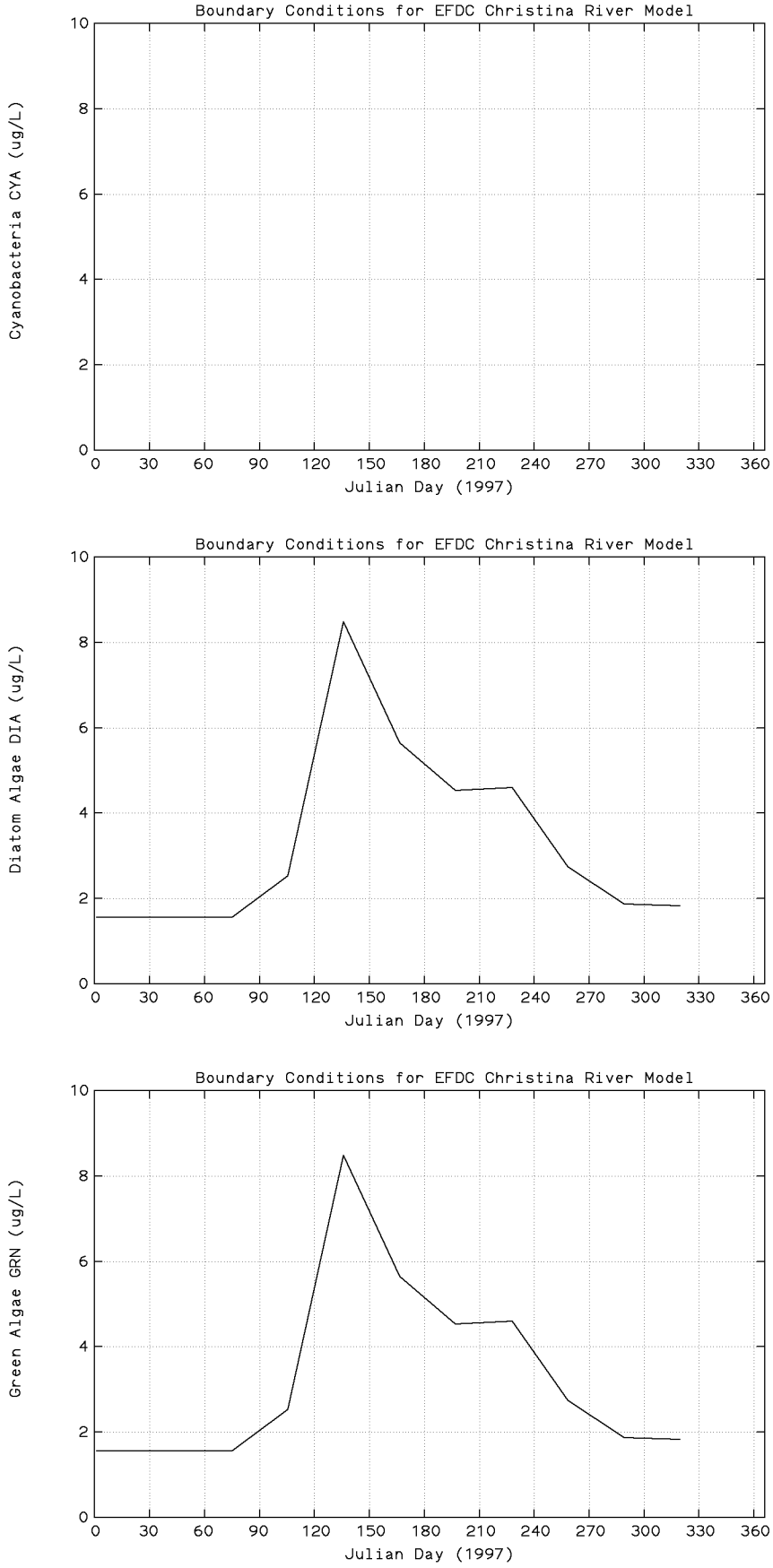

Figure 8-1. Boundary concentrations for CYA, DIA, and GRN algae.

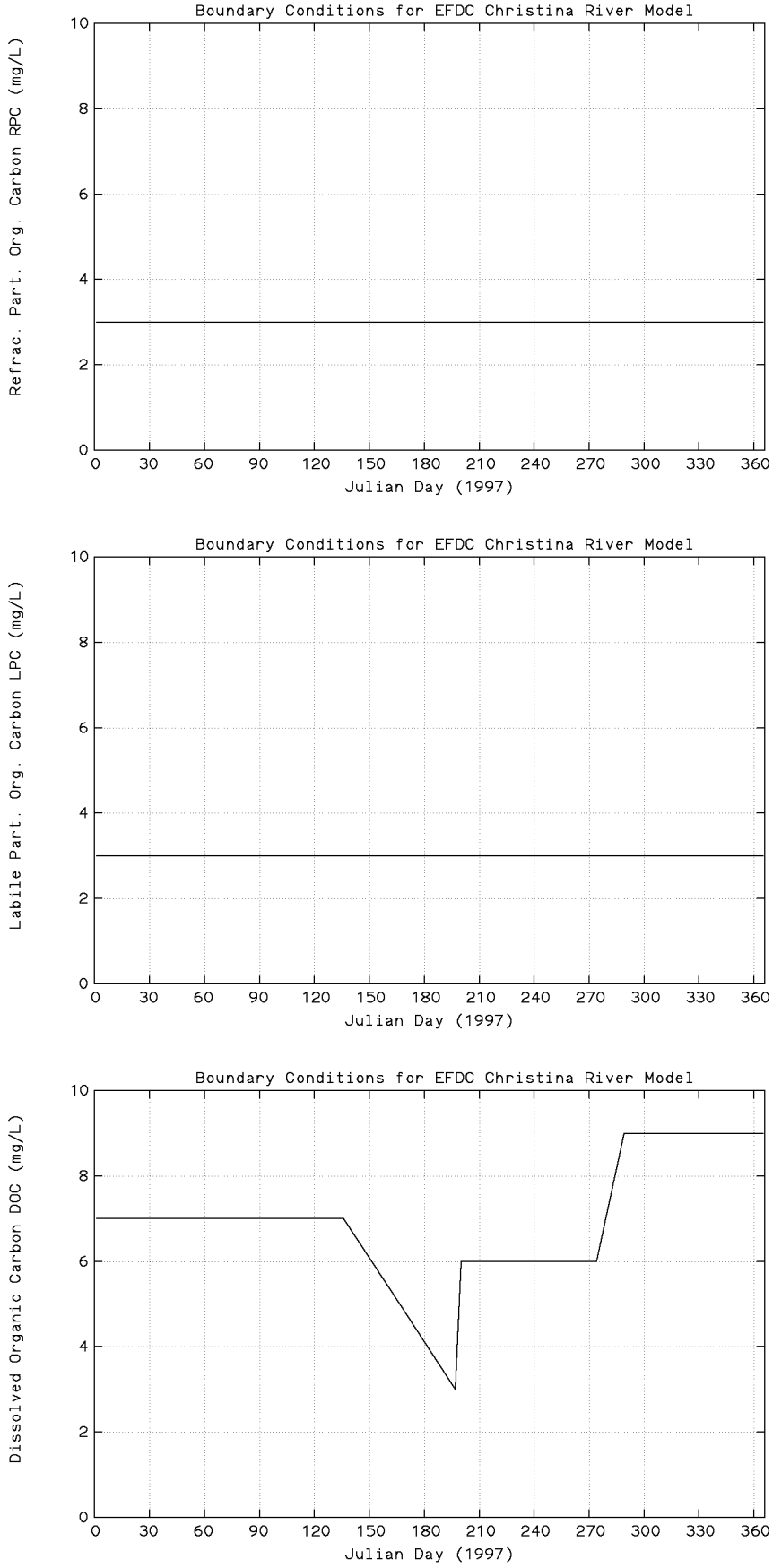

Figure 8-2. Boundary concentrations for RPC, LPC, and DOC.

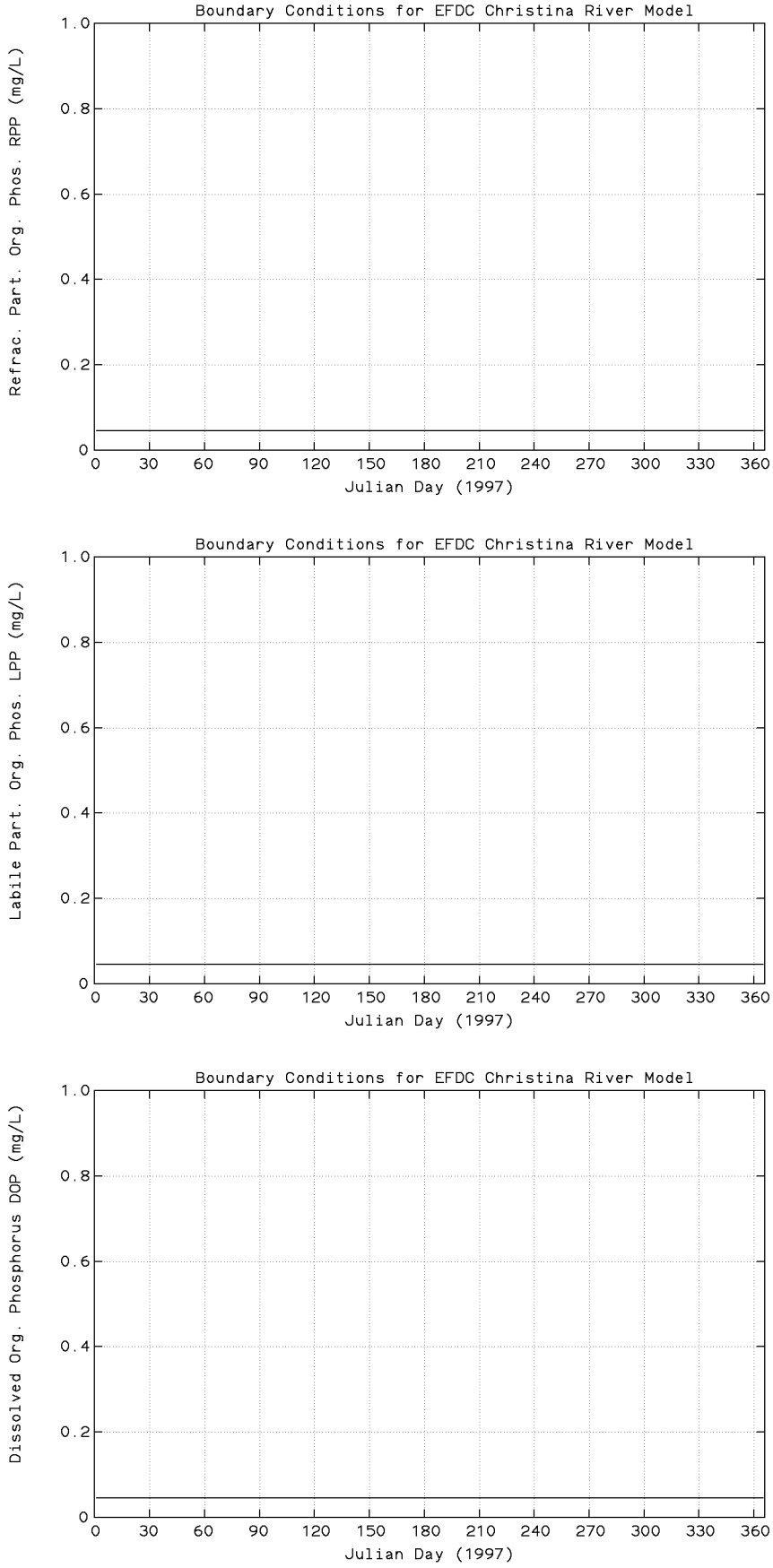

Figure 8-3. Boundary concentrations for RPP, LPP, and POC.

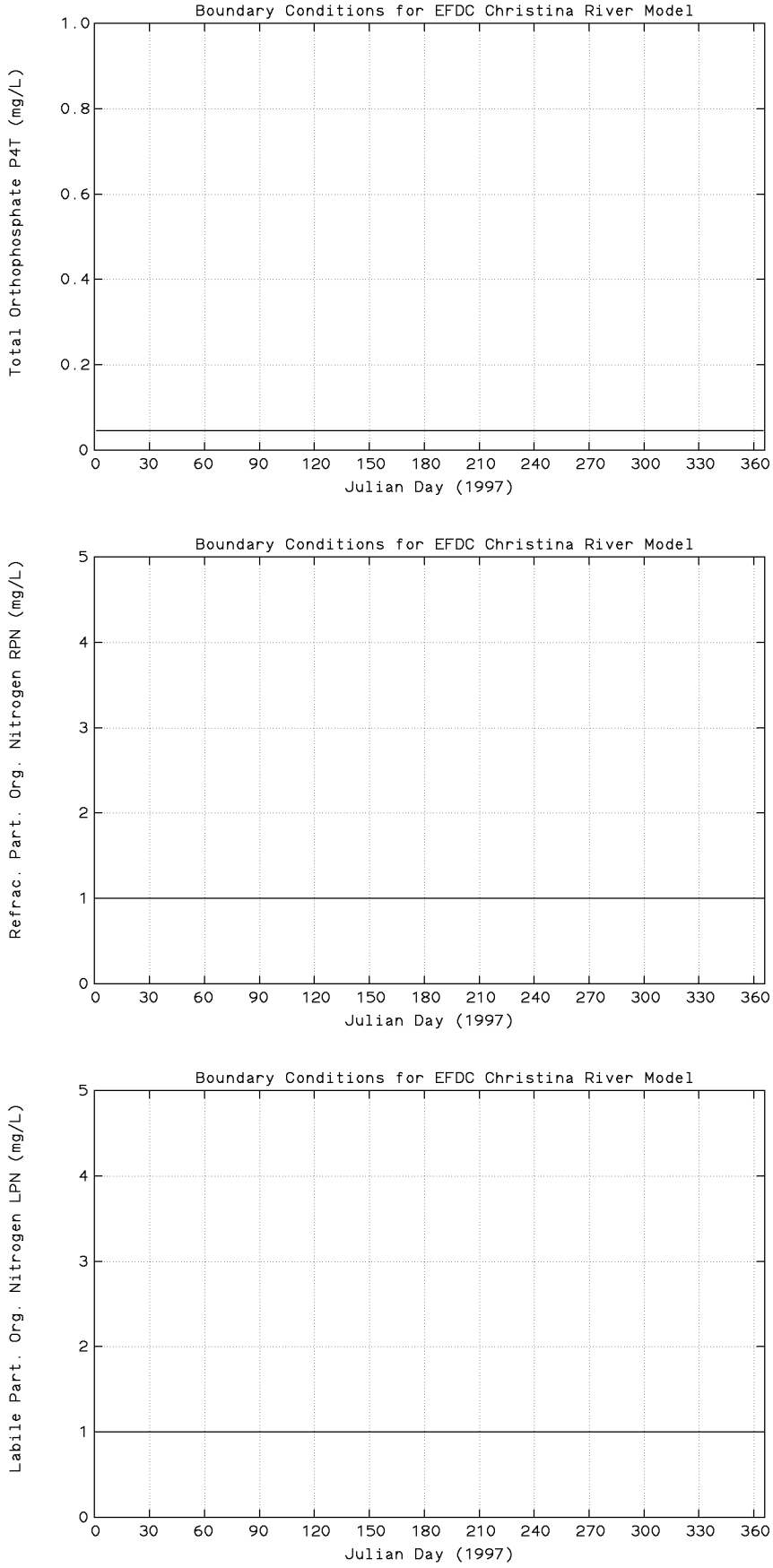

Figure 8-4. Boundary concentrations for P4T, RPN, and LPN.

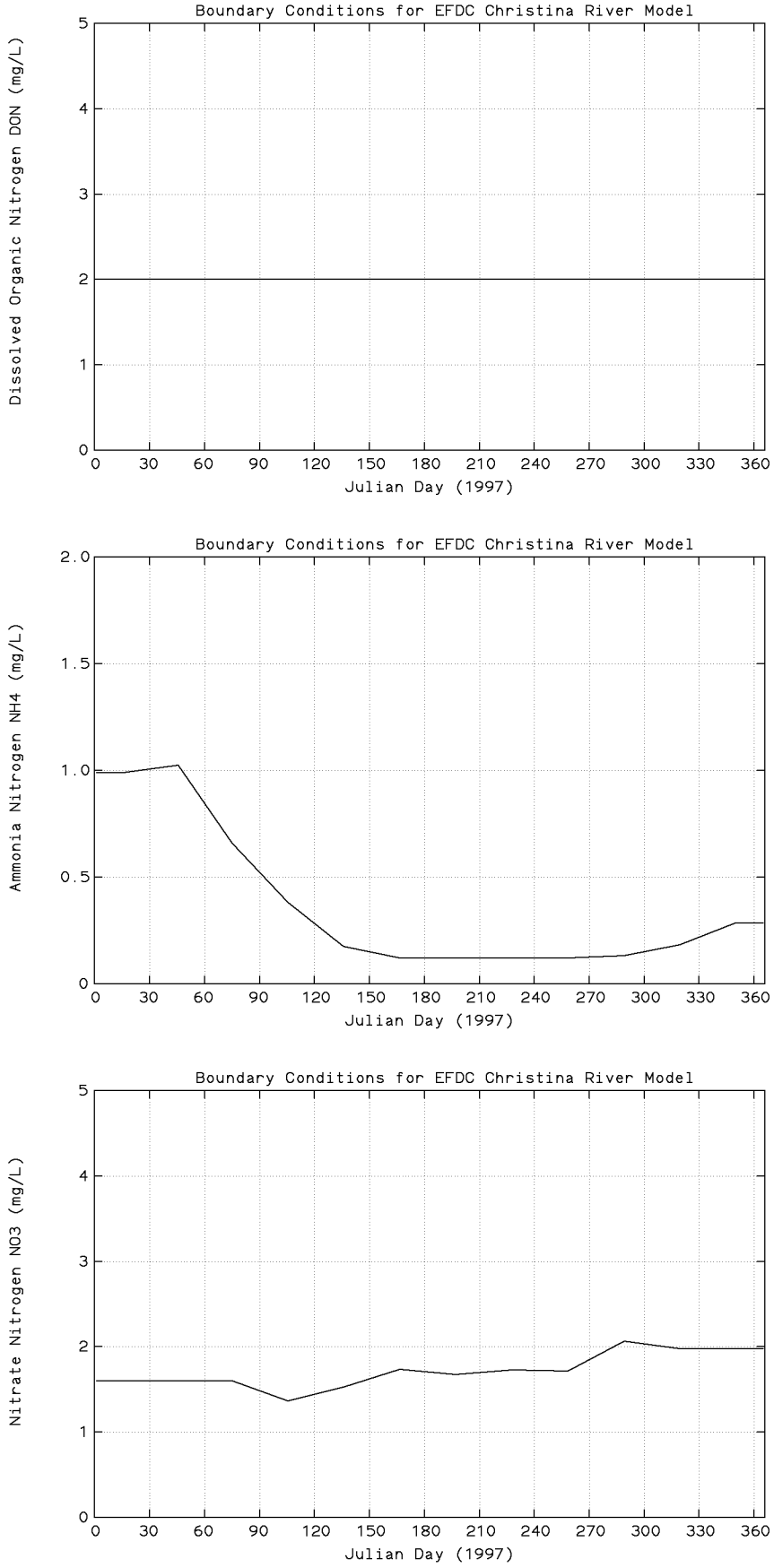

Figure 8-5. Boundary concentrations for DON, NH4, and NO3.

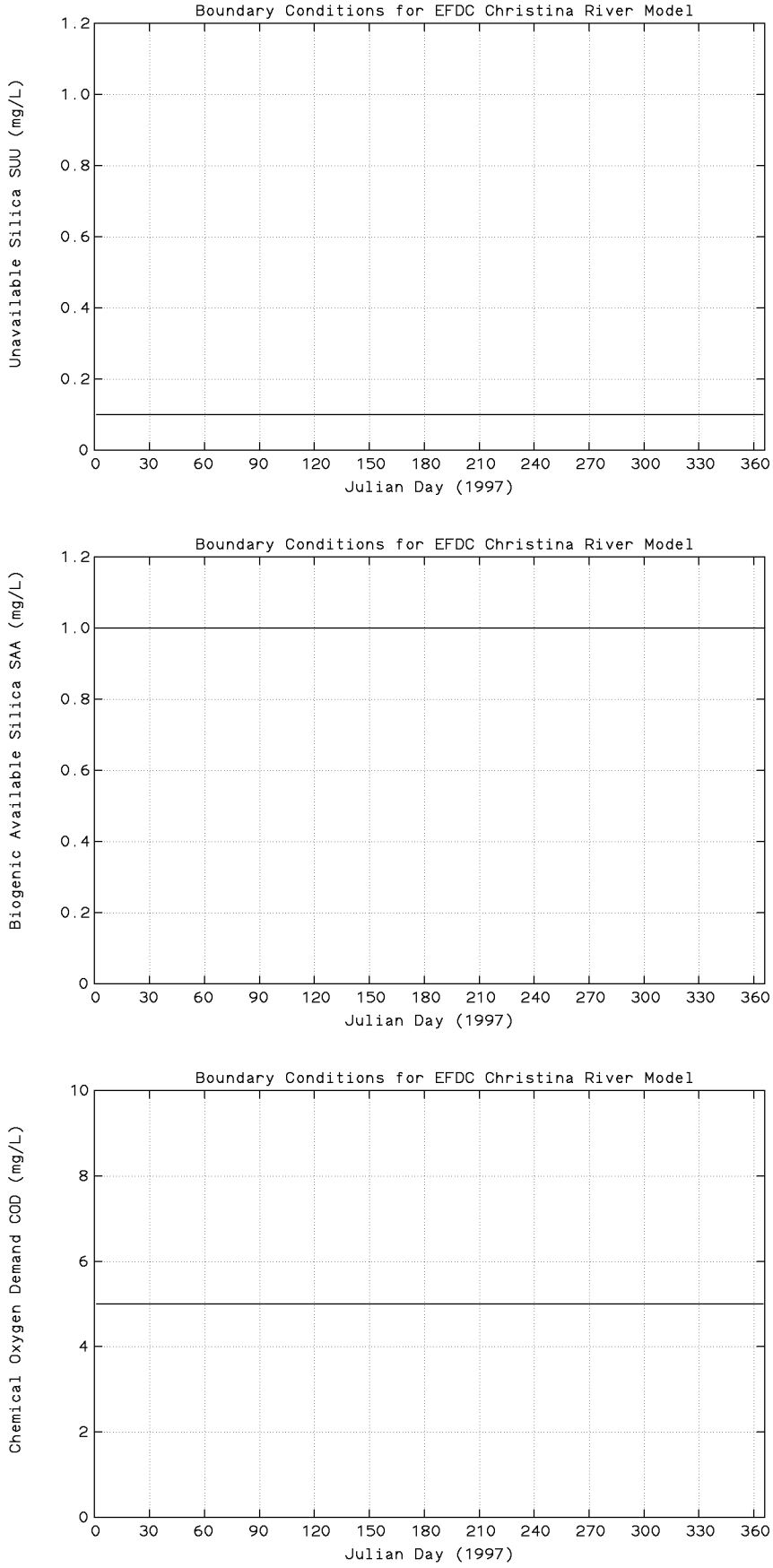

Figure 8-6. Boundary concentrations for SUU, SAA, and COD.

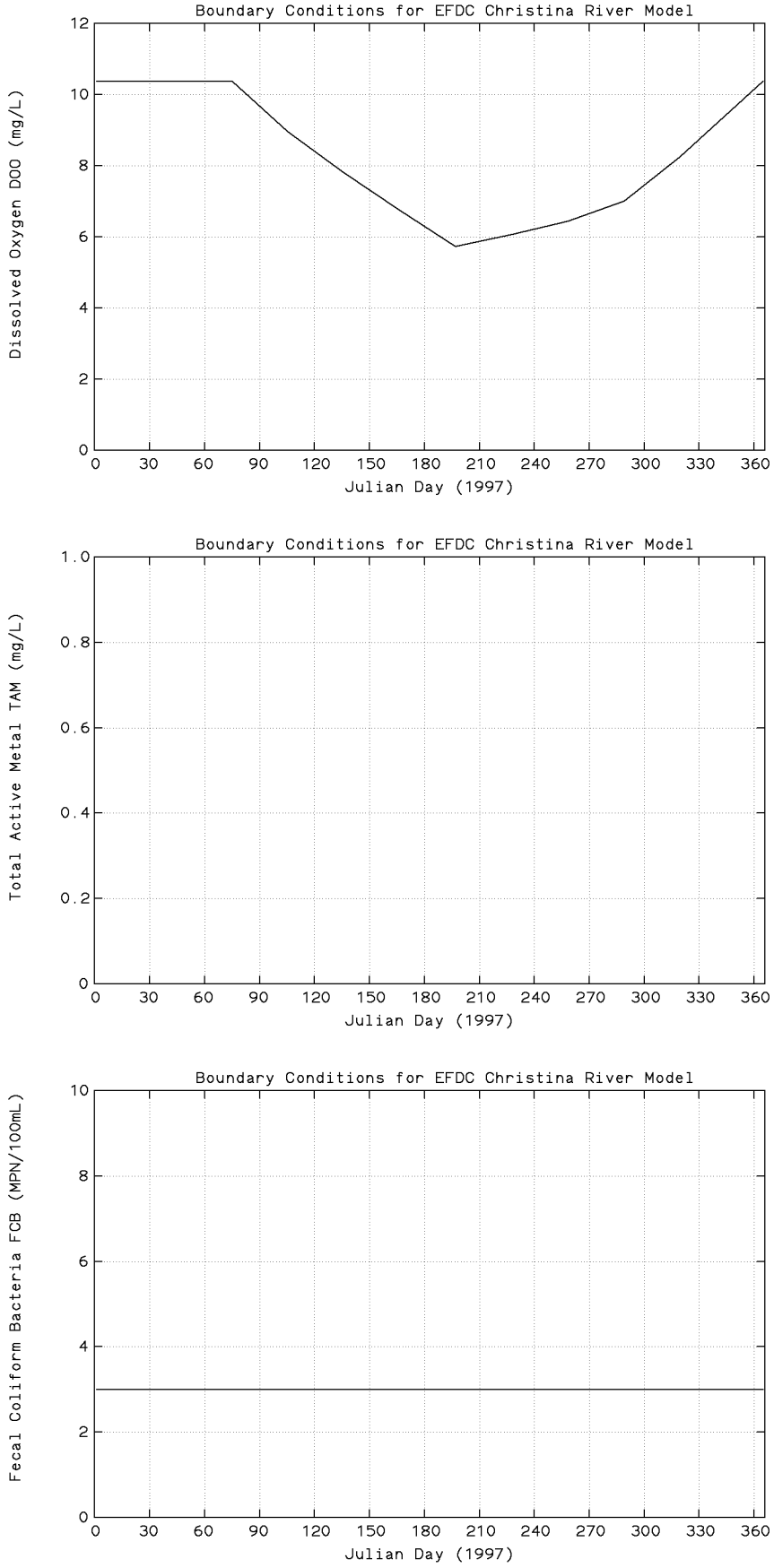

Figure 8-7. Boundary concentrations for DOO, TAM, and FCB.

This page intentionally left blank

9 - MODEL CALIBRATION

Model calibration involves the adjustment of certain model input quantities in an attempt to achieve a specified level of model performance. An extensive set of field data were gathered, processed, and displayed for modeling hydrodynamics and water quality transport in the Christina River Basin. The data set included database files containing more than 40,000 records at about 200 stations scattered throughout the interior of the basin as well as in the Delaware River itself. This section presents the results of the calibration of the EFDC hydrodynamic and water quality model. Parameters considered for calibration include flow rate, tidal surface elevation, chlorides, and a suite of water quality parameters.

9.1 Computational Grid

The basic equations in EFDC were solved using the finite-difference method. The grid was designed to resolve velocity shears both axially and laterally, and at the same time allow a time step suitable for efficient computation. Solutions to the hydrodynamics were obtained using a 60-second time step. The spatial domain of the study area was divided into a grid of discrete cells. To achieve close conformance of the grid to the estuary geometry, the cells in the Delaware River were represented using curvilinear horizontal grid cells constructed using an orthogonal mapping procedure (Ryskin and Leal 1983) to form a 2-D grid domain. The cells in the narrow tidal and nontidal streams were represented in a 1-D Cartesian coordinate system (see Figure 9-1). To obtain adequate resolution in the streams, longitudinal cells were configured to lengths ranging from 500 to approximately 1,000 meters. Cell widths were adjusted according to estimated stream channel widths. Velocities were computed on the boundaries between cells, and temperature, salinity, and density were computed at the center of each cell. The numerical grid consisted of 406 cells in the horizontal plane and a single vertical layer. A single layer was chosen because the estuary and streams are well mixed, thereby implying that stratification would not be an issue. In addition, field data available from STORET and from Davis (1998) did not distinguish vertical sample depths.

9.2 Model Configuration

The general procedure for application of the EFDC model to the Christina River Basin followed a sequence of steps beginning with model set up or configuration and continued through model execution of the calibration time period. Model configuration involved the construction of the horizontal grid for the waterbodies in the basin, interpolation of bathymetric data to the grid, construction of EFDC input files, and compilation of the FORTRAN source code with appropriate parameter specification of array dimensions. The model included 120 point source discharges (see Figure 9-1) and 28 consumptive use water withdrawals (see Figure 9-2).

The numerical model domain includes the tidal Delaware River from Reedy Point on the south to Chester on the north. Both the tidal and nontidal Christina River are included in the model. The lower Christina River is directly connected to the Delaware River. The nontidal Christina River is connected to the tidal portion by a dam control structure at Smalley's Pond. The tidal Brandywine Creek is connected to the Christina River by means of an inlet control structure. The tidal White Clay Creek is also connected to the Christina River via an inlet control structure. There are 27 control structures in the model, 4 inlet structure pairs, 11 confluence connections, and 12 control structures. These control structures represent low head dams and abrupt bottom elevation changes at bridge crossings as well as larger dams. The locations of the control structures are shown in Figure 9-1 and are described below in Table 9-1.

Table 9-1. Hydraulic control structures in Christina River Basin EFDC model.

Structure ID	Description	Structure ID	Description
1	Dam at Smalley's Pond, Christina River	18	Fall line, lower Red Clay Creek
2, 3	Tidal inlet, mouth of Brandywine Creek	19	Connection, E. Br. Red Clay to Red Clay Creek
4, 5	Tidal inlet, Nonesuch Cr.-Christina River	20	Connection, W. Br. Red Clay to Red Clay Creek
6, 7	Tidal inlet, Nonesuch Cr.-Christina River	21	Fall line, lower White Clay Creek
8, 9	Tidal inlet, mouth of White Clay Creek	22	Bridge culvert, Harmony Rd., White Clay Creek
10	Low dam, lower Brandywine Creek	23	Low dam, White Clay Creek
11	Submerged weir, Lenape, Brandywine Creek	24	Bridge culvert, Hopkins Road, White Clay Creek
12	Connection, Brandywine Cr to East Branch	25	Connection, E. Br. White Clay to White Clay Creek
13	Submerged weir, Embreeville, E.Br. Brandywine	26	Connection, W. Br. Christina to Christina River
14	Submerged weir, Mortonville, E.Br. Brandywine	27	Connection, Little Mill Creek to Christina River
15	Submerged weir, South Coatesville, E.Branch	28	Connection, Burroughs Run to Red Clay Creek
16	Dam, Icedale Lake, E.Br. Brandywine Creek	29	Connection, Mill Creek to White Clay Creek
17	Connection, Buck Run to E.Br. Brandywine Cr.	30	Connection, Pike Creek to White Clay Creek
		31	Connection, Muddy Run to White Clay Creek

9.3 Calibration Period

The time period for model calibration, May 1 to September 21, 1997, was selected because it included the detailed field survey period in which water quality data were collected by Davis (1998) as well as other monitoring data from DNREC, PADEP, USGS, and others. During the August and early September 1997 time period, stream flow throughout the basin was near the 7Q10 flow rate. Data for comparison to the model water quality results for stream reaches, other than those sampled by Davis

(1998) and three USGS locations, were generally monitored on a bimonthly basis during the calibration period.

9.4 Hydrodynamic and Hydraulic Calibration

Calibration of the hydrodynamic model involved adjustment of the open boundary water surface elevation forcing, the bottom boundary roughness, and local bathymetry. The open boundary tidal elevation, specified as a linear variation of the tidal constituent amplitudes and phases, was adjusted until predicted amplitudes and phases agreed with those obtained from an analysis of the USGS tide gage records at the Port of Wilmington and Newport. The model was executed for a period of 143 days from May 1 to September 21, 1997. The model results were then compared against available observations at interior monitoring stations. Comparisons were made for tide height and phase, flow rate, and chloride concentration at various locations in the model.

9.4.1 Calibration of Tide Elevation

Calibration of the model with respect to water surface elevation was accomplished by analysis of observed and model predicted time-series data at two interior tide stations. For tidal waters, least squares harmonic analysis is the most commonly utilized procedure (Oey, Mellor, and Hires 1985; Cheng et al. 1993; Shen et al. 1999). Tide elevation data were obtained from the USGS tide stations on the Christina River at the Port of Wilmington near the mouth and at Newport about 7.0 miles upstream of the mouth. These data were compared with surface elevations computed by the model at cell 56,13 (Port of Wilmington) and 45,13 (Newport). The time-series of tide elevations for the month of August 1997 for both the field data and model results were subjected to a harmonic analysis. The five most important astronomical harmonic constituents (M2, S2, N2, K1, and O1) were computed for both the field data and model simulation results. The harmonic analysis results, shown in Table 9-2, indicate the model is in good agreement with the measured tide data for both amplitude and phase. The model-data amplitudes for the M2 harmonic constituent agree within 5 cm (6%) and the phases agree to within 4 degrees (3%). Time-series graphs (Figure 9-3) of the observed and model tide elevations at both the Port of Wilmington and Newport covering a 15-day period (August 1 - 15, 1997) provide a visual means of assessing the skill of the model in simulating tidal elevations. The model tides are forced at the north and south boundaries in the Delaware River based on the NOAA predictions at the Reedy Point and Chester subordinate stations (NOAA 1998). These predictions do not consider low-frequency phenomenon caused by regional low pressure systems or storms that will be found in the signal of the tide data collected at the two USGS tide stations on the Christina River.

Table 9-2. Harmonic analysis of tides at Port of Wilmington and Newport.

Harmonic Constant	Port of Wilmington		Newport	
	Amplitude (m)	Phase (degrees)	Amplitude (m)	Phase (degrees)
M2 - observed	0.7594	130.382	0.6901	153.634
M2 - model	0.7135	134.180	0.6768	155.560
Difference	0.0459	-3.798	0.0133	-1.926
S2 - observed	0.0894	20.621	0.0900	36.374
S2 - model	0.1001	30.806	0.0890	59.180
Difference	-0.0107	-10.185	0.0010	-22.806
N2 - observed	0.1271	323.153	0.1275	345.054
N2 - model	0.1383	336.181	0.1240	3.603
Difference	-0.0112	-13.028	0.0035	-18.549
K1 - observed	0.0802	174.059	0.0615	184.740
K1 - model	0.0633	178.335	0.0606	190.948
Difference	0.0169	-4.276	0.0009	-6.208
O1 - observed	0.0626	316.879	0.0546	332.386
O1 - model	0.0546	326.765	0.0514	337.937
Difference	0.0080	-9.886	0.0032	-5.551

9.4.2 Hydraulic Flow Balance

Calibration of the hydraulic flow balance in the model system was determined by comparing the model and observed hydrograph at 12 USGS stream gage locations in the Christina River Basin for the calibration period. Estimates of unit discharge rates (cfs per square mile) were determined for each of the 39 subwatersheds for each day in the calibration period. The daily flow rates for each subwatershed were then distributed uniformly among each of the grid cells within a subwatershed, except for headwater grid cells, which were assigned a flow rate in accordance with the contributing area to that cell. The model was then run for the 143-day period, and the flow rate at the appropriate gage location was compared with the model results. The model flow rates compared reasonably well with the daily average flows at the stream gages (see Figures 9-4 to 9-7). The purpose of the hydraulic flow balance comparison to the USGS gage data was to determine whether the runoff rates from the contributing subwatersheds were properly apportioned to the model grid cells. Normally, a watershed runoff model would be used to provide flows to the receiving water model. However, the calibrated HSPF watershed model will not be available for a few more years. The model hydrograph agrees well with the stream gage data during periods between storm runoff events. At certain locations, the model tends to underpredict the peak flow rates of the storm events. The use of a watershed runoff model in the future will likely improve the peak flow calibration because the timing of the peak runoff from each subwatershed will be taken into account (a procedure that was not possible in the present model application).

9.4.3 Water Depth and Stream Velocity

Measurements of flow, water depth, and stream velocity were made at eight locations during the August 1997 field survey (Davis 1998). The field measurements were made on the following dates: East Branch Brandywine Creek (08/12 - 08/14/97), West Branch Brandywine Creek (08/19 - 08/20/97), West Branch Red Clay Creek (08/05 - 08/07/97 and 08/12 - 08/14/97), and East Branch White Clay Creek (08/26 - 08/28/97). A comparison of these measurements with the model results at the appropriate grid cell location is given in Table 9-3.

Table 9-3. Model-data comparison of velocity, flow, and geometry (August 1997 data).

Stream Reach	EFDC Cell	Velocity (fps)		Depth (ft)		Flow (cfs)		Rect. Channel Width (ft)	
		Field	EFDC	Field	EFDC	Field	EFDC	Field	EFDC
East Branch Brandywine Creek	54,61	0.33	0.48	0.82	0.87	14.5	25.6	53.6	52.5
East Branch Brandywine Creek	54,56	0.85	0.56	1.02	1.11	34.3	34.5	39.6	52.5
West Branch Brandywine Creek	19,79	0.40	0.41	1.09	0.94	9.5	14.9	45.0	42.6
West Branch Brandywine Creek	26,79	0.41	0.36	0.70	0.82	32.0	32.9	111.5	111.5
East Branch White Clay Creek	19,31	0.44	0.40	0.93	0.96	5.30	5.33	13.0	12.8
East Branch White Clay Creek	19,29	0.42	0.41	0.85	0.86	7.35	7.34	20.6	20.3
West Branch Red Clay Creek	29,43	0.35	0.44	0.75	0.78	3.55	3.35	13.5	13.5
West Branch Red Clay Creek	33,43	0.49	0.52	0.90	0.94	5.45	4.92	12.4	12.4

9.4.4 Chloride Concentrations

The ability of a numerical hydrodynamic model to predict the transient distribution of chlorides or salinity is viewed as the most important measure calibration skill if the ultimate use of the model is prediction of the transport and fate of dissolved contaminants. Since chloride distribution is a direct consequence of physical transport by advection and turbulent diffusion, chloride calibration substantiates advective and diffusive transport on a global flux scale rather than the point scale addressed by water surface elevation calibration. An acceptable chloride calibration supports the accuracy of global scale transport even under conditions of marginal verification of the model's ability to predict velocity and water surface elevation at specific observation points. The model-data comparisons of chloride concentration for the longitudinal transects representing the stream reaches included in the model are presented in figures in Appendix A. The "box-and-whisker" data shown on these graphs were obtained from STORET over the period June 1 to September 30, 1997. The box-and-whisker data points represent the average, median, 25th percentile, 75th percentile, minimum, and maximum. The sample data collected during the August 1997 field survey (Davis 1998) are also shown on these graphs as the mean and

standard deviation. Chloride concentrations computed by the EFDC model compare well with the observed data for all stream reaches.

9.5 Water Quality Calibration Results

Each observation in STORET was collected at an instant in time and at a single point in space. Time scales realistically represented in the EFDC model were determined by time scales of primary forcing functions: 60-second tidal hydrodynamics, hourly meteorological updates, monthly ocean boundary conditions, constant nonpoint source concentration estimates, daily nonpoint source flows, monthly point source loads, and hourly atmospheric wet deposition. The minimum model spatial scales were determined by the size of the grid cells, ranging from 500 to about 1,000 meters in the longitudinal direction along the streams. Data for longitudinal transect comparisons were averaged over the period June 1 to September 30, 1997. The disparity in the temporal and spatial scales between the model and prototype, especially for the nonpoint and point source loads, meant that individual observations may not be directly comparable with model prediction at a specific time in a given model grid cell.

Model-data comparisons will be made by means of longitudinal transect plots as well as time-series plots for the 11 major stream reaches in the study area: Brandywine Creek, East Branch Brandywine Creek, West Branch Brandywine Creek, Buck Run, Christina River (tidal), Christina River (nontidal), Red Clay Creek, West Branch Red Clay Creek, White Clay Creek, East Branch White Clay Creek, and the Delaware River. The transects are delineated in river miles referenced to River Mile 74.9 located at the mouth of the Christina River based on EPA REACH FILE 1 (Table 9-4). Longitudinal transect plots for each water column parameter are presented in Appendix A arranged by stream reach. There are 18 transect plots for each reach, representing 18 different water quality parameters. The model results for the transect plots were averaged over the period August 5 to August 20, 1997. The horizontal axis of each plot represents the river mile from the mouth of the Christina River measured along the stream network. The vertical axis represents the water column parameter concentration. The observed data are shown as "box-and-whisker" symbols indicating the maximum, minimum, 25^{th} percentile, 75^{th} percentile, mean, and median statistics. The model output results are represented by three lines, the solid line indicates the mean over the averaging period at a given model grid cell and the two dashed lines represent the minimum and maximum values simulated over the averaging period.

The time-series plots are provided in Appendix B and cover the entire 143-day calibration period beginning on May 1 (day 121) and continuing to September 21, 1997 (day 264). The time-series model-data comparisons were made at 16 monitoring locations on the various stream reaches in the study area (see Figure 9-8). The concentrations of the nonpoint source loads were considered to be constant throughout the calibration period, and the loads vary in accordance with the changes in nonpoint source

flow rate. The nonpoint source concentrations were based on the summer low-flow monitoring data and are representative of background water quality conditions. In reality, the concentrations of the various water quality parameters will vary in relation to storm events and changes in watershed runoff. Determination of the time-varying nonpoint source concentrations was outside the scope of the present study, but will be addressed in the future following completion of the HSPF watershed model of the Christina River Basin.

Table 9-4. Stream reaches included in EFDC Christina River Basin water quality model.

Stream Reach	River Mile at Mouth	River Mile at Upstream Extent
Christina River (tidal)	74.9	89.6
Christina River (nontidal)	89.6	103.0
Christina River West Branch	98.5	100.4
Brandywine Creek (main stem)	76.3	95.8
Brandywine Creek East Branch	95.8	113.7
Brandywine Creek West Branch	95.8	120.7
Buck Run	106.6	117.3
Red Clay Creek and East Branch	87.6	104.9
Red Clay Creek West Branch	100.3	104.9
White Clay Creek and Middle Branch	85.6	109.7
White Clay Creek East Branch	99.9	107.1
Delaware River	62.6	86.5
Little Mill Creek	79.8	85.4
Mill Creek	87.9	94.7
Burroughs Run	97.1	100.2
Pike Creek	90.6	95.9
Muddy Run	93.2	96.5

9.5.1 Brandywine Creek Main Stem Water Quality Calibration Results

The transect plots for all water quality parameters for the main stem of Brandywine Creek are shown in Figures A01 - A03, and the time-series plots at stations 104021 and WQN0105 are shown in Figures B01 - B04. The conservative constituents (chlorides and TSS) match the observed data very well in both the transect and time-series plots. The time-series of TSS shows little variation because a constant nonpoint source concentration was used for the entire time period, whereas in reality the TSS concentrations would increase during storm runoff events. The grab samples of dissolved oxygen all lie within the minimum and maximum range computed by the model for both the transect and time-series views. The observed organic carbon indicates an increasing trend in the downstream direction that is stronger than computed by the model. This is likely due to missing sources of organic carbon. Also, the total phosphorus and dissolved orthophosphate indicate an increasing concentration in the downstream direction that is not simulated in the model. The nitrogen species (total nitrogen, ammonia nitrogen, and nitrate nitrogen) all match the observations along the transect quite well.

9.5.2 Brandywine Creek East Branch Water Quality Calibration Results

The transect plots for all water quality parameters for the East Branch Brandywine Creek are shown in Figures A04 - A06, and the time-series plots at station 01480870 are shown in Figures B05 and B06. The Downingtown WWTP (PA0026531) discharges at river mile 103.7, which accounts for the spike in concentrations of various water quality parameters at that location. Along the transect, all water quality parameters are in agreement with observations. The time-series plots also indicate the model is in agreement with observations with the exception of fecal coliform bacteria, which is underpredicted in the model. This is most likely due to nonpoint sources that are not accounted for in the model.

9.5.3 Brandywine Creek West Branch Water Quality Calibration Results

The transect plots for all water quality parameters for the West Branch Brandywine Creek are shown in Figures A07 - A09, and the time-series plots at station 01480617 are shown in Figures B07 and B08. The South Coatesville WWTP (PA0036987) and Coatesville City WWTP (PA0026859) discharge at river mile 110.4 and 111.0, respectively. The spike in the concentrations of various water quality parameters is due to these two discharges. The model agrees with the observed data very well for chlorides, TSS, dissolved oxygen, chlorophyll-*a*, organic carbon, total nitrogen, ammonia nitrogen, and nitrate nitrogen. The model somewhat underpredicts the phosphorus species downstream of the two aforementioned WWTPs. The reason for this is not clear because phosphorus was a measured parameter reported on the discharge monitoring records at these two WWTPs and was not based on default estimates. Fecal coliform bacteria (see Figure B08) simulated by the model are about an order of magnitude less than the observations. This is likely due to nonpoint sources that are not accounted for in the model.

9.5.4 Buck Run Water Quality Calibration Results

The transect plots for all water quality parameters for Buck Run are shown in Figures A10 - A12. No time-series plots are presented for Buck Run. No observed data were available for Buck Run during the calibration period, so calibration cannot be assessed in this stream reach.

9.5.5 Christina River (Tidal) Water Quality Calibration Results

The transect plots for all water quality parameters for the tidal Christina River are shown in Figures A13 to A15, and the time-series plots at stations 106291 and 106021 are shown in Figures B23 to B26. The lower portion of the Christina River is strongly influenced by the Delaware River because of tidal excursion. The transect plots indicate the model agrees well with the data for all water quality parameters with the exception of total nitrogen, which is slightly high in the model. The time-series plots also indicate similar good model-data agreement. The two observations of chlorophyll-*a* at station 106021 reach levels of about 108 ug/L in late May and 67 ug/L in mid-July whereas the model computes a maximum concentration of about 40 ug/L in late May. One possibility for this discrepancy may be influences from nearby Churchman's Marsh, which is not included in the model.

9.5.6 Christina River (Nontidal) Water Quality Calibration Results

The transect plots for all water quality parameters for the nontidal Christina River are shown in Figures A16 - A18, and the time-series plots at station 106031 are shown in Figures B27 and B28. Along the transect, all water quality parameters agree with the observations quite well. The spike in chlorides concentration at river mile 98.1 is due to the West Branch Christina River, which carries loads from the two Maryland WWTPs (MD0022641 and MD0065145).

9.5.7 Red Clay Creek and East Branch Water Quality Calibration Results

The transect plots for all water quality parameters for Red Clay Creek and East Branch Red Clay Creek are shown in Figures A19 to A21, and the time-series plots at stations 103031, WQN0150, and RCEB04 are shown in Figures B09 to B14. The West Branch Red Clay Creek enters at river mile 100.3 and accounts for the spikes in concentration that are evident in a number of the transect plots. Overall, the model does a reasonable job of simulating the observations for both the transect and time-series views. At stations 103031 and WQN0150, the total phosphorus and dissolved orthophosphate data indicate an increasing trend from May to September (see Figures B10 and B12). This tends to support the hypothesis that the primary sources for phosphorus may be from a relatively steady-state source (i.e., point source or groundwater source) because as the stream flow decreases in the summer months, the concentration of phosphorus is increasing.

9.5.8 Red Clay Creek West Branch Water Quality Calibration Results

The transect plots for all water quality parameters for West Branch Red Clay Creek are shown in Figures A22 - A24, and the time-series plots at station RCWR2 are shown in Figures B15 and B16. The Kennett Square WWTP (PA0024058) discharges at river mile 103.9, accounting for the spike in concentrations at that location. The simulated concentrations of all water quality parameters agree with the observed data along the transect. Station RCWR2 is Reach 2 of the August 1997 study (Davis 1998). Dissolved oxygen is controlled by reaeration, sediment oxygen demand, nitrification, denitrification, decay of organic substances, photosynthesis of algae, and respiration of algae. The model represents both the mean and the range of dissolved oxygen very well. The observations indicate a strong oxygen sag occurring about 1.0 mile downstream of the Kennett Square WWTP where the daily minimum dissolved oxygen decreases from about 8.0 mg/L above the WWTP to about 1.9 mg/L at the maximum sag location. In the model, the minimum dissolved oxygen decreases from 7.5 mg/L above the WWTP to a value of 1.7 mg/L below the WWTP discharge. At river mile 103.1, the observed data indicate chlorophyll-*a* levels as high as 42 ug/L, whereas the model indicates concentrations of about 7 ug/L. It is possible that the measured chlorophyll-*a* may have contained periphyton cells that detached from the stream bottom.

9.5.9 White Clay Creek and Middle Branch Water Quality Calibration Results

The transect plots for all water quality parameters for White Clay Creek and Middle Branch White Clay Creek are shown in Figures A25 - A28, and the time-series plots at stations 105151 and WQN0149 are shown in Figures B17 - B20. The transect plots indicate good model-data agreement for all parameters except phosphorus. Downstream of river mile 103, the monitoring data indicate total phosphorus concentrations in the 0.1 to 0.6 mg/L range, whereas the model computes concentrations of about 0.1 mg/L. The reason for this discrepancy is not clear but may be due to inadequate nonpoint source loadings since the only two NPDES point sources downstream of mile 103 are small (Avon Grove School District and FMC Corp.).

9.5.10 White Clay Creek East Branch Water Quality Calibration Results

The transect plots for all water quality parameters for White Clay Creek East Branch are shown in Figures A28 - A30, and the time-series plots at stations WCER2 are shown in Figure B21. Station WCER2 is Reach 2 from the August 1997 study (Davis 1998). The Avondale Borough WWTP (PA0025488) is the largest point source on this stream and discharges at river mile 106.6. The model results are in reasonable agreement for all parameters along the transect and in the time-series views.

9.5.11 Delaware River Water Quality Calibration Results

The transect plots for all water quality parameters for the Delaware River are shown in Figures A31 - A33. The model indicates reasonable agreement for all water quality parameters. One surprising result was the simulated dissolved oxygen sag at river mile 82 that reaches a minimum value of about 2.1 mg/L. The model results can not be validated at that location since no observed data were available.

9.5.12 Muddy Run and Pike Creek Water Quality Calibration Results

Time-series plots for all water quality parameters for Muddy Run (station 105131) and Pike Creek (station 105101) are shown in Figures B29 to B32. The model results agree well with the observations for all parameters with the exception of an apparent algae bloom in mid-July (day 195) at the Muddy Run station. The data indicate a chlorophyll-*a* concentration of about 11 ug/L, whereas the model computes about 2.5 ug/L. However, in late May and mid-September the model agrees very well with the chlorophyll-*a* measurements.

9.6 Diel Dissolved Oxygen Calibration Results

An important feature of the Christina River Basin water quality model is the ability to compute the daily dissolved oxygen range as well as the daily average value. Water quality standards for dissolved oxygen in the Christina River Basin must meet two criteria, one for the daily average and one for the daily minimum concentration. The data available for model calibration included diel dissolved oxygen at a number of locations. The August 1997 survey (Davis 1998), used automatic monitors to record dissolved oxygen concentrations at 15-minute intervals over 2-day periods at locations on the East Branch Brandywine Creek, West Branch Brandywine Creek, West Branch Red Clay Creek, and East Branch White Clay Creek. In addition, the USGS collected diel dissolved oxygen data at three gages for the entire May-September 1997 calibration period: (1) 01480870 at Downingtown on the East Branch Brandywine Creek, (2) 01480617 at Modena on the West Branch Brandywine Creek, and (3) 01481000 at Chadds Ford on the main stem Brandywine Creek.

Achieving the proper range in daily dissolved oxygen is primarily a function of the community periphyton biomass available at a given model grid cell. The periphyton growth and basal metabolism rates as well as the growth rate density limitation parameters were adjusted to simulate the periphyton biomass needed to achieve reasonable daily DO ranges at the monitoring sites during August 1997, the critical low-flow period. The monitored daily minimum, maximum, and average dissolved oxygen concentrations at the three USGS gage locations are shown in Figure 9-9 along with the model results. It is evident that the model does a reasonable job of simulating the daily DO range at these three locations during the month of August. The daily minimum, maximum, and average water temperatures at the three USGS gage locations and the simulated model temperatures are shown in Figure 9-10. Again, the model

is in good agreement with the data for the entire 5-month simulation period. The time-series of periphyton biomass at the three gage locations is shown in Figure 9-11. The periphyton biomass has been displayed in units of ug/L of chlorophyll-*a* for comparison with the floating chlorophyll-*a* concentrations. Thus, the periphyton biomass (50 - 1,000 ug/L) is as much as two orders of magnitude greater than the floating chlorophyll-*a* biomass (3 - 10 ug/L) in these stream reaches. This means that an off-the-shelf model, such as WASP or QUAL2E, which does not include a periphyton state variable, would not be able to simulate the diel DO range by use of floating chlorophyll-*a* alone.

No measurements of periphyton biomass were available for the 1997 calibration period. However, in 1985 a study was conducted on the East Branch Brandywine Creek and periphyton biomass was measured at six locations during the period July 15 to August 7, 1985 (Knorr and Fairchild 1987). The conditions in the stream may have been different between 1985 and 1997 because of changes in wastewater treatment and the magnitude of nutrient loads reaching the stream. Nonetheless, these periphyton measurements represent the only data available for assessing the validity of the model periphyton calculations. A comparison of the periphyton biomass measured in 1985 with the biomass computed by the model is given in Table 9-5. The model biomass for August 4, 1999 (day 216) is reported in the table and is in reasonable agreement with the 1985 biomass measurements. The model periphyton biomass at sites 1 and 3 upstream of the Downingtown WWTP (river mile 103.7) is somewhat less than reported in 1985. The periphyton biomass computed by the model at sites 4 and 5 downstream of the Downingtown WWTP is slightly higher than the 1985 measurements, and at site 6 the model periphyton biomass is within the range reported in 1985.

Table 9-5. Comparison of model periphyton with 1985 measurements (Knorr and Fairchild 1987).

Site ID	River Mile	1985 Periphyton Biomass (ug chlorophyll-*a* / cm^2)	EFDC Grid Cell	Model Periphyton (ug chlorophyll-*a* / L)	Water Depth (m)	Model Periphyton Biomass (ug chlorophyll-*a* / cm^2)
1	109.3	6.2 - 10.2	54,69	70	0.30	2.1
2	NA	8.0 - 16.5	NA	NA	NA	NA
3	106.2	8.5 - 13.0	54,64	160	0.33	5.3
4	102.4	9.0 - 17.0	54,58	550	0.36	19.8
5	101.2	11.5 - 21.0	54,56	700	0.37	25.9
6	96.1	8.0 - 14.3	54,48	240	0.35	8.4

As stated in Section 4.13, periphyton growth is limited by a number of factors including the availability of nitrogen, phosphorus, and solar radiation, as well as by temperature, stream velocity, and biomass density limitations. Time-series plots of each of these limitation factors are presented in Figures 9-12 to 9-16 for five locations. All five locations indicate that there is an abundance of nitrogen available

and that parameter is not limiting periphyton growth. Phosphorus is the more limiting of the two nutrients according to the model calculations.

The model-data diel dissolved oxygen comparisons for the automatic monitors deployed in the August 1997 survey (Davis 1998) are presented in Figure 9-17 (East Branch Brandywine Creek); Figure 9-18 (West Branch Brandywine Creek); Figures 9-19 and 9-20 (West Branch Red Clay Creek); and Figures 9-21 and 9-22 (East Branch White Clay Creek). Considering that the model simulation began 3 months prior to the August time period, the fact that the diel dissolved oxygen agrees so well with the monitor data is noteworthy. At most monitor locations, the model agrees with both the minimum recorded dissolved oxygen and the dissolved oxygen range. The magnitude of the diel dissolved oxygen range is a very localized phenomenon related to sunlight and periphyton biomass. The resolution of the model grid and the temporal resolution of the various nutrient sources as well as the lack of canopy shading information are all possible contributors to deviations in the model versus monitored diel dissolved oxygen. Nonetheless, even with these sources of uncertainty in model resolution, the diel dissolved oxygen computed by the model agrees very favorably with the observations measured by the automatic monitors.

9.7 Sediment Oxygen Demand and Benthic Nutrient Flux Rates

The need for a predictive benthic sediment submodel for water quality modeling projects has been apparent for some time. When using a water quality model for management scenario analysis, one of the biggest sources of uncertainty involves what to use for the future sediment flux rates after a proposed management control has been implemented. The predictive sediment submodel in EFDC helps address this uncertainty with two fundamental capabilities: (1) the ability to predict effects of management alternatives on sediment-water exchange processes and (2) the ability to predict the time scale for alterations in the sediment-water exchange processes. To meet these requirements, a predictive sediment process model was incorporated into the EFDC model framework and was based on DiToro and Fitzpatrick (1993). The sediment submodel is driven by net settling of organic matter from the water column to the sediments. In the benthos, the sediment submodel simulates the decay (diagenesis) of organic matter, which produces oxygen demand and inorganic nutrients. Oxygen demand takes three paths out of the sediments: (1) export to the water column as chemical oxygen demand, (2) oxidation at the sediment-water interface as sediment oxygen demand, or (3) burial to a deep, inactive sediment layer. The inorganic nutrients produced by diagenesis can take two pathways out of the bottom sediment: (1) release back to the overlying water column or (2) burial to the deep, inactive sediment layer.

In the predictive sediment submodel, benthic sediments are represented as two layers with a total depth of 10 cm. The upper benthic layer is in contact with the water column and may be oxic or anoxic

depending on the dissolved oxygen concentration in the water. The lower benthic layer is permanently anoxic. The thickness of the upper benthic layer is determined by the penetration of oxygen into the sediments, and at its maximum thickness, the oxic layer depth is a small fraction of the total thickness. The sediment submodel consists of three basic processes:

- Particulate organic matter settles from the water column to the sediments. Because of the negligible thickness of the upper benthic layer, deposition proceeds from the water column directly to the lower anoxic layer.
- Within the lower layer, organic matter is subject to decay (diagenesis).
- The flux of substances produced by diagenesis moves to the upper benthic layer, to the water column, and to the deep, inactive benthic layer (burial). The flux portion of the sediment submodel is the most complex. The computation of flux requires consideration of (1) reactions in both benthic layers, (2) sedimentation from the upper to lower benthic layer as well as from the lower benthic layer to the deep inactive sediments, (3) particle mixing between layers, (4) diffusion between layers, and (5) mass transfer between the upper layer and the water column.

No field data were available during the calibration period to verify the flux rates computed by the predictive sediment submodel. However, SOD rates were measured in July and August 1996, at three locations in the tidal Christina River and Brandywine Creek. An SOD rate of 0.5 g/m^2/day was used in the tidal Delaware River in another model study conducted by HydroQual for DRBC and was also adopted for this study. The simulated SOD rates were converted to rates at 20°C and are compared with the measured data in Table 9-6. The relative errors were less than 13% at all locations. Time-series plots of sediment oxygen demand, benthic ammonia flux, benthic nitrate flux, benthic phosphate flux, benthic COD flux, benthic silica flux, and sediment temperature at the same 16 monitoring stations used for the water quality calibration are presented in Appendix C. Transect plots of these sediment flux parameters for the 11 major stream reaches in the model are presented in Appendix D.

Table 9-6. Model-data comparison of sediment oxygen demand rates (g/m^2/day).

Location	Sampling Date	Monitored SOD at 20°C	1997 Calibration Model SOD at 20°C	Relative Error
Christina River at I-495 bridge	Aug 12, 1996	0.81	0.91	12.9%
Christina River at Newport, Rt. 141 bridge	Jul 10, 1996	1.67	1.56	6.5%
Brandywine Creek, 0.6 mi. from mouth	Aug 12, 1996	1.23	1.19	3.4%
Delaware River (from HydroQual study)	-	0.50	0.46	8.8%

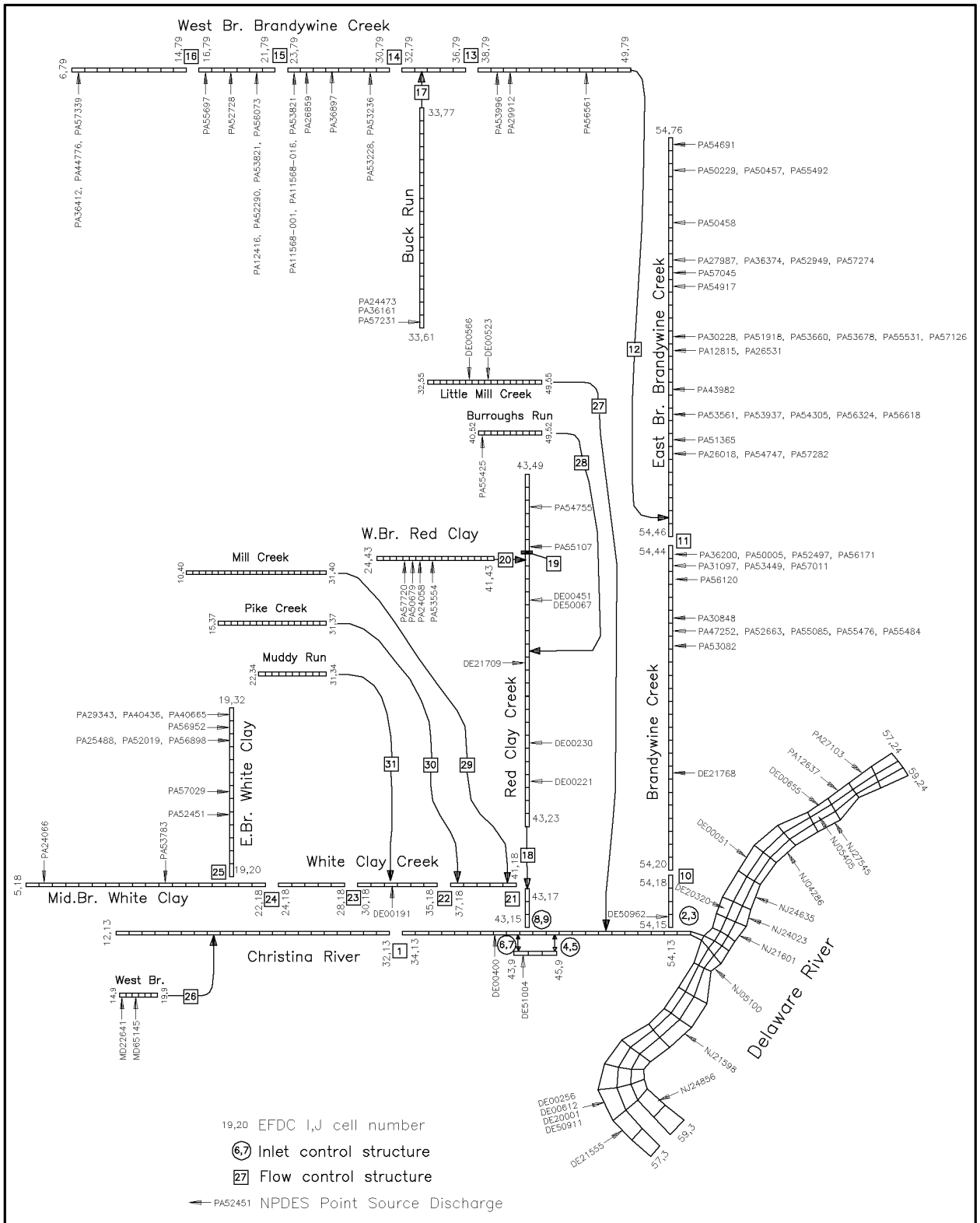

Figure 9–1. Schematic of EFDC model of Christina River Basin.

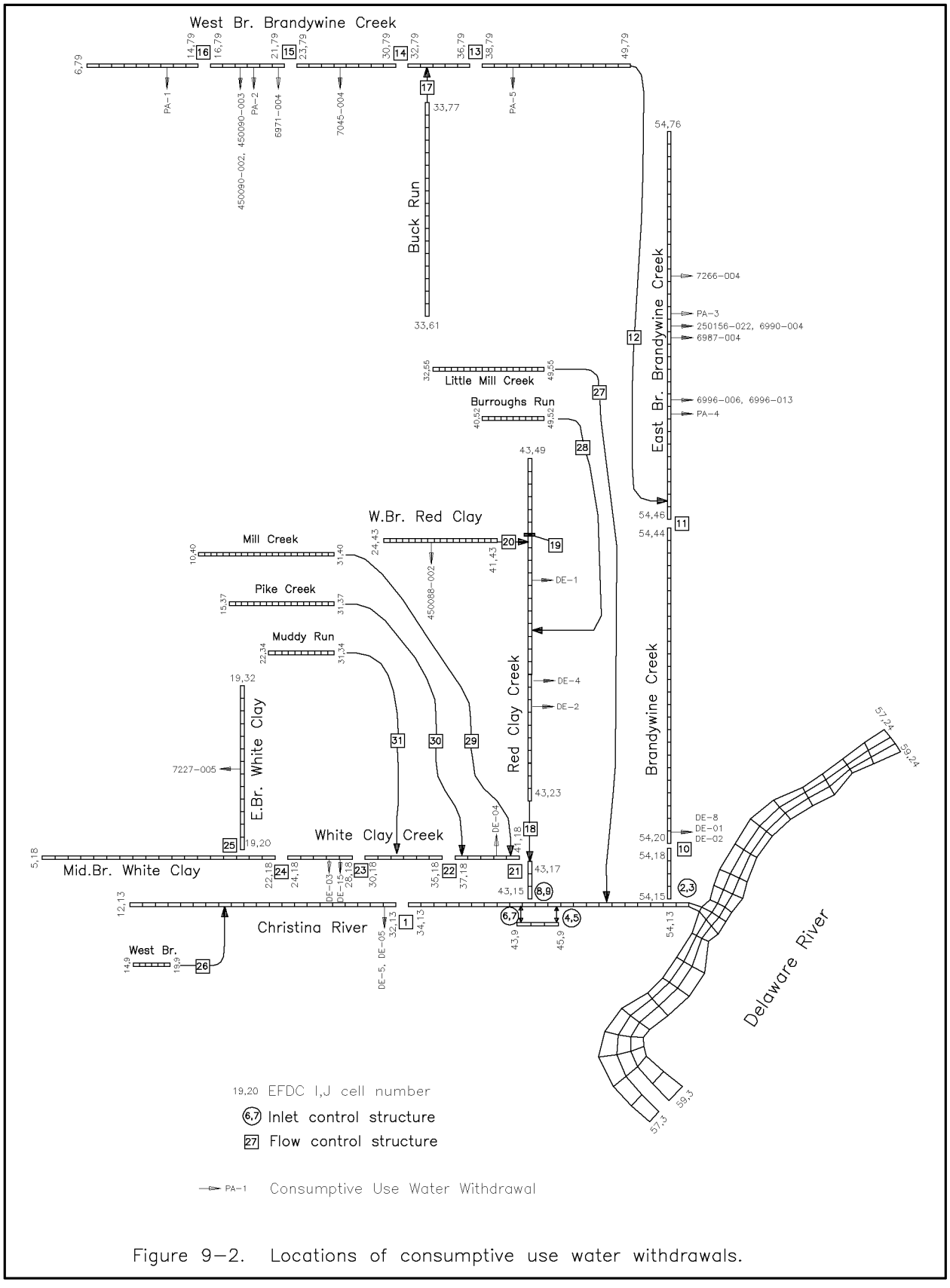

Figure 9–2. Locations of consumptive use water withdrawals.

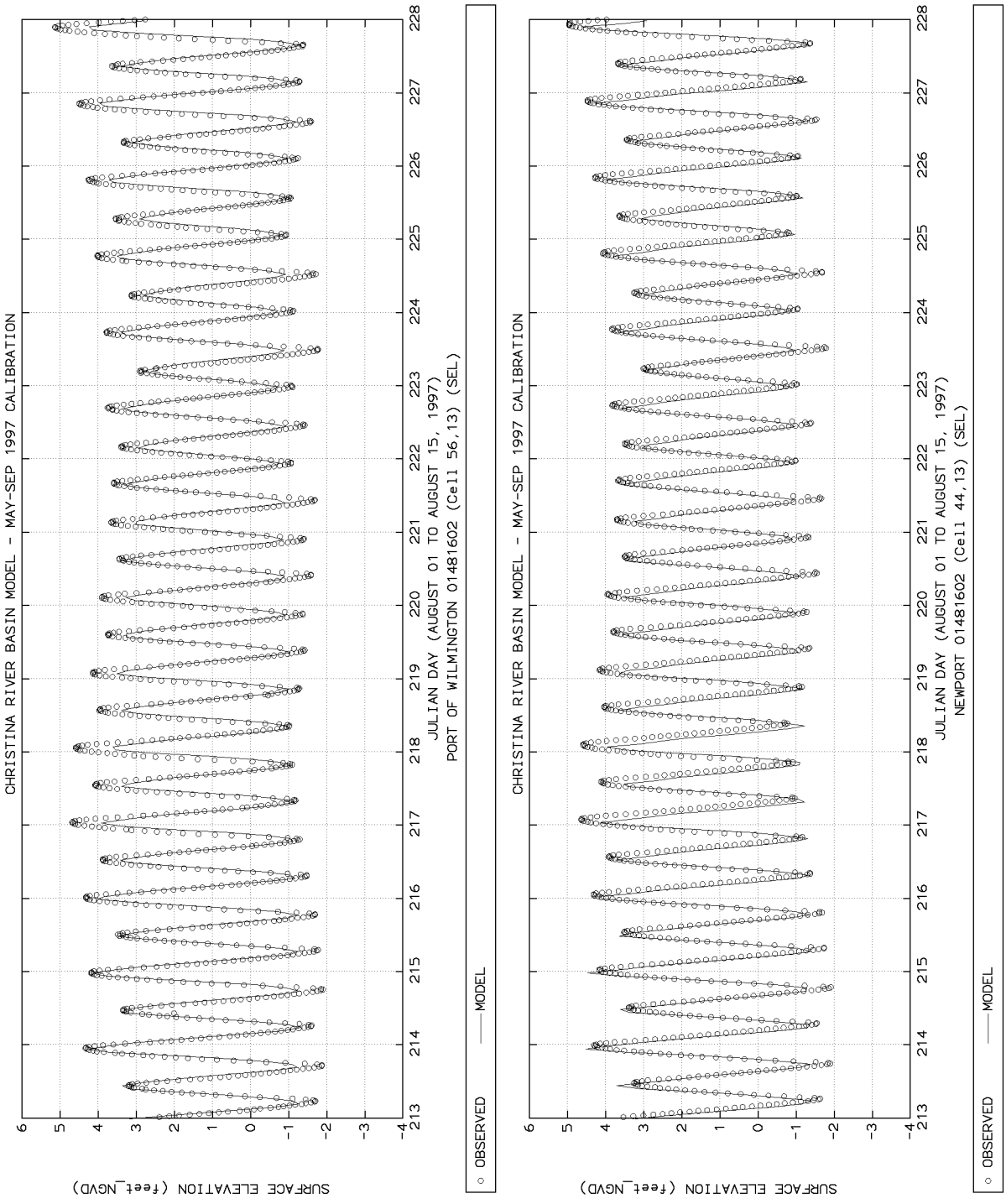

Figure 9-3. Model-data comparison of tides at Port of Wilmington and Newport (Aug 1997).

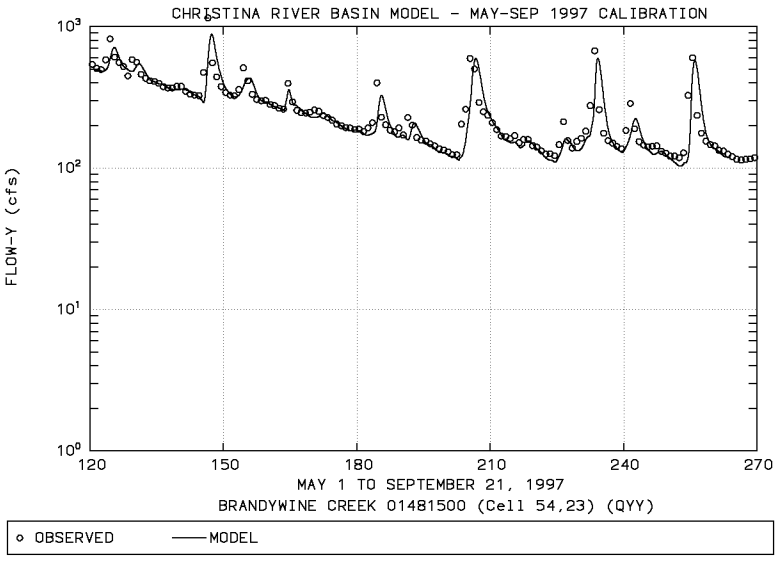

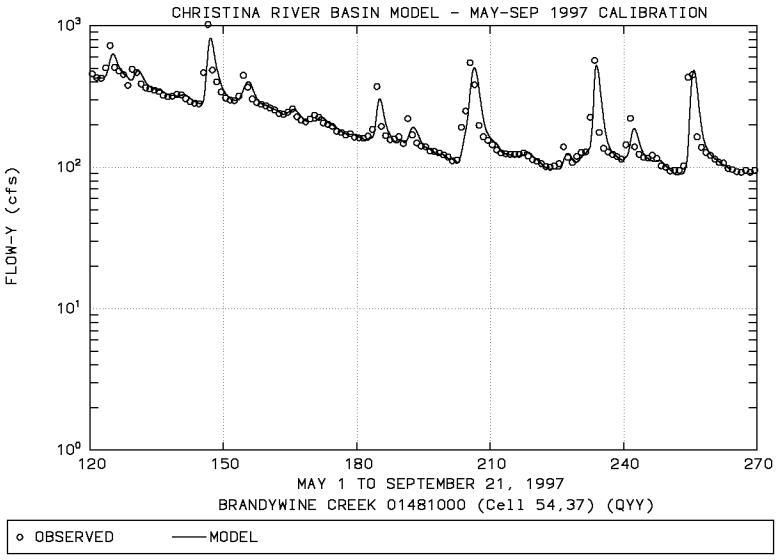

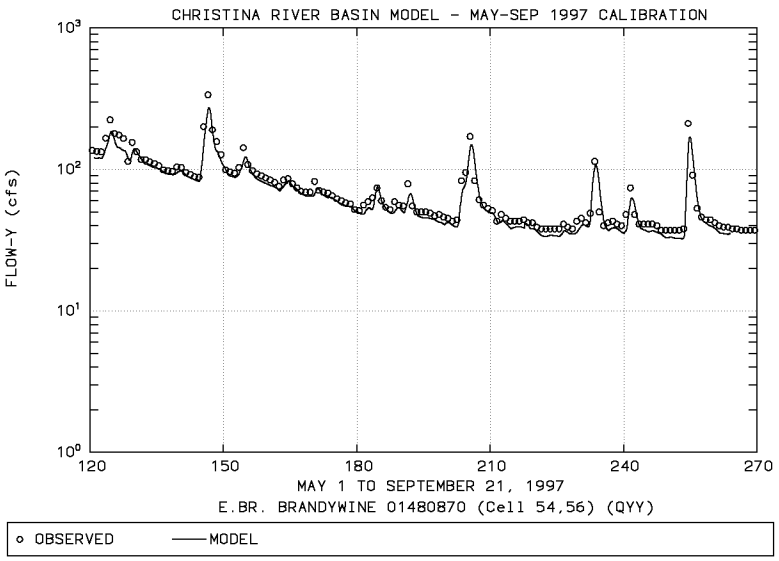

Figure 9-4. Model-data hydrographs, Brandywine Creek and E. Br. Brandywine Creek.

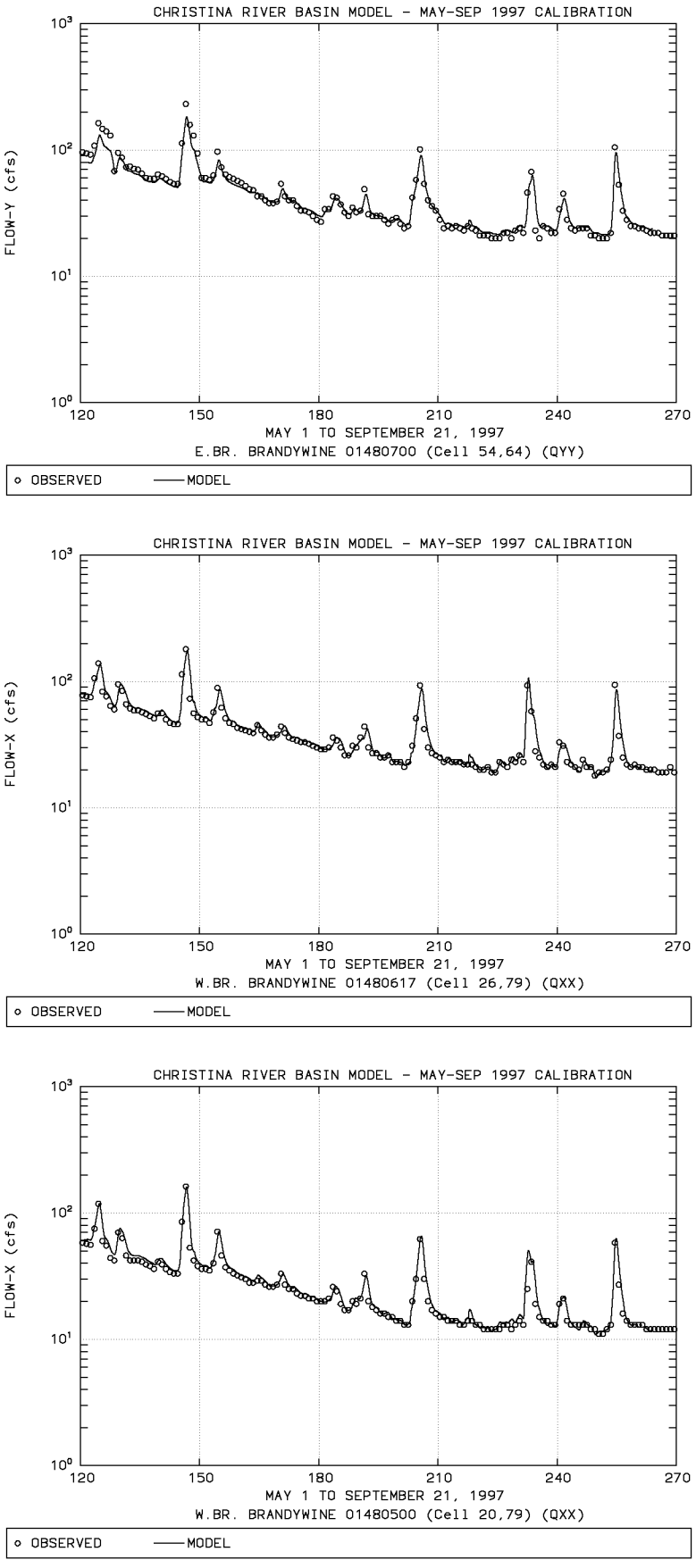

Figure 9-5. Model-data hydrographs, E. Branch and W. Branch Brandywine Creek.

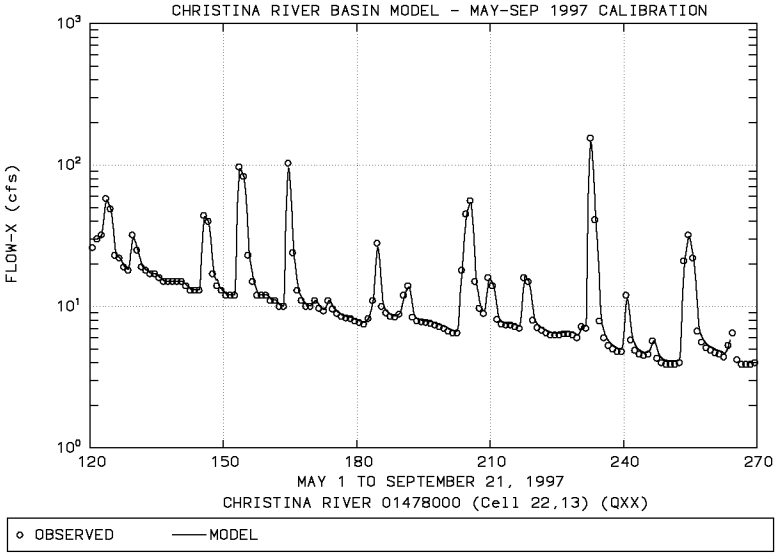

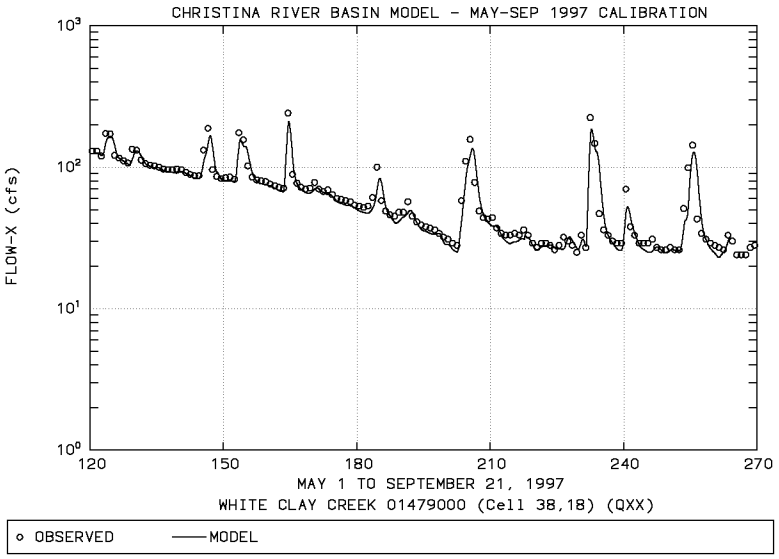

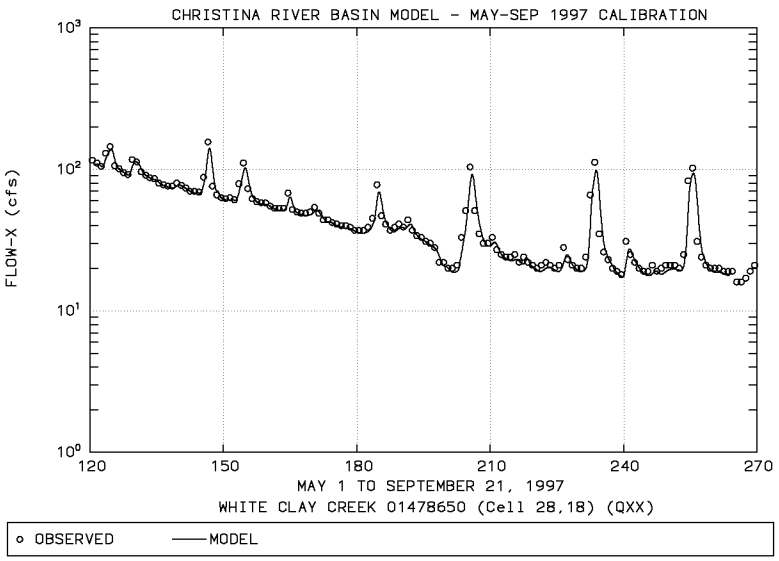

Figure 9-6. Model-data hydrographs, Christina River and White Clay Creek.

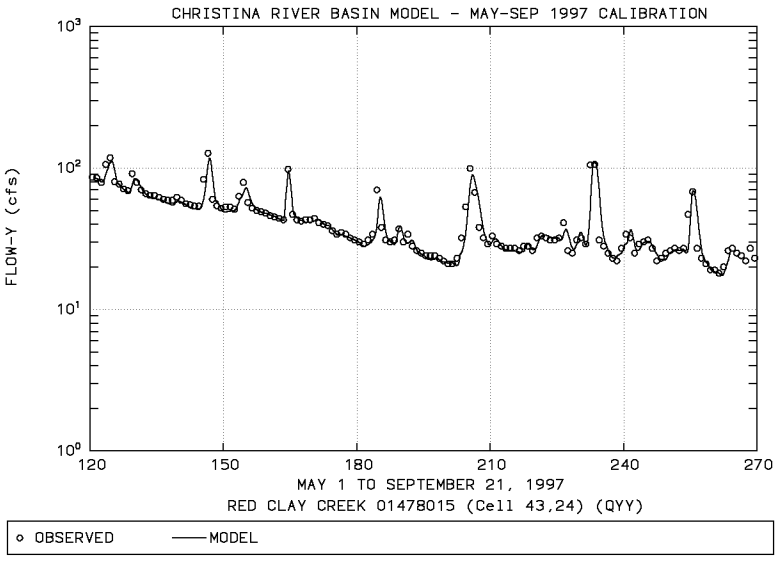

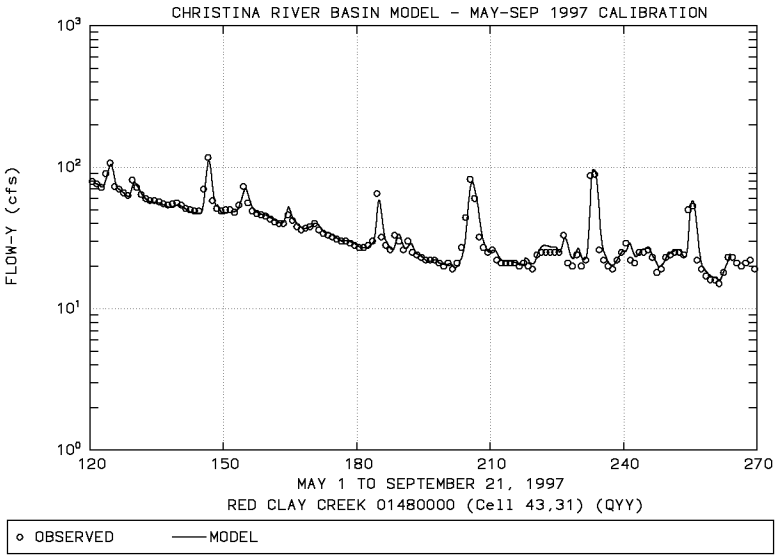

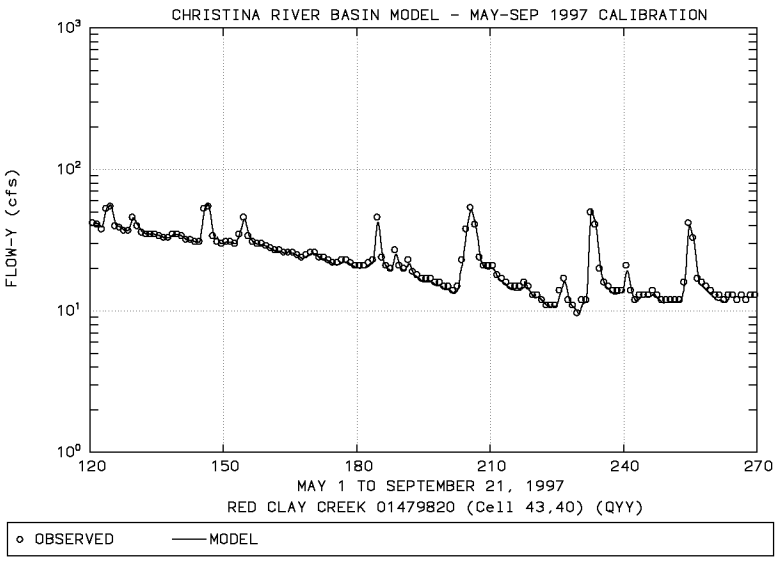

Figure 9-7. Model-data hydrographs, Red Clay Creek.

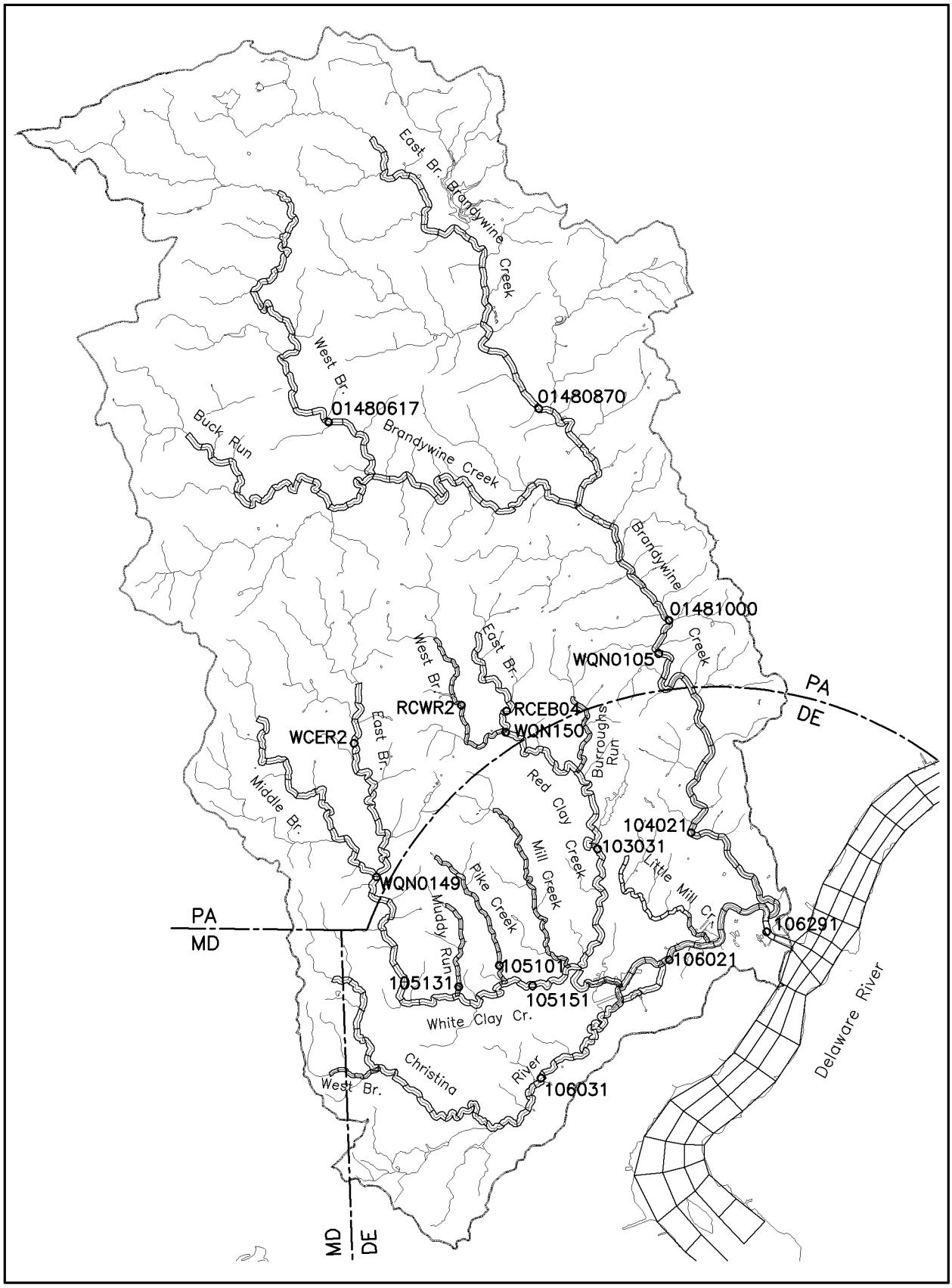

Figure 9-8. Monitoring stations used for model-data time-series comparisons.

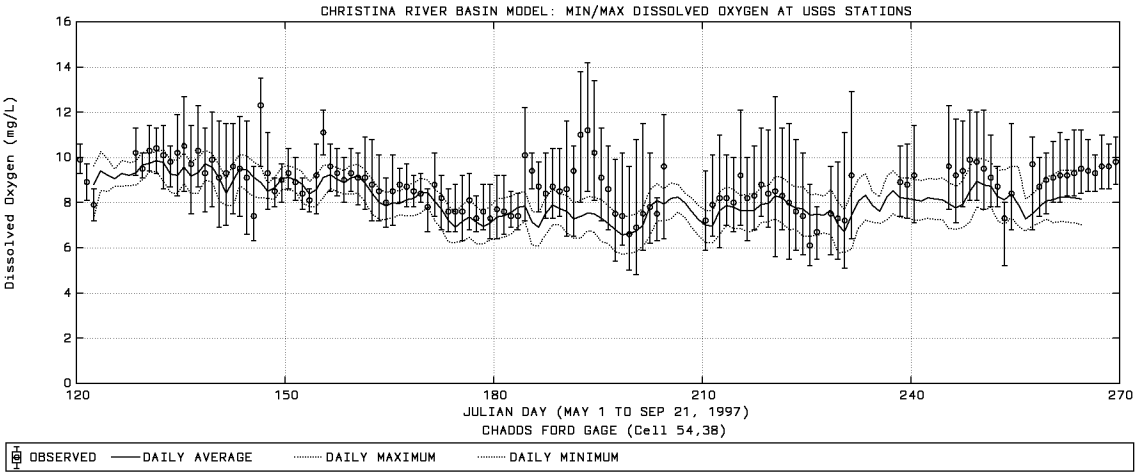

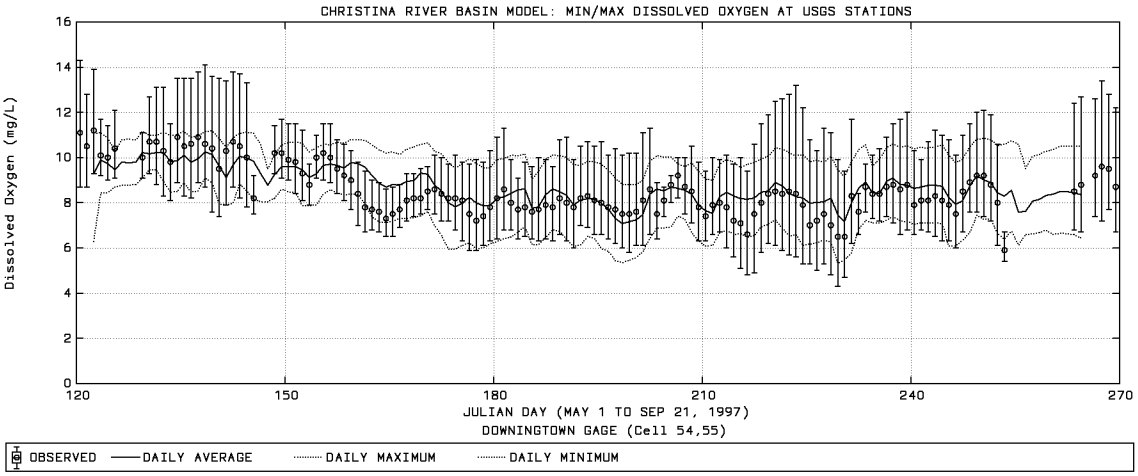

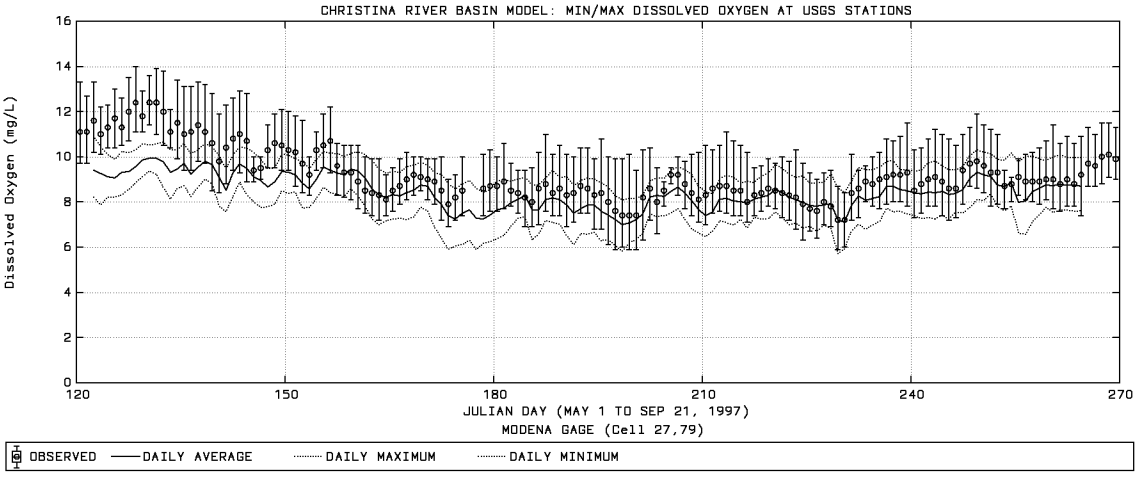

Figure 9-9. Diel dissolved oxygen at USGS monitoring stations.

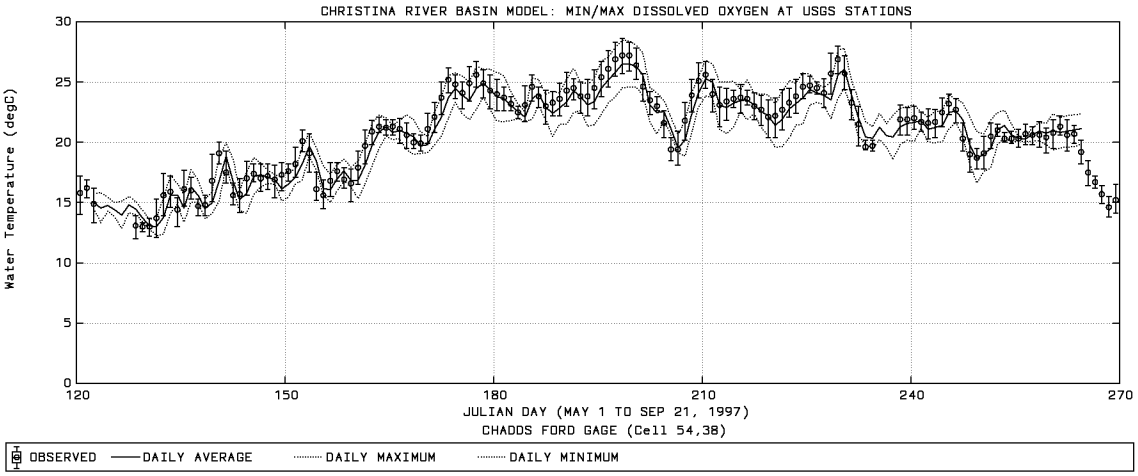

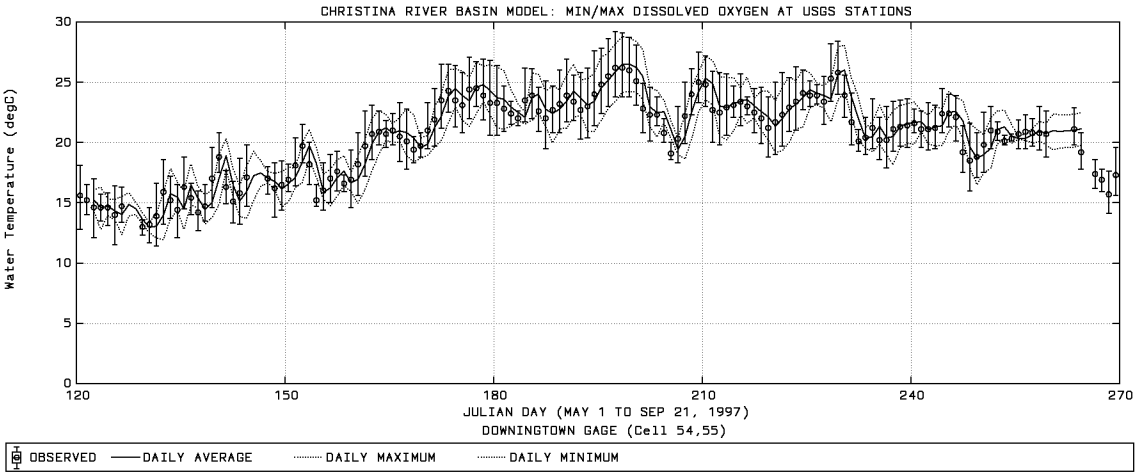

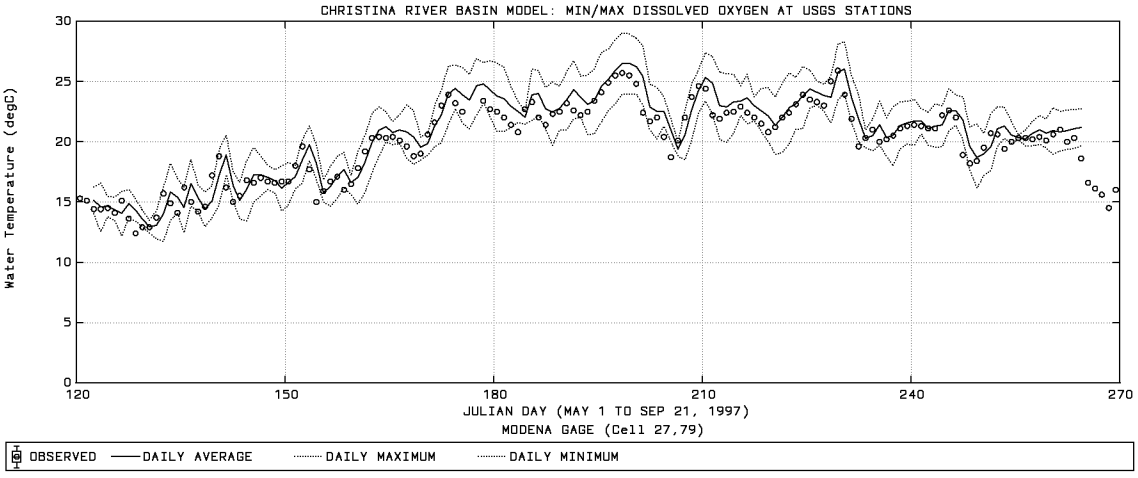

Figure 9-10. Water temperature at USGS monitoring stations.

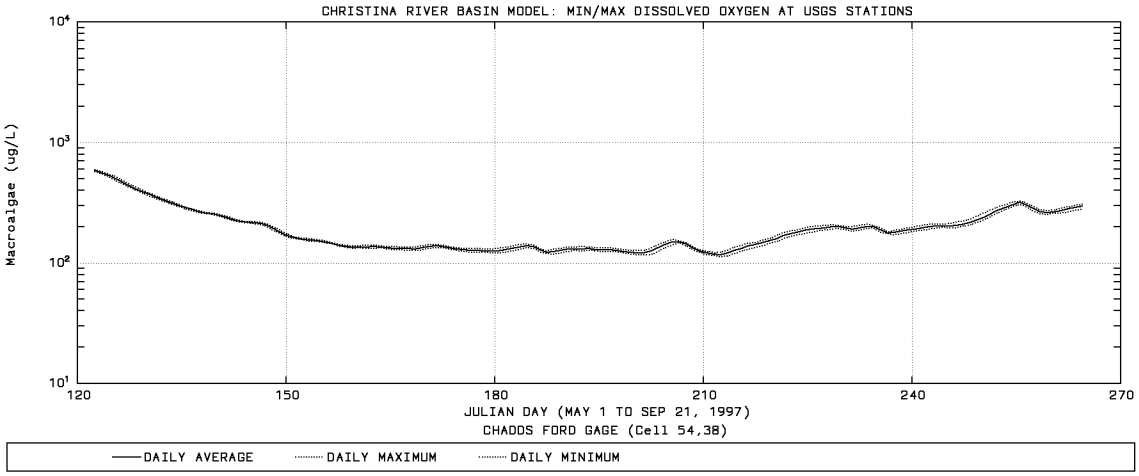

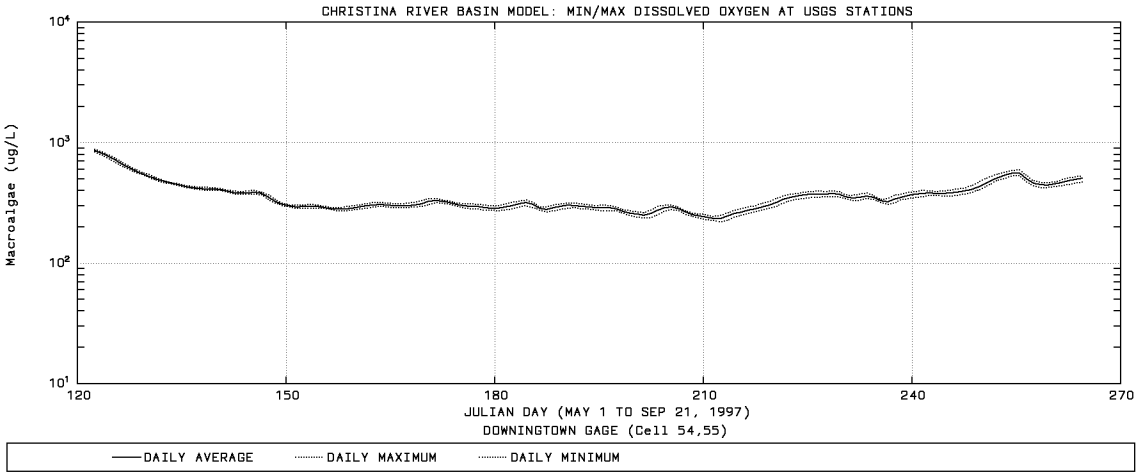

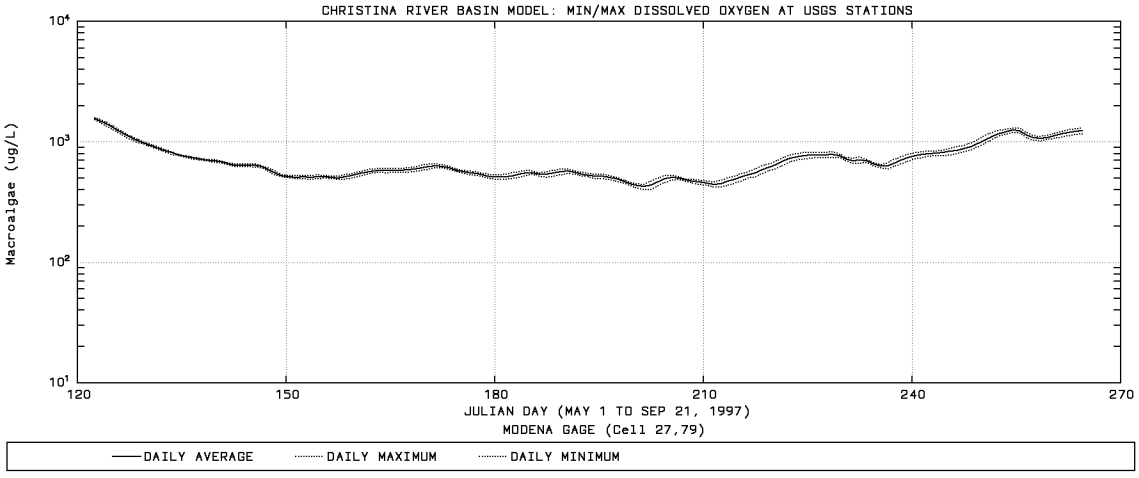

Figure 9-11. Periphyton biomass at USGS monitoring stations.

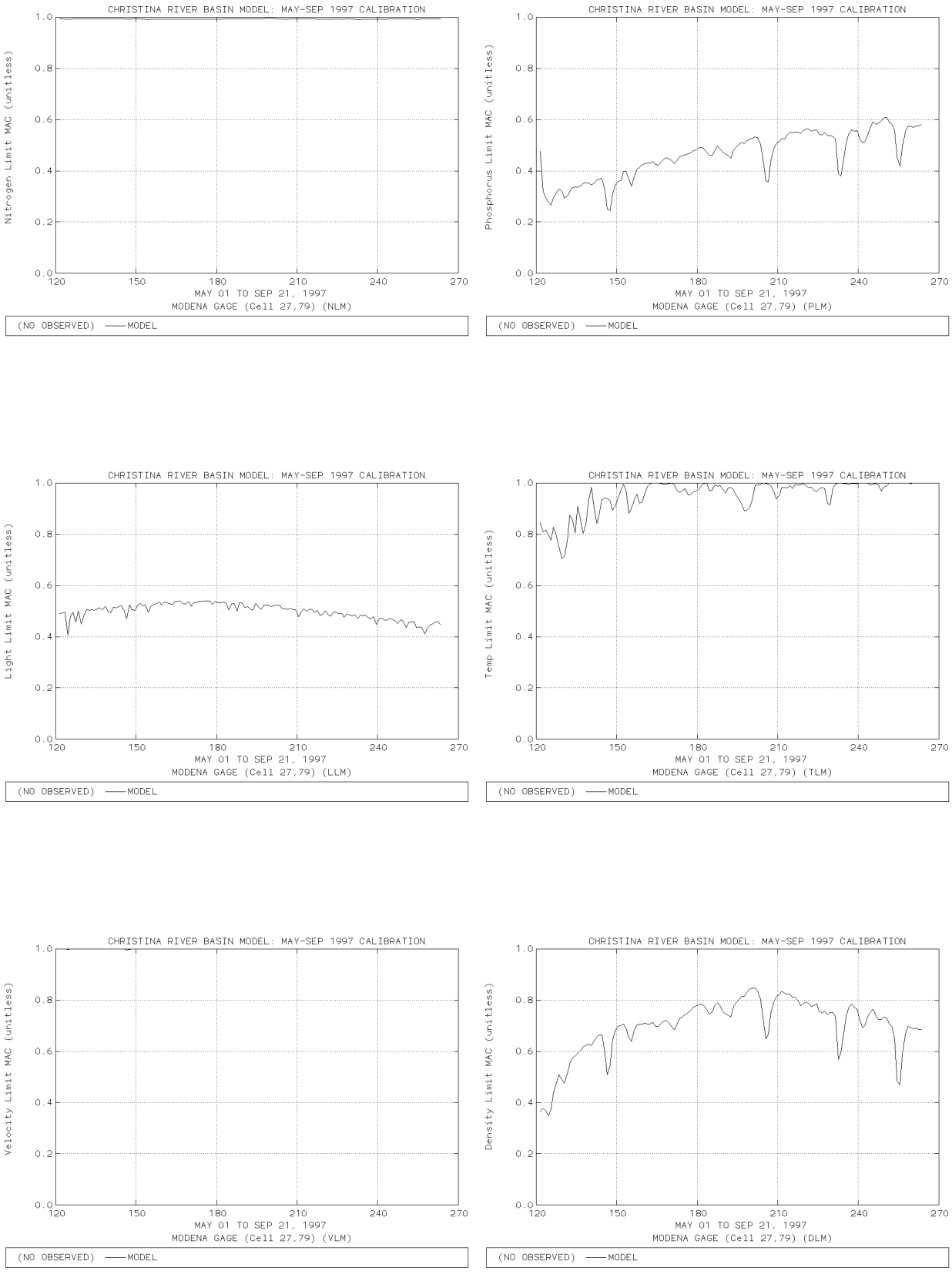

Figure 9-12. Periphyton limitation factors (Modena gage, W. Br. Brandywine Cr.).

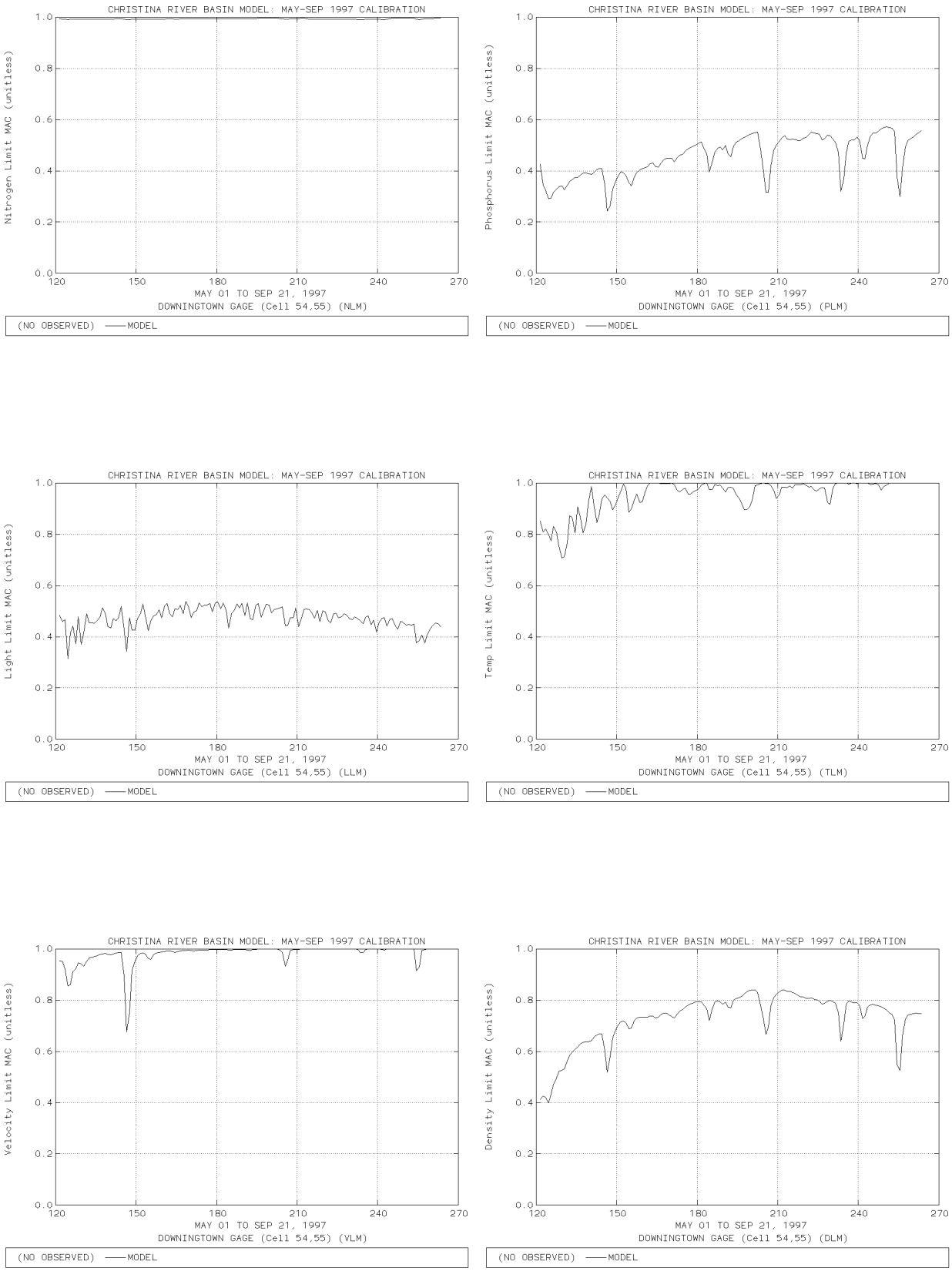

Figure 9-13. Periphyton limitation factors (Downingtown gage, E. Br. Brandywine Cr.).

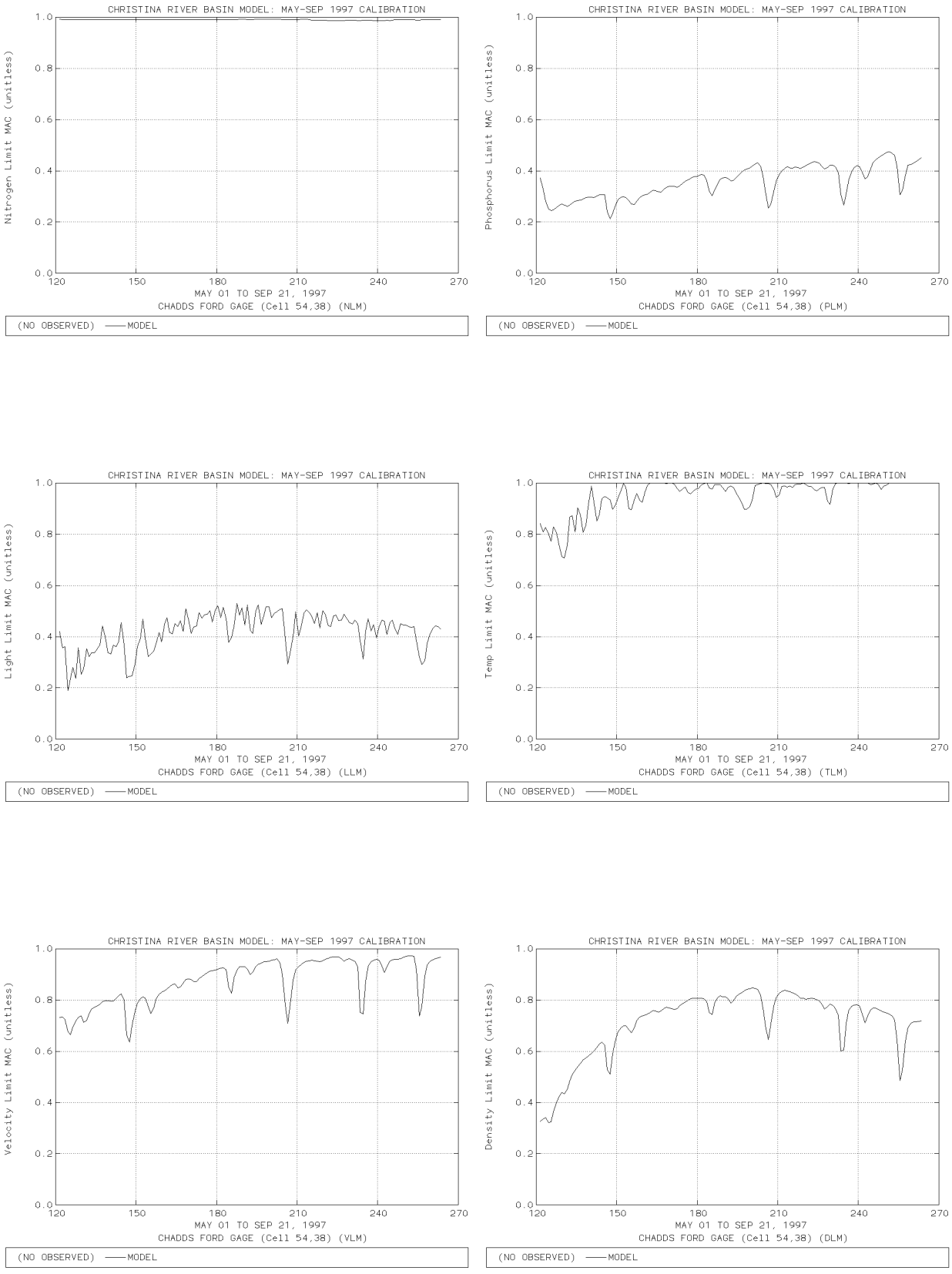

Figure 9-14. Periphyton limitation factors (Chadds Ford gage, Brandywine Cr.).

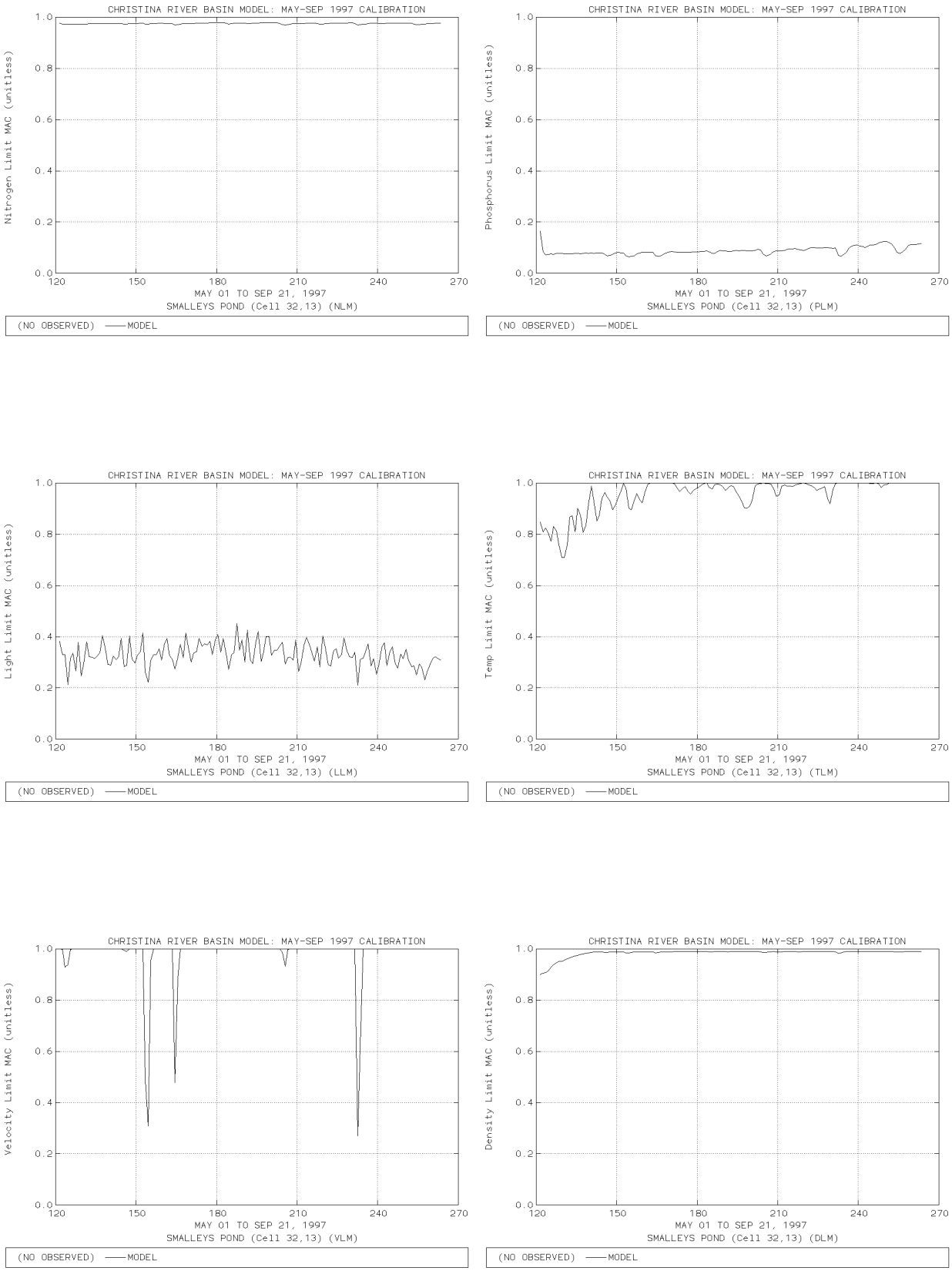

Figure 9-15. Periphyton limitation factors (Smalleys Pond, Christina River).

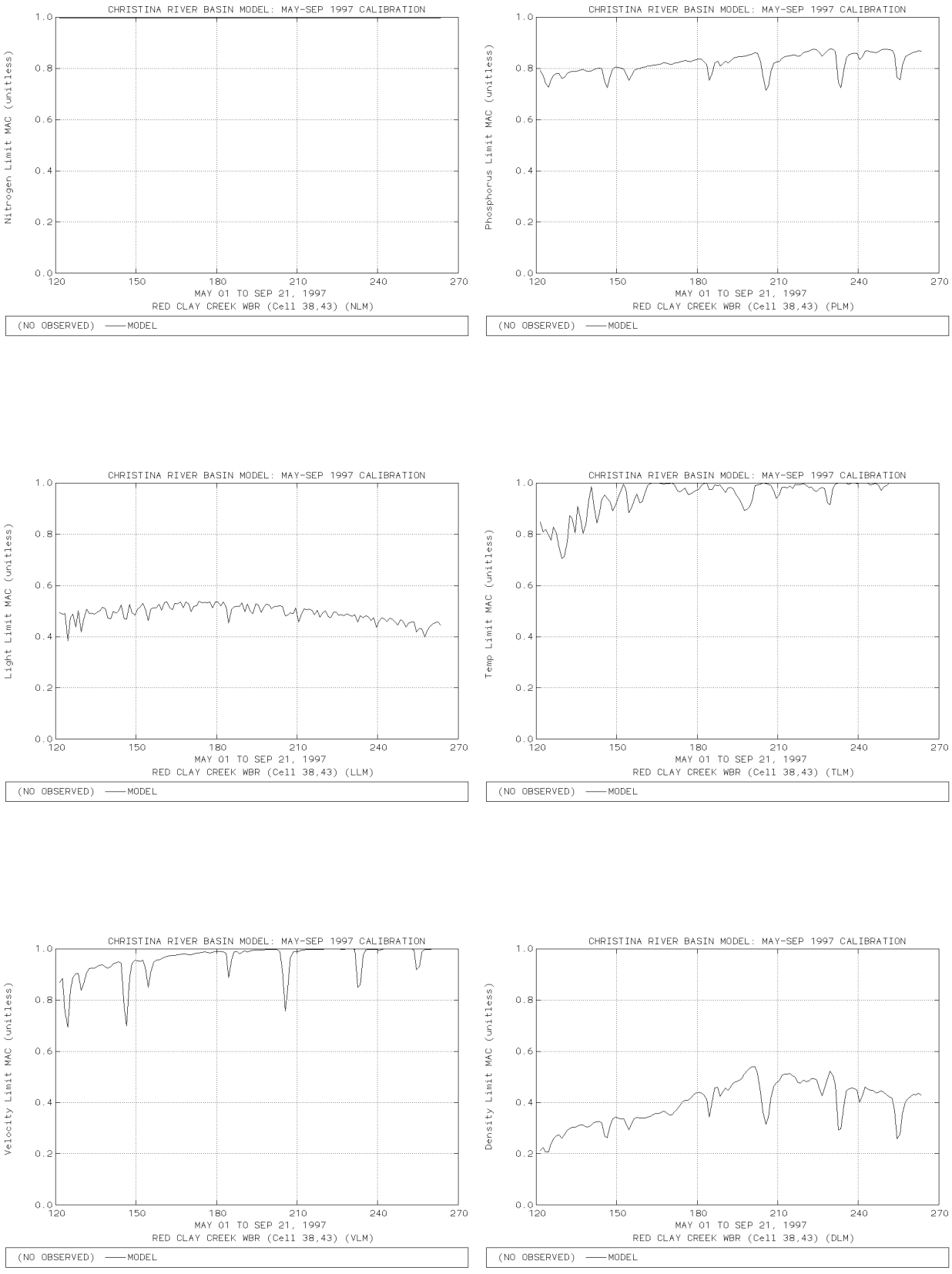

Figure 9-16. Periphyton limitation factors (W. Br. Red Clay Creek).

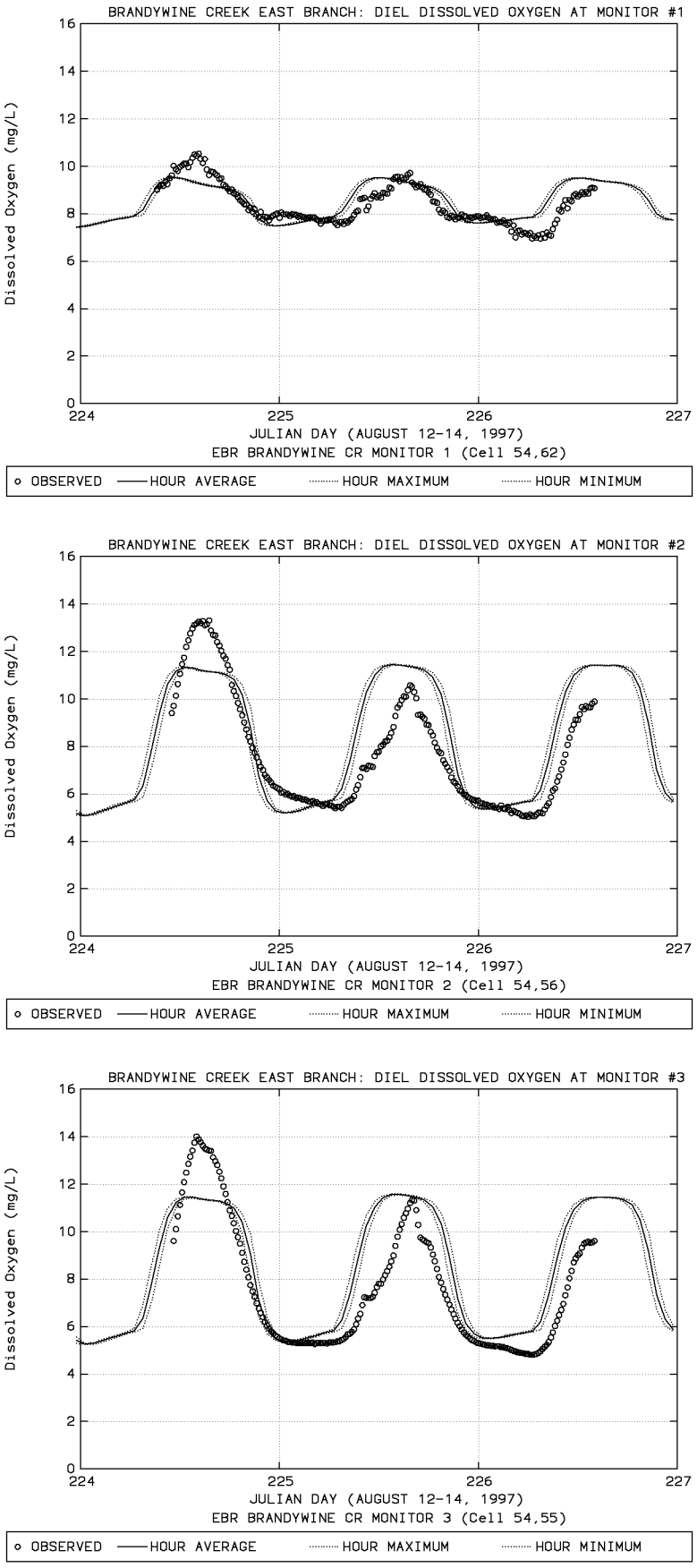

Figure 9-17. Model-data diel D.O. comparison, Brandywine Creek East Branch.

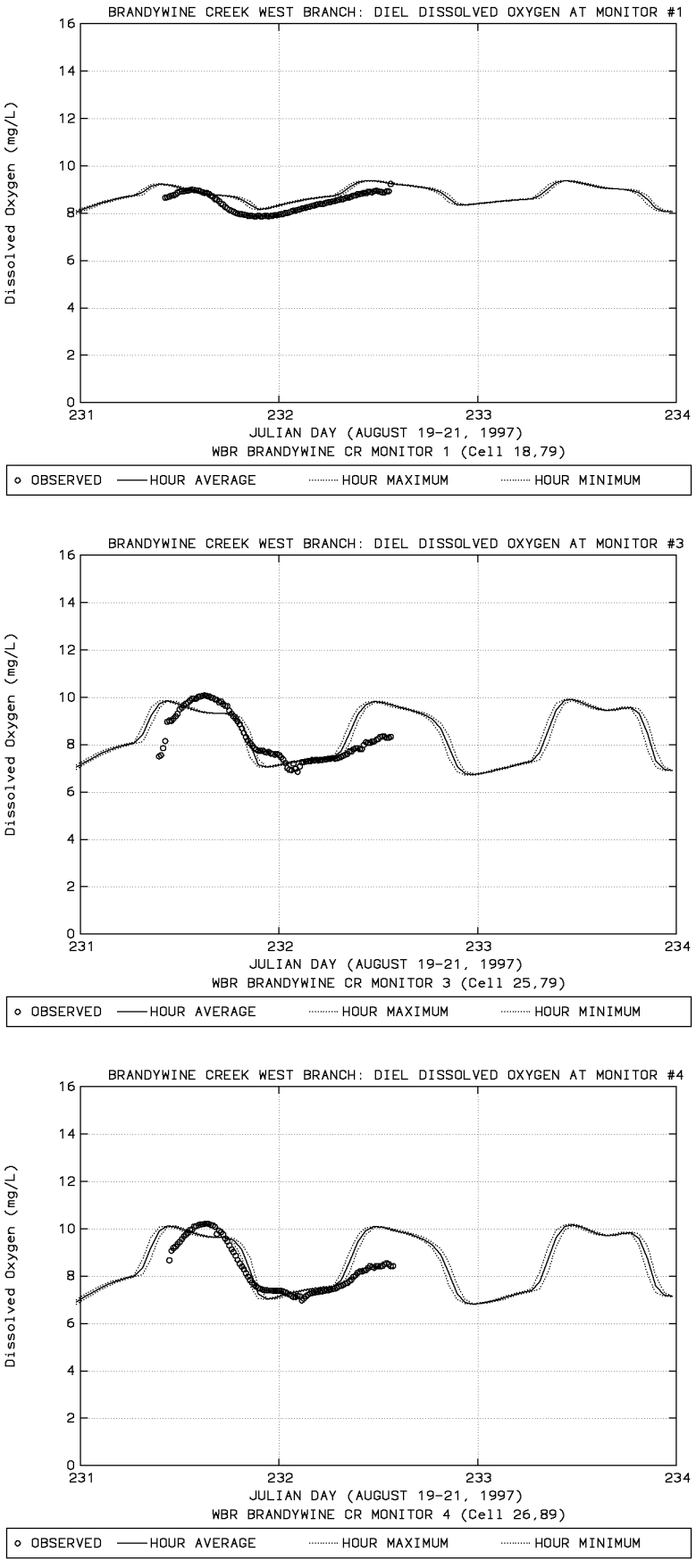

Figure 9-18. Model-data diel D.O. comparison, Brandywine Creek West Branch.

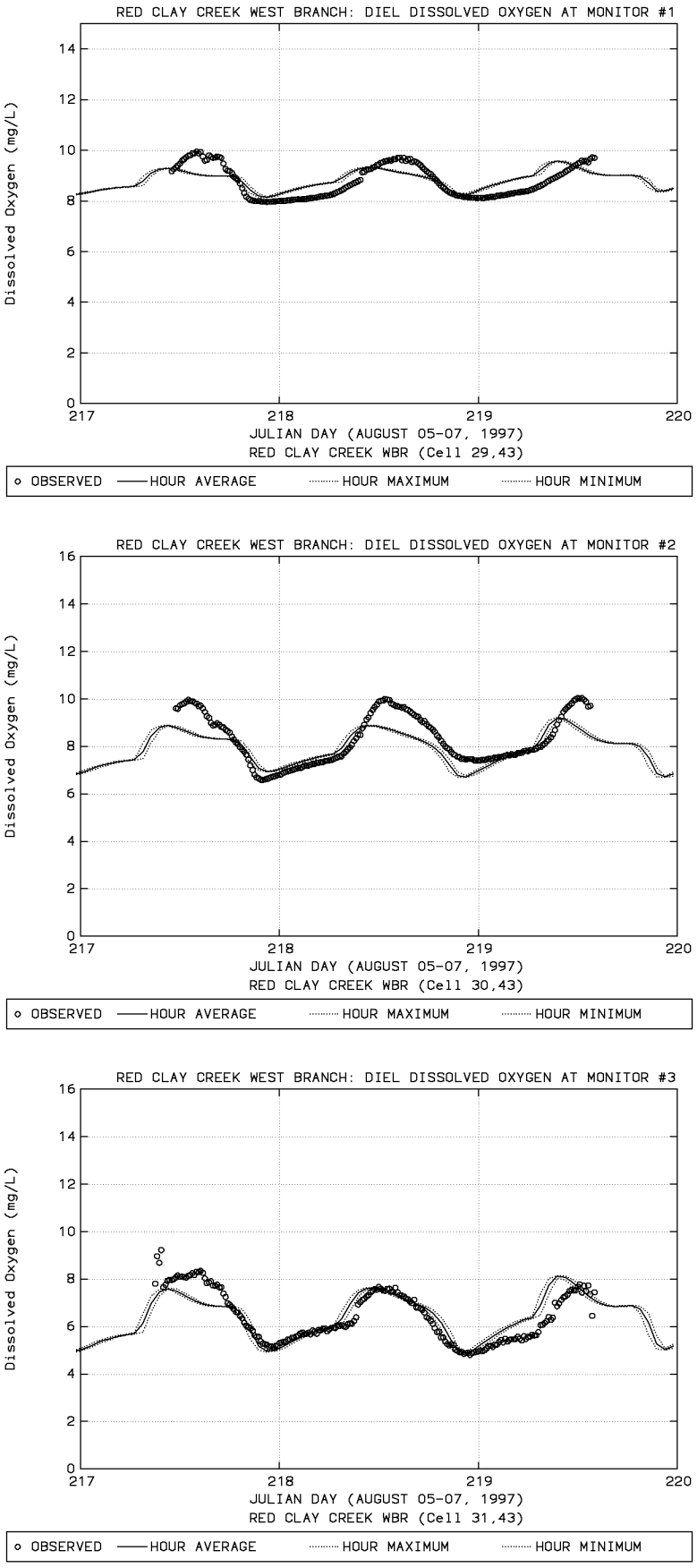

Figure 9-19. Model-data diel D.O. comparison, Red Clay Creek West Branch

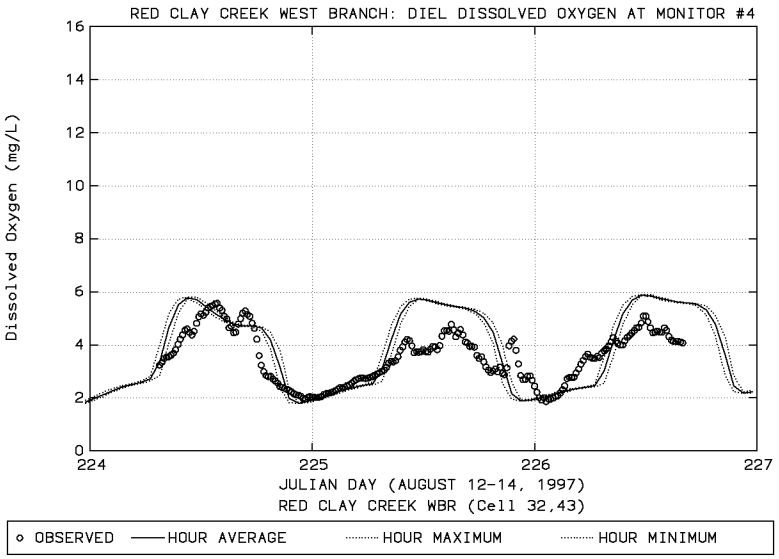

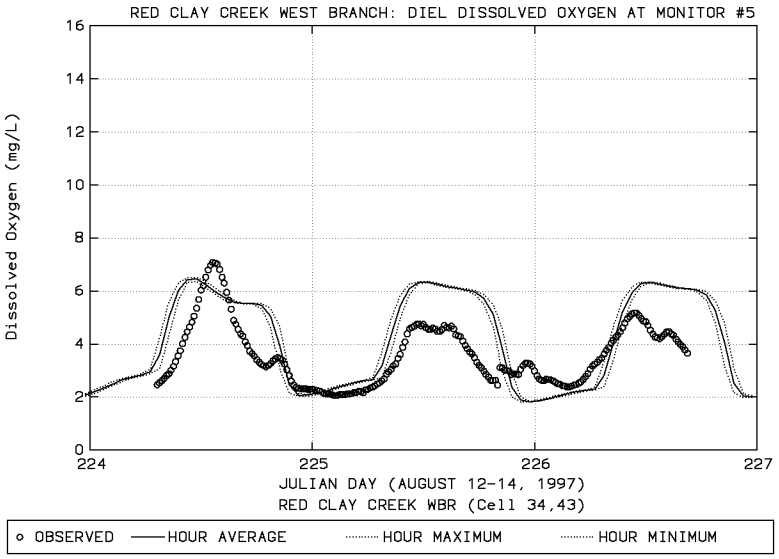

Figure 9-20. Model-data diel D.O. comparison, Red Clay Creek West Branch

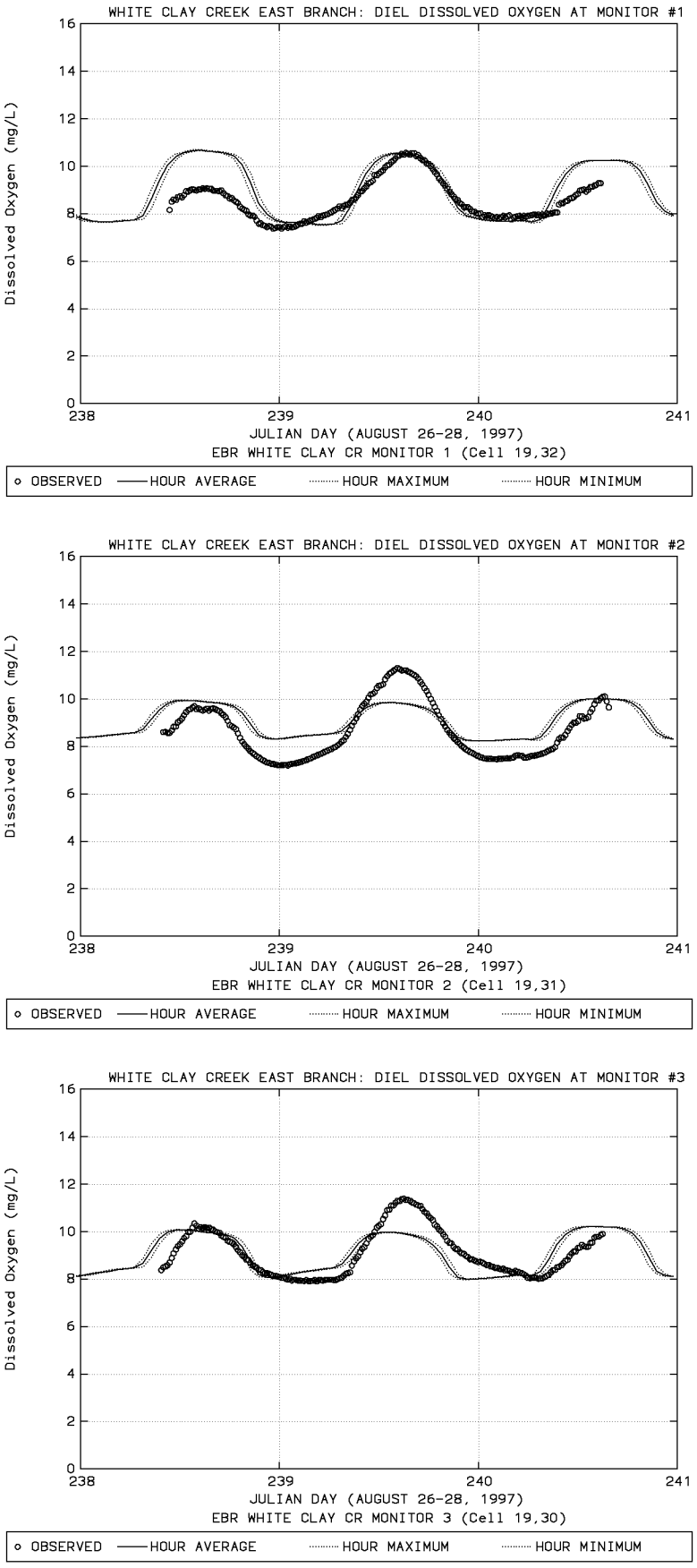

Figure 9-21. Model-data diel D.O. comparison, White Clay Creek East Branch

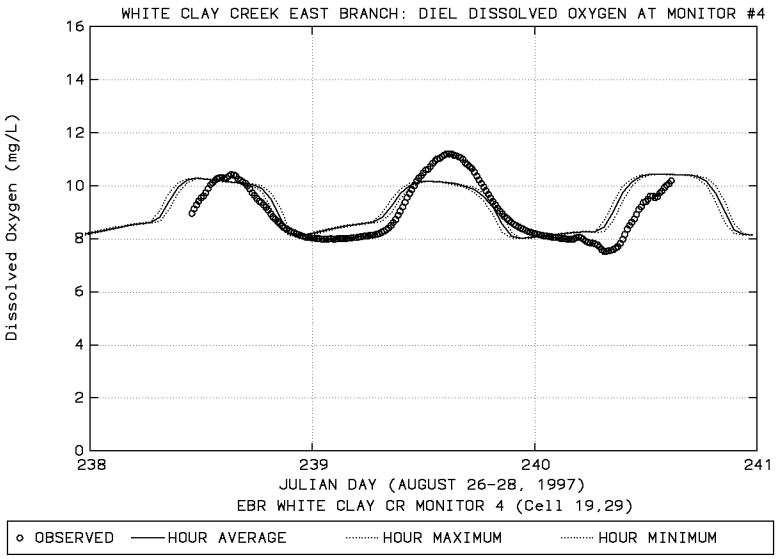

Figure 9-22. Model-data diel D.O. comparison, White Clay Creek East Branch

10 - MODEL VALIDATION

Model validation involved the application of the calibrated model using a different time period, namely, May 1 to September 21, 1995. This period was characterized by extremely low stream flows from late August to the middle of September. An extensive field monitoring program was conducted by the states of Delaware and Pennsylvania during the summer of 1995 in which grab samples were collected at a number of locations throughout the basin at a frequency of at least once a month. These data were assembled into an electronic database and were used to assess the model validation simulation. This section presents the results of the validation of the EFDC hydrodynamic and water quality model. Parameters considered for validation include flow rate, tidal surface elevation, chlorides, and a suite of water quality parameters including dissolved oxygen, nitrogen species, phosphorus species, organic carbon, chlorophyll-*a*, total suspended solids, and fecal coliform bacteria.

10.1 Validation Period

The time period for model validation, May 1 to September 21, 1995, was selected because it included an ambitious field monitoring program conducted by DNREC, PADEP, USGS, and others. During the late-August to mid-September 1995 time period, stream flow throughout the basin was below historical 7Q10 flow rates. Data for comparison to the model water quality results for stream reaches were monitored generally on a monthly basis during the validation period. The USGS maintained continuous monitors at three locations (Chadds Ford, Downingtown, and Modena) to record daily minimum and maximum values of dissolved oxygen, temperature, and pH.

10.2 Hydrodynamic and Hydraulic Validation

Assessment of the validation of the hydrodynamic model was accomplished by comparing model results to field observations of flow and tidal elevation. Tidal constituent amplitudes and phases were compared with those measured at two USGS tide gages on the Christina River at the Port of Wilmington and at Newport. The model was executed for a period of 143 days from May 1 to September 21, 1995. The simulated model stream flow rates were compared with available observations at 12 USGS stream gages

10.2.1 Validation of Tide Elevation

Validation of the model with respect to tidal water surface elevation was accomplished by analysis of observed and model predicted time-series data at interior tide stations. For tidal waters, least squares harmonic analysis is the most commonly utilized procedure (Oey, Mellor and Hires 1985; Cheng et al. 1993; Shen et al. 1999). Tide elevation data were obtained from the USGS tide stations on the Christina River at the Port of Wilmington near the mouth. No tidal data were available for the Newport

station during the validation period. These data were compared with surface elevations computed by the model at cell 56,13 (Port of Wilmington). The time-series of tide elevations for the month of August 1995 for both the field data and the model results were subjected to a harmonic analysis. The five most important astronomical harmonic constituents (M2, S2, N2, K1, and O1) were computed for both the field data and model simulation results. The harmonic analysis results, shown in Table 10-1, indicate the model is in reasonable agreement with the measured tide data for both amplitude and phase. The model-data amplitudes for the M2 harmonic constituent agree within 6 cm (8%) and the phases agree to within 7 degrees. Time-series graphs (Figure 10-1) of the observed and model tide elevations at the Port of Wilmington covering a 31-day period (August 1-31, 1995) provide a visual means of assessing the skill of the model in simulating tidal elevations. The model tides are forced at the north and south boundaries in the Delaware River based on the NOAA predictions at the Reedy Point and Chester subordinate stations (NOAA 1998). These predictions do not consider the low-frequency phenomenon caused by regional low pressure systems or storms that will be found in the signal of the tide data collected at the two USGS tide stations on the Christina River.

Table 10-1. Harmonic analysis of tides at Port of Wilmington and Newport.

Harmonic Constant	Port of Wilmington (USGS #01481062)		Newport (USGS #01480065)	
	Amplitude (m)	Phase (degrees)	Amplitude (m)	Phase (degrees)
M2 - observed	0.7755	303.381	-	-
M2 - model	0.7148	310.070	0.7287	316.763
Difference	0.0607	-6.698	-	-
S2 - observed	0.0962	26.056	-	-
S2 - model	0.1017	31.289	0.1031	41.384
Difference	-0.0055	-5.233	-	-
N2 - observed	0.1251	294.181	-	-
N2 - model	0.1348	326.473	0.1347	335.573
Difference	-0.0097	-32.292	-	-
K1 - observed	0.1119	186.070	-	-
K1 - model	0.0646	172.191	0.0646	175.690
Difference	0.0473	13.879	-	-
O1 - observed	0.0696	147.329	-	-
O1 - model	0.0595	151.881	0.0598	154.997
Difference	0.0101	-4.552	-	-

10.2.2 Hydraulic Flow Balance

Validation of the hydraulic flow balance in the model system was determined by comparing the model and observed hydrograph at 12 USGS stream gage locations in the Christina River Basin for the validation period. Estimates of unit discharge rates (cfs per square mile) were estimated for each of the 39 subwatersheds for each day in the validation period. The daily flow rates for each subwatershed were

then distributed uniformly among each of the grid cells within a subwatershed, except for headwater grid cells which were assigned a flow rate in accordance with the contributing area to that cell. The model was then run for the 143-day simulation period, and the flow rate at the appropriate gage location was compared with the model results. The model flow rates compared reasonably well with the daily average flows at the stream gages (see Figures 10-2 to 10-5). The purpose of validating simulated hydraulic flow balance to the USGS gage data was to determine whether the runoff rates from the contributing subwatersheds were properly apportioned to the model grid cells. Normally, a watershed runoff model would be used to provide flows to the receiving water model. However, the calibrated HSPF watershed model will not be available for a few more years. The model hydrograph agrees well with the stream gage data during periods between storm runoff events. At certain locations, the model tends to under predict the peak flow rates of the storm events. The use of a watershed runoff model in the future will likely improve the peak flow validation because the timing of the peak runoff from each subwatershed will be taken into account (a procedure that was not possible in the present model application).

10.3 Water Quality Validation Results

Each observation in STORET was collected at an instant in time and at a single point in space. Time scales realistically represented in the EFDC model were determined by time scales of primary forcing functions: 60-second tidal hydrodynamics, hourly meteorological updates, monthly ocean boundary conditions, constant nonpoint source concentration estimates, daily nonpoint source flows, monthly point source loads, and hourly atmospheric wet deposition. The minimum model spatial scales were determined by the size of the grid cells, ranging from 500 to about 1000 meters in the longitudinal direction along the streams. Data for longitudinal transect comparisons were averaged over the period August 1 to September 30, 1995. The disparity in the temporal and spatial scales between the model and prototype, especially for the nonpoint and point source loads, meant that individual observations may not be directly comparable with model prediction at a specific time in a given model grid cell.

Model-data comparisons will be made by means of longitudinal transect plots as well as time-series plots for the 11 major stream reaches in the study area: Brandywine Creek, East Branch Brandywine Creek, West Branch Brandywine Creek, Buck Run, Christina River (tidal), Christina River (nontidal), Red Clay Creek, West Branch Red Clay Creek, White Clay Creek, East Branch White Clay Creek, and the Delaware River. The transects are delineated in river miles referenced to River Mile 74.9 located at the mouth of the Christina River based on EPA REACH FILE 1 (see Table 9-4). Longitudinal transect plots for each water column parameter are presented in Appendix E arranged by stream reach. There are 18 transect plots for each reach, representing 18 different water quality parameters. The model results for the transect plots were averaged over the period August 25 to September 10, 1995. The horizontal axis of each plot represents the river mile from the mouth of the Christina River measured

along the stream network. The vertical axis represents the water column parameter concentration. The observed data are shown as "box-and-whisker" symbols indicating the maximum, minimum, 25th percentile, 75th percentile, mean, and median statistics. The model results are represented by three lines: the solid line is the mean over the averaging period at a given model grid cell and the two dashed lines are the minimum and maximum values simulated over the averaging period.

The time-series plots are presented in Appendix F and cover the entire 143-day validation period beginning on May 1 (day 121) and continuing to September 21, 1995 (day 264). The time-series model-data comparisons were made at 16 monitoring locations on the various stream reaches in the study area (Figure 9-8). The concentrations of the nonpoint source loads were considered to be constant throughout the validation period, and the loads vary in accordance with the changes in nonpoint source flow rate. The nonpoint source concentrations were based on the summer low-flow monitoring data and are representative of background water quality conditions. In reality, the concentrations of the various water quality parameters will vary in relation to storm events and changes in watershed runoff. Determination of the time-varying nonpoint source concentrations was outside the scope of the present study, but will be addressed in the future following completion of the HSPF watershed model of the Christina River Basin.

10.3.1 Brandywine Creek Main Stem Water Quality Validation Results

The transect plots for all water quality parameters for the main stem of Brandywine Creek are shown in Figures E01 to E03, and the time-series plots at stations 104021 and WQN0105 are shown in Figures F01 to F04. The conservative constituents (chlorides and TSS) match the observed data reasonably well in both the transect and time-series plots. The time-series of TSS shows little variation because a constant nonpoint source concentration was used for the entire time period, whereas in reality the TSS concentrations would increase during storm runoff events. The grab samples of dissolved oxygen generally lie within the minimum and maximum range computed by the model for both the transect and time-series views. The observed organic carbon indicates an increasing trend in the downstream direction that is not reflected by the model. This is likely due to missing sources of organic carbon. The total phosphorus and dissolved orthophosphate indicate a decreasing concentration in the downstream direction that is simulated in the model. The nitrogen species (total nitrogen, ammonia nitrogen, and nitrate nitrogen) all match the observations along the transect reasonably well. Total nitrogen simulated by the model is slightly higher than the observations and may be due to excess dissolved organic nitrogen since the other species agree well with the data.

10.3.2 Brandywine Creek East Branch Water Quality Validation Results

The transect plots for all water quality parameters for the East Branch Brandywine Creek are shown in Figures E04 to E06, and the time-series plots at station 01480870 are shown in Figures F05 and

F06. The Downingtown WWTP (PA0026531) discharges at mile 103.7, which accounts for the abrupt change concentrations of some of the water quality parameters at that location. Along the transect, all water quality parameters are in reasonable agreement with observations. The time-series plots also indicate the model is in agreement with observations. The exception is fecal coliform bacteria, which does not agree well with observations due to nonpoint sources that are not accounted for in the model.

10.3.3 Brandywine Creek West Branch Water Quality Validation Results

The transect plots for all water quality parameters for the West Branch Brandywine Creek are shown in Figures E07 to E09, and the time-series plots at station 01480617 are shown in Figures F07 and F08. The South Coatesville (PA0036987) and Coatesville City (PA0026859) WWTPs discharge at river mile 110.4 and 111.0, respectively. The spike in the concentrations of various water quality parameters is due to these two discharges. The model agrees with the observed data very well for chlorides, TSS, dissolved oxygen, chlorophyll-*a*, organic carbon, total nitrogen, ammonia nitrogen, and nitrate nitrogen. Fecal coliform bacteria (see Figure F08) simulated by the model are about an order of magnitude less than the observations. This is likely due to nonpoint sources that are not accounted for in the model.

10.3.4 Buck Run Water Quality Validation Results

The transect plots for all water quality parameters for Buck Run are shown in Figures E10 to E12, and the time-series plots are shown in Figures F09 and F10. No observed data were available for Buck Run during the validation period, so validation cannot be assessed in this stream reach.

10.3.5 Christina River (Tidal) Water Quality Validation Results

The water-quality transect plots for the tidal Christina River are shown in Figures E13 to E15, and the time-series plots at stations 106291 and 106021 are shown in Figures F23 to F26. The lower portion of the Christina River is strongly influenced by the Delaware River due to tidal excursion. The transect plots indicate the model agrees well with the data for all parameters with the exception of total nitrogen, which is slightly high in the model; ammonia nitrogen, which is low in the model; and total organic carbon, which is about 2.5 mg/L low in the model. The time-series plots also indicate similar reasonable model-data agreement with the exception of the above-mentioned three parameters.

10.3.6 Christina River (Nontidal) Water Quality Validation Results

The transect plots for all water quality parameters for the nontidal Christina River are shown in Figures E16 to E18, and the time-series plots at station 106031 are shown in Figures F27 and F28. Along the transect, all water quality parameters agree with the observations quite well. The spike in chlorides concentration at river mile 98.1 is due to the West Branch Christina River, which carries loads from the two Maryland WWTPs (MD0022641 and MD0065145).

10.3.7 Red Clay Creek and East Branch Water Quality Validation Results

The transect plots for all water quality parameters for Red Clay Creek and East Branch Red Clay Creek are shown in Figures E19 to E21, and the time-series plots at stations 103031, WQN0150, and RCEB04 are shown in Figures F09 to F14. The West Branch Red Clay Creek enters at river mile 100.3 and accounts for the spikes in concentration that are evident in a number of the transect plots. Overall, the model does a reasonable job of simulating the observations for both the transect and time-series views. At station WQN0150 the total phosphorus and dissolved orthophosphate data indicate an increasing trend from May to September (see Figure F12). This tends to support the hypothesis that the primary sources for phosphorus may be from a relatively steady-state source (i.e., point source or groundwater source) because as the stream flow decreases in the summer months, the concentration of phosphorus is increasing.

10.3.8 Red Clay Creek West Branch Water Quality Validation Results

The transect plots for all water quality parameters for West Branch Red Clay Creek are shown in Figures E22 to E24, and the time-series plots at station RCWR2 are shown in Figures F15 and F16. The Kennett Square WWTP (PA0024058) discharges at river mile 103.9, accounting for the spike in concentrations at that location. The observed data shown on the transect plots were not measured in the West Branch Red Clay Creek, but rather were measured in two tributaries (the NVF tributary and the Toughkenamon tributary). Thus, a direct model-data comparison should not be assumed for any of the transect plots for the West Branch Red Clay Creek.

10.3.9 White Clay Creek and Middle Branch Water Quality Validation Results

The transect plots for all water quality parameters for White Clay Creek and Middle Branch White Clay Creek are shown in Figures E25 to E28, and the time-series plots at stations 105151 and WQN0149 are shown in Figures F17 to F20. The transect plots indicate reasonable model-data agreement for all parameters except dissolved orthophosphate phosphorus. Downstream of river mile 103 the monitoring data indicate dissolved orthophosphate concentrations in the 0.1 to 0.2 mg/L range, whereas the model computes concentrations of about one-half of the observed values.

10.3.10 White Clay Creek East Branch Water Quality Validation Results

The transect plots for all water quality parameters for White Clay Creek East Branch are shown in Figures E28 to E30, and the time-series plots at station WCER2 are shown in Figures F21 and F22. Station WCER2 is Reach 2 from the August 1997 study (Davis 1998), and no observed data were available for the 1995 validation period. The Avondale Borough WWTP (PA0025488) is the largest point source on this stream and discharges at river mile 106.6. No data were available downstream of the Avondale WWTP to compare to the model results.

10.3.11 Delaware River Water Quality Validation Results

The transect plots for all water quality parameters for the Delaware River are shown in Figures E31 to E33. The model indicates reasonable agreement for most water quality parameters. The largest discrepancies occur for chlorophyll-*a* (model is higher than the observations) and total organic carbon (model is lower than the observations). The simulated dissolved oxygen sag at river mile 82 reaches a minimum value of about 2.4 mg/L. The model results cannot be validated at that location since no observed data were available.

10.3.12 Muddy Run and Pike Creek Water Quality Validation Results

Time-series plots for all water quality parameters for Muddy Run (station 105131) and Pike Creek (station 105101) are shown in Figures F29 to F32. The model results agree well with the observations for all parameters with the exception of an apparent algae bloom in mid-July (day 198) at the Muddy Run station. The data indicate a chlorophyll-*a* concentration of about 16 ug/L, whereas the model computes about 3.0 ug/L. However, in May to June and August to September the model agrees well with the chlorophyll-*a* measurements.

10.4 Diel Dissolved Oxygen Validation Results

An important feature of the Christina River Basin water quality model is the ability to compute the daily dissolved oxygen range as well as the daily average value. Water quality standards for dissolved oxygen in the Christina River Basin must meet two criteria, one for the daily average and one for the daily minimum concentration. The data available for model validation included diel dissolved oxygen at several locations. The USGS collected diel dissolved oxygen data at three gages for the entire May to September 1995 validation period: (1) 01480870 at Downingtown on the East Branch Brandywine Creek, (2) 01480617 at Modena on the West Branch Brandywine Creek, and (3) 01481000 at Chadds Ford on the main stem Brandywine Creek.

Achieving the proper range in daily dissolved oxygen is primarily a function of the community periphyton biomass available at a given model grid cell. The periphyton growth and basal metabolism rates as well as the growth rate density limitation parameters were adjusted to simulate the periphyton biomass needed to achieve reasonable daily DO ranges at the monitoring sites during mid-August to mid-September 1995, the critical low-flow period. The monitored daily minimum, maximum, and average dissolved oxygen concentrations at the three USGS gage locations are shown in Figure 10-6, along with the model results. It is evident that the model does a reasonable job of simulating the daily DO range at these three locations during the critical low-flow period (August 15 to September 15, 1995; day 228 to 259). At the Downingtown station, the dissolved oxygen does not agree with the observed data from

May 1 to about July 31, 1995. The reason for this may be due to the Broad Run WWTP (PA0043982), which is discharging ammonia nitrogen at a concentration of 12 to 15 mg/L during the May to July period. In August and September the effluent ammonia concentration drops to between 0.8 and 5.3 mg/L at this WWTP. The daily minimum, maximum, and average water temperatures at the three USGS gage locations and the simulated model temperatures are shown in Figure 10-7. The model is in good agreement with the measured temperature data for the entire 5-month simulation period. The time-series of periphyton biomass at the three gage locations is shown in Figure 10-8. The periphyton biomass has been displayed in units of ug/L of chlorophyll-*a* for comparison with the floating chlorophyll-*a* concentrations. The periphyton biomass (500 to 1,000 ug/L) is as much as two orders of magnitude greater than the floating chlorophyll-*a* biomass (3 to 10 ug/L) at these three locations.

10.5 Sediment Oxygen Demand Rates

No field data were available during the 1995 validation period to verify the flux rates computed by the predictive sediment submodel. However, SOD rates were measured in July and August 1996, at three locations in the tidal Christina River and Brandywine Creek. An SOD rate of 0.5 g/m^2/day was used in the tidal Delaware River in another model study conducted by HydroQual for DRBC and was also adopted for this study. The simulated SOD rates were converted to rates at 20 °C and are compared with the measured data in Table 10-2. The relative errors vary from 2.2% on the Christina River at Newport to 22.5% at the mouth of Christina River.

Table 10-2. Model-data comparison of sediment oxygen demand rates (g/m^2/day).

Location	Sampling Date	Monitored SOD at 20°C	1995 Validation Model SOD at 20°C	Relative Error
Christina River at I-495 bridge	Aug 12, 1996	0.81	0.99	22.5%
Christina River at Newport, Rt. 141 bridge	Jul 10, 1996	1.67	1.63	2.2%
Brandywine Creek, 0.6 mi. from mouth	Aug 12, 1996	1.23	1.48	20.0%
Delaware River (from HydroQual study)	-	0.50	0.52	4.8%

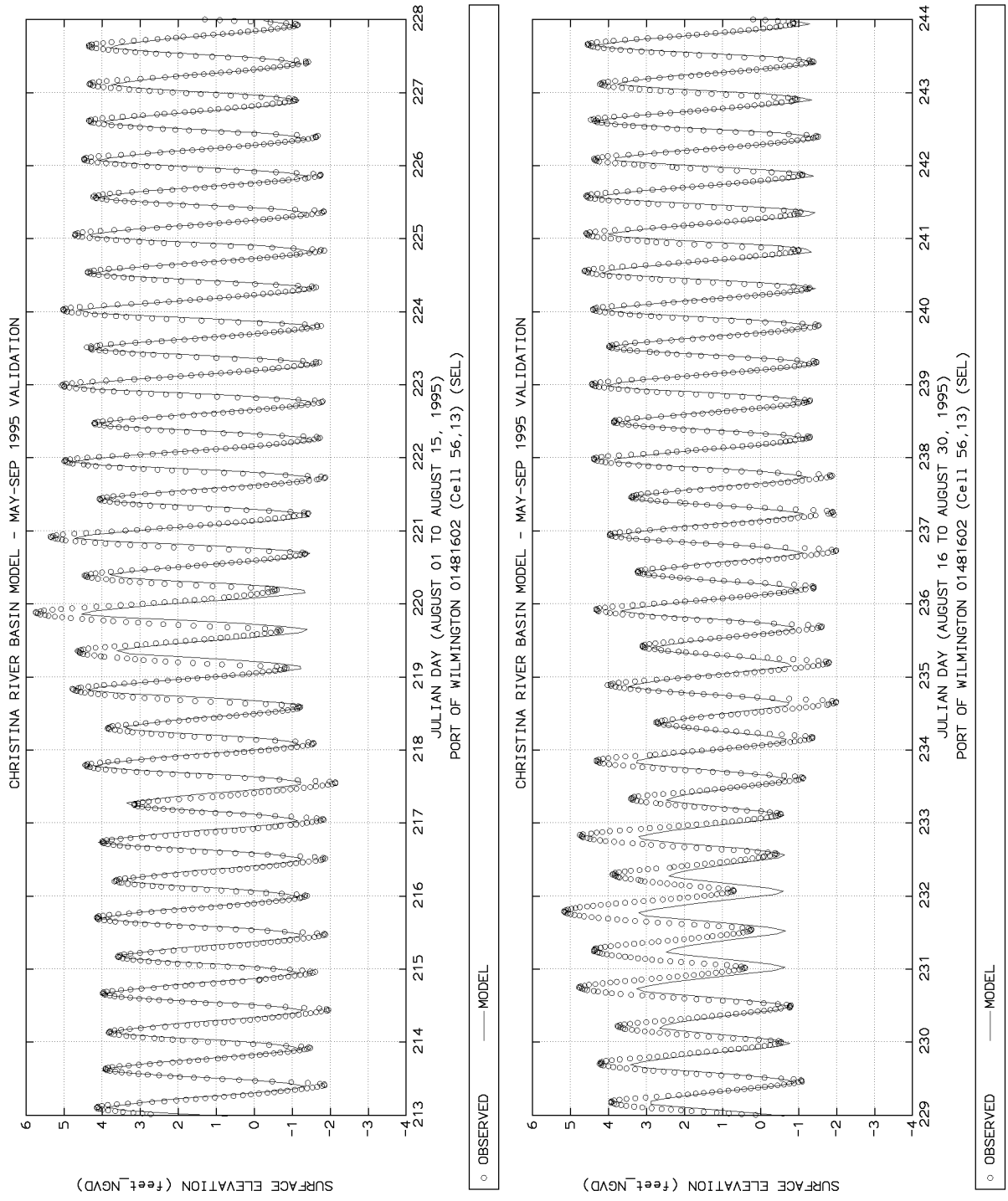

Figure 10-1. Model-data comparison of tides at Port of Wilmington (Aug 1995).

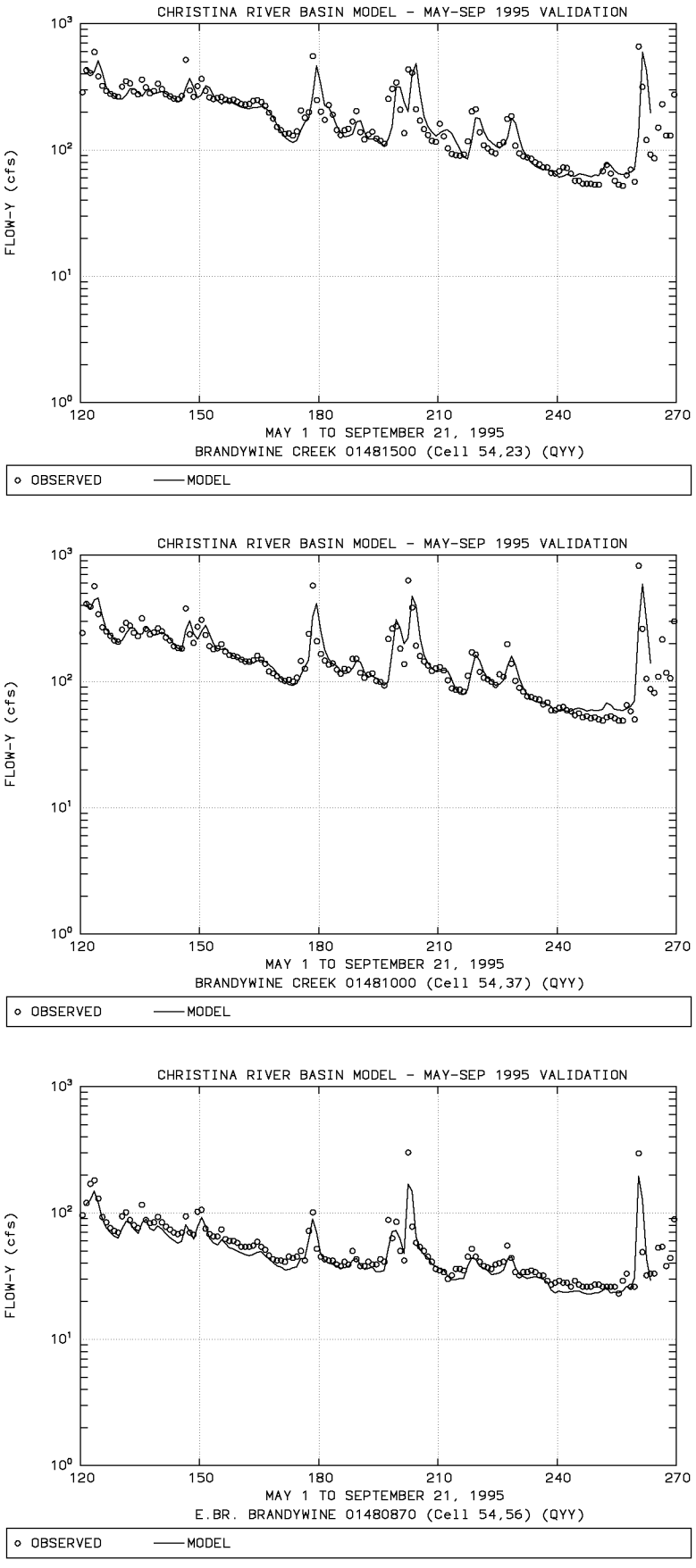

Figure 10-2. Model-data hydrographs, Brandywine Creek and E. Br. Brandywine Cr.

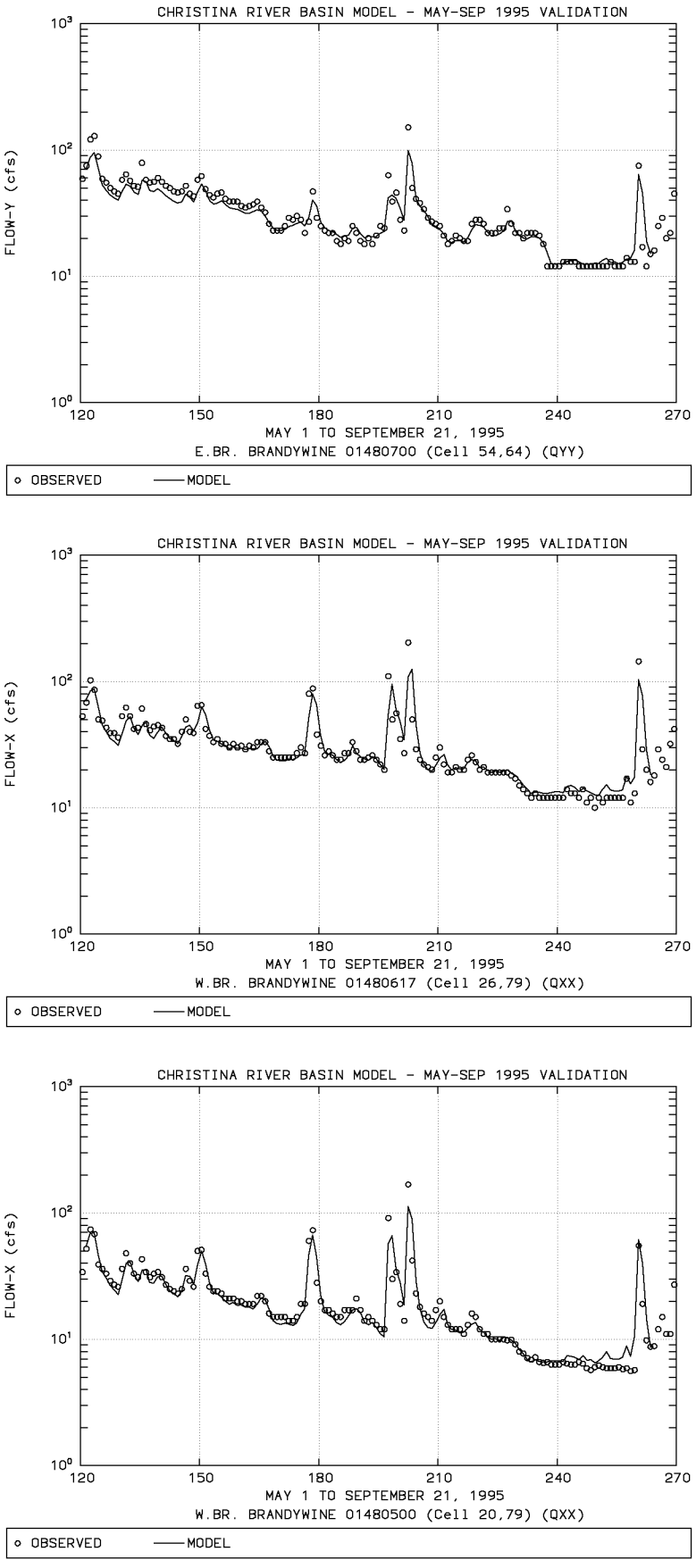

Figure 10-3. Model-data hydrographs, E. Br. Brandywine Cr. and W. Br. Brandywine Cr.

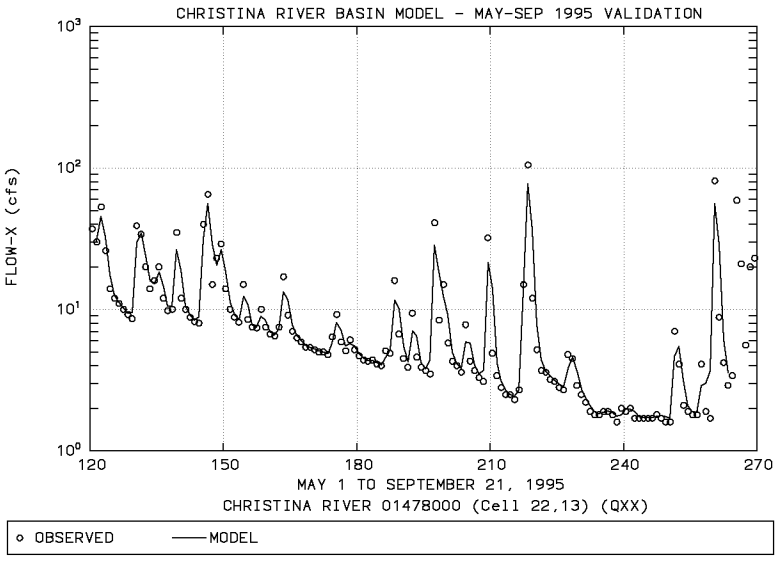

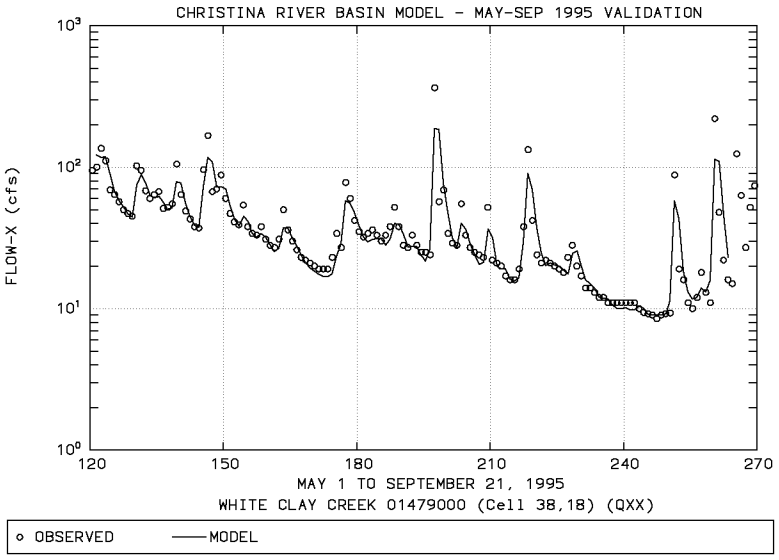

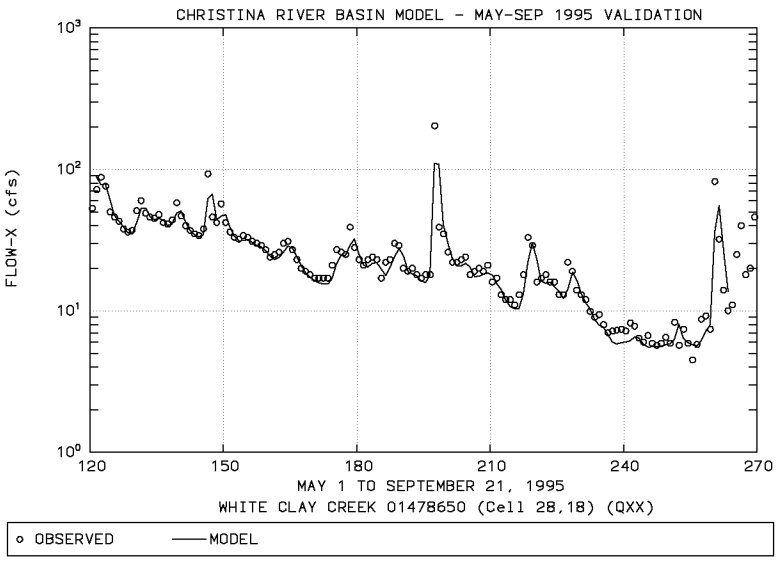

Figure 10-4. Model-data hydrographs, Christina River and White Clay Creek.

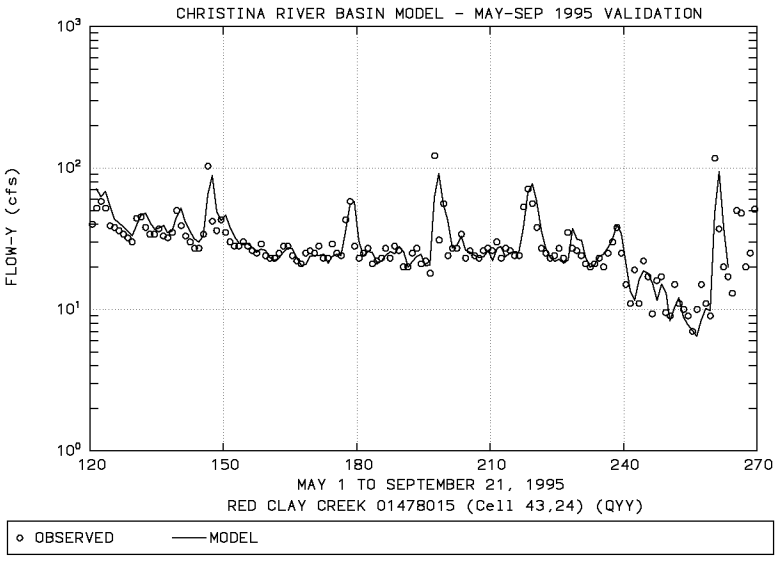

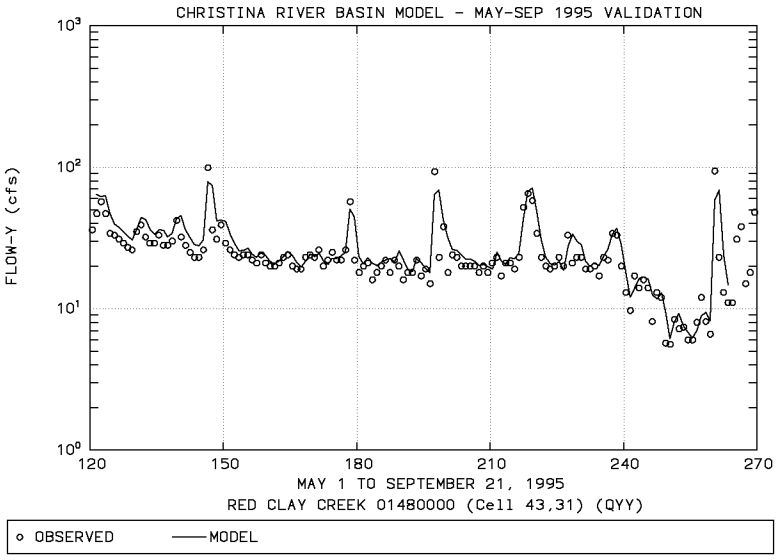

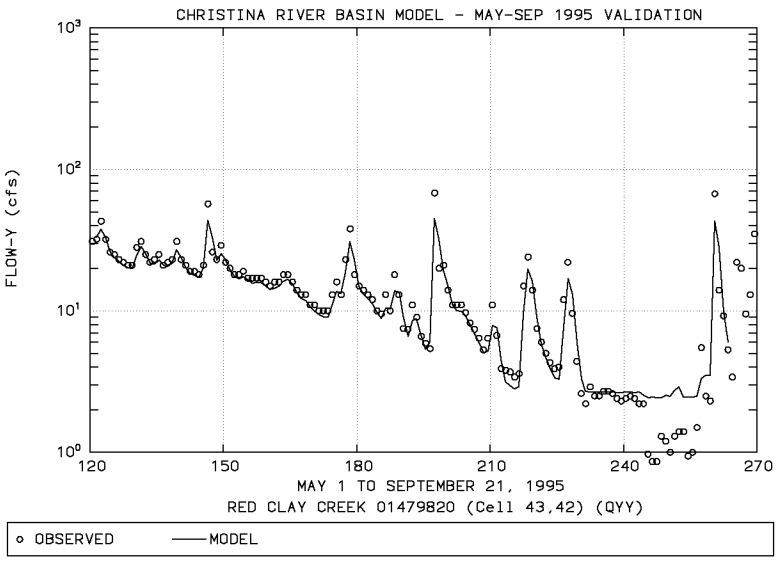

Figure 10-5. Model-data hydrographs, Red Clay Creek.

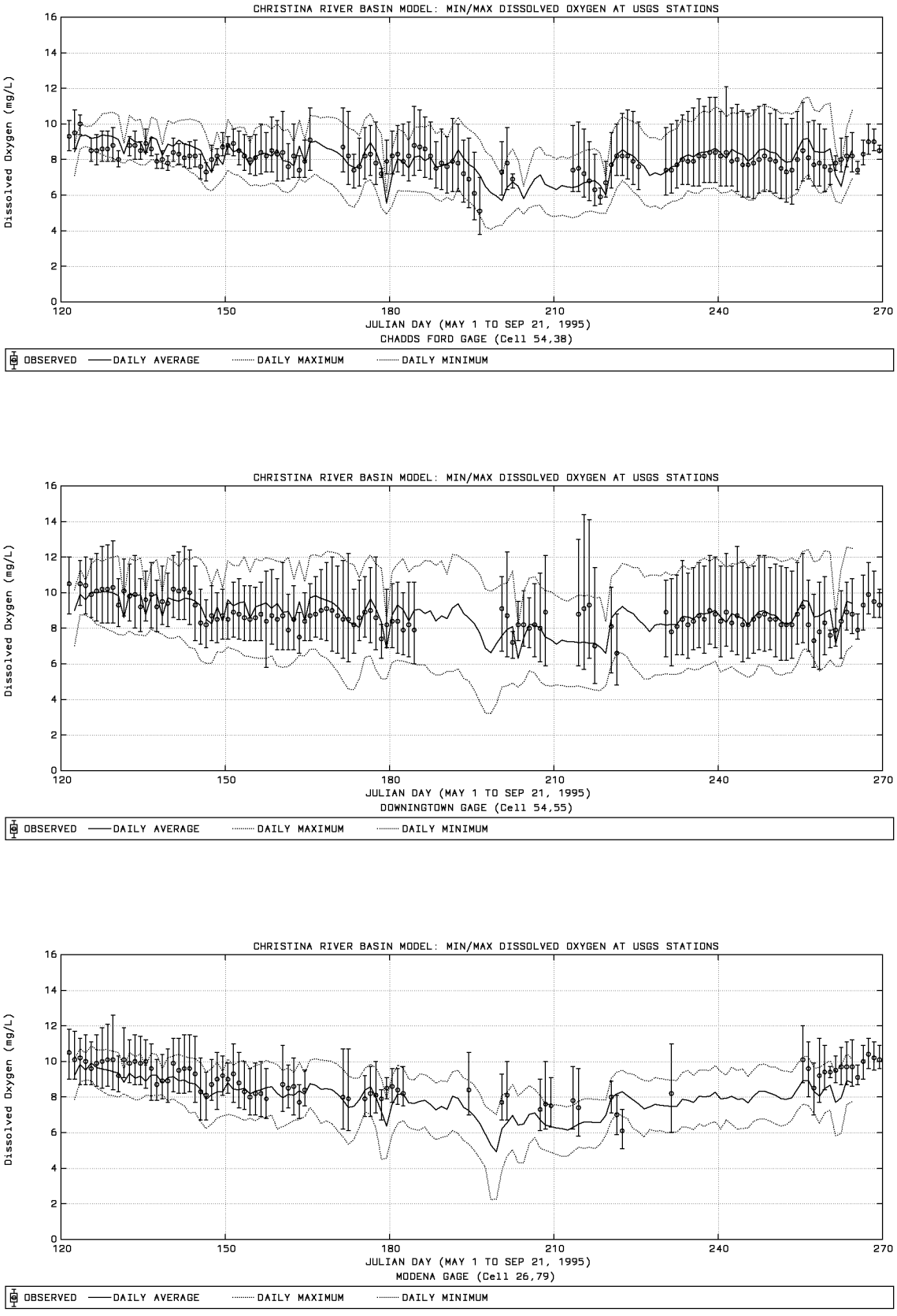

Figure 10-6. Diel dissolved oxygen at USGS monitoring stations.

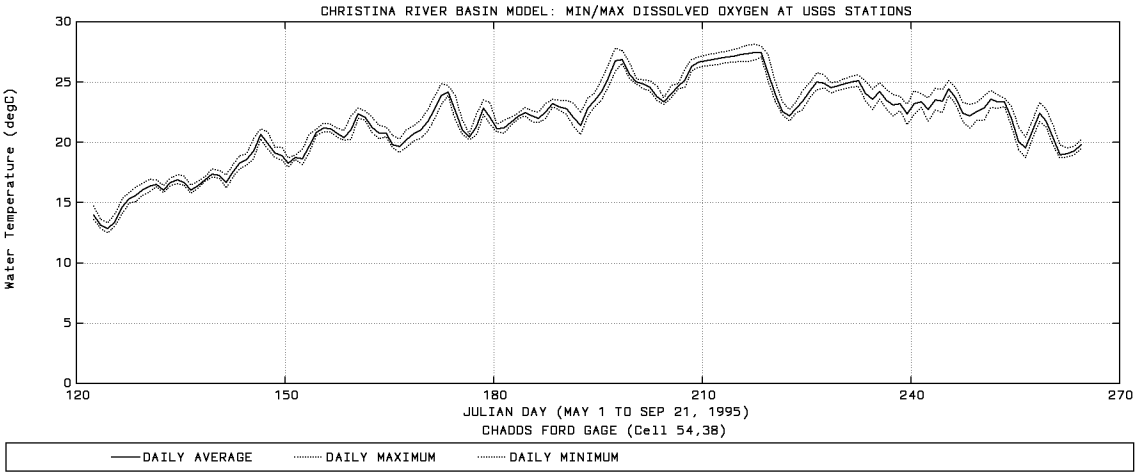

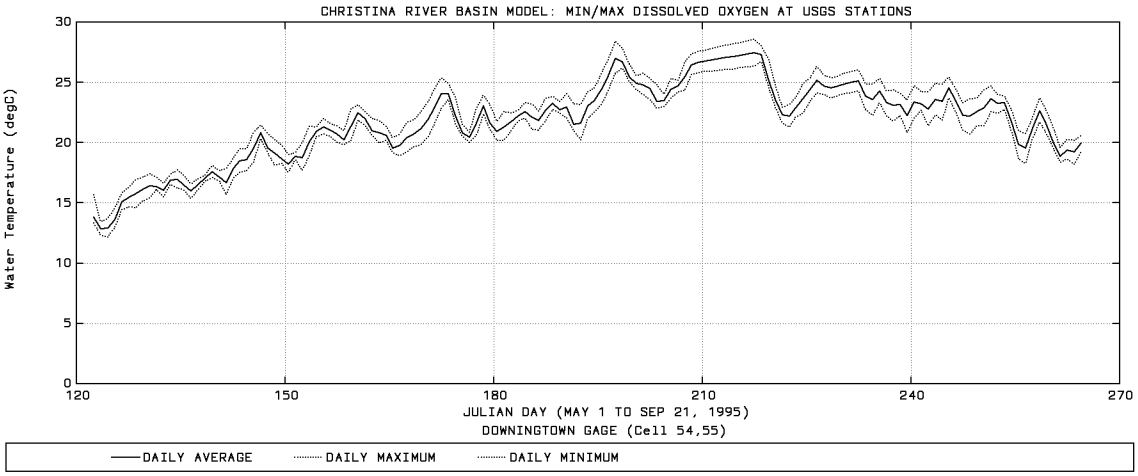

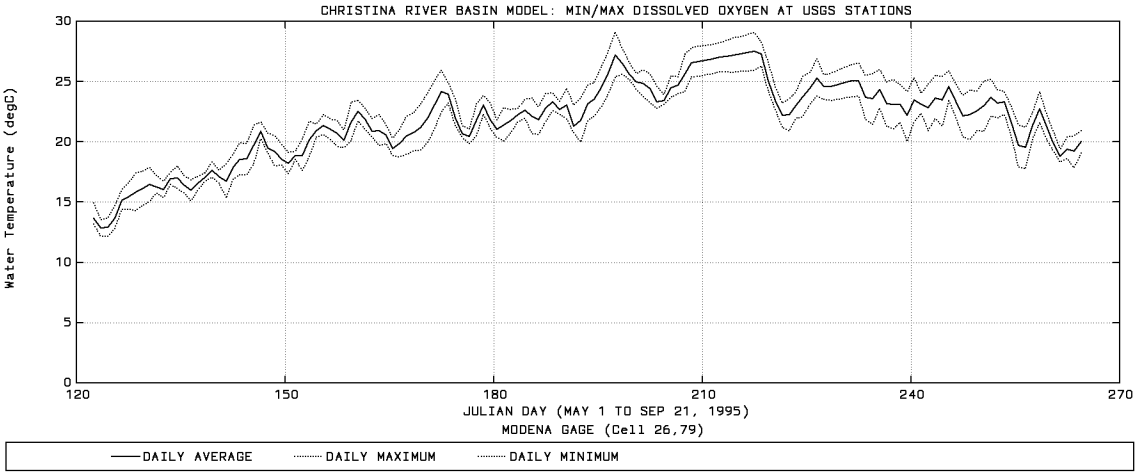

Figure 10-7. Water temperature at USGS monitoring stations.

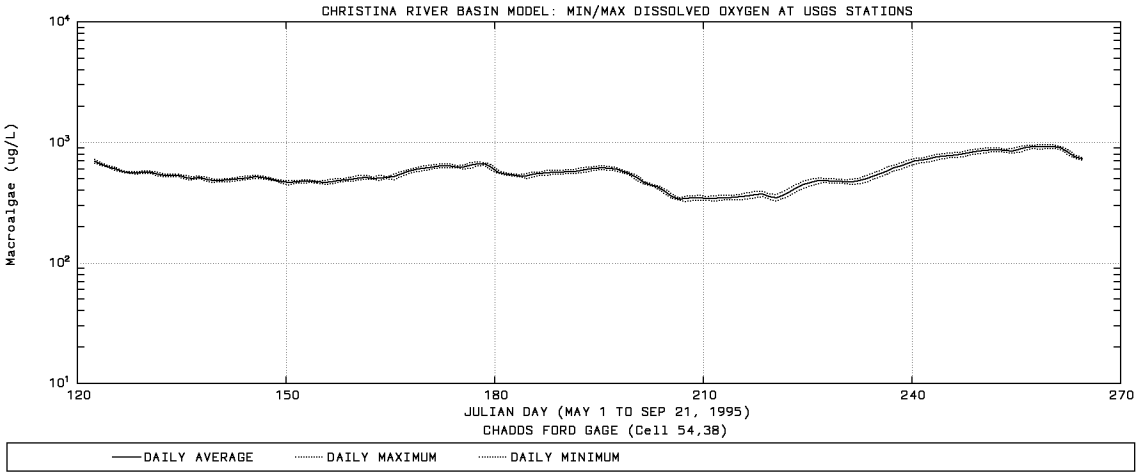

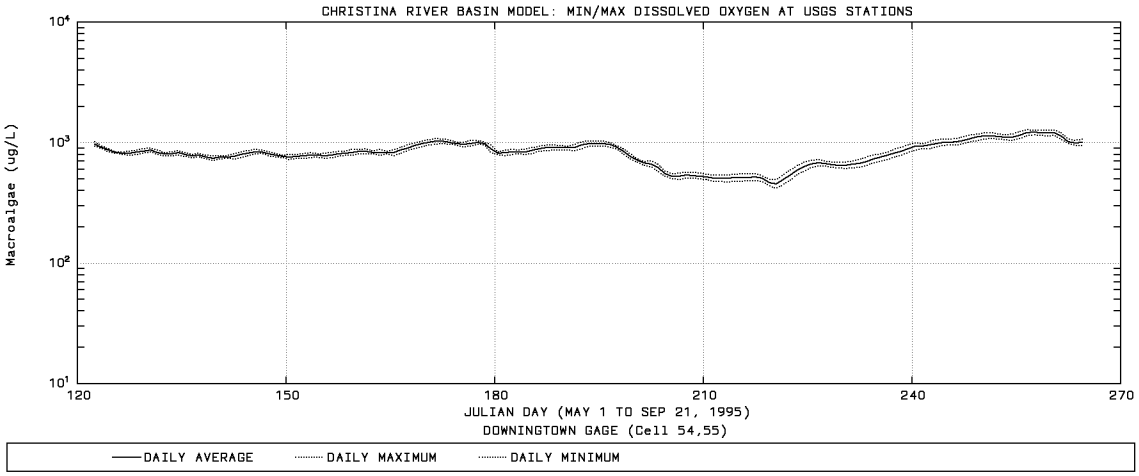

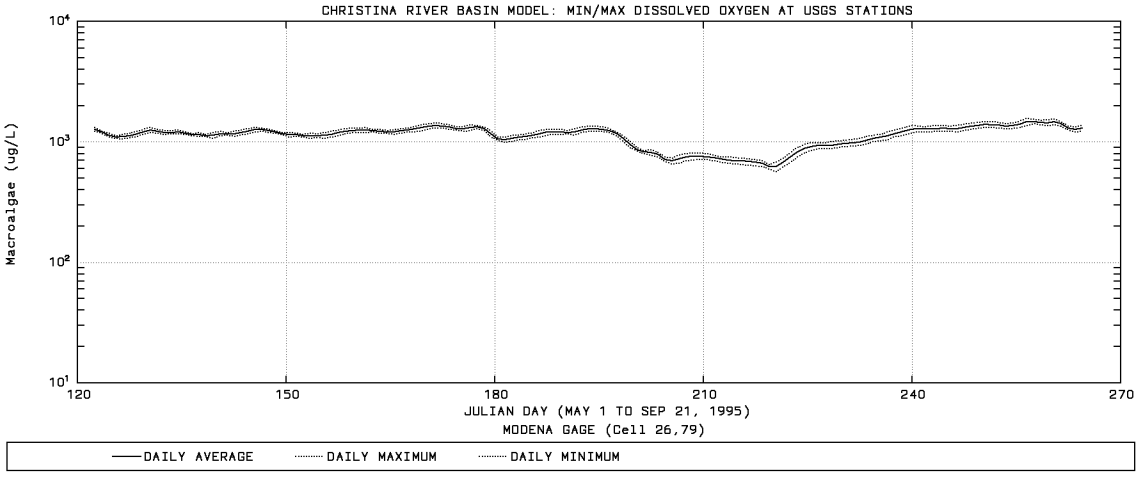

Figure 10-8. Periphyton biomass at USGS monitoring stations.

11 - STATISTICAL SUMMARY OF CALIBRATION AND VALIDATION

The model-data comparisons in Appendices A and B (1997 calibration) and in Appendices E and F (1995 validation) provide a qualitative evaluation of model performance. A seasoned modeler can examine the plots and form an experience-based judgment on the status of model calibration and verification. In this section, model-data comparisons are presented as quantitative statistical summaries. This presentation provides a different perspective on model-data comparison that numerically quantifies the state of model calibration/verification (sometimes referred to as model "skill assessment").

Although numerous methods exist for analyzing and summarizing model performance, there is no consensus in the modeling community on a standard analytical suite. A set of basic statistical methods were used to compare model predictions and sampling observations which included the mean error statistic, the absolute mean error, the root-mean-square error, and the relative error. The observations and model predictions were analyzed over the period May 1 to September 21 for both the 1997 calibration data set and the 1995 validation data set at 20 monitoring locations throughout the Christina River Basin.

11.1 Mean Error Statistic

The mean error between model predictions and observations is defined in Eq. 11-1. A mean error of zero is ideal. A non-zero value is an indication that the model may be biased toward either over- or underprediction. A positive mean error indicates that on average the model predictions are less than the observations. A negative mean error indicates that on average the model predictions are greater than the observed data. The mean error statistic may give a false ideal value of zero (or near zero) if the average of the positive deviations between predictions and observations is about equal to the average of the negative deviations in a data set. Because of that possibility, it is never a good idea to rely solely on this statistic as a measure of performance. Instead, it should be used in tandem with the other statistical measures that are described in this section.

$$E = \frac{\Sigma\ (O - P)}{n} \qquad (11\text{-}1)$$

where:

E = mean error
O = observation, aggregated by month and over the water column
P = model prediction, aggregated by month and over vertical layers
n = number of observed-predicted pairs

11.2 Absolute Mean Error Statistic

The absolute mean error between model predictions and observations is defined in Eq. 11-2. An absolute mean error of zero is ideal. The magnitude of the absolute mean error indicates the average deviation between model predictions and observed data. Unlike the mean error, the absolute mean error cannot give a false zero.

$$E_{abs} = \frac{\Sigma\ |O - P|}{n} \tag{11-2}$$

where:

E_{abs} = absolute mean error.

11.3 Root-Mean-Square Error Statistic

The root-mean-square error (E_{rms}) is defined in Eq. 11-3. A root-mean-square error of zero is ideal. The root-mean-square error is an indicator of the deviation between model predictions and observations. The E_{rms} statistic is an alternative to (and is usually larger than) the absolute mean error.

$$E_{rms} = \sqrt{\frac{\Sigma\ (O - P)^2}{n}} \tag{11-3}$$

where:

E_{rms} = root-mean-square error

11.4 Relative Error Statistic

The relative error between model predictions and observations is defined in Eq. 11-4. A relative error of zero is ideal. The relative error is the ratio of the absolute mean error to the mean of the observations and is expressed as a percent.

$$E_{rel} = \frac{\Sigma\ |O - P|}{\Sigma\ O} \tag{11-4}$$

where:

E_{rel} = relative error.

11.5 Evaluation of Results

Summary statistics have been developed for each of the individual monitoring locations as well as for the entire Christina River Basin (i.e., all monitoring stations taken together as a whole) for both the 1997 calibration period and the 1995 validation period. A summary of the error statistics for all water quality parameters for the 1997 model calibration simulation is given in Table 11-1, and the 1995 validation summary is given in Table 11-2. The relative error statistic permits comparisons between the various water quality substances. Temperature and dissolved oxygen were the parameters with the smallest relative error. The results for temperature indicate a relative error of 5.0% or less, and the relative error for dissolved oxygen was less than 7.1% for both the calibration and validation runs. The relative error for total nitrogen was less than 18%, total phosphorus was less than 35%, and total organic carbon was less than 36% for both the calibration and validation runs. The relative error for chlorophyll-*a* was about 19% in the calibration run and 37% in the validation run. The variability of the chlorophyll-*a* parameter reflects the nonconservative behavior of algal dynamics and the approximate nature of mathematical models of biological processes. A rule of thumb for chlorophyll-*a* monitoring is that at any given station and any given time, the sampled concentrations can vary by a factor of one-half to double. The highly dynamic, short-term variations of the chlorophyll-*a* parameter are extremely difficult to model. Eutrophication models are better suited to simulating the long-term (daily to monthly time scale) chlorophyll-*a* levels rather than the short-term (hourly) concentrations.

The relative errors for total nitrogen and total phosphorus for the combined 1995 and 1997 simulation periods for the individual stream reaches are presented in Table 11-3. The relative errors in total nitrogen for the primary stream reaches are as follows: West Branch Brandywine Creek (5.2%), East Branch Brandywine Creek (12.6%), Brandywine Creek main stem (14.4%), West Branch Red Clay Creek downstream of Kennett Square (9.4%), and East Branch White Clay Creek (18.7%). The relative errors in total phosphorus for these same stream reaches are West Branch Brandywine Creek (27.8%), East Branch Brandywine Creek (23.6%), Brandywine Creek main stem (32.8%), West Branch Red Clay Creek downstream of Kennett Square (16.5%), and White Clay Creek (35.4%).

Table 11-1. Statistical summary of Christina River model 1997 calibration results.

Parameter	Mean Error	Absolute Mean Error	RMS Error	Relative Error	No. Samples
Chlorides (mg/L)	0.2684	2.8507	4.6268	11.40%	55
Chlorophyll-a (ug/L)	0.3741	0.8374	1.3293	18.67%	34
Dissolved Oxygen (mg/L)	0.2598	0.6224	0.9063	7.10%	68
Total Organic Carbon (mg/L)	-0.6543	1.7280	2.4286	35.92%	37
Diss. Organic Carbon (mg/L)	-0.1237	1.4143	2.1255	34.00%	37
Total Nitrogen (mg/L)	0.0617	0.4686	0.6689	13.61%	51
Ammonia Nitrogen (mg/L)	0.0283	0.0322	0.0820	44.58%	55
Nitrate Nitrogen (mg/L)	-0.0106	0.3933	0.5334	14.69%	58
Total Phosphorus (mg/L)	-0.0025	0.0618	0.1143	34.17%	53
Diss. Orthophosphate P (mg/L)	-0.0147	0.0324	0.0536	31.37%	52
Temperature (degC)	-0.6974	0.9147	1.2818	4.72%	70

Table 11-2. Statistical summary of Christina River model 1995 validation results.

Parameter	Mean Error	Absolute Mean Error	RMS Error	Relative Error	No. Samples
Chlorides (mg/L)	2.6778	4.5443	6.0969	18.43%	63
Chlorophyll-a (ug/L)	-0.2194	1.1667	2.2680	53.42%	38
Dissolved Oxygen (mg/L)	0.1747	0.5204	0.7058	6.30%	89
Total Organic Carbon (mg/L)	-0.0552	2.0567	2.9104	33.27%	63
Diss. Organic Carbon (mg/L)	0.2037	1.8365	2.4630	36.43%	63
Total Nitrogen (mg/L)	-0.4560	0.5863	1.0084	21.57%	63
Ammonia Nitrogen (mg/L)	0.0301	0.0347	0.0617	59.06%	63
Nitrate Nitrogen (mg/L)	-0.2554	0.4711	0.7607	22.35%	63
Total Phosphorus (mg/L)	-0.0077	0.0407	0.0593	27.99%	63
Diss. Orthophosphate P (mg/L)	0.0059	0.0246	0.0333	30.37%	15
Temperature (degC)	-0.8597	1.0222	1.3666	5.04%	90

Table 11-3. Relative error of total nitrogen and total phosphorus for 1995 and 1997 simulation periods.

Location	Total Nitrogen		Total Phosphorus	
	Relative Error	No. Samples	Relative Error	No. Samples
Christina River (Smalleys Pond)	22.6%	8	35.6%	8
Brandywine Creek main stem	14.4%	21	32.8%	23
Brandywine Creek East Branch	12.6%	12	23.6%	14
Brandywine Creek West Branch	5.2%	11	27.8%	13
Red Clay Creek	23.0%	12	31.9%	14
Red Clay Creek West Branch below Kennett Square	1.5%	3	16.5%	2
White Clay Creek	18.7%	22	35.4%	21
White Clay Creek East Branch	9.9%	3	48.1%	3
Muddy Run	28.5%	8	20.4%	7
Pike Creek	25.8%	8	28.6%	6

11.6 Comparison with Other Model Studies

The combined 1997 calibration and 1995 validation results of the Christina River EFDC model were compared with results from a number of other water quality model studies. Some of these results were presented in the Chesapeake Bay model report (Cerco and Cole 1994) and were incorporated into this study. The model studies that will be considered in the comparison include Peconic Estuary (Tetra Tech 1999), Long Island Sound (HydroQual 1991), Massachusetts Bay (HydroQual 1995), Chesapeake Bay (Cerco and Cole 1994), Delaware Inland Bays (Cerco et al. 1993), Tolo Harbour (Chau and Jin 1998), New York Bight (Hall and Dortch 1993), Chesapeake Steady-State model (HydroQual 1987), Potomac Estuary model (Thomann and Fitzpatrick 1982), Gunston Cove (Cerco 1985), Eau Galle Reservoir (Wlosinski and Collins 1985), and Lake Ontario (Thomann et al. 1979).

Comparing statistics from different model studies is not straightforward. In contrast to classical statistics, no standard methodology has existed for determining model performance statistics. Various treatments of predictions and observations among different model studies (for example, aggregation of data temporally and spatially) affect the statistical results and complicate comparisons between studies. Since these conflicts cannot be avoided without reworking past modeling results, a review of model application and statistical computation methods used in the past studies is warranted to provide a better understanding of the interstudy comparisons. The reviews in Sections 11.6.5 to 11.6.12 were adopted from the Chesapeake Bay model report (Cerco and Cole 1994). A summary of the characteristics of the various model applications is given in Table 11-4. It is noteworthy to compare and contrast the duration of the simulations among the various model applications in the comparison group. With the exception of the Lake Ontario model, the Peconic Estuary model was run for the longest duration (8 continuous years of simulation) of any model in the group. Some models were run for as little as a summer season (3 months) whereas others were steady-state simulations. This is important to keep in mind since user-specified initial conditions can impact model results for several months or even up to as much as a year beyond model startup. The longer a simulation is run, the less effect initial conditions have on water quality predictions.

11.6.1 Peconic Estuary Study

The Peconic Estuary model (Tetra Tech 1999) was a three-dimensional application of EFDC, a fully coupled hydrodynamic and water quality model. The water quality model simulated 22 state variables. The Peconic model was calibrated and validated over an 8-year continuous time period from October 1988 to October 1996. Model-data comparisons were computed using the same statistics defined earlier in this section of the report.

Table 11-4. Summary of various models in comparison group.

Model Application (code)	Spatial Dimensions	Simulation Time	State Variables	Dynamic or Steady-State	Sediment Fluxes
Christina River Basin (CRB)	2D	5 months 05/95-09/95 05/97-09/97	22	Dynamic	Predicted
Peconic Estuary (PE)	3D	8 years 10/88-10/96	22	Dynamic	Predicted
Long Island Sound (LIS)	3D	18 months 4/88 - 10/89	25	Dynamic	Predicted
Massachusetts Bay (BEM)	3D	18 mo. / 1 yr. 10/89 - 4/91 1/92 - 12/92	24	Dynamic	Predicted
Chesapeake Bay (CB)	3D	3 years 1/84 - 12/87	21	Dynamic	Predicted
Tolo Harbour (TH)	2D-horizontal 2-layer vertical	2 years 1/88 - 12/89	9	Dynamic	Specified
Delaware Inland Bays (DIB)	3D	3 years	21	Dynamic	Specified
New York Bight (NYB)	3D	one summer	21	Dynamic	Specified
Chesapeake Bay Steady-State (CBS)	3D	3 individual summers (1964, 1984, 1985)	NA	Steady-state	Specified
Potomac River Estuary (PR)	1D	6 individual summers (1968, 69, 70, 77, 78, 79)	9	Dynamic	Specified
Gunston Cove (GC)	2D	one summer	NA	Dynamic	Specified
Eau Galle Reservoir (EGR)	1D	two 6 mo. periods (Apr - Nov)	NA	NA	Specified
Lake Ontario (LO)	2D	10 years	NA	Dynamic	Specified

NA - not available.

11.6.2 Long Island Sound Study

The Long Island Sound Study model (HydroQual 1991) was a three-dimensional application of a hydrodynamic model linked to a 25-state variable water quality model. The LISS model was calibrated over a period of 18 months (April 1988 to September 1989). Model-data comparison statistics were not presented in the model report. Instead, the various time-series graphs in the report showing model predictions and observed data were digitized and reverse engineered to create data files that were then used to compute statistics according to Eq. 11-1 to 11-4. It is possible that only the “best fit” model-data comparison graphs were presented in the LISS model report; therefore, the statistics computed using these graphs may overstate model performance to a certain degree.

11.6.3 Massachusetts Bay

The Massachusetts Bay Eutrophication model (HydroQual 1995), called BEM, was a 3-D application of a hydrodynamic model (ECOM) linked to a 24-state variable water quality model (BEM). The model was calibrated using data for two time periods, October 1989 through April 1991, and January through December 1992. Since model-data statistics were not presented in the model report, the various time-series graphs showing observed data and model predictions were digitized and reverse engineered into data files for computing statistics according to Eq. 11-1 to 11-4. It is possible that only the "best fit" model-data comparison graphs were presented in the BEM model report. Therefore, any statistics computed using these graphs may overstate model performance to a certain degree.

11.6.4 Chesapeake Bay

The Chesapeake Bay model (Cerco and Cole 1994) was a three-dimensional application of the hydrodynamic model CH3D-WES and eutrophication model CE-QUAL-IC. The sediment processes model (DiToro and Fitzpatrick 1993) was activated. The model was run continuously for a period of 3 years. Statistics were computed according to the formulas presented earlier in this section. Observations and predictions were aggregated by season, by spatial zone, and by vertical level. The water quality model was essentially identical to the EFDC model used in this study.

11.6.5 Tolo Harbour

A two-layer, two-dimensional hydrodynamic model was integrated with a two-layer, two-dimensional eutrophication model and applied to Tolo Harbour, Hong Kong (Chau and Jin 1998). The water quality model simulated the transport and transformation of nine water quality constituents associated with eutrophication. Sediment oxygen demand and benthic nutrient fluxes were specified based on field monitoring data. The model was run for a period of 2 years (January 1985 through December 1986). Model-data statistics were not presented in the journal article; however, the various time-series graphs showing model-data comparisons were digitized and used to compute statistics according to Eq. 11-1 to 11-4. The model-data comparison graphs presented in the journal article represented four of seven monitoring stations in Tolo Harbour, so the computed statistics may not be a true indicator of overall model performance.

11.6.6 Delaware Inland Bays

The Delaware Inland Bays model (Cerco et al. 1993) was a two-dimensional application of the hydrodynamic (CH3D-WES) and eutrophication (CE-QUAL-IC) components of the Chesapeake Bay model. The sediment processes model was not activated. The model was run continuously for 3 years. Statistics were computed according to the formulas presented earlier in this section. Reported results were for spatial and temporal aggregations comparable to the Chesapeake Bay model study.

11.6.7 New York Bight

The New York Bight model (Hall and Dortch 1993) was a three-dimensional application of the hydrodynamic (CH3D-WES) and eutrophication (CE-QUAL-IC) components of the Chesapeake Bay model. The sediment processes model was not activated. The model was run for one summer. Statistics were computed according to formulas presented earlier in this section. Reported results were for one-to-one comparisons of predictions and observations (i.e., no aggregration).

11.6.8 Chesapeake Bay Steady-State Model

The steady-state model study of Chesapeake Bay (HydroQual 1987) was a three-dimensional eutrophication model applied to summer-average conditions. Statistics were reported individually for 3 years (1964, 1984, and 1985). Computation of statistics differed from those shown earlier in this section. The median absolute error and the median of individual relative errors were selected for comparison with absolute mean error and relative error in the Peconic Estuary study. The steady-state nature of the model implied temporal aggregation of model and observations.

11.6.9 Potomac River Estuary Model

The Potomac River Estuary model (Thomann and Fitzpatrick 1982) included a one-dimensional eutrophication model coupled to a rudimentary sediment model. The median of individual relative errors was reported for 6 different years (1968, 1969, 1970, 1977, 1978, and 1979). Observations from June through September in the upper 83 km of the Potomac Estuary were compared to model results. Unfortunately, the Potomac River Estuary model was compared to various data sets by readjusting the model parameters for each of the six calibration years. This is not an accepted practice since the purpose of model calibration and verification is not to “force fit” the model to the data.

11.6.10 Gunston Cove

The Gunston Cove model (Cerco 1985) was a two-dimensional eutrophication model applied for one summer period to an embayment of the tidal Potomac River. For statistical evaluation, observations and model predictions were aggregated spatially but not temporally. The root-mean-square error was used in the computation of the relative error.

11.6.11 Eau Galle Reservoir

The Eau Galle Reservoir model (Wlosinski and Collins 1985) was a one-dimensional eutrophication model. The model was executed for the period April through November for 2 years. The relative error was computed as shown in Eq. 11-4 except that “O” was the mean of the observations and “P” was the mean of the model predictions.

11.6.12 Lake Ontario

The Lake Ontario model (Thomann et al. 1979) was a two-layer eutrophication model. The median relative error was reported for an analysis of 10 years of data.

11.6.13 Comparison of Absolute Mean Errors

Absolute mean errors for salinity, chlorophyll-*a*, total nitrogen, total phosphorus, and dissolved oxygen for the various water quality model studies are shown in Figure 11-1. The absolute mean error of salinity was near zero for the Christina River model since this was a freshwater system. The other model studies are for estuary environments having larger salinity values. The absolute mean error of dissolved oxygen (0.53 mg/L) for the Christina River model for the combined 1995 and 1997 validation periods was among the better predicting models included in the study. The absolute mean error of chlorophyll-*a* (0.80 ug/L) in the Christina River model was less than most of the other models. The absolute mean error of total phosphorus (0.05 mg/L) and total nitrogen (0.47 mg/L) in the Christina River model was larger than most of the other models. This was expected since the magnitude of total nitrogen and total phosphorus in the Christina River system was higher than in the other estuarine models. For example, the highest total nitrogen concentrations in the Peconic Estuary range from about 0.3 to 1.0 mg/L, whereas the typical total nitrogen concentrations in the Christina River system were in the 2 to 8 mg/L range.

11.6.14 Comparison of Mean Errors for Dissolved Oxygen

Based on the mean error statistic, 6 of the 11 models for which data were available indicate that predicted dissolved oxygen concentrations are higher than observations (see Figure 11-2). Only the Gunston Cove model under predicted dissolved oxygen by a significant amount (about 1.9 mg/L). The Christina River model under predicted dissolved oxygen during the 1995 and 1997 periods by about 0.20 mg/L. Based on the mean error statistic, the Christina River model is ranked as the fourth best predictor of dissolved oxygen behind only the Peconic Estuary model, the Massachusetts Bay model (BEM), and the Tolo Harbor model. The Peconic Estuary model and Massachusetts Bay model have a mean dissolved oxygen error of near zero which, when considered by itself, may mislead the reader to assume an almost perfect model-data match. However, by also considering the absolute mean error statistic shown in Figure 11-1, the reader will understand that offsetting positive and negative "O-minus-P" pairs of data points in Eq. 11-1 resulted in a mean error of near zero for these two models. The magnitude of mean errors for the models in this comparative study were Massachusetts Bay (+0.03 mg/L), Peconic Estuary (+0.10 mg/L), Tolo Harbour (+0.16 mg/L), Christina River (+0.20 mg/L), Chesapeake Bay (-0.50 mg/L), Delaware Inland Bays (-1.25 mg/L), New York Bight (-0.55 mg/L), Gunston Cove (+1.8 mg/L), Eau Galle Reservoir 1981 (-1.1 mg/L), and Eau Galle Reservoir 1982 (-3.0 mg/L). Although the sample size is small, a common characteristic of eutrophication models seems

to be a general inability to simulate minimum dissolved oxygen levels as inferred by the tendency toward a negative value of the mean error statistic.

11.6.15 Comparison of Relative Errors

The comparisons of relative errors for dissolved oxygen, chlorophyll, total nitrogen, and total phosphorus for several model studies are shown in Figures 11-3 to 11-6. Nearly 20 years ago, the median relative error in a summary of dissolved oxygen models was reported as about 10% (Thomann 1982). Despite tremendous improvements in model formulation, it is apparent that with the exception of the Peconic Estuary and BEM models, the 10% relative error standard has not changed much in the past 2 decades. The median relative error in dissolved oxygen derived from models completed after 1982 was about 9% (not including the Christina River and Peconic Estuary models). The relative error in dissolved oxygen in the Christina River model was 6.3%, which ranks as 2nd best of the 20 models included in the comparative study. The average relative error for dissolved oxygen for all the models is 15.1%. The degree of realism in present-day eutrophication models has improved tremendously. This realism has removed degrees of freedom available to the modeler to calibrate the model. In other words, some of the calibration processes are not as amenable to subjective manipulation by the modeler as they were in the past. For example, the 2-D and 3-D hydrodynamic models have eliminated the use of a dispersion parameter to transport mass about an estuarine system. The predictive sediment model has eliminated the oftentimes subjective specification of benthic nutrient fluxes and sediment oxygen demand. The use of organic carbon as a state variable instead of BOD has eliminated flexibility in converting short-term measures of BOD to long-term values, which impacts the rate of oxygen consumption.

The relative error of chlorophyll-*a* for the recent generation of water quality models (Peconic Estuary, Long Island Sound, Massachusetts Bay, Chesapeake Bay, Tolo Harbour, and Delaware Inland Bays) ranges from 27 to 75% (Figure 11-4). The Christina River model is the best of this group with a relative error of 26.9%. The average relative error for chlorophyll-*a* for all the models is 35.2%. Some of the older models (Chesapeake Bay Steady-State, Potomac Estuary, Gunston Cove, Eau Galle Reservoir, and Lake Ontario) seem to give better results, with relative errors in chlorophyll-*a* ranging from 10 to 32%. However, most of these models were applied over a short-term duration (a single season) rather than a full year or multiple years, which removes the seasonal variation from the statistics and helps to produce a lower relative error. Also, the Potomac River Estuary model was compared to various data sets by readjusting the model parameters for each calibration run, which improves the fit. In the Christina River model, the important chlorophyll type is attached algae (periphyton) rather than floating algae. The floating algae biomass is small compared to the periphyton in the freshwater streams of the Christina River Basin.

The relative error of total nitrogen for the various models is shown in Figure 11-5. The Christina River model has a relative error of 15.9%, which ranks as 8th best of the 15 models included in the comparative study. The average relative error for total nitrogen for all the models is 17.1%. The relative error of total phosphorus for the various models is presented in Figure 11-6. The Christina River model has a total phosphorus relative error of 29.8%, which ranks 11th of the 16 models in the comparison group. This value is only slightly larger than the average relative error for total phosphorus for all the models (26.2%) in the comparison group. The larger than average relative error for total phosphorus in the Christina River model may be due to one or more of the following reasons: (1) the NPDES point source discharges were characterized based on monthly average flows and loads, whereas the in-stream monitoring data were grab samples taken at a single point in time and therefore reflect any short-term variations in the point source loading that the model would not be able to resolve; (2) phosphorus loads from nonpoint sources are based on a constant concentration whereas during storm events, the concentration would likely increase because of runoff from the watershed; and (3) uptake by aquatic macrophytes. The model simulates floating algae and periphyton but no other types of macrophytes.

According to the *Technical Guidance Manual for Performing Waste Load Allocations* (USEPA 1990), acceptable relative error statistic criteria are 15% for dissolved oxygen and 45% for nutrient parameters (nitrogen, phosphorus, and carbon). The overall relative error statistics for the Christina River model were 6.3% for dissolved oxygen, 15.9% for total nitrogen, 29.9% for total phosphorus, and 32.6% for total organic carbon. The relative error statistics for the Christina River water quality model meet the general guidance criteria published in USEPA (1990).

11.7 References for Section 11

Cerco, C. 1985. Water quality in a Virginia Potomac embayment: Gunston Cove. Virginia Institute of Marine Science, Gloucester Point, VA.

Cerco, C., B. Bunch, M. Cialone, and H. Wang. 1993. Hydrodynamic and eutrophication model study of Indian River-Rehoboth Bay Delaware. U.S. Army Engineer Waterways Experiment Station, Vicksburg, MS.

Cerco, C.F., and T.M. Cole. 1994. Three-Dimensional Eutrophication Model of Chesapeake Bay. Volume I: Main Report. Technical Report EL-94-4. U.S. Army Corps of Engineers, Waterways Experiment Station, Vicksburg, MS, May 1994.

Chau, K.W. and H. Jin. 1998. Eutrophication Model for a Coastal Bay in Hong Kong. *ASCE J. Environ. Engr.* 124(7):628-638.

Hall, R., and M. Dortch. 1993. New York Bight study report 2 - development and application of a eutrophication/general water quality model. Technical Report EL-93-xx, U.S. Army Engineer Waterways Experiment Station, Vicksburg, MS.

HydroQual. 1987. A steady-state coupled hydrodynamic/water quality model of the eutrophication and anoxia process in Chesapeake Bay. Final report. HydroQual Inc., Mahwah, NJ.

HydroQual. 1991. Water quality modeling analysis of hypoxia in Long Island Sound. HydroQual Inc., Mahwah, NJ.

HydroQual. 1995. A water quality model for Massachusetts and Cape Cod Bays: calibration of the Bays Eutrophication Model (BEM). HydroQual, Inc., Mahwah, NJ.

Tetra Tech. 1999. Three-dimensional hydrodynamic and water quality model of Peconic Estuary. For Peconic Estuary Program, Suffolk County Department of Health Services, Riverhead, NY. By Tetra Tech, Inc., Fairfax, VA.

Thomann, R., R. Winfield, and J. Segna. 1979. Verification analysis of Lake Ontario and Rochester Embayment three-dimensional eutrophication models. EPA-600/3-79-094. U.S. Environmental Protection Agency, Duluth, MN.

Thomann, R. 1982. Verification of water quality models. *ASCE J. Environ. Engr.* 108(EE5):923-940.

Thomann, R., and J. Fitzpatrick. 1982. Calibration and verification of a mathematical model of the eutrophication of the Potomac Estuary. HydroQual Inc., Mahwah, NJ.

USEPA. 1990. *Technical Guidance Manual for Performing Waste Load Allocations, Book III Estuaries, Part 2, Application of Estuarine Waste Load Allocation Models*. EPA823-R-92-003. U.S. Environmental Protection Agency, Office of Water. May 1990.

Wlosinski, J., and C. Collins. 1985. Confirmation of the water quality model CE-QUAL-RI using data from Eau Galle Reservoir, Wisconsin. Technical Report E-85-11. U.S. Army Engineer Waterways Experiment Station, Vicksburg, MS.

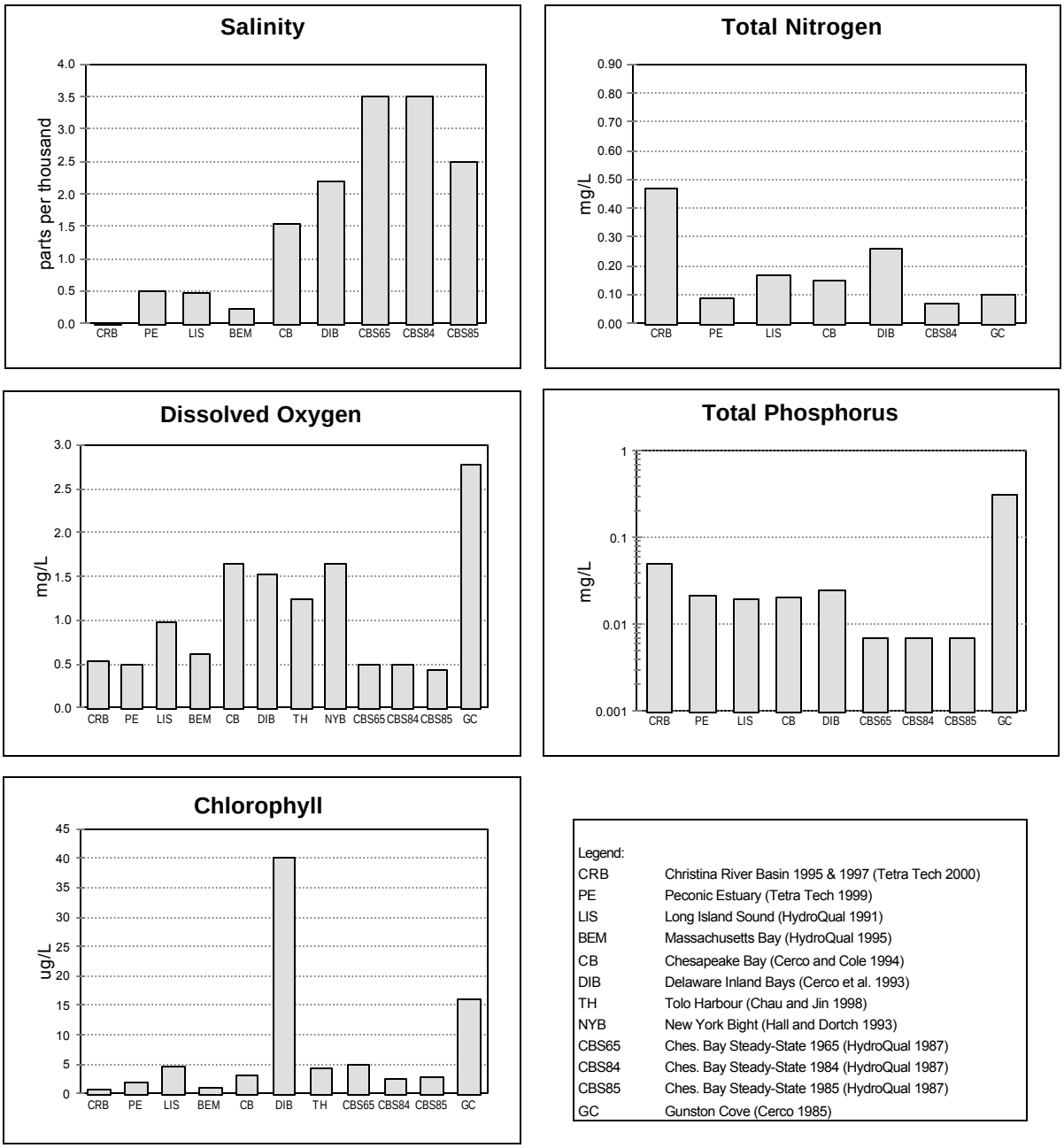

Figure 11-1. Absolute mean error for several model studies.

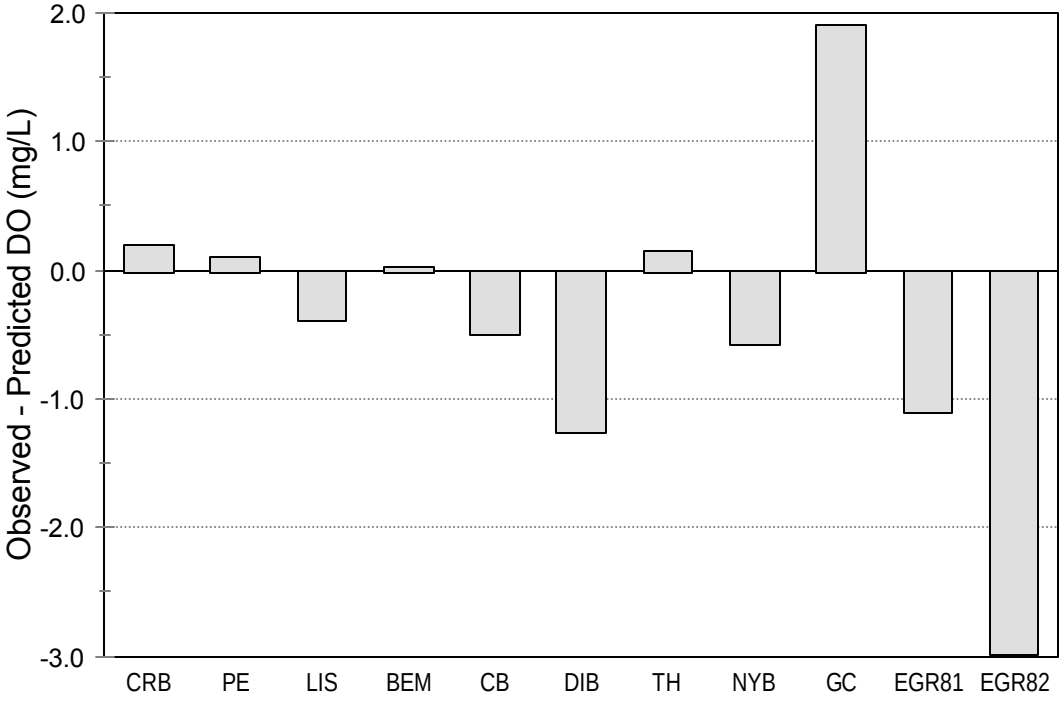

Legend:		
	CRB	Christina River Basin 1995 & 1997 (Tetra Tech 2000)
	PE	Peconic Estuary (Tetra Tech 1999)
	LIS	Long Island Sound (HydroQual 1991)
	BEM	Massachusetts Bay (HydroQual 1995)
	CB	Chesapeake Bay (Cerco and Cole 1994)
	DIB	Delaware Inland Bays (Cerco et al. 1993)
	TH	Tolo Harbour (Chau and Jin 1998)
	NYB	New York Bight (Hall and Dortch 1993)
	GC	Gunston Cove (Cerco 1985)
	EGR81	Eau Galle Reservoir 1981 (Wlosinski and Collins 1985)
	EGR82	Eau Galle Reservoir 1982 (Wlosinski and Collins 1985)

Figure 11-2. Mean dissolved oxygen error for several model studies.

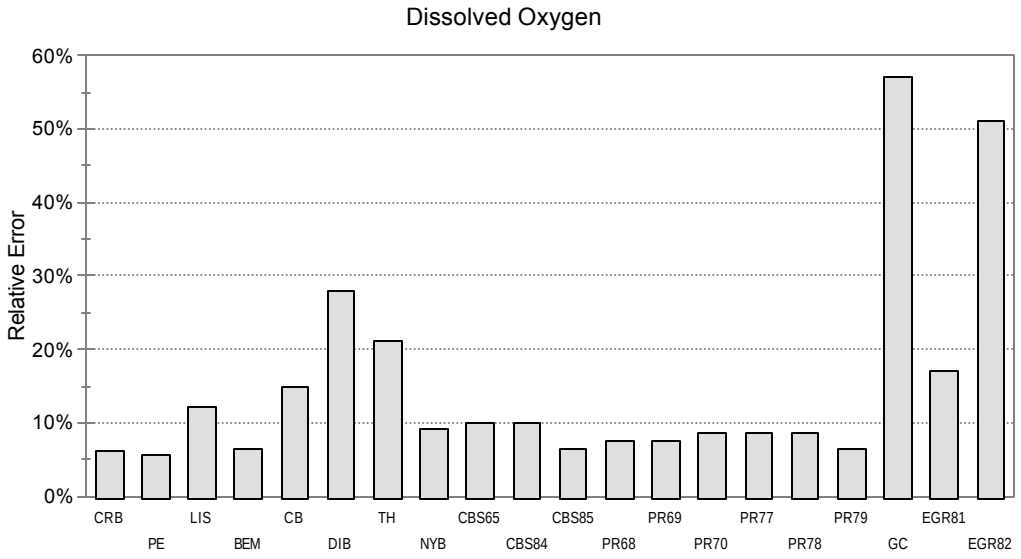

Figure 11-3. Relative error in dissolved oxygen for several water quality models.

Legend:			
CRB	Christina River Basin 1995 & 97 (Tetra Tech 2000)	TH	Tolo Harbour (Chau and Jin 1998)
PE	Peconic Estuary (Tetra Tech 1999)	CBS	Chesapeake Bay Steady-State (HydroQual 1987)
LIS	Long Island Sound (HydroQual 1991)	PR	Potomac River (Thomann & Fitzpatrick 1982)
BEM	Massachusetts Bay (HydroQual 1995)	GC	Gunston Cove (Cerco 1985)
CB	Chesapeake Bay (Cerco & Cole 1994)	EGR	Eau Galle Reservoir (Wlosinski & Collins 1985)
DIB	Delaware Inland Bays (Cerco et al. 1993)	LO	Lake Ontario (Thomann et al. 1979)

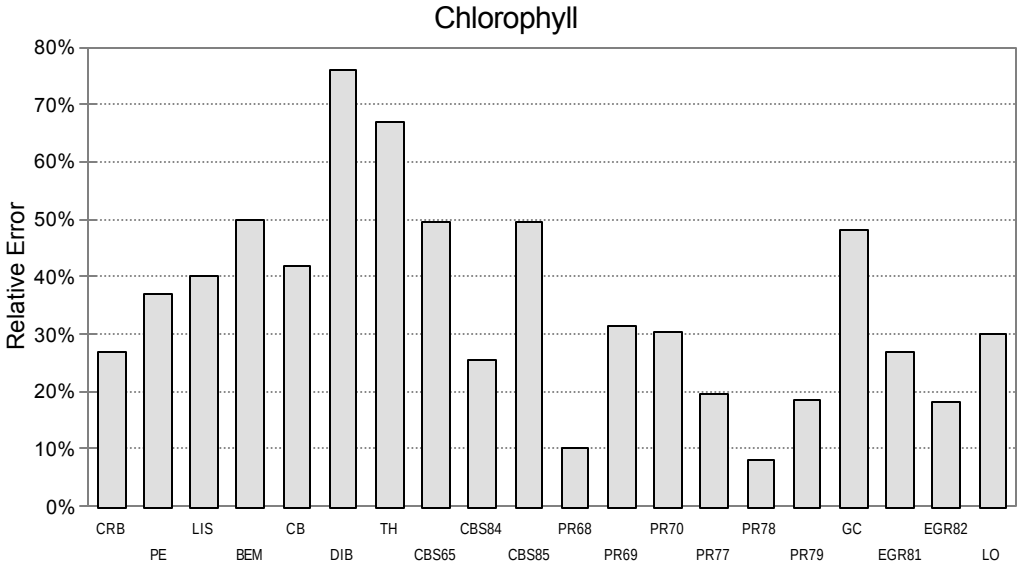

Figure 11-4. Relative error in chlorophyll for several water quality models.

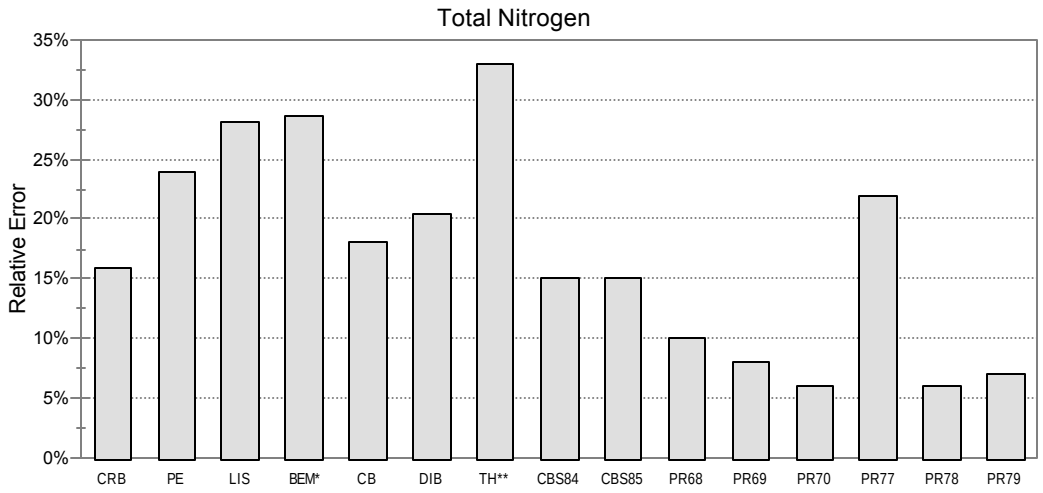

Figure 11-5. Relative error in total nitrogen for several water quality models.
* Total nitrogen not available for BEM; relative error in DIN is shown instead.
** Total nitrogen not available for TH; relative error in DON is shown instead.

Legend:			
CRB	Christina River Basin 1995 & 97 (Tetra Tech 2000)		
PE	Peconic Estuary (Tetra Tech 1999)	TH	Tolo Harbour (Chau and Jin 1998)
LIS	Long Island Sound (HydroQual 1991)	CBS	Chesapeake Bay Steady-State (HydroQual 1987)
BEM	Massachusetts Bay (HydroQual 1995)	PR	Potomac River (Thomann & Fitzpatrick 1982)
CB	Chesapeake Bay (Cerco & Cole 1994)	GC	Gunston Cove (Cerco 1985)
DIB	Delaware Inland Bays (Cerco et al. 1993)	EGR	Eau Galle Reservoir (Wlosinski & Collins 1985)

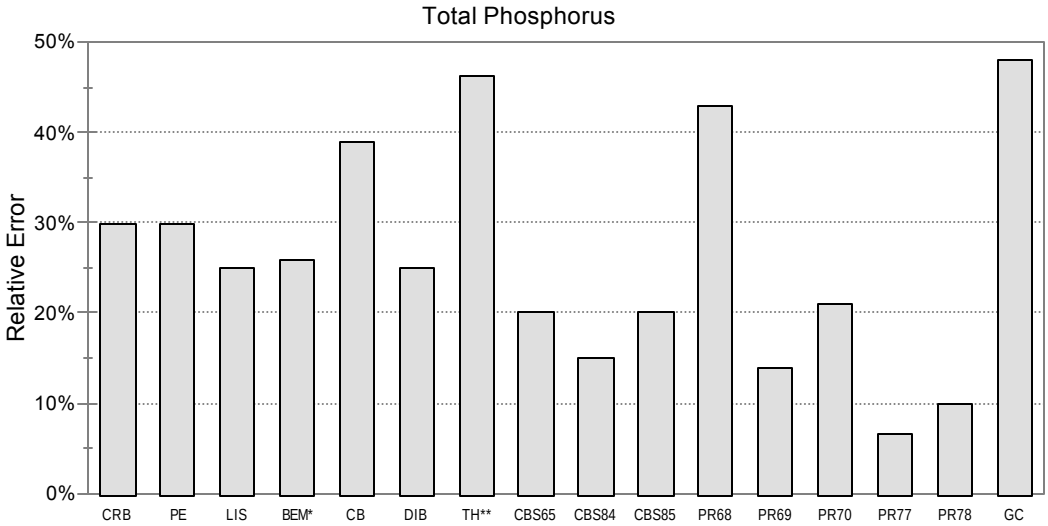

Figure 11-6. Relative error in total phosphorus for several water quality models.
* Total phosphorus not available for BEM; relative error in DIP is shown instead.
** Total phosphorus not available for TH; relative error in DOP is shown instead.

12 - SUMMARY AND CONCLUSIONS

12.1 Summary of EFDC Hydrodynamic and Water Quality Model Framework

The time-dependent, multidimensional Environmental Fluid Dynamics Code (EFDC) provided the modeling framework for this study. EFDC solved prognostic equations for free-surface elevation, velocity components, temperature, salinity, and turbulence energy. All equations were written in curvilinear, coastline-fitted coordinate systems combined with a free-surface and bottom following sigma-coordinate system. An imbedded turbulence closure submodel was employed to provide vertical mixing coefficients for momentum, temperature, and salinity.

A high spatial resolution grid was employed to resolve the important physical processes operating in the Christina River Basin. The horizontal grid spacing along the streams ranged from 500 to about 1,000 meters to provide adequate resolution. The vertical direction was resolved by a single layer. The model was driven by data sets of tidal elevations, salinity, and temperature at the north and south open boundaries, as well as by winds, solar radiation, and point and nonpoint source discharges.

A suite of 22 state variables was required to model the eutrophication processes in the water column (see Table 4-1). Three variables (salinity, water temperature, and total suspended sediment), which are necessary for certain computations involving the 22 state variables, were provided by the EFDC hydrodynamic model. The interactions among the state variables were shown in Figure 4-1.

Kinetic interactions affecting the state variables were described in over 80 partial differential equations that required evaluation of more than 130 parameters. The kinetics described carbon, phosphorus, nitrogen, and silica cycles as well as the dissolved oxygen balance. Algal production is the primary source of carbon, although carbon also enters the system through external loads. Predation on algae releases particulate and organic carbon to the water column, a portion of which undergoes first-order dissolution to dissolved organic carbon, and the remainder settles to the bottom sediments. The kinetic rates used for model calibration are provided in the listing of the model input data in Appendix G.

External loads provide the ultimate source of phosphorus to the system. Dissolved phosphate is consumed by algae during growth and is released through respiration and predation as phosphate and organic phosphorus. A portion of the particulate organic phosphorus hydrolyzes to dissolved organic phosphorus, and the remaining balance settles to the bottom. Dissolved organic phosphorus in the water column is mineralized to phosphate, a portion of which sorbs to inorganic solids and settles to the

bottom. Within the sediment layer, particulate phosphorus is mineralized and recycled back into the water column as dissolved phosphate.

External loads provide the primary source of nitrogen to the Christina River Basin system. Inorganic nitrogen is consumed by algae and released as ammonia and organic nitrogen through respiration and predation. A portion of the particulate organic nitrogen hydrolyzes to dissolved organic nitrogen and the remaining balance settles to the bottom sediments. Dissolved organic nitrogen in the water column is mineralized to ammonia. Depending on the concentration of oxygen in the water column, a fraction of the ammonia is oxidized to nitrate through the nitrification process, or nitrate is lost to nitrogen gas through denitrification. Particulate nitrogen settles to the bottom where it is mineralized and recycled to the water column as ammonia. Nitrate moves in both directions across the sediment-water interface depending on the relative concentrations in the water column and sediment pore water.

In the silica cycle, diatoms consume the available silica and recycle both available and particulate biogenic silica through the actions of metabolism and predation. Particulate silica dissolves in the water column or settles to the bottom. A portion of the settled particulate biogenic silica dissolves within the sediments and returns to the water column as available silica. The sources and sinks of dissolved oxygen in the water column are algal photosynthesis, algal respiration, atmospheric reaeration, nitrification, and chemical oxygen demand.

12.2 Summary of Hydrodynamic Results

An extensive water quality database was used to calibrate a high-resolution, physically comprehensive hydrodynamic and water quality model of the freshwater and tidal streams in the Christina River Basin. The model was driven by data sets of tidal elevations, salinity, and temperature at the north and south open boundaries on the Delaware River, as well as by winds, solar radiation, and point and nonpoint source discharges.

The period May 1 to September 21, 1997, was chosen for model calibration because of available detailed field measurements by Davis (1998) and because the month of August during this period was characterized by stream flows approaching the 7Q10 flow rate. The month of August 1997 was used for tide calibration because tide elevation data were available from two USGS tide gages on the Christina River. Model-data comparisons included water surface elevations, stream flow, velocity, and chlorides. It was apparent from the calibration results that the model is well suited to predict the hydrodynamic characteristics of both the freshwater and the tidal streams in the Christina River Basin. The model was validated during the period May 1 to September 21, 1995.

12.3 Summary of Water Quality Results

It can be debated that using a highly sophisticated, fully dynamic hydrodynamic and eutrophication model such as EFDC is not warranted for a steady-state, low-flow study. However, this calibrated model represents the first phase of a much larger project that will require the dynamic capabilities of EFDC, namely, linking to an HSPF watershed runoff model of the Christina River Basin. The calibration period for the water quality component (May 1 to September 21, 1997) included substantial instream and point source monitoring data collected by PADEP, DNREC, USGS, and Davis (1998) for model calibration. The model was validated during the period May 1 to September 21, 1995. Comparison of the EFDC water quality model predictions with observations indicated the following characteristics:

- Particular attention was given to reproduction of the August 1997 water column concentrations of chlorides, chlorophyll, carbon, nitrogen, and phosphorus in the estuary and freshwater stream reaches. Comparisons of predicted and observed data for all parameters were considered to be reasonable in all 11 major stream reaches included in the model.
- The magnitude of the chlorophyll-*a* concentrations was replicated quite well in all 11 stream reaches.
- The longitudinal concentration gradients of phosphorus, nitrogen, and organic carbon species were replicated reasonably well throughout the system.
- The daily average dissolved oxygen concentrations as well as the daily range in DO agreed well with the observations.
- The model results during the validation period, which experienced flow rates below 7Q10 values, agreed with the observations in a manner similar to the calibration period.
- Although no data were available to compare with the predicted sediment oxygen demand and benthic nutrient flux rates during the calibration and validation periods, the fact that the water column concentrations of oxygen and nutrients compared well with the data provides an indirect confirmation that the predictive sediment submodel is operating reasonably well. Also, SOD data were available from July and August 1996 at two locations in the tidal Christina River and one location in the tidal Brandywine Creek, and the model agreed reasonably well with these limited observations.

12.4 Sources of Uncertainty

In modeling any large and complex system the size of the Christina River Basin, there will always be many possible uncertainties in the model input data (e.g., boundary conditions, loadings, and kinetic rate parameters). The EFDC model incorporates 22 water quality state variables, and 19 of those were required for the Christina River Basin application. The nutrients require the partitioning of carbon,

nitrogen, and phosphorus organic material into dissolved and particulate forms, and the particulate matter is further split into labile and refractory matter. This detailed information was not available from the point source monitoring records or from the STORET monitoring data. To fill in these data gaps, an assumption was made that the organic matter from point and nonpoint sources was generally partitioned into 50% dissolved, 25% labile particulate, and 25% refractory particulate. In addition, the only nutrients generally available from discharge monitoring records were ammonia nitrogen and total phosphorus. The rules for estimating the other nitrogen and phosphorus species were presented in Table 6-4, Table 6-5, and Table 7-4.

The estimated loadings from nonpoint sources are also subject to uncertainty. For this low-flow study, nonpoint source loading rates were computed using a constant concentration reflective of conditions in low-flow periods in the summer and estimates of daily discharge rates. In reality, the concentrations of the various water quality parameters will also change in accordance with storm events due to associated runoff from the watersheds. When the HSPF watershed runoff model of the Christina River Basin is completed, the uncertainty in the nonpoint source loading rates should be reduced because the watershed model will be computing calibrated washoff loads. It was beyond the scope of this study to estimate the watershed runoff loading during rain events.

Detailed information on stream geometry was available only at selected locations, including the four areas sampled in the August 1997 study (Davis 1998), as well as at several cross-sections in the tidal Christina River, Red Clay Creek, and some of the other smaller tributaries. Very crude information on stream geometry was obtained from HEC-2 cross-section data obtained from FEMA. However, since the HEC-2 data were developed for flood studies, they do always include sufficient detail to resolve the low-flow stream channels. Vegetative cover shields many portions of the stream reaches from direct sunshine, which can have a profound effect on localized chlorophyll photosynthesis. The present model incorporates a light reduction factor due to vegetative shading that is adjustable for each grid cell. However, for this calibration the shade factor has been set to 1.0 (i.e., no light reduction due to shade cover) for all grid cells because detailed information on areas affected by canopy cover was not available.

The WWTPs have permit limits for CBOD5 and the discharge monitoring records report CBOD5, whereas the model uses organic carbon instead of CBOD. A special study was conducted in August and September 1999 in which 14 of the largest dischargers in the Christina River Basin were asked to collect effluent data and analyze it for CBOD5, CBOD20, total organic carbon, and dissolved organic carbon content. These data were used to determine the CBODu/CBOD5, DOC/TOC, and TOC/CBODu ratios for the rules listed in Table 7-4.

12.5 Conclusions

The dynamic simulation of eutrophication in a freshwater and estuarine system is a very complicated and computationally intensive endeavor because a large number of chemical, biological, and biochemical processes interact, and the reaction rates and external inputs vary with time. In addition, the flow rates and associated circulation are also time-varying, having time scales ranging from minutes to months or even years in the case of sediment flux recovery.

The present EFDC hydrodynamic and water quality model of the freshwater and tidal streams in the Christina River Basin represents the current state of the art in eutrophication modeling. The original scope of work for this project was designed around a model framework based on EPA's WASP model. The framework was changed to the EFDC model because it provides several advances over a WASP model application. First, the coupling of the model to a three-dimensional, time-varying hydrodynamic model provides more realistic circulation physics of the tidal waters in the system. Second, the water quality model itself includes an expanded suite of 22 state variables (the EPA WASP model includes only 8 state variables). Third, the coupling to a fully predictive sediment process model allows the simulation of sediment oxygen demand and nutrient fluxes. Fourth, the model simulates the growth of attached algae (periphyton), which is the primary force driving the large diel dissolved oxygen swings observed in certain stream reaches (WASP does not include a periphyton state variable).

The EFDC hydrodynamic and water quality model of the Christina River Basin meets or exceeds the goals specified at the initiation of the project. Even though a number of potential sources of uncertainty were outlined in Section 12.4, the model exhibits a high degree of correspondence to observations monitored in the estuary and stream reaches. The calibration and validation statistics for the Christina River water quality model were presented in Chapter 11. According to the *Technical Guidance Manual for Performing Waste Load Allocations* (USEPA 1990), acceptable relative error statistic criteria are 15% for dissolved oxygen and 45% for nutrient parameters (nitrogen, phosphorus, and carbon). The overall relative errors of the Christina River model were 6.3% for dissolved oxygen, 15.9% for total nitrogen, 29.9% for total phosphorus, and 32.6% for total organic carbon. Based on the calibration and validation results, the model is considered to be adequately calibrated and is acceptable as a tool for TMDL management of nutrient, dissolved oxygen, and eutrophication issues in the Christina River Basin.

This page intentionally left blank

13 - REFERENCES

Ambrose, R.B., T.A. Wool, and J.L. Martin. 1993. The water quality analysis and simulation program, WASP5: Part A, model documentation version 5.1. U.S. Environmental Protection Agency, Environmental Research Laboratory, Athens, GA, 210 pp.

Andrews, D.G., and M.E. McIntyre. 1978. An exact theory for of nonlinear waves on a Lagrangian flow. *J. Fluid Mech.* 89:609-646.

Banks, R.B. and F.F. Herrera. 1977. Effect of wind and rain on surface reaeration. *ASCE J. of the Environ. Engr. Div.* 103(EE3):489-504.

Barrow, N.J. 1983. A mechanistic model for describing the sorption and desorption of phosphate by soil. *J. of Soil Science* 34:733-750.

Bennett, A.F. 1976. Open boundary conditions for dispersive waves. J. Atmos. Sci. 32:176-182.

Bennett, A.F., and P.C. McIntosh. 1982. Open ocean modeling as an inverse problem: tidal theory. *J. Phys. Ocean.* 12:1004-1018.

Bennett, J.R., and A.H. Clites. 1987. Accuracy of trajectory calculation in a finite-difference circulation model. *J. Comp. Phys.* 68:272-282.

Blumberg, A.F., and L.H. Kantha. 1985. Open boundary condition for circulation models. *J. Hydr. Engr.* 111:237-255.

Blumberg, A.F., and G.L. Mellor. 1987. A description of a three-dimensional coastal ocean circulation model. *Three-Dimensional Coastal Ocean Models, Coastal and Estuarine Science, Vol. 4,* ed. N.S. Heaps, pp. 1-19. American Geophysical Union.

Boni, L., E. Carpené, D. Wynne, and M. Reti. 1989. Alkaline phosphatase activity in *Protogonyaulax tamarensis*. *J. of Plankton Research* 11(5):879-885.

Boudreau, B.P. 1991. Modelling the sulfide-oxygen reaction and associated pH gradients in porewaters. *Geochimica et Cosmochimica Acta*, 55:145-159.

Bowie, G.L., W.B. Mills, D.B. Porcella, C.L. Campbell, J.R. Pagenkopf, G.L. Rupp, K.M. Johnson, P.W.H.Chan, S.A. Gherini, and C.E. Chamberlin. 1985. Rates, constants and kinetics formulations in surface water quality modeling (2nd edition). EPA/600/3-85/040, U.S. Environmental Protection Agency, Environmental Research Lab., Athens, GA, 455 pp.

Boynton, W., W. Kemp, and C. Keefe. 1982. A comparative analysis of nutrients and other factors influencing estuarine phytoplankton production. *Estuarine Comparisons*, Academic Press. pp 69-90.

Burban, P.Y., W. Lick, and J. Lick. 1989. The flocculation of fine-grained sediments in estuarine waters. *J. Geophys. Res.* 94:8323-8330.

Burban, P.Y., Y.J. Xu, J. McNeil, and W. Lick. 1990. Settling speeds of flocs in fresh and seawater. *J. Geophys. Res.* 95:18,213-18,220.

Carritt, D.E. and S. Goodgal. 1954. Sorption reactions and some ecological implications. *Deep-Sea Research* 1:224-243.

Caupp, C.L., Brock, J.T., and Runke, H.M. 1991. Application of the dynamic stream simulation and assessment model (DSSAM III) to the Truckee River below Reno, Nevada: Model formulation and program description.

Report prepared by Rapid Creek Water Works for Nevada Division of Environmental Protection, Carson City and Washoe County Dept. Of Comprehensive Planning, Reno, NV.

Cerco, C.F., and T. Cole. 1993. Three-dimensional eutrophication model of Chesapeake Bay. *J. Environ. Engnr.* 119:1006-1025.

Cheng, R.T., V. Casulli, and J.W. Gartner. 1993. Tidal, residual, intertidal mudflat (TRIM) model and its applications to San Francisco Bay, California. *Estuarine, Coastal, and Shelf Science* 36: 235-280.

Chróst, R.J. and J. Overbek. 1987. Kinetics of alkaline phosphatase activity and phosphorus availability for phytoplankton and bacterioplankton in Lake Plußsee (North German eutrophic lake). *Microbial Ecology* 13:229-248.

Cline, J.D. and F.A. Richards. 1969. Oxygenation of hydrogen sulfide in seawater at constant salinity, temperature and pH. *Environmental Science & Technology*, 3(9):838-843.

Cole, T.M., and E.M. Buchak. 1994. CE-QUAL-W2: A two-dimensional laterally averaged, hydrodynamic and water quality model, Version 2.0, Report ITL-93-7. U. S. Army Corps of Engineers, Waterway Experiment Station, Vicksburg, MS.

Davis, J. 1998. Measurement of community photosynthesis and respiration rates for selected reaches of the Christina Watershed. Prepared for Pennsylvania Department of Environmental Protection and Delaware Department of Natural Resources and Environmental Control, March 1998.

Diaz, R.J. and R. Rosenberg. 1995. Marine benthic hypoxia: a review of its ecological effects and the behavioural responses of benthic macrofauna. *Oceanography and Marine Biology: an Annual Review* 33:245-303.

DiToro, D.M. 1980. Applicability of cellular equilibrium and Monod theory to phytoplankton growth kinetics. *Ecological Modelling* 8:201-218.

DiToro, D.M., P.R. Paquin, K. Subburamu, and D.A. Gruber. 1990. Sediment oxygen demand model: methane and ammonia oxidation. *ASCE J. Environ. Engr.* 116(5):945-986.

DiToro, D.M., and J.F. Fitzpatrick. 1993. Chesapeake Bay sediment flux model. Contract Report EL-93-2. Prepared by HydroQual, Inc. for U. S. EPA Chesapeake Bay Program, U. S. Army Engineer District, Baltimore, MD, and U.S. Army Engineer Waterways Exp. Station.

Frick, W.E. 1984. Non-empirical closure of the plume equations, *Atmos. Environ.* 18:653-662.

Froelich, P.N. 1988. Kinetic control of dissolved phosphate in natural rivers and estuaries: a primer on the phosphate buffer mechanism. *Limnol. and Oceanogr.* 33(4, part 2):649-668.

Galperin, B., L.H. Kantha, S. Hassid, and A. Rosati. 1988. A quasi-equilibrium turbulent energy model for geophysical flows. *J. Atmos. Sci.* 45:55-62.

Genet, L.A., D.J. Smith, and M.B. Sonnen, M.B. 1974. Computer program documentation for the dynamic estuary model. Prepared for U.S. Environmental Protection Agency, Systems Development Branch, Washington, D.C.

Grant, W.D., and O.S. Madsen. 1986. The continental-shelf bottom boundary layer. *Annual Review of Fluid Mechanics*, ed. M. Van Dyke et al., pp. 365-306, Annual Review, Inc.

Giordani, P. and M. Astorri. 1986. Phosphate analysis of marine sediments. *Chemistry in Ecology* 2:103-112.

Hamrick, J.M. 1992a. A Three-Dimensional Environmental Fluid Dynamics Computer Code: Theoretical and Computational Aspects, Special Report 317. The College of William and Mary, Virginia Institute of Marine Science. 63 pp.

Hamrick, J.M. 1992b. Estuarine environmental impact assessment using a three-dimensional circulation and transport model. Estuarine and Coastal Modeling, Proceedings of the 2nd International Conference, M. L. Spaulding et al, Eds., American Society of Civil Engineers, New York, 292-303.

Hamrick, J. M. 1994: Linking hydrodynamic and biogeochemcial transport models for estuarine and coastal waters. *Estuarine and Coastal Modeling, Proceedings of the 3rd International Conference*, ed. M.L. Spaulding et al., pp. 591-608. American Society of Civil Engineers, New York.

Hamrick, J.M. 1996. A User's Manual for the Environmental Fluid Dynamics Computer Code (EFDC), Special Report 331. The College of William and Mary, Virginia Institute of Marine Science. 234 pp.

Hamrick, J.M., and T.S. Wu. 1996. Computational design and optimization of the EFDC/HEM3D surface water hydrodynamic and eutrophication models. *Computational Methods for Next Generation Environmental Models*, ed. G. Delich. Society of Industrial and Applied Mathematics, Philadelphia.

Hecky, R. and P. Kilham. 1988. Nutrient limitation of phytoplankton in freshwater and marine environments: a review of recent evidence on the effects of enrichment. Limnol. And Oceanogr. 33(4):796-822.

Horner, R.R., E.B. Welch, M.R. Seeley, and J.M. Jacoby. 1990. Responses of periphyton to changes in current velocity, suspended sediment, and phosphorus concentration. *Freshwater Biol.* 24(2):215-232.

HydroQual. 1991. Draft Water Quality Modeling Analysis of Hypoxia in Long Island Sound. Prepared for Management Committee Long Island Sound Estuary Study and New England Interstate Water Pollution Control Commission. Prepared by HydroQual, Inc., Mahwah, NJ. Job Number: NENG0012. July 1991.

Jirka, G. H., and R.L. Doneker. 1991. Hydrodynamic classification of submerged single-port discharges, *J. of Hydr. Engr.* 117:1095-1112.

Jirka, G.H., and P.J. Akar. 1991. Hydrodynamic classification of submerged multiport-diffuser discharges, *J. of Hydr. Engr.* 117:1113-1128.

Kang, I.S., and L.G. Leal. 1992. Orthogonal grid generation in a 2D domain via the boundary integral technique. *J. Comp. Phys.* 102:78-87.

Knorr, D.F. and G.W. Fairchild. 1987. Periphyton, benthic invertebrates and fishes as biological indicators of water quality in the East Branch Brandywine Creek. *Proceedings of the Pennsylvania Academy of Science* 61(1):62-66.

Kremer, J.N. and S.W. Nixon. 1978. A coastal marine ecosystem: simulation and analysis. *Ecological Studies 24*, Springer-Verlag, New York. 217 pp.

Lebo, M.E. 1991. Particle-bound phosphorus along an urbanized coastal plain estuary. *Marine Chemistry* 34:225-246.

Lee, J.H.W., and V. Cheung. 1990. Generalized Lagrangian model for buoyant jets in a current. *J. Environ. Engrg.* 116:653-662.

Lijklema, L. 1980. Interaction of ortho-phosphate with iron (III) and aluminum hydroxides. *Environmental Science & Technology*, 14(5):537-541.

Madsen, P.A., and J. Larsen. 1987. An efficient finite-difference approach to the mild-slope equation. *Coastal Engr.* 11:329-351.

Mancini, J.L. 1983. A method for calculating effects, on aquatic organisms, of time varying concentrations. *Water Research* 17(10):1355-1362.

Matisoff, G. 1982. Mathematical models of bioturbation, ed. P.L. McCall and M.J.S. Tevesz, pp. 289-330. *Animal-Sediment Relations: The Biogenic Alteration of Sediments*, Plenum Press, NY.

Mellor, G.L., and T. Yamada. 1982. Development of a turbulence closure model for geophysical fluid problems. *Rev. Geophys. Space Phys.*, 20:851-875.

Millero, F.J. 1986. The thermodynamics and kinetics of the hydrogen sulfide system in natural waters. *Marine Chemistry* 18:121-147.

Mobley, C.D., and R.J. Stewart. 1980. On the numerical generation of boundary-fitted orthogonal Curvilinear coordinate systems. *J. Comp. Phys.* 34:124-135.

Morel, F. 1983. *Principles of Aquatic Chemistry*. John Wiley & Sons, New York, NY. 446 pp.

Morse, J.W., F.J. Millero, J.C. Cornwell, and D. Rickard, D. 1987. The chemistry of the hydrogen sulfide and iron sulfide systems in natural waters. *Earth-Science Reviews* 24:1-42.

Moustafa, M.Z., and J.M. Hamrick. 1994. Modeling circulation and salinity transport in the Indian River Lagoon. *Estuarine and Coastal Modeling, Proceedings of the 3rd International Conference*, ed. M. L. Spaulding et al., pp. 381-395. American Society of Civil Engineers, New York.

McIntire, C.C. 1973. Periphyton dynamics in laboratory streams: a simulation model and its implications. *Ecological Monographs.* 43:399-420.

Nixon, S. 1981. Remineralization and nutrient cycling in coastal marine ecosystems. *Estuaries and Nutrients*, ed. Neilson and Cronin. pp.111-138. Humana Press, Clifton, NJ.

NOAA. 1998. Tide Tables 1998. National Oceanographic and Atmospheric Administration, National Ocean Service, Silver Spring, MD.

O'Connor, D.J. and W.E. Dobbins. 1958. Mechanism of reaeration in natural streams. *Transactions of the American Society of Civil Engineers*, 123(2934):641-684.

Odum, E.P. 1971. *Fundamentals of ecology (3rd edition).* W.B. Saunders Co., Philadelphia, PA. 574pp.

Oey, L.-Y., G.L. Mellor, and R.I. Hires. 1985. A three-dimensional simulation of the Hudson Raritan estuary. *J. Phys. Oceanogr.* 15:1676-1720.

Park, K., A.Y. Kuo, J. Shen, and J.M. Hamrick. 1995. A three-dimensional hydrodynamic-eutrophication model (HEM3D): description of water quality and sediment processes submodels, Special Report 327. The College of William and Mary, Virginia Institute of Marine Science. 113 pp.

Parsons, T.R., M. Takahashi, and B. Hargrave. 1984. *Biological oceanographic processes (3rd edition).* Pergamon Press. 330 pp.

Pfeifer, R.F., and McDiffett, W. 1975. Some factors affecting primary production of stream communities. *Archives of Hydrobiol.* 75:306-317.

Press, W.H., B.P. Flannery, S.A. Teukolsky, and W.T. Vetterling. 1986. *Numerical recipes: the art of scientific computing*. Cambridge University Press. 818 pp.

Redfield, A.C., B.H. Ketchum, and F.A. Richards. 1963. The influence of organisms on the composition of sea-water, ed. M.N. Hill, Chapter 2, pp 26-77. *The Sea - Ideas and Observations on Progress in the Study of the Seas: Vol. 2, Composition of Sea Water, Comparative and Descriptive Oceanography*, Interscience Publishers.

Reif, A.G. 1999. Physical, chemical, and biological data collected for selected streams in Chester County, Pennsylvania, 1981-1994.

Rennie, S., and J.M. Hamrick. 1992. Techniques for visualization of estuarine and coastal flow fields. *Estuarine and Coastal Modeling, Proceedings of the 2nd International Conference*, ed. M. L. Spaulding et al., pp. 48-55. American Society of Civil Engineers, New York.

Robbins, J.A., T. Keilty, D.S. White, and D.N. Edgington. 1989. Relationships among tubificid abundances, sediment composition and accumulation rates in Lake Erie. *Canadian J. of Fisheries & Aquatic Sciences*, 46(2):223-231.

Rosati, A.K., and K. Miyakoda. 1988. A general circulation model for upper ocean simulation. *J. Phys. Ocean*, 18:1601-1626.

Ross, P.J. 1983. Dynamics of periphyton communities. *Periphyton in Freshwater Ecosystems*, ed. R.G. Wetzel, pp. 5-10. Junk, Boston, MA, 5-10.

Runke, H.M. 1985. Simulation of the lotic periphyton community of a small mountain stream by digital computer. PhD thesis, Utah State University, Logan, Utah.

Ryskin, G. and L.G. Leal. 1983. Orthogonal mapping. *J. Comp. Phys.* 50:71-100.

Sand-Jensen, K. 1983. Physical and chemical parameters regulating the growth of periphyton communities. *Periphyton in Freshwater Ecosystems*, ed. R.G. Wetzel, pp. 63-71. Junk, Boston, MA.

Senior, L.A. 1999. Background concentrations for Christina River Model. U.S. Geological Survey, Malvern, PA. Memorandum to M.R. Morton, Tetra Tech, Inc. dated August 6, 1999.

Shen, J., J. Boon, and A.Y. Kuo. 1999. A numerical study of a tidal intrusion front and its impact on larval dispersion in the James River estuary, Virginia. *Estuary* 22(3A):681-692.

Smolarkiewicz, P.K., and T.L. Clark. 1986. The multidimensional positive definite advection transport algorithm: further development and applications. *J. Comp. Phys.* 67:396-438.

Smolarkiewicz, P.K., and W.W. Grabowski. 1990. The multidimensional positive definite advection transport algorithm: nonoscillatory option. *J. Comp. Phys.* 86:355-375.

Smolarkiewicz, P.K., and L.G. Margolin. 1993. On forward-in-time differencing for fluids: extension to a curvilinear framework. *Mon. Weather Rev.* 121:1847-1859.

Steele, J.H. 1962. Environmental control of photosynthesis in the sea. *Limnol. and Oceanogr.* 7(2):137-150.

Stevenson, R.J., and Glover, R. 1993. Effects of algal density and current on ion transport through periphyton communities. *Limnol. and Oceanogr.*, 38(6):1276-1281.

Strickland, J. 1960. Measuring the production of marine phytoplankton. *Fisheries Research Board of Canada Bulletin* 122:172.

Stumm, W. and J.J. Morgan. 1981. *Aquatic chemistry, an introduction emphasizing chemical equilibria in natural waters (2nd edition).* John Wiley & Sons, Inc. 780 pp.

Thomann, R.V., N.J. Jaworski, S.W. Nixon, H.W. Paerl, and J. Taft. 1985. The 1983 algal bloom in the Potomac Estuary. The Algal Bloom Expert Panel, pepared for the Potomac Strategy State/EPA Management Committee, US Environmental Protection Agency, Region III, Philadelphia, PA.

Thomann, R.V. and J.A. Mueller. 1987. *Principles of surface water quality modeling and control.* Harper & Row, Publishers, Inc. 644 pp.

Troup, R. 1974. The interaction of iron with phosphate, carbonate and sulfide in Chesapeake Bay interstitial waters: a thermodynamic interpretation. Ph.D. Dissertation, Johns Hopkins University, MD. 114 p.

USEPA. 1990. *Technical Guidance Manual for Performing Waste Load Allocations, Book III Estuaries, Part 2, Application of Estuarine Waste Load Allocation Models*. EPA823-R-92-003. U.S. Environmental Protection Agency, Office of Water. May 1990.

USEPA. 1995. *Technical Guidance Manual for Developing Total Maximum Daily Loads, Book II: Streams and Rivers, Part 1: Biochemical Oxygen Demand/Dissolved Oxygen and Nutrients/Eutrophication.* EPA 823-B-95-007. U.S. Environmental Protection Agency, Office of Water. September 1995.

Warwick, J.J., D. Cockrum, and M. Horvath. 1997. Estimating non-point source loads and associated water quality impacts. *ASCE J. Water Res. Plan. and Manage.* 123(5):302-310.

Westrich, J.T. and B.A. Berner. 1984. The role of sedimentary organic matter in bacterial sulfate reduction: the G model tested. *Limnol. and Oceanogr.* 29(2):236-249.

Wezernak, C.T. and J.J. Gannon. 1968. Evaluation of nitrification in streams. *ASCE J. Sanitary Engr. Div.* 94(5):883-895.

Whitford, L.A. and G.J. Schumacher. 1964. Effect of current on respiration and mineral uptake of Spirogyra and Oedogonium. *Ecology* 45:168-170.

Wu, T.S., J.M. Hamrick, S.C. McCutechon, and R.B. Ambrose. 1996. *Benchmarking the EFDC/HEM3D surface water hydrodynamic and eutrophication models. Computational Methods for Next Generation Environmental Models*, ed. G. Delich. Society of Industrial and Applied Mathematics, Philadelphia.

Yamamoto, S., J.B. Alcauskas, and T.E. Crozler. 1976. Solubility of methane in distilled water and seawater. *J. of Chemical and Engineering Data* 21(1):78-80.